2018

Investigation of the Effect of Tuning Mechanisms on the Operational and Survival State of a Floating Oscillating Water Column Wave Energy Converter

York Stanham

University of Wollongong

UNIVERSITY OF WOLLONGONG

Department of Engineering

Investigation of the Effect of Tuning Mechanisms on the Operational and Survival State of a Floating Oscillating Water Column Wave Energy Converter

York Stanham

This thesis is part of the requirements for the award of the Degree of Doctorate of Engineering of the University of Wollongong

May 2018

Abstract

This research was undertaken to determine the characteristics governing a thin-walled cylindrical, floating oscillating water column wave energy device with regards to power production and device integrity. This investigation considers how such an oscillating water column wave energy device can be optimised for power production yet still be robust enough to withstand unfavourable storm conditions by tuning mechanisms such as heave added mass changes, power take-off damping changes, and stiffness changes. The investigation also considers how the initial device and oscillating water column sizing affects performance in favourable and unfavourable sea conditions.

This research was undertaken by utilising WAMIT and OrcaFlex. These are two industry accepted analysis tools. This thesis examines the power take-off efficiency of the device in moderate frequency waves and employs wave conditions from DNV standards during survival studies.

It is conjectured that installation sites with moderate to low energy are more feasible for motion dependent wave energy converters than sites with higher concentrations of energy because the unfavourable storm conditions are not as severe. It was determined that a system with an oscillating water column natural frequency designed to match the mean peak wave frequency of the desired installation site, and operating within a structure with a natural frequency approximately 0.66 times the oscillating water column natural frequency, produced the most efficient system. This ratio ensured sufficient spacing between the natural frequencies. This spacing allows increased velocity differentials with a single forcing frequency. Achieving this ratio of natural frequencies is most feasible through tuning of the heave mass of the structure.

This thesis concludes that such a device can withstand unfavourable storm conditions if the structure natural frequency can be altered. Adjusting the heave mass to move the natural frequency of the structure away from the peak wave frequency reduces the peak heave displacement and hence the peak mooring line tensions. Tuning during the operational and survival states is most feasible through changing the heave added mass of the device by employing or withdrawing heave plates.

Acknowledgements

First, I would like to send a huge thanks to my primary research supervisor, Professor Timothy McCarthy. This thank you is also extended to my secondary supervisor Dr. Brad Stappenbelt. Their guidance and knowledge has been essential to the direction and completion of this thesis.

Secondly, I would like to extend my appreciation for the work of Daryl Trkulja for ensuring that OrcaFlex and WAMIT were operating when simulations needed to be completed.

Contents

List of Figures

List of Tables

Glossary of Terms

OWC	Oscillating water column
WED	Wave energy device
CSIRO	Commonwealth Scientific and Industrial Research Organisation
IPCC	International Panel on Climate Change
TWh/y	Terawatt hours per year
kW/m	Kilowatts per metre
WAMIT	Wave Analysis MIT
ISSC	International Ship and Offshore Structures Congress
JONSWAP	Joint North Sea Wave Project
PTO	Power take-off
RAO	Response amplitude operator
FPS	Free pressure surface
ULS	Ultimate limit state
ALS	Accidental limit state
FLS	Fatigue limit state

Chapter 1 Introduction

1.1 Introduction

Wave energy converters are potentially one of the larger areas of growth, not only in the realm of renewable energy but as a viable alternative to non-renewable resources that Australia and the world so heavily depend on. The Australian Academy of Science predicts that wave energy has the potential to account for 5% of Australia's total energy needs within twenty years and approximately 25% by 2060. The utilisation of wave energy is not limited to Australia; it is also forecast that wave energy has the potential to be the source of about 10% of the world's energy in 50 years (Williamson and Dopita, 2010). The Commonwealth Scientific and Industrial Research Organisation (CSIRO) predicts that wave power has the potential to deliver up to 11% of Australia electricity needs by 2050 (Behrens et al. 2012). There have been a number of estimates for the total global wave energy available. The Intergovernmental Panel on Climate Change (IPCC) estimate that a theoretical potential of approximately 29,500 TWh/yr is available if all areas with energy densities greater than 5 kW/m were considered (Lewis et al. 2011). In 2007 the IPCC assessed that there is approximately 146 TWh/yr available assuming that energy capturing devices are installed along approximately 2% of the world's coastline that contains power density greater than 30 kW/m (Sims et al., 2007). The inherent issue with this abundance of wave energy is that the energy is often located in large densities where the forces associated with the waves are often too large for a device to handle.

Currently, wave energy is a secondary option in the effort to increase the use of renewable energy sources. The Clean Energy Council estimates that marine energy contributed approximately 0.001% of total renewable energy resources used in Australia in 2011 (Clean Energy Australia, 2012). The main reason for the slow implementation is that, compared to other renewable sources such as solar, wind and geothermal, wave energy is seen as being inefficient and hard to maintain at a cost that makes it viable. Levelised cost of energy is defined as the total installation cost divided by the total lifetime energy output of the device. The estimated levelised cost for a 10 MW wave energy farm is $500-$1000 AUD/MWh (SI Ocean, 2013). Other renewable systems include hydro (~$175/MWh), wind (~$75/MWh) photovoltaic (~$120/MWh) and biomass (~$90/MWh) (Hayward et al., 2011).

This increased cost of energy is based partly on the inherent problems of the energy source as well as the limited research being undertaken in the area. The overall efficiency of wave energy devices is dependent on numerous factors. These include the environmental conditions, the design of the device, the depth of the sea, and weather patterns (Halloran, 2010). Despite the bleak assessment of the potential for using wave energy there is a vast amount of energy present in the ocean.

1.2 Wave Energy Location, Capacity and Cost

Clean Energy Australia (2011) estimates that approximately 80% of the Australian population lives within 50 kilometres of the coast. Clean Energy Australia (2011) highlighted that current interest in wave energy development has focused on the southern, southwestern and southeastern coastline of Australia. This places wave energy in close proximity to the majority of the intended users. Geosciences Australia have highlighted these areas as having a total annual wave energy greater than 0.5 TJ/m (Willcock, Che, and McCluskey, 2013). Hughes and Heap (2010) have estimated that the total energy crossing the 25 metre isobaths along the southern coastline of Australia is approximately 1329 TWh/yr. This equates to approximately five times Australia's energy usage in 2010 (Hughes and Heap, 2010). The isolation of this area provides obvious obstacles meaning 100% capture is highly improbable; however, if say only 10% of this energy is collected it has the potential to provide half of Australia's energy needs.

A report published in 2011 by the CSIRO estimated that the levelised cost of electricity produced from potential wave energy systems could be brought down to below $100 per MWh if suitable wave energy converters can be developed (Hayward et al., 2011). A prediction for the year 2030 was made by the CSIRO. In this prediction, wave energy had a long-term levelised cost of approximately $105/MWh. This prediction shows that wave energy can compete on cost when compared to other established renewable energy systems. These systems include hydro (~$175/MWh), wind (~$75/MWh) photovoltaic (~$120/MWh) and biomass (~$90/MWh) (Hayward et al., 2011).

It is evident that wave energy has potential as an energy source from a cost and location standpoint and is an abundant resource for commercial scale use within Australia. This is provided a suitable wave energy converter can be developed.

1.3 Wave Energy Devices

Wave energy converters can be broadly categorised based on their means of capturing power from wave loading. Wave energy converters either aim to remain still and use the motion of the water to generate power or aim to use the motion of the converter itself to generate power; this gives rise to the categories of motion-dependent and motion-independent wave energy generating devices (Johanning et al., 2006).

In 2015 there were two wave energy facilities operating within Australia. The largest system was the bioWAVE unit developed by BioPower Systems. This device was rated at 250 kW. It is located at Port Fairy in Victoria. This device is a fixed pivoting device operating in depths of approximately 30 m. The second device is located at Garden Island in Western Australia and was operated by Carnegie Wave Energy. This system is known as the CETO5 system and was rated at 240 kW. This wave energy converter is a floating buoy-type device. Carnegie Wave Energy does have plans to develop and install the CETO6 device. The device is rated at 1MW and can be installed up to 10 km offshore. This point absorber device is expected to be fully installed by the end of 2017 (Carnegie Wave Energy, 2015). The largest wave energy facility operated within Australia was operating at Port Kembla, New South Wales in February and March 2010. This facility was the oscillating water column converter operated by Oceanlinx. It was rated at 0.5 MW. This device is no longer in operation due to a mooring line failure in May 2010.

There are numerous wave energy companies either investigating or testing various devices around Australia. These are listed in Table 1.1.

Table 1.1: Existing and Planned Wave Energy Facilities in Australia

Owner	Location	State	Status of Device
AquaGen Technologies	Lorne	VIC	1.5 kW device installed at Lorne Pier in 2010
BioPower Systems	King Island	TAS	Preliminary investigation and design completed
	Port Fairy	VIC	250 kW device installed in 2015
	Flinders Island	TAS	Preliminary investigation and design completed
Carnegie Wave Energy	Perth	WA	CETO5 units installed and operated for over 13,000 hours
			CETO6 units under development. To be installed in 2017.
Protean Wave Energy	Geraldton	WA	Scale testing complete. Demonstration wave farm testing has commenced.

1.4 Aims and Objectives

This thesis aims to develop a thorough explanation of how the structural dynamics and sizing of floating offshore oscillating water column wave energy devices affect the response of such a wave energy device in a range of wave conditions. This aim includes improving the existing knowledge of how the real and added mass, stiffness, and power take-off damping affect the heave motions and, by extension, the power output and robustness of the device. The aim of this research is to investigate the effect of the structure and oscillating water column sizing on the structural dynamics of wave energy device.

The specific objectives of this work are to:

1. Develop an explanation of how and why existing design methodologies, standards, and design are employed in the offshore industries with a focus on the oil and gas, and offshore wind turbine industries.
2. Explain how the existing designs (from objective 1) affect the dynamics of an offshore floating vessel.
3. Understand ocean wave spectra and how these are developed and influenced.
4. Develop a theoretical explanation of how power is produced in a floating oscillating water column wave energy device.
5. Detail the key structural characteristics, and the parameters that govern them, of the floating vessel and oscillating water column and their effect on the response of the device.
6. Develop a framework for the appropriate sizing of both the oscillating water column and structure for an OWC wave energy converter.
7. Determine and assess appropriate tuning mechanisms to increase power output during favourable conditions and to maintain structural integrity during unfavourable conditions.

1.5 Research Questions

The following are the questions this study answers. Each question is explored with further questions. These questions guided the path of the investigation.

1. Existing design methodologies.
    a) What are the current moored offshore floating vessel design methodologies and parameters?
    b) What are the current motion-dependent floating wave energy converter design methodologies and parameters?
    c) How applicable are traditional design methodologies and parameters to motion-dependent wave energy converter design and operation?
    d) What are the requirements of a motion-dependent wave energy converter system?

These research questions aim to answer objectives 1 and 2. These objectives are concerned with the control of the structural dynamics of moored floating offshore vessels. Answering these questions will provide an initial design methodology and provide evidence for how and why design aspects are employed in the offshore industry.

2. Operational stage wave energy converter moorings.
    a) Can a system be developed that allows the vessel to experience increased motion from first order wave loading?
    b) Over what range of wave frequencies can this system operate?
    c) Is a tuneable system likely to increase the range of wave conditions in which the wave energy converter is able to provide increased motion and power?
    d) What are the most viable methods to create a tuneable system that is able to meet objective 2?
    e) To what extent is the efficiency of a motion-dependent wave energy converter increased during periods of optimal wave induced motion?

The research questions covered in the second point aim to answer objectives concerned with how power is produced in a floating OWC device. Answers to these questions will be used to complete objectives 3 to 7.

3. Survivability stage wave energy converter moorings.
    a) Can the system developed in objective 5 withstand unfavourable conditions through the tuning (i.e. reduction of first order motion response) without compromising the operational phase motion of the wave energy converter?
    b) If the answer to 3a is no then what is the most feasible design that will meet the survivability requirement of a wave energy converter?

The two research questions covered in point 3 aim to determine how the structural integrity of the OWC device will be ensured during unfavourable conditions. The questions in point 3 will provide evidence for the completion of objective 5 to 7.

4. System integration.
    a) Can the operational system and survivability system be integrated into one system without compromising efficiency or increasing risk of failure?
    b) If the answer to 4a is negative then can both systems be implemented with one floating vessel?
    c) If the answer to 4b is positive then what is the best method to transition between the systems?
    d) What are the environmental conditions that determine which system is in use?

Point 4 asks four research questions concerned with the implementation of two systems. These systems are the system aimed at power production and system integrity. These questions will be used to develop evidence for objective 7.

5. Design parameters and concerns
    a) What are appropriate factors of safety during analysis for wave energy converters?

b) Where are the most feasible locations for the installation of the wave energy converter investigated in this study?

Point 5 addresses questions concerned with the practical implementation of OWC devices around the world. These questions are answered to develop a guideline for the conditions likely to determine whether an installation location is suitable. These questions are also concerned with the applicability of existing design guidelines to OWC devices. Answering these questions will provide further evidence of the completion of objective 1.

1.6 Scope of this Research

This research is primarily concerned with the design and analysis of a wave energy converter will influence the dynamics of vessel and its response to single waves and wave spectra. The design component of this present study is limited to sizing of wave energy converter and oscillating water column. This includes specification of system characteristics such as mass, damping, and stiffness. The key areas of interest are the structure's geometry, vertical and horizontal stiffness, heave mass, and the power take-off for a floating wave energy converter. The wave energy converter of concern is an open bottom, motion-dependent, oscillating water column device.

Ideally, this wave energy converter should be able to respond freely to wave loading in a manner that will increase power production. The aforementioned system characteristics were investigated to enable the creation of a system that is able to achieve increased power production yet allow the system to remain on station during unfavourable conditions.

The environmental conditions for design and analysis were chosen that correspond to locations with relatively calm seas. The reason for focussing on calm seas is explored in Chapter 2. The calmer sea states correspond to lower energy density areas. These areas also have lower wave forces. These sea states typically have wave periods of eight to twelve seconds and wave heights from one to three metres. The research is mostly concerned with use of wave energy within Australian waters. Applicability to other locations can be extrapolated from the results of this research.

1.7 Research Methodology

The methodology used is to develop a case study of a floating, oscillating water column, wave energy converter. The behaviour of this wave energy converter is simulated using commercially available software (OrcaFlex and Wave Analysis MIT (WAMIT)) in sea states defined in offshore industry standards (DNV-OS-301). These simulations allow for investigation into how the characteristics of a wave energy device such as power take-off damping, stiffness, heave mass, and geometry can be used to tune the structure and oscillating water column. This tuning is aimed at increasing power take-off in moderate sea states and at increasing survivability in storms. The model used in the case study has been developed in WAMIT. This model is based on existing designs identified in the literature.

The areas of knowledge developed during the study are highlighted in Figure 1.1

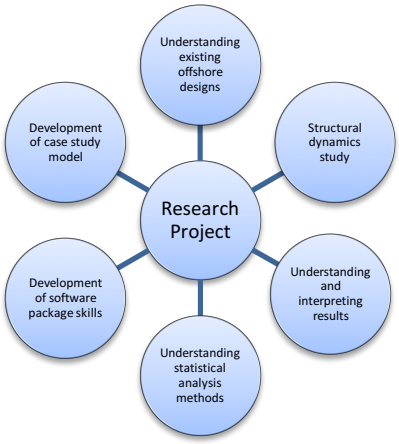

Figure 1.1: Research project constituents

Investigation of the effect of tuning mechanisms on the operation and survival of a floating, oscillating, water column, wave energy converter requires a thorough understanding of existing offshore technologies and the reasons for their implementation. The investigation also requires an advanced understanding of how power is generated by oscillating water column wave energy devices and what is likely to lead to their failure. Understanding the terminology used in the offshore oil and gas industry is a prerequisite for further study into how existing technologies can be transferred into the renewable energy sector.

A literature review of existing offshore vessels, such as oil and gas platforms, was conducted to identify possible tuning mechanisms that can be employed on a floating wave energy

converter. Such traditional offshore moored vessels serve as the basis of this investigation because this industry has been long established. Floating wind turbine platforms are also investigated to determine how traditional designs have been applied to a technology where the budget is much more constrained. Identification of the key parameters used in these industries to control the motion of the vessel during various storms provide a starting point for mechanisms likely to be used for tuning a floating, oscillating water column, wave energy device.

OrcaFlex was chosen as the commercial software package for this research. Alternatives to OrcaFlex do exist. These include packages such as Flexcom, AQUA, ARIANE, and ANSYS. OrcaFlex was chosen for a number of reasons. The reasons are that the researcher had prior experience with OrcaFlex gained during enrolment in an honours programme and the University of Wollongong has a license for OrcaFlex. The second software package chosen was WAMIT. This package was chosen because there is a precedent for using WAMIT and OrcaFlex in combination and an existing tool for importing WAMIT results to OrcaFlex.

A prerequisite for the simulations of the wave energy device in WAMIT and OrcaFlex is a thorough understanding of both software packages. This understanding is not limited to the workings of the packages but also includes an understanding of how best to create a model within the package. This understanding was developed through experience gained by running tutorial simulations and through development of simple models with existing solutions. This process served to establish the tacit knowledge required to complete this research project. Offshore dynamic simulations are often run to standards established in various guidelines. The most prominent of these guidelines are those stipulated by the DNV.

Assessment of the results obtained using OrcaFlex and WAMIT is essential in developing solutions and answering the research questions of this research. Assessment of the results was through statistical analysis of the results. Various weaknesses with this method can exist. Examples of these include applying the wrong statistical analytical method to the data or not collecting enough data to ensure adequate distribution of the results. Appropriate statistical analysis methods are defined in existing offshore design standards and statistical analysis textbooks. A statistical analysis is strengthened through an increase in data. To ensure sufficient data was available, the simulations were run according to standards defined by DNV and employed in the offshore oil and gas industry.

1.8 Implications of this Research

This research develops a new explanation of the coupled response of an open bottom, floating, oscillating water column wave energy device to calm seas and to storm seas. A better understanding of these responses allows for the ultimate goals of the study to be achieved.

The ultimate goals of this research are twofold. One component of the goal is to establish guidelines pertaining to the optimal geometry, stiffness, power take-off damping, and heave mass of a wave energy converter that is capable of allowing the device to respond to first order wave loading. Part of this goal includes determining how tuning of the structure and oscillating water column can be used to increase the power take-off of wave energy converter during lower energy sea states.

The second component is to ensure the design specifications are also able to ensure the wave energy converter is structurally sound during unfavourable environmental conditions. The second component includes how to detune the wave energy converter will ensure structural integrity during these conditions. Minimal compromise between these two objectives is ideal. This device will potentially fill the existing void of wave energy devices operating in sheltered, lower energy sea states.

Achievement of the primary goal may lead to a system that can be installed in various low energy density locations around Australia and across the world. This will allow for a device that can capture energy from smaller waves and avoid the risks that large storm swells of unsheltered areas provide. As outlined in section 1.1, there is a substantial amount of wave energy available for capture in locations around Australia. The installation of suitable motion-dependent wave energy converters has the potential to reduce Australia's dependence on non-renewable resources and the potential to lower carbon emissions. Unlike the majority of the energy currently produced in Australia and the world, motion-dependent wave energy converters will be sustainable.

The assessment of current offshore design methodology applicable to motion-dependent wave energy converters will allow for the development of new design framework. This new design framework will contain relevant design procedures and factors of safety that reflect the different functional requirements and lower risk associated with wave energy converters when compared to traditional offshore oil and gas vessels.

1.9 Arrangement of the Thesis

The summary of the thesis chapters is as follows:

A review of the current design methodologies of floating wave energy converter systems and traditional offshore vessels is undertaken in Chapter 2. Chapter 2 presents a literature review of traditional offshore floating and production systems and their applicability to floating wave energy converters. Possible optimisation techniques are discussed. The literature is critiqued and through this critique the research questions were developed.

An oscillating water column wave energy converter and methods for sizing the water column and structure are presented in Chapter 3. An oscillating water column wave energy converter is sized for waves experienced off the east coast of Australia. Wave kinematics and particle motions are presented and their importance discussed. Wave spectra used in this study are presented. These include the ISSC and JONSWAP spectra. This investigation allows an initial sizing to be made so that the device is suited to the installation location. This sizing is then used in the computer simulations.

The frequency domain analysis computer package called Wave Analysis MIT (WAMIT) is introduced in Chapter 4. The testing undertaken in the frequency domain is then presented. Previous design guidelines are assessed and improved guidelines regarding structure geometry, stiffness, and damping are developed and tested. These results were used as the intial descriptors of the device in OrcaFlex.

Implementation of the frequency domain analysis results to the time domain is undertaken in Chapter 5. This is achieved using the computer software package called OrcaFlex. Chapter 5 is primarily concerned with investigating the optimal system setup during ideal power production conditions. Testing is undertaken to determine the sensitivity of the frequency domain analysis conclusions using sinusoidal waves and wave spectra. Conclusions are drawn regarding this sensitivity. This chapter includes further design recommendations based on the wave spectra analysis. The recommendations include structure geometry, power take-off damping, and total stiffness. New design assessment tools are proposed.

Further investigation of the time domain results using OrcaFlex with DNV defined storms is undertaken in Chapter 6. This chapter is concerned with developing and testing tuning mechanisms that may allow the wave energy converter to be more robust during storm conditions. Investigation into the mooring line tensions during different 1-in-100 year storm

spectra provides a conclusion about which tuning mechanism is likely to be the most viable in a 1-in-100 year storm.

Chapter 7 presents the experimental work undertaken during this thesis. This experimental work details the models used, the experimental methodology, the results, and a discussion into the findings. These finding are compared with the numerical analysis undertaken during Chapter 4 and Chapter 5 of this thesis.

A general discussion of the results of the study is undertaken in Chapter 8. Chapter 8 answers the questions proposed in Chapter 1. In doing so, Chapter 8 presents a roadmap for the design of a tuneable oscillating water column wave energy converter. This chapter also presents evidence of the completion of the objectives outlined in section 1.4.

Chapter 9 concludes the study. It summarises the study and the implications of the research. This chapter details the original contributions made by the author to the offshore wave energy industry. Chapter 9 concludes by highlighting areas where further research will be beneficial to this field of study.

Appendix A contains background theory and information on how WAMIT produces results. Appendix B contains the operational files for WAMIT. These files were using this thesis to produce the results in Chapter 4. Appendix C provides the mathematical background to fast fourier transforms. Appendix D contains the MATLAB FFT code used to automate the FFT. This information has used in to analysis the results produced using OrcaFlex

Chapter 2 A Review of Offshore Design Methodologies

2.1 Introduction

This chapter discusses the literature regarding the areas investigated in this study. The chapter begins by presenting an overview of wave energy converters and continues by discussing the current wave energy converter design philosophy, site selection and the potential drawbacks of traditional methods of offshore oil and gas platform designs. The traditional methodology of floating offshore vessels is explored and assessed with a focus on its applicability to wave energy converters. This chapter details the method used in the offshore industry in the assessment of feasible designs and touches on software packages that can be applied to each method. A strong focus is applied to how heave plates are using the offshore industry and their applicability to wave energy converters. The chapter also presents various design wave conditions and wave conditions typically seen along the east coast of Australia.

2.2 Introduction to Wave Energy Converters

There are over 100 wave energy projects in development around the world and over 1000 patents relating to wave energy devices have been filed; Girard and Sons filed the first patent in 1799 (Day et al. 2015). To develop a context and understanding of how certain devices work and differ, a selection of existing energy converters are explored in this chapter. An extensive overview of current and past oscillating water column wave energy converters can be seen in Falcão and Henriques, 2016.

The classification of wave energy technologies is seen in Figure 2.1 (adapted from Perez and Iglesias, 2012). Wave energy converters can be broadly categorised based on their means of capturing power from wave loading (Falcão, 2010). Wave energy converters either aim to remain still and use the motion of the water to generate power or aim to use the motion of the vessel itself to generate power. This gives rise to the categories of motion-dependent and motion-independent devices (Johanning et al. 2006).

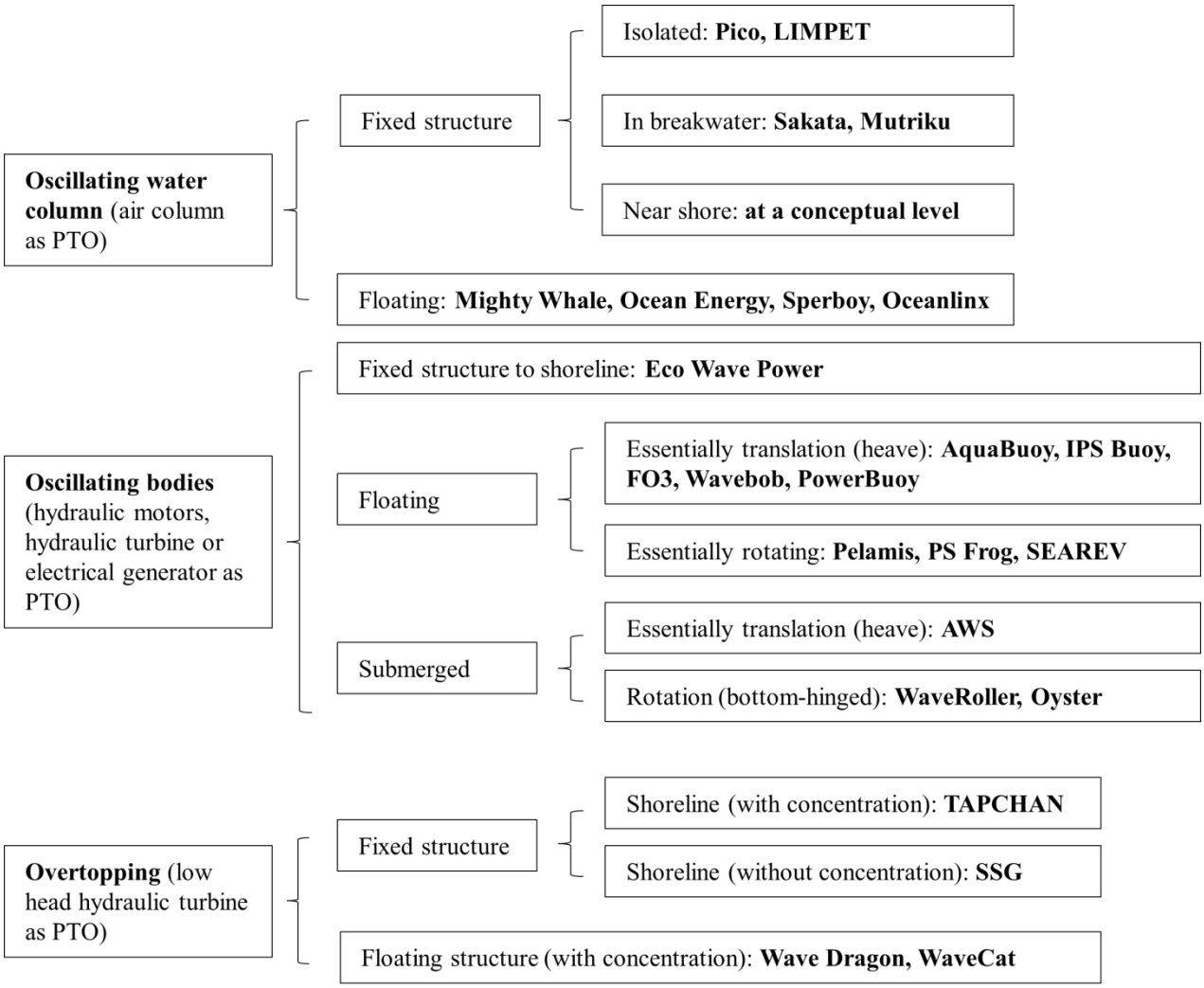

Figure 2.1: Classification of wave energy technologies (Falcao (2010)).

2.2.1 Oscillating Water Columns

The oscillating water column device, the device this present research is concerned with, operates by pushing air through a self-rectifying turbine. The device can be fixed or floating. Oscillating water column WEDs are either near shore fixed devices or moored floating devices; both operate by employing the same principles. Water is forced into the lower opening and pressurises the air in the chamber, forcing the air out of the top opening. In doing so, the air is passed through a turbine. The water is then evacuated from the chamber through the natural motion of the wave, which pulls air through the top opening and, once again, past the turbine, the movement of air drives the turbine to generate energy. The turbine which is usually employed is the Wells turbine which allows rotation in one directed despite the change in the direction of airflow (Gomes et al., 2012). The near shore devices are constructed with the base on land, extending into the ocean; an example of this is seen in Figure 2.2.

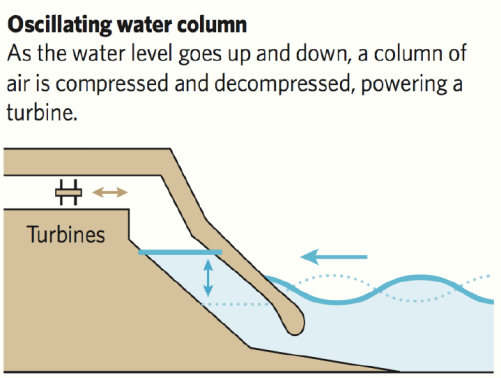

Figure 2.2: Near shore oscillating water column wave energy device (Space for News, 2012)

A shoreline oscillating water column wave energy device was installed and was providing power to the gird on the Scottish island of Islay. The Islay 500 kilowatt LIMPET (land installed marine power energy transmitter) was installed in 2000 after a 75-kilowatt prototype was built and tested in same location in 1991. The wave energy converter was downgraded to 250 kilowatts in 2007 by removing one turbine, and is now used as a grid connected testing device for further implementation of shoreline wave energy generation.

There is interest in installing offshore floating oscillating water column wave energy devices offshore because the wave energy is greater in deeper waters and because a larger number of devices can be installed in offshore regions as site selection is not limited in the same way it is for near shore devices (Wilson, 1984). Another advantage of the floating offshore

oscillating water column is the theoretical ability to tune the floating structure so resonance of the structure is achieved (Godoy-Diana and Czitrom, 2007). This will increase the length of the water column; hence allowing more air to be driven through the turbine leading to greater energy extraction (Oceanlinx, 2012). A simple schematic of the process is detailed in Figure 2.3.

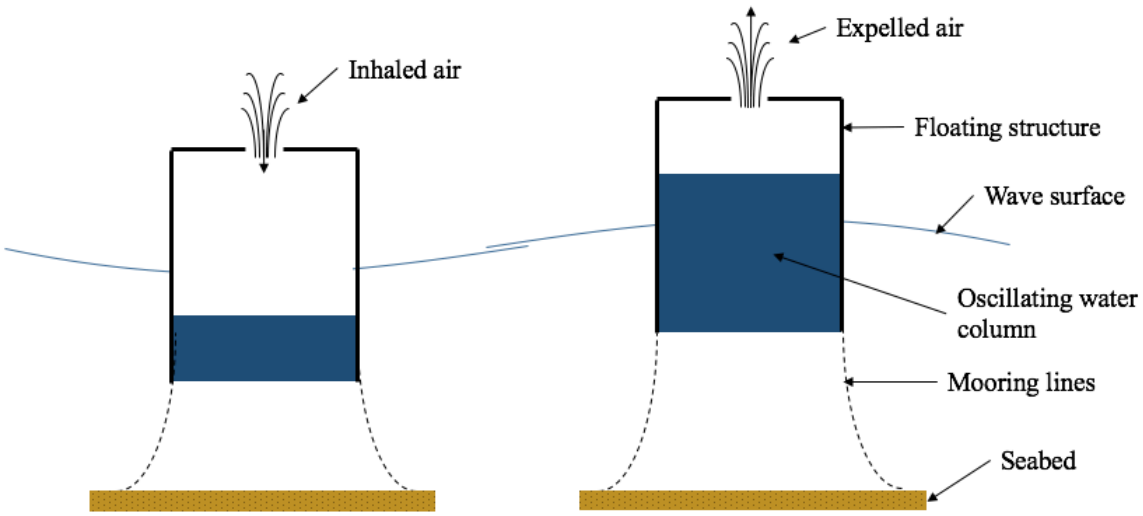

Figure 2.3: Oscillating water column schematic

2.2.2 Oscillating Bodies

Reacting bodies are sometimes also called attenuators or linear absorbers. They are generally of a size comparable to the wavelength of the incoming waves and are lined up parallel to the direction of the income wave. Attenuators are floating devices that require mooring systems that will allow them to maintain their proper alignment to the incoming wave to ensure maximum efficiency. As illustrated in Figure 2.4, the attenuator 'rides' the wave and this motion generates energy.

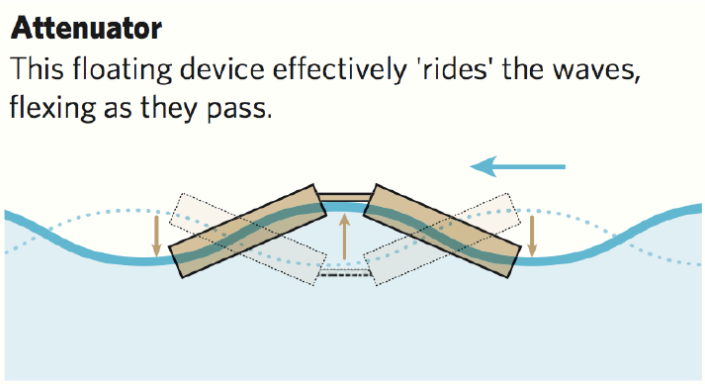

Figure 2.4: How energy is created using an attenuator (Space for News, 2012)

The most notable project utilising this technology is the Pelamis Wave Power generator. This generator is designed to withstand a 1 in 100-year storm and operate efficiently in wave heights ranging from 2 m to 30 m (Pelamis Wave Power, 2013). The first Pelamis prototype device was installed in 2004 and tested in the period up to 2007. It was located off the coast of Orkney, Scotland, it was rated at 750 kilowatts and was the world's first offshore wave energy device to supply electricity to the grid system.

After the prototype proved successful, the world's first wave energy farm was installed off the coast of Portugal in 2008. The Aguçadoura Wave Farm consisted of three 140 m Pelamis devices but the farm was discontinued due to a mechanical malfunction of three devices a few months after deployment. The project did, however, prove that wave farms could be used as a significant source of energy.

Other oscillating bodies include single-body heaving buoys and two-body heaving systems. Single-body buoys are generally reacting against a fixed point. These are generally floating or submerged point absorbers attached to the ocean floor. The CETO wave energy converter deployed off the coast of Western Australia is an example of such a device. A two-body heaving system uses the difference in motion between each body to generate power. These systems are generally used in locations where a fixed point, such as the sea floor, are not available; this is often due to depth. An example of such a system is the PowerBuoy. A 40 kW prototype was deployed off the coast of Santona in Northern Spain in September 2008.

2.2.3 Overtopping Devices

Overtopping devices require the water to move over the device to create a low hydraulic head and then flow, usually, through a turbine and back into the ocean (see Figure 2.5). Overtopping devices can be fixed or floating.

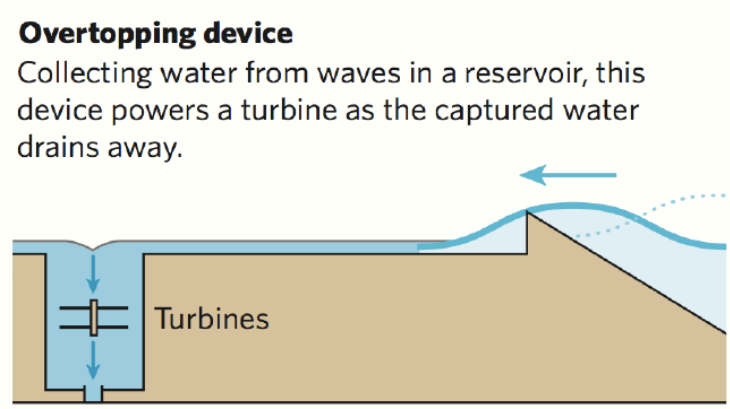

Figure 2.5: Overtopping wave energy conveter (Space for News, 2012)

A floating overtopping WED, called the Wave Dragon, began prototype testing off the coast of Denmark in 2003 and ended in 2005 with favourable results. In 2006 the 237 tonne device was moved to another site off the coast of Denmark for testing in differing conditions.

2.3 Wave Energy Design Philosophy

The first stage of the conventional approach for the design of a wave energy device is the selection of an installation site. This selection is often based on estimations of wave energy available at a number of preselected sites. Johanning et al. (2006) supports this ideology. Johanning et al. argue that wave energy converters must be installed in unsheltered high energy density locations to be economically viable. Iglesias and Carballo (2011) suggest that one of the fundamental objectives of identifying potential wave energy converter installation locations is to determine locations where wave energy is concentrated. The selected sites are then evaluated and ranked in order of the total percentage of energy that is predicted to be captured (Iglesias and Carballo, 2011). This is done in an effort to increase the profitability of the device (Harris et al., 2004).

However, Leijon (2006) states that “the large waves dictate the costs while the small and medium waves give the incomes.” With this in mind, there are two paths available for design. The device can either include large safety margins to ensure it can survive the large waves or

it can be placed in areas where the large waves are less likely to occur. Selecting large safety margins is likely to increase the total levelised cost of the wave energy device. There is little scope to increase the cost of wave energy devices because it is already higher than other alternative renewable energy sources (Astariz and Iglesias, 2015).

Bernhoff et al. (2006) have suggested that developing smaller wave energy converters and installing them in a farm type setup in calmer waters may be a feasible design option to reduce the effect of large storm swells on the levelised cost of wave energy devices. While there are areas of significant wave energy concentration around the world, large quantities of wave energy exists in calmer sea states. Examples of such seas include the Baltic Sea where the average significant wave height is approximately one metre and the peak wave period between three and five seconds (Soomere, 2014), the Beibu Gulf of China where the average significant wave height is 0.6 metres and peak wave period is 3.6 seconds (Zhou, 2015), and along the Lithuanian coast of the Baltic Sea where the average significant wave height is approximately 0.5 metres and the average peak wave period is approximately 3.25 seconds (Kasiulis, Punys, and Kofoed, 2015). Similar conditions exist along the east coast of Australia (Behrens et al. 2012) where the significant wave height is approximately 1.5 metres and the peak wave period is approximately 8 seconds (Hughes and Heap, 2010). Hughes and Heap have produced data for Australian shelf waters detailing the total wave energy available during the average year (see Figure 2.6). As discussed earlier, Australia's southern coastline has the best potential for wave energy devices if assessed purely on available energy. This is supported by the data in Figure 2.6.

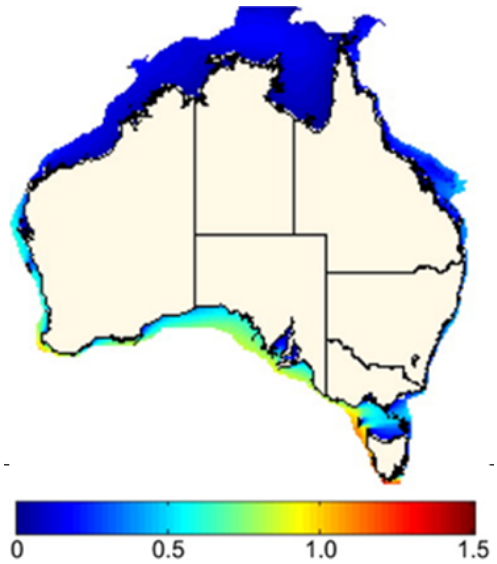

Figure 2.6: Total Wave energy delivered in an average year (TJ/m) in Australian shelf waters (Hughes and

Heap, 2010).

Inherent issues arise when the selection of location is simply a function of estimated power output. Locations with substantial wave energy are also locations with the greatest significant wave height, peak period and an increased chance of delivering conditions unfavourable to wave energy converters. Behrens et al. (2012) support this idea when looking at wave energy as a function of wave height and peak wave period around the coast of Australia. shows the 50^{th} percentile wave energy flux, significant wave height and wave peak period for the Australian coastline and near waters. For example, the southern coastline has the largest amount of energy available per metre per year but also has much larger peak wave periods (~15 seconds) and peak significant wave heights (~3 metres). The areas with the largest energy also have larger wave heights and higher peak periods. It may seem ideal to develop a wave energy converter to operate in areas of the highest energy density in an effort to achieve more produced energy; however, this design methodology increases the risk of failure of the wave energy converter due to increased wave periods and significant heights. The design methodology might be the reason for the lack of widespread wave energy converters despite the identification of substantial available energy. Despite arguing for installation in the highest energy sea state, Johanning et al., (2006) do touch on the ideology of a wave energy system that may be installed in calmer sea states. They argue an idealised resonating OWC converter will be out of phase with the incident wave allowing for the expansion and contraction of an air column. This is not possible if the vertical wave motion and device heave are identical. A resonating structure will lead to higher efficiency of the device.

Developing a wave energy converter to operate in calmer, more protected areas such as the east coast of Australia will present opportunity for more feasible designs because total cost can be reduced. Here the peak wave period lies between seven and ten seconds and the significant wave height is approximately 1.5 metres. This combination can potentially produce more cost efficient wave energy converters. Since the sea state will be calmer, an efficient wave energy converter is likely to be a motion-dependent device. Movement of the floating wave energy converter might be one way to overcome the lower energy associated with waves in calmer sea states. One possible method by which this increase in movement can be achieved is through the development of a resonating device. Again, Johanning et al. (2006) argue that a resonating device is essential in wave energy converters. Stappenbelt and Cooper (2010) have shown that through control of floating oscillating water column wave energy converters, greater energy output is possible. Stappenbelt and Cooper (2010) suggest

this control may be achieved through a stiffness increase through mooring line tensioning. Other device characteristics such as the geometry, mass, damping, and the motion of the oscillating water column, have the potential to be used to tune the device. Control of these characteristics was shown to be vital to the power output of a floating point absorber wave energy device (Beirao, 2014). Investigation is needed into how control of the system through the chosen structure geometry, stiffness, and power take-off damping can best be achieved. This will require an investigation into the design methodology of similar offshore systems. In addition, the extent to which the vessel motion can be controlled through manipulating these variables is paramount.

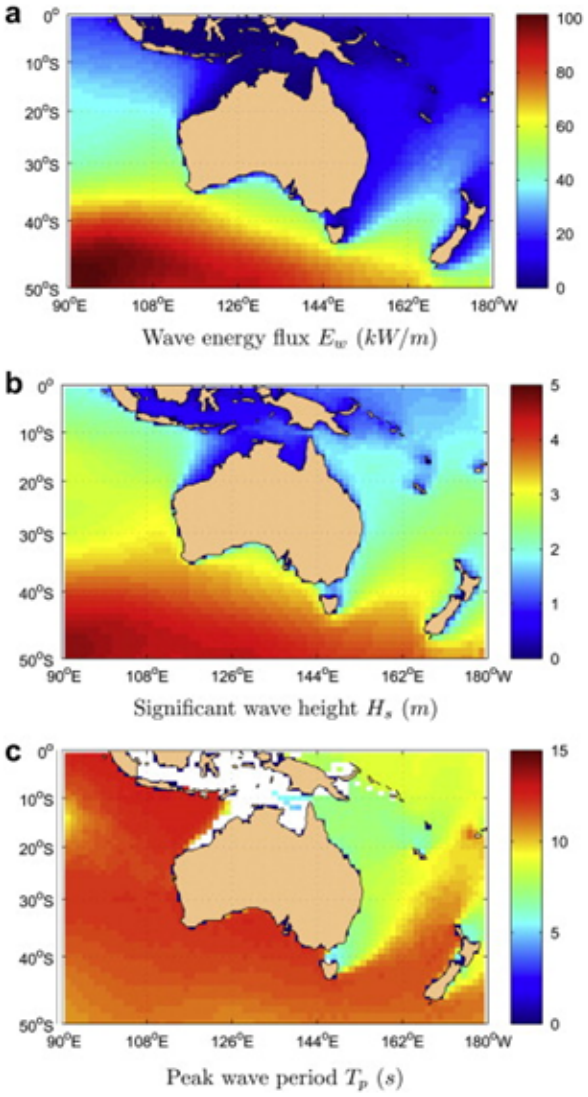

Figure 2.7: 50th percentile wave data for Australia (Behrens et al., 2012)

2.4 Existing Offshore Designs

The design methodology of traditional floating offshore oil and gas extraction vessels often serves as the starting point for the design of a floating offshore wave energy device because the oil and gas industry is already established and various design standards have already been developed. A notable influence of traditional design methodologies on novel systems is seen in Roddier et al. (2010) where the design methodologies and standards were applied to a floating platform for a wind turbine generator. Application of the design methodology often employed in the oil and gas industry is complex and intricate with each stage having an influence over the next or previous.

The traditional offshore design methodology is heavily governed by existing international standards. Det Norske Veritas (DNV) and the American Petroleum Institute (API) are the most notable producers of these design standards. As with offshore wind turbines there are no standards that explicitly apply to offshore wave energy converters. The design methodology for oil and gas platforms can be broken into two distinct stages: the design of the structure and the testing of the structure with the application of mooring lines.

The primary concern for any design process is to ensure the design meets the requirements of the system. The primary requirement of the design of a traditional offshore oil or gas vessel is to reduce movement in all degrees of freedom. This reduction in movement is done in an effort to remain on station with minimum stresses induced in the oil or gas riser. The first stage of design takes into consideration the metacentric height, centre of gravity and natural periods in heave, and pitch and roll, with the first two considerations being significantly simpler to achieve than the last. Reduction of the heave response amplitude operator (RAO) through natural period manipulation is often essential to produce a compliant system. Reduction of the heave response is often undertaken by ensuring the mass of the structure is large enough to have the natural period at least double the peak wave period at the installation site. A general ‘rule of thumb’ regarding the natural period for semi-submersibles, ship shaped FPSOs and spar buoys is seen in Table 2.1.

Table 2.1: Configuration Sizing 'Rule of Thumb' for Catenary Moored Offshore Vessels [3]

Floater Type	Criteria
Semi-submersible	Metacentric height greater than 5 metres under normal operating conditions.
	Heave period greater than 20 seconds.
Ship shaped FPSO	Provisions for process, quarters, turret and oil storage govern the configuration sizing.
Spar	Maximum heel angle 5 degrees in 100 year storm.
	Heave period ~2 times peak storm wave period.

Often smaller structures cannot have a mass large enough to ensure that its natural period falls within the DNV recommended range. Heave plates are used to overcome this smaller mass (Moreno et al., 2015). These heave plates increase the added mass and hence add to the dynamic mass of the structure. This is discussed in the next section.

The effect of the natural period on the heave RAO for different vessels is shown in Figure 2.8. This figure is used to illustrate the increased heave experienced when the forcing frequency coincides with the natural heave frequency of the vessel. This is seen in the area between 20 and 25 seconds for semi-submersible vessels where the RAO value increases from approximately 0.1 m/m to over 2.4 m/m once the frequencies are somewhat similar. Avoiding this matching of frequencies is a key design parameter for oil and gas vessels as it allows the vessel to avoid large periods of heave, increases production time and hence profits, and ensures lower forces are experienced by the mooring lines when restoring the vessel to the desired location.

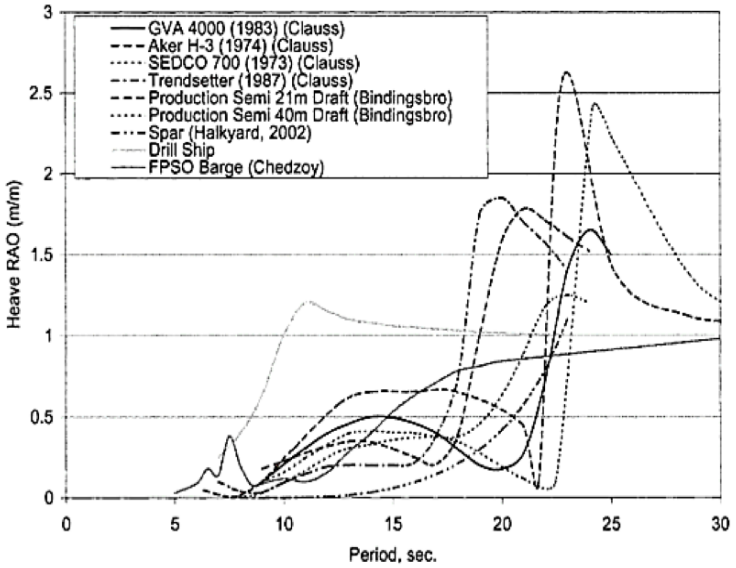

Figure 2.8: Heave RAO of Various Floaters (Chakrabarti, 2005)

Adjustment of the natural period is undertaken using a number of methods, most notably by adjusting the mass and/or stiffness of the vessel. A change in heave mass is often accomplished by adding mass through the geometrical design of the structure. A way to increase the heave mass of a floating offshore structure without increasing draft is to introduce heave plates into the system (Koh and Cho, 2011). The increase in heave mass is also often accompanied by an increase in heave damping. This method of natural period adjustment in an effort to avoid the majority of the wave energy is also employed when designing floating offshore wind turbine platforms.

The WindFloat platform has successfully used heave plates on the base of three pontoon columns to increase the natural period of the floater to more than 20 seconds. This is well outside the range of expected wave periods (Roddier et al., 2010). There is a design conflict when trying to implement this ideology into wave energy converters when considering what Johanning et al., (2006) recommend about resonance of wave energy devices for which the natural period of the device must be matched to the expected wave period to create the maximum heave motion.

The desire for the floating vessel to be minimally influenced by environmental loading is reversed when considering the production stage of motion-dependent devices such as a wave energy device. These devices rely directly on exaggerated motion to produce power (Fitzgerald and Bergdahl, 2008). An ideal motion-dependent device will respond freely to first order wave loading in a resonant fashion (Johanning, 2007). Stappenbelt and Cooper (2010) developed a mass spring damper model of an oscillating water column wave energy device. By using this model it was concluded that the system heave was a function of two natural frequencies; the oscillating water column natural frequency and the structure natural frequency. Power output peaks were seen at frequency values equal to the oscillating water column natural frequency and structure natural frequency depending on the configuration of the oscillating water column device. The largest relative area (oscillating water column plane area vs the structure water plane area) showed the largest normalized power peak at the corresponding natural frequency. The most favourable setup was when the oscillating water column area constituted 90% of the total base area when including the structure.

Stappenbelt and Cooper (2010) argue that tuning the device so that the natural frequency of either the structure or oscillating water column matches the forcing frequency can lead to greater power output of the device. This is true when there is sufficient separation between

the values of the oscillating water column natural frequency and the structure natural frequency. Various ratios were tested. A ratio of 1.5 for the oscillating water column natural frequency to the structure natural frequency showed good results when assessed from a power production viewpoint. The primary tuning mechanisms suggested is a tensioning of the mooring system to increase stiffness and the use of heave plates to minimise the structure waterplane area. Stappenbelt and Cooper (2010) did not investigate how tuning of the device can be used to withstand unfavourable conditions.

2.4.1 Natural Period Manipulation through Heave Plate Adoption

Heave plate applications in wave energy devices have been generally limited to point absorber devices installed in deep water. Here the heave plate is used to maintain tension in the power take-off line rather than tethering the device to the sea floor. Examples of this system are seen in Davis (2014) and Brown and Thomson (2015). A simple diagram of this system is seen in Figure 2.9.

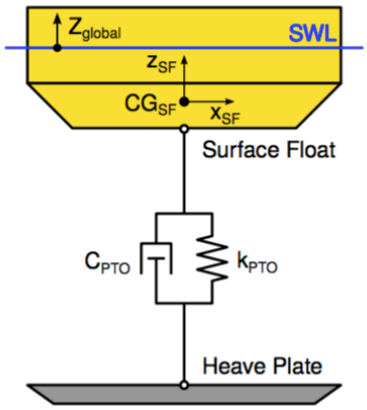

Figure 2.9: Point absorber using a heave plate to maintain tension on the power take-off line (Brown and Thomson, 2015).

Heave plates have been used in the offshore oil and gas industry since 1999 to stabilise deep-water spar platforms (Lake et al, 2000). The effect of heave plates on the added mass and damping of a submerged floating cylinder has been investigated by Koh and Cho (2011). They investigated various parameters of heave plates including the location of installation on the cylinder, the diameter of the plate, and the total depth of the floating cylinder. Koh and Cho's research is primarily concerned with application of heave plates to spar buoys in the oil and gas industry.

Koh and Cho investigated the heave plate diameter (*a*) to cylinder diameter (*b*) ratios (*a/b*) ranging from 1 to 1.8, cylinder draft (*d*) to depth ratios (*h*) of 0.1 to 0.4 (*d/h*). Both tests were conducted at a depth to cylinder diameter ratio (*b/h*) of 5.0. A simple diagram detailing these parameters is seen in Figure 2.10.

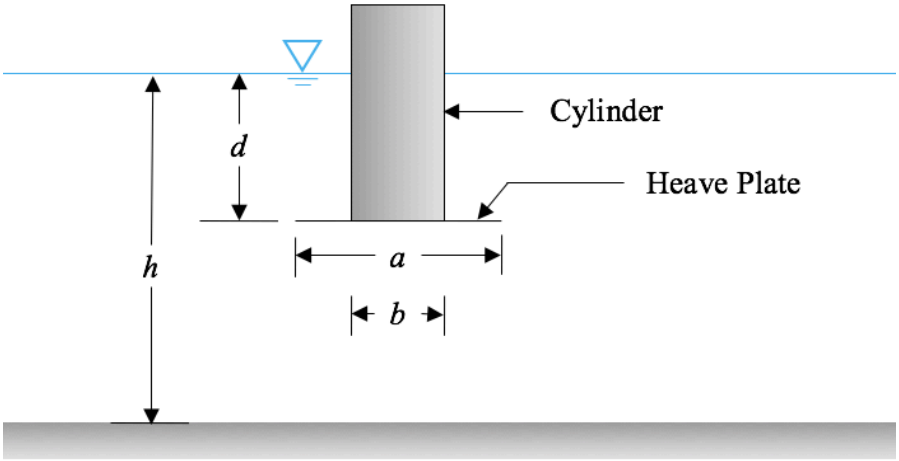

Figure 2.10: Heave plate investigation parameters (Adapted from Koh and Cho (2011))

It was determined that an increase in the heave plate diameter for a fixed cylinder diameter caused a linear increase in added mass however this was not the case with the damping increases. Damping was shown to increase at an *a/b* value of 1.8 while decreasing when *a/b* went from 1.2 to 1.4. Damping is the effect of the increased drag of the system due to the plates. This drag is related to the number and strengths of the vortices induced around the edges of the heave plates during motion (Brown and Thomson, 2015).

Increasing the depth of water (*h*) the cylinder was in (*d/h* going from 0.4 to 0.1) resulted in a larger added mass at $\omega^2 h/g < 7$ but showed a reduction in the added mass for $\omega^2 h/g < 7$ where ω is the wave angular frequency. The damping exhibited little change at values where $\omega^2 h/g < 2$ however there was a large increase where $\omega^2 h/g > 2$. It can be concluded that a shallower depth will allow the heave plate to provide a greater reduction of the cylinder RAO. Koh and Cho have stated that this is due to the heave plate being located closer to the free surface; hence, more radiation damping is created. This means that heave plates can provide a greater reduction in the RAO of the structure if they are placed closer to the surface of the water.

Koh and Cho have also shown that the frequency dependent, non-dimensional added mass of the structure can be increased up to seven times that of a cylinder without a heave plate. This increase was found with an *a/b* value of 1.8. The frequency dependent, non-dimensional damping for an *a/b* of 1.4 value increased approximately four times above the base level. It is important to note that the non-dimensional, added mass remained approximately constant when $\omega^2 h/g < 3$ before dropping when $\omega^2 h/g > 3$. The non-dimensional damping exhibited a much more pronounced peak at approximately $\omega^2 h/g = 5$ before dropping off when $3< \omega^2 h/g < 6$. The significance of this is that a large increase in added mass is attainable without the associated increase in system damping. This will allow the natural frequency of the total structure to be reduced without reducing the response amplitude operator.

Subbulakshmi et al. (2015) have investigated the effects of using numerous heave plates on the added mass and radiation damping on floating spar platforms. This was done in an effort to increase the natural period and damping of spar buoys used in the oil and gas industry. Subbulakshmi et al. (2015) have undertaken two studies; the first used a single heave plate and the second used two heave plates. The first study investigated the effect of adjusting the heave plate diameter of a heave plate attached to the keel of a buoy. Heave plate to buoy diameter ratios of 1.1, 1.2, 1.3, and 1.4 were tested. The second study investigated the effect of the location of the second heave plate on the damping and added mass. The second study used two equal heave plates with a diameter ratio of 1.3. The distance between the two heave plates was varied. The ratio of the distance between the heave plates to the heave plate diameter was used as the marker. Ratios of 0.1, 0.2, 0.3, and 0.4 were studied.

The effect of the heave plate diameter and heave plate spacing on the heave added mass and added mass coefficients of the structure is shown in Table 2.2 andTable 2.3.

Table 2.2: Heave added mass and added mass coefficient for a spar buoy with one heave plate (Subbulakshmi et al., 2015)

Diameter Ratio	Added Mass (t)	Added Mass Coefficient
1.1	14463	0.06
1.2	20469	0.084
1.3	28072	0.115
1.4	37339	0.153

Table 2.3: Heave added mass and added mass coefficient for a spar buoy with two heave plates (Subbulakshmi et al., 2015)

Relative Spacing	Added Mass (t)	Added Mass Coefficient
0.1	32269	0.132
0.2	35949	0.147
0.3	38593	0.158
0.4	39683	0.162

Subbulakshmi et al. (2015) have shown that using heave plates has the ability to increase the added mass of the structure and, hence, the natural period of the structure. They have also shown that utilising two heave plates is able to increase the added mass of the structure further. The further apart these plates are spaced the greater the increase in added mass.

The results from these studies regarding the effect of heave plates on the heave RAO of the spar are shown in Table 2.4 and Table 2.5.

Table 2.4: Heave RAO of a spar buoy with one heave plate

Diameter Ratio	Heave RAO	Reduction in Heave RAO (%)
1	3.15	-
1.1	2.45	22.2
1.2	2.2	30.2
1.3	1.7	46
1.4	1.55	50.8

Table 2.5: Heave RAO of a spar buoy with two heave plates

Relative Spacing	Heave RAO	Reduction in Heave RAO (%)
0.1	2.7	14.3
0.2	1.85	41.3
0.3	1.4	55.6
0.4	1.25	60.3

Subbulakshmi et al. (2015) have shown that utilising heave plates can reduce the RAO of a spar buoy. Increasing the heave plate diameter for a fixed cylinder diameter will further reduce the RAO of the spar buoy. It has also been shown that utilising two heave plates can reduce the heave of the structure even further. The further apart the heave plates are spaced the greater the reduction in heave RAO of the buoy. This 2015 investigation did not determine the heave RAO of the buoy as a function of the forcing frequency so it is not known if this RAO reduction is the reduction of the peak RAO value across all frequencies or if it is the peak RAO value that falls within the likely value of the forcing wave frequencies.

2.4.2 Mooring System Design

The second stage of a design for an offshore oil or gas platform is aimed at producing a vessel able to meet its functional requirements is the addition of mooring lines to vessel. Unless installed in waters less than 100 metres in depth (DNV-OS-E301, 2010), mooring lines do not often have significant influence over oil and gas platform motions other than to reduce the excursion area. However, failure of mooring lines can often lead to failure of the entire system; hence, mooring lines are key components ensuring the integrity of the system and allowing it to meet the functional requirements established at the outset.

The key design goal concerning mooring lines for oil and gas platforms is to produce a system that is able to withstand the largest load case caused by an event with a predetermined probability while still maintaining the vessel on station. It is important to note that the mooring lines are often not considered in the hydrodynamic design of the vessel. It is expected that the vessel will behave in a compliant manner before mooring lines are considered. The mooring lines serve only to reduce movement in an effort to keep the vessel in place rather than influence or control the reaction of the vessel to environmental loading.

Mooring line design is currently reflected in the design for motion dependent wave energy converters. Harris et al. (2004) argue that the primary mooring objective for a wave energy converter mooring system is much the same as the objective of the system for a floating oil or gas vessel. The primary function of mooring lines is to maintain a floating wave energy converter on station during both normal operating conditions and extreme environmental conditions. This is desirable for floating oil or gas vessels because it will protect the riser from over extension (Wang, 2012).

Harris et al. (2004) call for wave energy converter mooring lines to be considered in the initial hydrostatic design of the vessel and also during motion analysis of the wave energy converter; hence, the wave energy converter design and analysis needs to be coupled with the mooring design and analysis stage (Fitzgerald and Bergdahl, 2008). The is unlike in the oil and gas industry where the device and moorings are not a component of the hydrostatic design and are only included in the motion analysis of the floater if the mooring depth is below 100 metres (DNV-OS-E301, 2010). Typically, offshore floating wave energy converters have been placed at depths ranging from 40 to 100 metres. This design

methodology is a major point of difference between design of traditional floating offshore vessels and motion-dependent wave energy converters (Falcão, 2010).

Normal operating conditions are the environmental conditions that are present the majority of the time. In these conditions, the wave energy converter should be expected to capture the majority of the energy. The wave energy converter and associated mooring system should be designed to operate effectively in these conditions as a coupled system (Fitzgerald and Bergdahl, 2008). Rather than just designing the mooring system to withstand extreme conditions, as is done in the oil and gas industry, the extreme conditions will be determined through a statistical analysis of the site over a period. Extreme operating conditions are those specified in DNV-OS-E301 (DNV-OS-312: Certification of Tidal and Wave Energy Coverters). These extreme operating conditions are a combination of conditions during a 1-in-100 year storm. These conditions have also been used in the wind turbine industry. The 1-in-100 year conditions were used to determine the intial viability of the WindFloat wind turbine floater before optimisation of the system (Roddier et al., 2010).

The event probability is dependent on the vessel type and location. The design procedure is a deterministic approach where the line tension, vessel offset and anchor loads are evaluated for environmental conditions and hence load cases defined by a yearly return period (DNV-OS-E301, 2010).

Harris et al. (2004) suggest the functional requirements for any mooring system, including wave energy converters, are:

- To maintain the vessel within a permissible offset. The riser in oil and gas platforms often determines this. In wave energy converters, the power umbilical is probably the determining factor along with the presence of other WECs if installed in a farm type setup.
- To meet the design lifetime
- To maintain stability
- To provide positioning ability

The offshore oil and gas industry recognises two cases of environmental conditions when evaluating the mooring design for a given vessel. These are the maximum design conditions and the maximum operating conditions (API-RP-2SK, 2005). Both are integral in allowing the vessel to fulfil the requirements established in the initial design stage. Maximum design

conditions are defined as the extreme load caused by a combination of environmental forces at the desired installation location. These forces are determined by a statistical history of the site (API-RP-2SK, 2005; DNV-RP-F205, 2010). The most often investigated force combinations in the oil and gas industries for permanent moorings are:

- The 100-year waves with associated winds and currents,
- The 100-year wind with associated waves and currents and,
- The 100-year current with associated waves and wind.

It is also important to consider directional combinations of the aforementioned forces when permanent installations are being considered. Lastly, special consideration should be given to vessels, such as ship shaped vessels, that are likely to be subject to considerable slow drift motions. For structures with a design life less than 20 years, API-RP-2SK allows for considerations when determining the yearly return period for maximum design conditions. In this case, it is suggested that the return period be determined by a risk analysis that takes into account the likely consequences of mooring failure. Vessels such as wave energy converters and floating wind turbine platforms are unlikely to encounter significant slow drift motions because they are smaller than FSPOs and other oil and gas platforms (Lupton and Langley, 2014). This is not the case with offshore wave energy devices because unfavourable locations can be avoided because they are not dictated by the presence of oil or gas deposits (Bernhoff et al. 2006).

Table 2.6 illustrates the different 100-year design conditions at various locations around the world. In this table H_s is the significant wave height, T_p is the peak wave period, U_w is the 1-hour average wind speed, and U_c is the current.

This is presented to highlight the importance of considering the location of the vessel during design, as one of the limiting factors in design of floating oil and gas platforms, and to a certain extent wind turbine platforms, is the constraint of the installation location. The platforms must operate within close vicinity to the hydrocarbon deposit or in an area of high winds; hence, the environmental conditions for design are a function of location and not an input of choice during the initial stage of design. Design and analysis requires careful consideration of the environmental loading for each installation site during design and analysis. This is not the case with offshore wave energy devices because unfavourable locations can be avoided (Bernhoff et al., 2006)

Table 2.6: DNV OS E-301 100-Year Storm and 10-Year Current Guidance Values (DNV-OS-E301, 2010)

Location	**H_S (m)**	**T_P (s)**	**γ***	**U_W (1-hr. avg.) (m/s)**	**U_C (m/s)**
Norwegian Sea	16.5	17.0-19.0	2	37	0.9
Northern North Sea	15	15.5-17.5	2	40.5	1.5
North Sea	14	15.0-17.0	2	34	0.55
Gulf of Mexico (GOM)	11.9	14.2	3	41.4	1.98
West Africa (swell)	3.6-4.1	15.5-16.0	1	16	0.9-1.85
West Africa (squalls)	2.0-2.7	7.0-7.6	1	22.0-30.0	1.6
Brazil	8	13	2	35	1.6
South China Sea (non-Typhoon)	7.3	11.1	3	28.6	0.85
South China Sea (Typhoon)	13.6	15.1	3	56.3	2.05

*γ = Peak enhancement factor of the JONSWAP wave spectrum.

Conditions for the east coast of Australia are shown in Table 2.7. Comparison of the conditions in Table 2.6 with the conditions shown in Table 2.7 shows the conditions along the east coast of Australia are typically less extreme than the conditions defined by the DNV standards. This is possibly because the east coast being relatively sheltered compared to locations such as the North Sea, and Gulf of Mexico.

Table 2.7: Wave Statistics from various Australian East Coast Locations

Location	Brisbane	Byron Bay	Coffs Harbour	Crody Head	Sydney	Botany Bay	Port Kembla	Batemans Bay	Eden	Average
Data Range	1976-2009	1976-2009	1976-2009	1985-2009	1987-2009	1971-200-	1974-2009	1986-2009	1978-2009	-
Effective record (yrs)	28.5	24.3	28.5	20.7	19	34	30.6	21.2	26.6	25.93
Signifcant wave height (m)										
Mean	1.63	1.66	1.58	1.61	1.63	1.6	1.58	1.43	1.64	1.6
Median	1.47	1.5	1.43	1.46	1.46	1.43	1.43	1.3	1.52	1.44
10% exceedence	2.57	2.59	2.44	2.48	2.55	2.54	2.47	2.22	2.43	2.48
1% exceedence	4.04	3.93	3.85	3.94	4.19	4.17	3.94	3.57	3.93	3.95
Maximum	7.36	7.64	7.37	7.35	8.43	8.86	8.43	7.19	7.14	7.75
Variance	0.51	0.48	0.44	0.46	0.54	0.55	0.48	0.39	0.42	0.47
Peak wave period (s)										
Mean	9.32	9.59	9.58	9.71	9.72	9.82	9.57	9.36	9.41	9.56
Median	9.31	9.5	9.5	9.5	9.77	9.38	9.5	9.5	9.5	9.5
10% exceedence	12.14	12.2	12.2	12.2	12.5	11.98	12.23	12.2	12.2	12.21
1% exceedence	14.67	15.1	15.1	15.1	15.1	14.38	15.1	15.1	15.1	14.97
Maximum	19.17	19.7	19.79	19.79	20	23.65	19.7	19.7	19.69	20.13
Variance	4.75	4.92	4.99	5.12	5.57	5.24	5.17	5.17	5.46	5.15

2.4.3 Mooring Design Factors of Safety

DNV-OSS-312 stipulates that mooring system analysis for wave energy converters be undertaken in accordance with DNV-OS-E301 with a Consequence Class 1 rather than a Consequence Class 2 where the Consequence Classes are defined as:

> Consequence Class 1: "where mooring system failure is unlikely to lead to unacceptable consequences such as loss of life, collision with an adjacent platform, uncontrolled outflow of oil or gas, capsize or sinking."
>
> Consequence Class 2: "where mooring system failure may well lead to unacceptable consequences of these types."

This definition of the Consequence Class 1 seems suitable for wave energy converters. A possible drawback to the design methodology outlined in both DNV-OSS-312 and DNV-OS-E301 is the failure to consider the type of wave energy converter in consideration; all wave energy converters will be classified as Consequence Class 1. This enveloping categorisation does not allow for individual treatment of the different functional requirements of motion-dependent and motion-independent wave energy converters. An additional categorisation of wave energy converters that considers the key requirements of the mooring system needs to be developed. This categorisation will, ideally, present factors of safety that consider the increased motion of motion-dependent wave energy converters derived through risk analysis. This risk analysis should be individualised for each wave energy converter system as the design location conditions can be chosen by the user; unlike oil and gas vessels which are constrained by the location of the hydrocarbon deposit. Treatment of the ULS, ALS and FLS analysis by DNV-OS-E301 should be explored to assess the applicability to wave energy converters.

The primary objective of DNV and API standards is to reduce risk associated with the design. Inherently, wave energy converters are systems of lower risk when compared to traditional oil and gas platforms. Wave energy converters are usually unmanned, do not contain a riser carrying hydrocarbons and produce significantly less revenue than large-scale oil and gas vessels. Hence, from a risk perspective, designing a motion-dependent wave energy converter in accordance with both DNV-OSS-312 and DNV-OS-E301 is likely to produce a system with overcompensation in regards to safety. The assessment of the applicability of these design standards to motion-dependent wave energy converters is essential. An assessment of

both the design methods and various factors of safety stipulated in the documents is likely to produce a more relevant design methodology for motion-dependent wave energy converters.

2.4.4 Design Analysis Methods

Once the environmental conditions have been determined, mooring strength analysis and design is the next stage in design. This stage will ensure the selected mooring system is able to withstand all conditions and hence produce a system that, in combination with the vessel, is able to meet the design specifications and deliver the functional requirements established at the outset of design. Mooring line analysis is first completed with an intact mooring system and then, depending on the vessel in question, an analysis of the mooring system is undertaken with the assumption that one mooring line has failed. The strength analysis is used to predict the maximum mooring line response characteristics which include mooring line tensions, and potential vessel offset and anchor loading patterns. These characteristics will be determined by the maximum combination of significant low frequency motions, maximum low frequency motions, and significant wave frequency motions.

API-RP-2SK initially splits the strength analysis into two parts; the first being the simulation of vessel dynamics and the second being a simulation of mooring line response. The simulation of vessel dynamics is undertaken using a frequency domain approach, a time domain approach or a combination of the two. It is important to note that each method utilises certain approximations and, hence, the results of different methods may not be the same. The desired outcomes of vessel dynamic simulations have been broken down into four components by DNV-OS-301 and Mombaerts (2006):

1. Mean displacement of the vessel when acted upon by mean environmental loads.
2. Low frequency displacements in the frequency range of the natural periods in surge, sway and yaw. These forces are usually due to wind loading and second order wave loading.
3. Oscillations due to first order wave loading.
4. Vortex induced motions when dealing with deep draught structures such as spar buoys

The mooring line analysis should encompass all forms of loading on the structure, mooring lines and risers. In some applications, these forces may be simplified to allow easier calculations. As suggested in DNV-OS-E301, treatment of these forces is as follows:

a. Mooring line restoring forces must be taken into account when determining the mean displacement of the vessel.
b. Restoring forces and damping effects of the mooring lines must be considered in the low frequency response of the vessel. Determination of the damping is often difficult and is best predicted using scale and full size modelling.
c. The effect of mooring lines on wave frequency response only if the depth of mooring is below 100 metres.
d. If multiple risers are employed on the vessel the effect of these on the vessel's motion must be considered.

This mooring analysis can be summarized into the flow diagram seen in Figure 2.11.

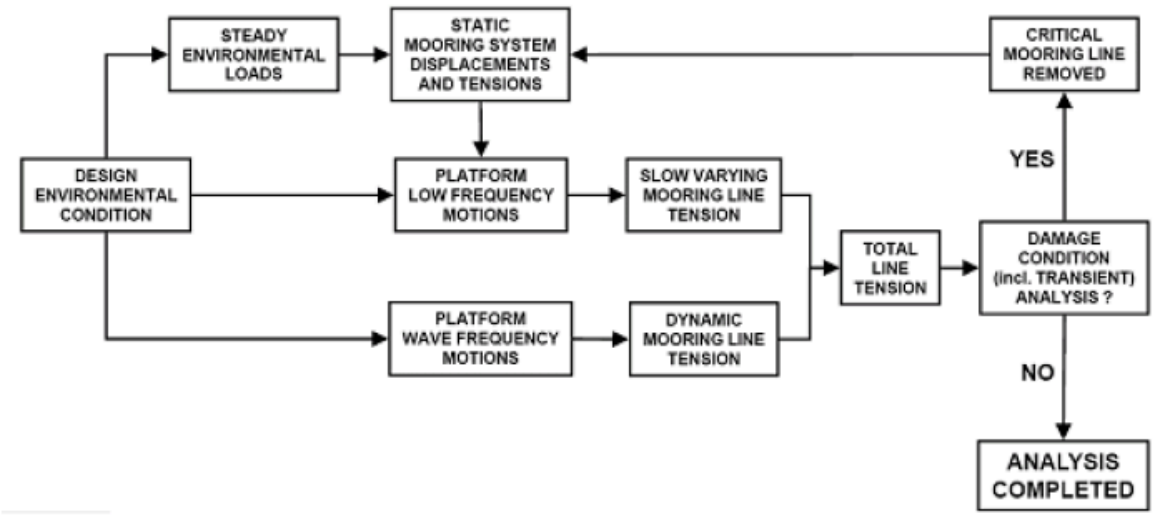

Figure 2.11: Mooring Line Analysis (Mombaerts, 2006)

Lupton and Langley (2014) have shown that slow drift motions for smaller structures, such as wind turbine pontoons and smaller wave energy converters, are much smaller than those experienced by the larger oil and gas platforms. This means that the majority of the total line tension in these smaller structures will come from the tension induced through first order wave loading.

Determination of the values governing the mooring analysis can be computed using two methods. These analyses are often conducted through a frequency domain and time domain.

A combination of these methods provides a total dynamic and static solution. These methods are considered in the next section.

2.4.5 Frequency domain approach

A frequency domain approach involves decoupling and analysing the motions separately for low, mean and wave frequency responses. Static equilibrium between the mooring line restoring force and environmental loading is used to determine the mean offset of the vessel while a combination of low and wave frequency responses is used to determine the statistically expected maximum combined vessel response. If the vessel is subject to weathervaning, the heading must be fixed at a specified angle taking into consideration low frequency yaw motions and mean equilibrium heading. The response spectrum of the platform is determined from the wave spectrum and the transfer function of the response in question (DNV-OS-E301, 2010). The platform response spectrum is as follows:

$$S_R(\omega) = |H(\omega)|^2 S(\omega) \tag{2.1}$$

Where

ω = wave frequency

H(ω) = transfer function of response in question

S(ω) = Wave spectrum

S_R(ω) = platform response spectrum

The wave spectrum is determined from a statistical analysis of the installation site. An example of this data is seen in section 3.2.2 Random Sea State Wave Spectra. The frequency domain analysis is well suited to systems exposed to statistically stationary random loads and situations where linearised analysis is able to produce satisfactory results. This stage of analysis is often undertaken in a computer simulation package such as WAMIT.

In an effort to reduce the need for scale model testing WAMIT has also been used to model oscillating water column wave energy devices in the frequency domain. Sheng et al. (2012) modelled both fixed and floating oscillating water column devices in an effort to validate the WAMIT as a means of testing. Good agreement was shown with both fixed and floating devices. Ribeiro et al. (2016) used WAMIT to investigate optimisation of a U shaped oscillating water column. Ning et al. (2015) investigated a fixed oscillating water column device using the higher order boundary element method implemented in WAMIT. Bull (2015) investigated the natural frequencies and coupling of moon pools in rigid bodies using

WAMIT. Sykes et al. (2008) showed that modelling thin walled floating oscillating water column using the higher order method in WAMIT produced favourable results when compared to the experimental results. The method of testing with WAMIT is further explained in Chapter 4.

2.4.6 Time domain approach

A time domain approach involves solving for the general equations of motion for the combined mean, low, and wave frequency motions of the vessel. This method allows a time history of the vessel motions to be developed. It is important to run the simulation based on the general equations for a sufficient amount of time so peak statistical values of the vessel response can be determined; API-RP-2SK uses a three-hour domain for time simulations which corresponds to the 57% percentile (DNV-OS-E301, 2010). An example of mooring line tension time history is seen in Figure 2.12. The method is often computationally intensive but can produce a large number of useful results. Line tension from both the low frequency and wave frequency is seen in Figure 2.12.

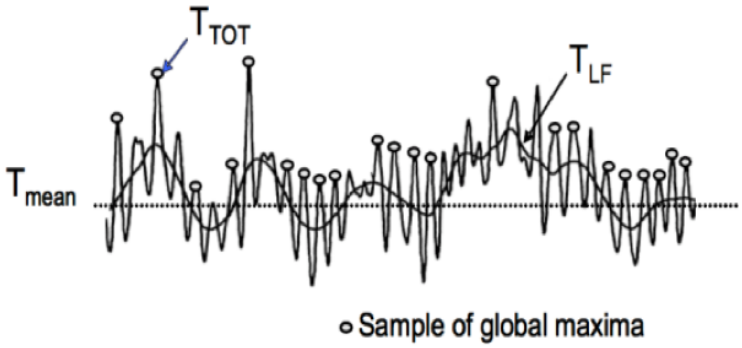

Figure 2.12: Mooring Line Tension Time History (DNV-OS-E301, 2010)

At the time of writing, two projects have utilized WAMIT and OrcaFlex when testing in the time domain. Testing in the time domain allows the sensitivity of the frequency domain results to be assessed. Rhinefrank (2010) used a combination of WAMIT and OrcaFlex to investigate the feasibly of a novel point absorber wave energy device. Rhinefrank (2011) then used OrcaFlex to investigate a 1:7 scale model of a point absorber wave energy device. This was used for a performance and mooring analysis. The approach to the time domain solution using OrcFlex is highlighted in Chapter 5.

2.4.7 Combination of frequency and time domain approach

A combination of the two aforementioned methods may be used to reduce the computational load of time domain analysis. The most often used method is to undertake a frequency domain analysis to produce the RAOs, added mass, and first order loading of the vessel. The time domain analysis is then computed to produce the low and mean vessel responses and to determine the statistical peaks through a suitable time history simulation. The results are then superimposed to determine the overall vessel response.

The simulation of mooring line responses is by quasi-static analysis and dynamic analysis. These two methods are most often used to determine the response to wave frequency environmental loadings as determination of the mean vessel offset and low frequency motions can be determined relatively accurately through static analysis.

2.5 Literature Critique

Previous attempts to determine installation locations for wave energy converters have focused on areas of the highest wave energy density (Johanning et al., 2006; Iglesias and Carballo, 2011; Harris et al., 2004). These areas are often areas of high refraction and shoaling. While these areas do contain the most energy they also often contain the largest wave forces. These large wave forces can often lead to a large increase in the capital cost of the device and hence overall levelised cost of energy. Various studies have suggested that there is a very large amount of energy in sheltered areas, including the east coast of Australia (Soomere, 2014; Zhou, 2015; Kasiulis, Punys, and Kofoed, 2015; Behrens et al., 2012). Utilising these calmer sea areas to develop electricity could significantly reduce the risks associated with areas of higher, more erratic sea states. Bernhoff et al. (2006) suggest there are potential benefits to developing a wave energy converter to operate in calm sea states. These include:

- Easier to predict wave characteristics
- Lower chance of unfavourable conditions
- Lower periods of 'down' time because of unfavourable operating conditions
- Longer periods of consistent conditions.

Developing a device that can efficiently capture the energy of calm sea sites by tuning to the conditions presents a possible method for reducing the overall cost of the system and increasing survivability. Johanning et al. 2006 have suggested that the efficiency of the device is likely to be increased if the device can respond in a resonant fashion to first order wave loading. This implies that a motion-dependent device is likely to be most suitable to calmer sea conditions in sheltered seas. One such device is the floating oscillating water column device.

Previous studies suggesting a resonant response is necessary to achieve efficiency have not considered the coupled dynamics of floating oscillating water column devices. It has been shown by Stappenbelt and Cooper (2010) that the structure and oscillating water column exhibit coupled, and potentially out of phase behaviour. Identifying the optimal phase difference between the oscillating water column, the structure, and the wave is likely to lead to a greater understanding of what is needed to obtain efficiency in such a system.

Motion dependent devices, such as oscillating water column devices do not have the same objectives as traditional platforms or wind turbine platforms during optimal power production conditions. The wave energy converter system needs to experience increased motion and in the case of oscillating water column wave energy converters they need an increase in heave motion due to wave loading. This increase in heave motion is intended to create a larger velocity differential between the structure and oscillating water column. For wave energy converters, the guidelines employed in the oil and gas industry need to be rethought. The natural periods of the oscillating water column devices need to be closer to the periods of the forcing waves during times when the forcing waves are optimal.

Floating motion-independent devices, such as an overtopping device like the Wave Dragon device, reflect the functional objectives of traditional offshore oil and gas vessels when considering hydrostatic analyses during unfavourable sea conditions. In unfavourable sea conditions the primary object of both vessels is to bypass as much wave energy as possible and so allow the device to experience minimal motion. Therefore, the existing design methodology and industry standards employed in the oil and gas industry can be applied to these devices when survivability is the paramount requirement. During unfavourable wave conditions, measures taken by these industries would be well placed in the wave energy converter industry. The measures primarily include manipulation of the natural period through initial sizing considerations and heave plates to avoid the most common wave periods.

Developing a wave energy converter that is able to act like a traditional oil and gas platform during unfavourable conditions and still experience an increase in first order loading during favourable conditions is likely to be able to operate efficiently in calmer sea states such as those found off the east coast of Australia.

A combination of the work by Koh and Cho (2011) and Subbulakshmi et al. (2015) regarding heave plate additions to spar buoys, and the work done by Stappenbelt and Cooper (2010) regarding optimal ratios of the structure's natural period to the oscillating water column natural period suggests a possible tuning mechanism for oscillating water column wave energy converters. If the system is setup in such a way that the water column has a natural period that falls within a region of low damping for the structure, an increase in power output can be obtained. This is possible because the structure and water column moving out of phase will produce more power but is reliant on the structure being able to oscillate. Koh and Cho

(2011) showed that the utilisation of heave plates is able to increase the added mass of the structure without a large increase in the viscous damping which is likely to reduce the heave RAO of the structure. The heave plate diameter must be kept to between 1.2 and 1.4 times the diameter of the structure for this to occur. If this size of heave plate does not provide a sufficient increase in the added mass of the structure then Subbulakshmi et al. (2015) showed that using two heave plates can further increase the added mass.

In the oil and gas industry, ensuring the integrity of the mooring system will result in a vessel that is able to remain on station, hence increasing production time and profits, while also posing minimal risk to the surrounding environment. Mooring system design standards currently only consider the mooring system with the fundamental aim of survivability, assessment of the ultimate limit state (ULS), accidental limit state (ALS) and fatigue limit state (FLS). It is assumed that if the mooring system can remain viable during extreme conditions it can maintain the station during normal operating conditions (DNV-OS-E301, 2010). As explained, this system is not ideal for a motion-dependent wave energy converter because the mooring lines can affect the structural dynamics through an addition of weight and damping. Therefore, mooring lines should be considered in the design of the system as a whole (Fitzgerald and Bergdahl, 2008).

In summary, the literature suggests that traditional wave energy design methodology has called for placing a robust device in sea states with significant energy densities. These wave energy converters have been designed in accordance with established oil and gas industry standards despite different functional objectives. There is evidence that designing a motion-dependent device for calmer sea states can produce efficient systems with lower probability of encountering unfavourable environmental conditions. Hence, with careful design an efficient system with relatively low risk appears feasible. This present research is aimed at developing a design framework through investigating the dynamics of a motion-dependent wave energy converter that can operate properly This study focuses on the structural dynamics of a floating oscillating water column device in regular and random sea states and identifies the optimal arrangements for a floating oscillating water column device with regards to power production and device safety.

2.6 Chapter Summary

This chapter has introduced the general concept of wave energy converters as a renewable energy system. A number of devices have been presented and categorised. The traditional wave energy installation location method has been presented and critiqued. The literature suggests that there are sheltered areas of significant wave energy that do not contain the larger sea states seen in unsheltered areas of higher energy density. The east coast of Australia is one such area. Here the average wave height is between one and two metres and the average wave period is approximately eight to ten seconds. These values were used as the starting point for the design and analysis in this present study.

Chapter 2 has made it evident that existing wave energy converter design recommendations have placed too much emphasis on traditional offshore oil and gas mooring design. This is highlighted by DNV-OS-E301 and DNV-OSS-312 recommendations for analysis and design. A rethinking of the design methodology and its applicability to motion-dependent wave energy converters is required. This is because the functional requirements of a motion-dependent wave energy converter vessel and mooring system and traditional offshore oil and gas vessels are different. Previous attempts to define applicable system requirements have been recorded in the literature; however, these requirements rely too heavily on traditional design methodology.

Evidence has been provided that suggests that it may be feasible to design a motion dependent oscillating water column wave energy device that can be installed in areas of lower energy density. This device has the potential to be tuned to increase power output in calmer sea states. There is also evidence that such a device can be tuned to withstand any unfavourable conditions. Various tuning mechanisms have been suggested. These include changing the heave mass, mooring line stiffness, and power take-off damping.

Lastly, this chapter considered the current analysis methods employed in the offshore industry. These methods usually consist of a combination of frequency domain testing using WAMIT and time domain testing using OrcaFlex.

Chapter 3 Ocean Waves and a Theoretical Development of an OWC Device

3.1 Introduction

This chapter presents relevant theory regarding oscillating water column wave energy converters and ocean wave theory about pressure, kinematics, and wave spectra. In this chapter the relationships that are used to determine the optimal and practical sizes of the oscillating water column and the wave energy converter are developed and presented. An oscillating water column and accompanying device is sized for an eight second wave. This wave is typical of the wave conditions along the sheltered east coast of Australia. This sizing will be utilised for testing with WAMIT and OrcaFlex in the following chapters. This present chapter discusses the theory required to develop and appropriately test an oscillating water column device and fills a gap identified in the literature review. The theory basis of the theory presented here is often seen in textbooks covering the topic. It has been presented to provide context to the conclusions drawn in relation to an oscillating water column wave energy device.

3.2 Wave Theory

3.2.1 Pressure and Kinematics

The horizontal *u*, and vertical *w*, components of orbital velocity of a water particle in an ocean wave can be determined from the velocity potential:

$$u = \frac{\partial \phi}{\partial x} \tag{3.1}$$

$$w = \frac{\partial \phi}{\partial z} \tag{3.2}$$

The velocity potential satisfies the Laplace equation:

$$\frac{\partial^2 \phi}{\partial x} + \frac{\partial^2 \phi}{\partial z^2} = 0 \tag{3.3}$$

Applying the kinematic boundary conditions at the free surface and seabed gives:

$$\phi = \frac{\omega}{k} a \frac{\cosh k(z+d)}{\sinh kd} \sin(kx - \omega t) \tag{3.4}$$

Where ω is the wave angular frequency, k is the wave number, d is the water depth, t is the time, x is the horizontal displacement, z vertical displacement, and a is the wave amplitude.

Partial differentiation of equation 3.1 and equation 3.2 produce the following relationships for the horizontal and vertical components of the water particle orbital velocity:

$$u = \frac{\pi H}{T} \frac{\cosh k(z+d)}{\cosh kd} \cos(kx - \omega t) \tag{3.5}$$

$$w = \frac{\pi H}{T} \frac{\sinh k(z+d)}{\cosh kd} \sin(kx - \omega t) \tag{3.6}$$

where H is the wave height, and T is the wave period.

The horizontal acceleration (a_x) of the particles can be determined through the following relationship:

$$a_x = u\frac{\partial u}{\partial x} + w\frac{\partial u}{\partial z} + \frac{\partial u}{\partial t} \tag{3.7}$$

The first two terms of the acceleration are known as the convective acceleration and the third term is the local acceleration. The convective acceleration is the acceleration of the particles due to a change in the position of the fluid within a fluid flow while the local acceleration is the acceleration of the particle with respect to time. The convective acceleration is mostly influenced by wave face steepness and is the same magnitude as the wave face steepness squared while the local acceleration is the same magnitude as the wave face steepness. Because of the nature of a small amplitude wave, the wave face steepness is often very small. Hence, the convective accelerations of the water particle are small enough to be negligible in the calculation of the acceleration of the water particle. Ignoring the convective acceleration produces the equation of the acceleration in the horizontal direction a_x, and in the vertical direction a_z:

$$a_x = \frac{2\pi^2 H}{T^2} \frac{\cosh k(z+d)}{\cosh kd} \sin(kx - \omega t) \tag{3.8}$$

$$a_z = -\frac{2\pi^2 H}{T^2} \frac{\cosh k(z+d)}{\cosh kd} \cos(kx - \omega t) \tag{3.9}$$

The next stage of analysis is determining the size of the water particle orbit about the centre point of the orbit. This is obtained by integrating the particle velocities with respect to time.

The horizontal displacement, ζ, and vertical displacement ε, of the water particle as a function of time is equal to:

$$\zeta = -\frac{H}{2}\frac{\cosh k(z+d)}{\sinh kd}\sin(kx-\omega t) \tag{3.10}$$

$$\varepsilon = \frac{H}{2}\frac{\sinh k(z+d)}{\sinh kd}\cos(kx-\omega t) \tag{3.11}$$

Investigating the orbital shapes in different water depths produces interesting results. As the water depth decreases (as *z* approaches *d*) the vertical displacement of the particles drops to zero as the denominator of equation 3.9 becomes increasingly large. The horizontal component does not change. This means that in shallow water waves, the orbits are more elliptical (with longer horizontal axes than vertical axes) than in the deep water waves. In turn it means that there is less vertical motion in shallow water waves than in deep water waves. This phenomenon may be critical in the choice of the location for a floating oscillating water column wave energy device because less vertical motion of the water column is likely to produce less power. Investigating the particle orbits in deep water show that as the depth is increased the particles remain circular but reduce in orbital radius. These orbits, as a function of depth in deep water and shallow water, are shown in Figure 3.1.

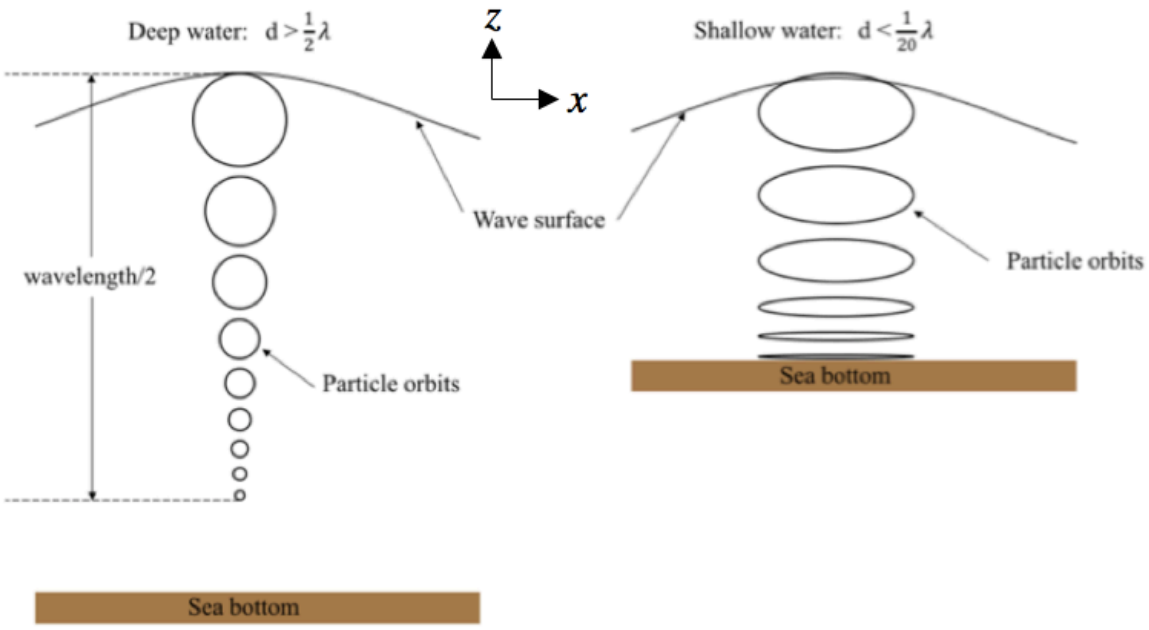

Figure 3.1: Deep and shallow water particle orbits

The orbital radius is practically zero when z = λ/2 in deep water. This depth may be considered the maximum practical length of a water column used in a floating wave energy device. Ideally the draft would be no larger than one quarter of the wavelength. At this depth (depth equal to λ/2) there is unlikely to be enough energy to allow the significant heave of a water column. Shallow water waves are also unlikely to be a targeted for oscillating water column wave energy devices.

This present analysis has determined key characteristics of the installation location using standard formula to identify wave length properties for an eight second wave. The water depth must be large enough to deem the waves as deep water waves and the wave length must be sufficient so that the draft of the water column does not have to exceed λ/2 in an effort to match the natural period of the water column with the ocean wave period. The maximum recommended draft for a structure tuned to an eight second wave in deep water is approximately 50 metres.

3.2.2 Estimating Wave Energy

For a sinusoidal waveform on which linear theory is based, the total energy per wavelength per metre can be expressed as:

$$E = \frac{1}{2}\rho g {A_m}^2 \text{ or } \frac{1}{8}\rho g H^2 \tag{3.12}$$

where

H = $2A_m$ for a sinusoidal wave where A_m is the mean wave amplitude (m)

E = Time-average energy per unit horizontal area (J/m^2)

ρ = Fluid density (kg/m^3)

Measuring the height of a particular ocean wave is difficult because it is composed of a large number of smaller waves. To overcome this, a few assumptions must be made. The significant wave height is equal to:

$$H_s = 4\sqrt{\sigma} \tag{3.13}$$

where σ is the variance in wave height in a random sequence.

Given that for a sinusoid waveform:

$$\sigma = \frac{1}{2}{A_m}^2 = \frac{1}{8}H^2 \tag{3.14}$$

this leads to:

$$H = \frac{H_s\sqrt{2}}{2} \tag{3.15}$$

Substituting equation 3.19 into equation 3.16, an equation can be developed for the energy of waves as a function of significant height per square metre:

$$E = \frac{1}{16}\rho g H_s^2 \quad \text{J/m}^2 \tag{3.16}$$

The product of the energy and wave group velocity then defines the wave power, P, per metr of wave crest:

$$P = EC_g = \frac{1}{32}\rho g H_s^2 \cdot \left[\frac{g}{k}\tanh kd\right]^{1/2} \cdot \left[1 + \frac{2kd}{\sinh(2kd)}\right] \text{ W/m} \tag{3.17}$$

where L is the wavelength and d is the water depth, and $k = \frac{2\pi}{L}$

In most data collection techniques, the period of the wave is usually collected rather than the wavelength, because the value of *k* is difficult to determine. A dispersion relationship for linear waveforms can be used to determine the value for *kd*. It is accurate to 0.1% for deep water scenarios (Hughes and Heap, 2010):

$$(kd)^2 = y^2 + y(1 + 0.666y + 0.355y^2 + 0.161y^3 + 0.0632y^4 + 0.0218y^5 + 0.00654y^6)^{-1} \tag{3.18}$$

where y = $\frac{\omega^2 d}{g}$

It is also possible to determine the wavelength and period through a Fast Fourier Transform of the measurement of the wave heights.

3.2.3 Random Sea State Wave Spectra

Various mathematical expressions of spectra exist that aim to provide a mathematical function that can describe the motion of the sea. As the sea is irregular, through Fourier transformations it can be broken down into the sum of an infinite number of cosine curves, each having a different wave height and period. This is where the definitions of peak frequency and significant wave height are established (Chakrabarti, 2005).

Peak Frequency: The frequencies at which the most number of individual cosine waves propagate. Peak frequency is usually noted as f_p and is proportional to the inverse of the peak period, T_P.

Significant Wave Height: Four times the standard deviation of the surface elevation. Significant wave height is usually notated as H_s.

A number of wave spectra have been developed and typically take the form:

$$S^{+}(\omega) = \frac{A}{\omega^5} e^{-B/\omega^4} \tag{3.19}$$

where:

A and B are constants

ω = the limiting frequency in rad/sec

The limiting frequency is a function of wind speed: $\omega \approx g/U_{wind}$

The wave spectra used for analysis in this is the Bretschneider spectrum (known in OrcaFlex as the ISSC spectrum) and the JONSWAP spectrum. The ISSC spectrum is suitable for use when modelling the waves along the southern and eastern coastline of Australia as the assumptions of the spectra are met. These assumptions include:

- Near unlimited Fetch
- Fully developed or developing seas
- Deep water

The JONSWAP spectrum is more suited to areas of limited fetch, such as the North Sea, and for storm swell conditions.

The ISSC spectrum is expressed mathematically as

$$S^{+}(\omega) = \frac{1.25}{4}\frac{\omega_m^4}{\omega^5}\left(H_{1/3}\right)^2 e^{-1.25(\omega_m/\omega)^4} \tag{3.20}$$

where: ω_m = Modal frequency =$0.4\sqrt{g/H_s}$

A standard ISSC spectral density curve with varying peak frequencies are shown in Figure 3.2. All the curves have a significant wave height of 1 metre but have peak wave periods of 8 seconds, 12 seconds, and 20 seconds.

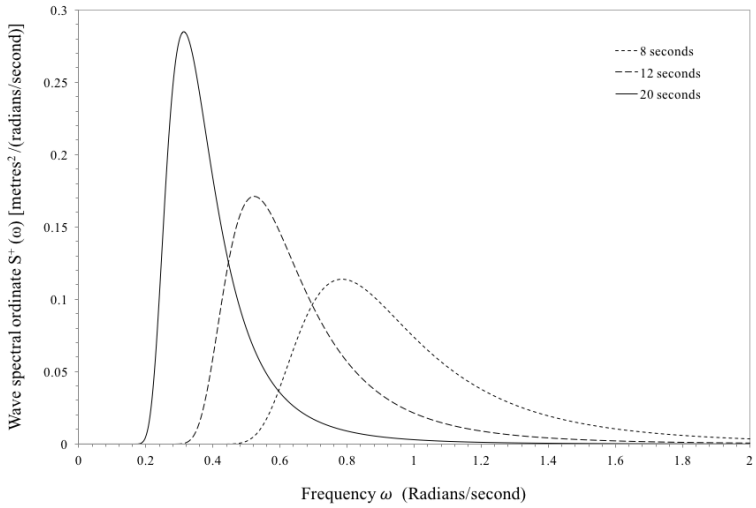

Figure 3.2: ISSC Wave spectra with varying peak wave periods

The JONSWAP (Joint North Sea Wave Project) wave spectrum was defined from empirical data and is meant to be used for sea states with limited fetch. The spectrum describes waves that are not fully developed. It is often used to describe storm swells around the world and is used in the DNV standards to describe the 100-years storms. It is expressed mathematically as:

$$S(\omega) = \frac{\alpha g^2}{\omega^5} e^{-1.25(\omega_p/\omega)^4} \gamma^a \tag{3.21}$$

where:

- $\alpha = e^{\left[-\frac{(\omega-\omega_p)^2}{2\omega_p^2\sigma^2}\right]}$
- $\sigma = \begin{cases} 0.07 \text{ if } \omega \leq \omega_p \\ 0.09 \text{ if } \omega > \omega_p \end{cases}$

- a is a constant dependent on the wind speed and fetch length. It typically falls between 0.0081 and 0.01
- ω = wave frequency
- ω_p = peak wave frequency
- γ = peak enhancement factor

A standard JONSWAP spectral density curve with varying peak frequencies is shown in Figure 3.3. The curves have a significant wave height of 1 metre and peak wave periods of 8 seconds, 12 seconds, and 20 seconds. All spectra have a peak enhancement factor of one and an *a* value equal to 0.0081.

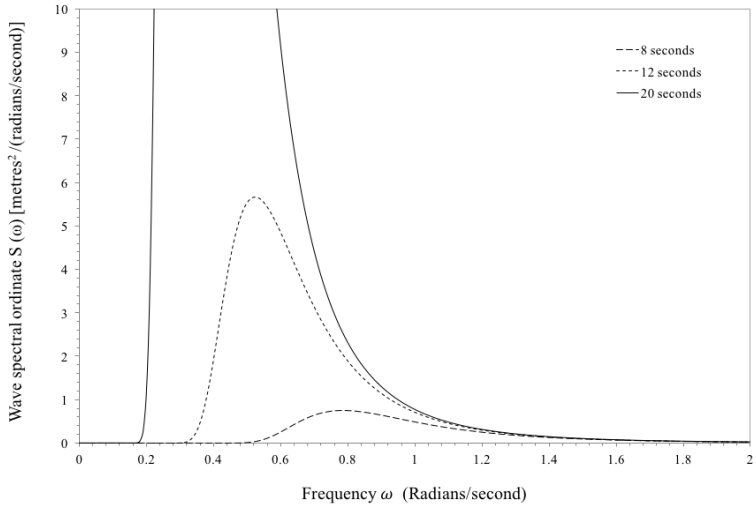

Figure 3.3: JONSWAP spectra with varying peak wave periods

Plotting a spectrum for a given significant wave height and peak frequency allows the total energy of the random sea state to be calculated. The area under the spectral density curve is equal to the power of the wave. The area is equal to the integral of the spectrum from negative infinity to positive infinity.

$$\int_{-\infty}^{\infty} S^{+}(\omega) = \text{Wave power (J/m}^2\text{)} \tag{3.22}$$

Generating a random wave

In the ocean, the wave energy converter will be subjected to an irregular wave rather than regular sinusoidal waves. The irregular sea state can be reduced to the sum of a number of

regular sinusoidal waves. Through superposition, the varying wave heights, frequencies and propagation directions can be added to produce one ocean state. This analysis will be limited to a two-directional wave; hence, propagation will be unidirectional for all wave components. This means that the surface elevation may be expressed as:

$$\zeta(x,t) = \sum_{n=1}^{N} A_n \sin(\omega t - k_n x + \varepsilon_n) \tag{3.23}$$

where A_n, k_n, ω and ε_n are the wave amplitude, wave number, wave frequency and wave phase angle for each wave component. The wave amplitude for each component can be expressed as:

$$\frac{1}{2}{A_n}^2 = S(\omega_n)\Delta\omega \tag{3.24}$$

where $S(\omega_n)$ is the wave spectrum best suited to the location of choice. This is graphically represented in Figure 3.4. This shows the ten wave components and the final irregular ocean wave constructed through superposition.

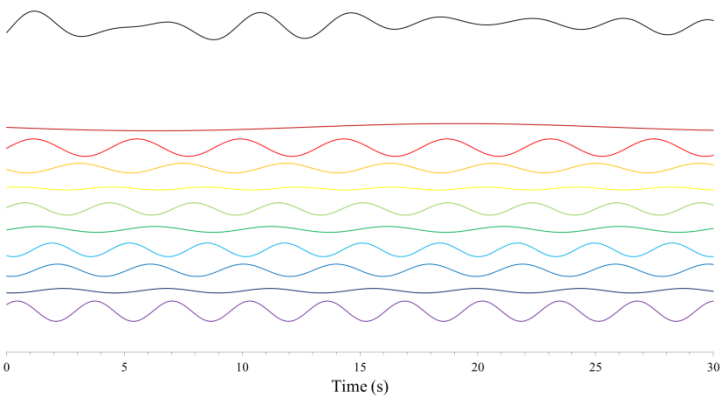

Figure 3.4: Construction of a random sea state from ten regular sinusoidal waves.

3.3 Water Column Sizing

The main parameters for a floating oscillating water column wave energy device are: surface area of the column and depth of the water column. Investigation into these parameters is undertaken in this section.

Stappenbelt and Cooper (2010) have provided a guideline for sizing the structure relative to the water column. They concluded that the water column natural frequency should match the frequency of the surrounding waves. Evans and Porter (1995) has provided a basic relationship between the water column draft and the water column natural frequency:

$$\omega_n = \sqrt{\frac{g}{D}} \tag{3.25}$$

where ω_n is the water column natural frequency in rad/sec, g is the acceleration due to gravity, and D is the water column draft or duct length in a bent duct device.

Veer and Thorlen (2008) built upon the work of Evans and Porter (1995) to include the effect of a larger water column surface area on the natural frequency. They found that an increase in water column surface area led to a non-negligible increase in added mass. This added mass caused a decrease in the natural frequency of the water column because of a non-physical increase in draft. They further deduced that the natural angular frequency of the water column could be expressed as:

$$\omega_n = \sqrt{\frac{g}{D + D_a}} \tag{3.26}$$

where D_a is the additional draft caused by the added mass of the water column. This draft can be thought of in the same manner as added mass. It is not real but the system behaves as if it were. Fukuda (1977) had previously shown that this additional draft is proportional to the surface area of the water column:

$$\mathrm{D_a} = 0.41\sqrt{\mathrm{S}} \tag{3.27}$$

where S is the water column surface area. Combining equation 3.24 with equation 3.25 yields an expression for the natural angular frequency for an oscillating water column in rad/sec.

$$\omega_n = \sqrt{\frac{g}{D + 0.41\sqrt{S}}} \tag{3.28}$$

Expressing equation 3.26 in terms of the period gives:

$$T_n = 2\pi\sqrt{\frac{D + 0.41\sqrt{S}}{g}} \tag{3.29}$$

Equation 3.27 can be used to size the water column if the target period is known. Average wave periods of sea states are easily found.

3.3.1 Water Column Sizing – A Numerical Investigation

Sizing the water column is the first step to sizing an oscillating water column wave energy device. This step is performed with the assumption that there is no physical limitation placed on device size by available device components. As Stappenbelt and Cooper (2010) have outlined, a good starting point for designing a water column natural period should be that it will match that of the forcing wave. The natural period is a function of both the surface area and draft of the water column. Investigation of the relative magnitudes of draft and surface area shows that the contribution of the added mass to the water column natural period is significant at lower draft values. This significance is further increased as the water column surface area is increased. This is seen in Figure 3.5, which is produced by plotting the draft divided by the sum of the draft and square root of the surface area for fixed OWC diameters against different draft values.

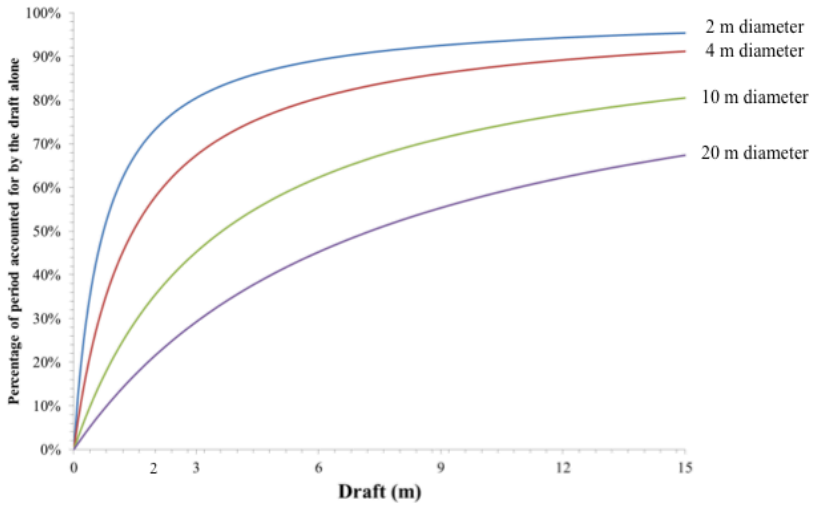

Figure 3.5: Percentage of the water column natural period accounted for by the draft alone

Figure 3.5 shows that as the draft increases for a fixed oscillating water column surface, the increase in the water column natural period increases at a diminishing rate. Limiting the draft

range from 2 to 15 metres, the draft can account for approximately 95% of the value of the water column natural period. The remaining 5% is accounted for by the surface area of the water column. Increasing the diameter of the water column will increase the natural period of the structure. A ten metre water column diameter leads to a large reduction in the contribution of the draft to the natural period when compared to a one metre water column diameter; at a 15 metre draft the value of the percent of the natural period that is accounted for by the draft alone is approximately 67% compared to 95%. This characteristic of oscillating water columns must be accounted for during design of wave energy converter, especially if altering the draft of the structure in an attempt to alter the natural period of the water column is a goal.

Veer and Throlen (2008) have shown that the effect of the added mass caused by the increase in surface area can have a significant effect on the natural period of a fixed oscillating water column and so it is important to consider both the draft and the surface area when sizing a column. Figure 3.6 has been developed to overcome dealing with two unknown quantities.

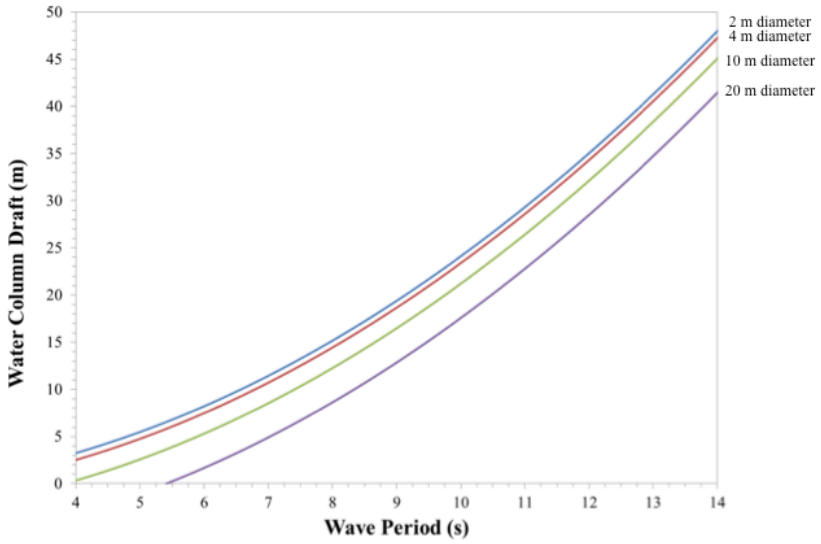

Figure 3.6: Approximate required water column draft for a given wave period and water column radius.

Figure 3.6 plots the water column draft against the natural period of the water column for various water column diameters. The required draft for the water column can be determined by first selecting an approximate radius for the water column, then the target natural period is selected; these two inputs determine the water column draft.

For example, a water column with a 10 metre diameter that will be placed in a location with a peak wave period of eight seconds will require a draft of approximately 12.3 metres (see equation 3.29.

$$D = g\left(\frac{T_n}{2\pi}\right)^2 - 0.41\sqrt{S} \tag{3.30}$$

$$D = 9.81\left(\frac{8}{2\pi}\right)^2 - 0.41\sqrt{25\pi} = 12.3m \tag{3.31}$$

While a water column with a 10 metre diameter that will be placed in a location with a peak wave period of twelve seconds will require a draft of approximately 32.1 metres (seen in equation 3.30.

$$D = 9.81\left(\frac{12}{2\pi}\right)^2 - 0.41\sqrt{25\pi} = 32.1m \tag{3.32}$$

The natural period of the water column is proportional to the square of the draft. This means that there must be some consideration of the practicalities of constructing a large structure when selecting installation sites. Using the above examples, selecting a location with a peak wave period of approximately eight seconds will result in a structure needing a significantly smaller draft than the same structure placed in a location with a twelve second peak wave period. In addition, using the conclusions from Sheng et al. (2012), a smaller target wave period will result in more power capture and greater energy conversion efficiency. This consideration will place a limit on installation locations around the world. Sheng et al. (2012) also highlight the limitations place on the maximum size of the oscillating water column. Too large a water column relative to the wave length of the ocean waves and the free surface of the oscillating water column will mean that the surface of the water column will be susceptible to sloshing. A that the work done by Veer and Thorlen (2008) and Fukuda (1977) and that was applied to fixed structures by Sheng et al. (2012) is applicable regardless of whether the surrounding structure is fixed or not.

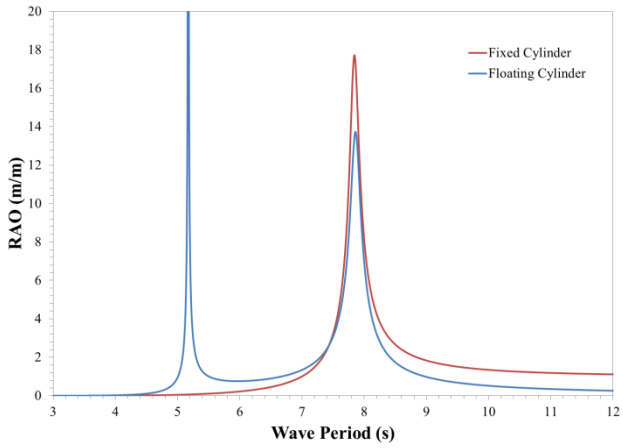

Figure 3.7: Water Column RAO for a fixed and floating structure

3.4 Structure Sizing

The size of the vessel will dictate the size of the oscillating water column. The heavier the vessel the greater the draft of the oscillating water column. The size of the structure also dictates the surface area of the oscillating water column, hence care must be taken to ensure the size and dimensions of the structure impact favourably on the dynamics of the both the structure and oscillating water column.

Stappenbelt and Cooper (2010) have studied the optimal sizing of the structure to accommodate the required water column. They concluded that a separation of the water column and structure natural frequencies would lead to a larger power capture. They suggest that the system should be established such that the structure has a lower natural frequency than the oscillating water column. Stappenbelt and Cooper used a ratio of a structure's natural frequency to water column natural frequency of approximately 0.66. This separation of natural frequencies also allows a phase difference between the structure and water column. They have also shown that when the wave frequency coincides with the natural frequency of the water column a phase difference between the structure and water column can be created.

3.4.1 Structure Sizing Numerical Investigation

To determine a sizing guideline, Stappenbelt and Cooper (2010) tested various water column diameters to structure outer diameter ratios. Practicalities dictate that a larger water column surface area will result in more airflow through the power take-off system, hence a larger power output. Stappenbelt and Cooper hypothesised this and Sheng et al. (2011) have mathematically proven that the power output is proportional to water column surface area cubed. Stappenbelt and Cooper (2010) used a diameter ratio of 0.9. They have shown that this value is equal to the proportion of the Froude-Krylov force acting on the water column.

Stappenbelt and Cooper (2010) showed that as the diameter ratio (ratio of the water column surface area to the total surface area of the structure and water column) tends towards 1.0, the power output is increased at wave period values coinciding with the natural period of the water column. The opposite is true when the diameter ratio tends towards zero; the power output peak moves to a value closer to the natural period of the structure. Practicalities dictate that a value closer to 1.0 will allow an easier structure to be developed. A value of 0.9 was adopted for this present research because it is unreasonable to assume negligibly thin walls of a practical floating device. This is likely to cause an unfavourably short metacentric height

because most of the necessary equipment is stored on top of the device. This may lead to the device overtopping.

Using the water column draft (12.3 m) for a sea with a peak wave period of eight seconds (see section 3.4), the structure sizing can be determined. If using the oscillating water column diameter (d_{wc}) of 10 metres, the outer diameter of the column, d_o, will be equal to:

$$d_o = \frac{d_{wc}}{0.9} = \frac{10\ m}{0.9} = 11.34\ m$$

The RAO from WAMIT (described in Chapter 4) for this structure is shown in Figure 3.8 and details much the same response as Figure 3.7. There is a distinct peak at the natural period of the structure (~5.2 seconds) and a smaller peak at the water column natural period (~8 seconds). The magnitude of the RAO at the structure's natural period is non-physical; meaning that this cannot be expected in a practical application. The structure has a 12.3 metre draft and the expected RAO at the natural period is equal to ~55. This means that the structure is expected to reach a heave amplitude of 55 times the wave amplitude. This has been read from Figure 3.8. This leads to amplitude of oscillation larger than the dimensions of the structure. This is not possible in a practical setting. This discrepancy is due to WAMIT not accounting for additional viscous damping within the system.

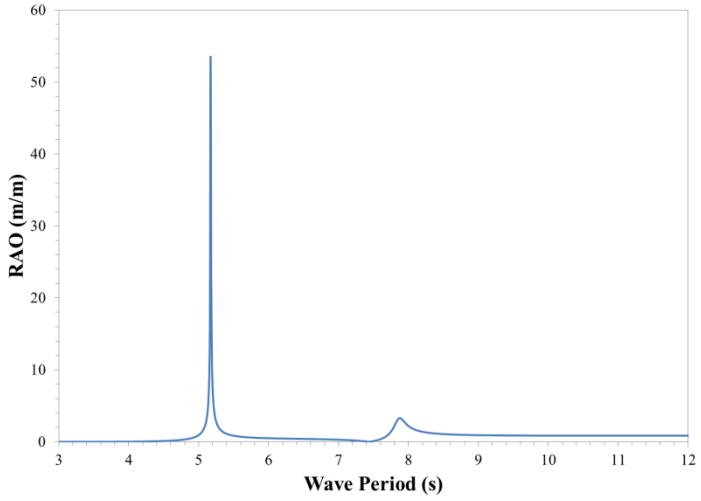

Figure 3.8: Structure RAO from WAMIT

3.5 Power Production in an OWC

The power production of an oscillating water column wave energy device is going to be directly related to the airflow through the turbine and the associated pressure drop. Sheng et al. (2012) developed a relationship between water column size and power take-off efficiency for fixed devices. This is extrapolated to floating devices here. If the non-dimensional oscillating water column response at a particular frequency is equal to ξ_7, then the vertical displacement of the water column as a function of time is equal to:

$$X_7(t) = \frac{H}{2}\xi_7 \sin \omega t \tag{3.33}$$

where H is the wave height, ω is the angular frequency, and t is time.

Differentiating the displacement with respect to time produces the water column velocity:

$$V_7(t) = \frac{H}{2}\omega\xi_7 \cos \omega t \tag{3.34}$$

If the air within the chamber is assumed to be incompressible then the airflow rate caused by the water column is equal to the airflow rate through the turbine. Folley and Whittaker (2005) have stated this assumption may lead to a slight overestimate of the power production of this model as the potential additional natural frequency of the system is removed. The magnitude of the overestimate increases as the size of the associated models moves toward a full-sized OWC.

Defining the water column surface area as A_0, the flow rate through the orifice can be expressed as:

$$Q(t) = C_d \mathrm{A}_1 V_1(t) = A_0 V_7(t) \tag{3.35}$$

where $V_1(t)$ is the airflow velocity through the orifice, A_1 is the orifice opening area, and C_d is the flow loss coefficient. The associated pressure drop because of the constriction can be expressed by:

$$\Delta p(t) = \frac{1}{2}\rho_a V_1^2(t) = \frac{\rho_a}{2C_d^2}\left(\frac{A_0}{A_1}\right)^2 V_7^2(t) \tag{3.36}$$

where ρ_a is the air density. The power extracted because of the pressure drop is equal to the product of the flow rate and the pressure drop:

$$P(t) = \Delta p(t) \times Q(t) = \frac{\rho_a A_0}{2C_d^2}\left(\frac{A_0}{A_1}\right)^2 |V_7^3(t)| \tag{3.37}$$

Expressing the total average power as a function of the inputs results in:

$$\bar{P} = \frac{1}{t_2 - t_1}\int_{t_1}^{t_2} P(t)\, dt = \frac{1}{t_2 - t_1}\int_{t_1}^{t_2} \frac{\pi^3 \rho_a A_0}{2C_d^2}\left(\frac{A_0}{A_1}\right)^2 |V_7^3(t)| dt \tag{3.38}$$

$$\bar{P} = \frac{2\pi^2 \rho_a A_0}{3C_q^2}\left(\frac{A_0}{A_1}\right)^2 \xi_7^3 H^3/T^3 \tag{3.39}$$

If the energy per unit width of the ocean wave is expressed as:

$$E = \frac{1}{8}\rho g H^2 \tag{3.40}$$

then the efficiency of the water column wave energy device can be expressed as:

$$\eta = \frac{64\pi^3 \rho_a}{3C_q^2 \rho_w g^2 B}\left(\frac{A_0}{A_1}\right)^2 A_0 \xi_7^3 H/T^4 \tag{3.41}$$

where *B* is the width of the water column perpendicular to the direction of wave propagation.

Equation 3.37 and equation 3.39 highlight important factors to consider when sizing an OWC water column and orifice. A larger water column to orifice ratio will result in increased power production (provided the flow rate of the air remains constant) because of the increase in pressure differential across the turbine. An increase in water column surface area with a fixed orifice diameter will also result in production of more power and in an energy conversion efficiency increase. If the flow rate is not kept constant, there exist an optimal water column to orifice ratio. If the orifice is too large the flow rate will decline; if the orifice is too small the pressure differential will decline.

3.6 Chapter Summary

This chapter discussed theory related to ocean waves, wave energy, wave energy devices, and oscillating water columns. The chapter has established the start for guidelines for the development of a model that can be investigated using WAMIT and OrcaFlex.

This model is designed so that the oscillating water column has a natural period of 8 seconds. This value was identified as a common wave period along the east coast of Australia. The vertical cylinder has a draft of 12.3 metres, an inner diameter of 10 metres and an outer diameter of 11.34 metres. The draft is significantly less than half the expected wavelength of the ocean waves in deep water (~50 m) and therefore avoids any negative wave attenuation effects at increased drafts. The internal diameter, and hence water column diameter, is also significantly smaller than the expected wavelength of the ocean waves (~100 m). This will avoid any excess sloshing within the chamber. These dimensions have been chosen based on the recommendations in the literature. These recommendations are further investigated in the coming chapters.

This chapter has also presented a derivation for calculation of the power output and hence efficiency rating of a floating oscillating water column device. These equations are used in the assessment of the device in coming chapters.

Lastly, this chapter has presented and discussed wave spectra. The wave spectra discussed are the ISSC (or Bretschneider spectrum) and the JONSWAP spectrum. The ISSC spectrum is often used to describe calm sea states with significant fetch. The JONSWAP spectrum is often used to describe unfavourable conditions and is used by DNV to define the 1-in-100 year storms. The ISSC spectrum is used in this study to assess the sensitivity of the frequency domain testing to wave spectra with regards to power production, and the JONSWAP spectrum is used to investigate the feasibility of tuning with regards to device integrity during unfavourable conditions.

Chapter 4 Understanding OWC WECs in the Frequency Domain

4.1 Introduction

This research used a software package known as Wave Analysis MIT (WAMIT) to investigate various floating water column wave energy device parameters and to draw conclusions related to both the testing procedures used and physical geometry of an ideal oscillating water column wave energy device.

This chapter discusses to use of WAMIT to investigate the effects of various sizing considerations put forward in previous works. These include the oscillating water column sizing recommendation by Sheng et al. (2012), and the ratio of the oscillating water column natural period to structure natural period suggested by Stappenbelt and Cooper (2010). Effects of varying system characteristics often seen in the oil and gas industry were determined. These characteristics include structure stiffness as suggested by Stappenbelt and Cooper (2010), different levels of power take-off damping as suggested and investigated by Stappenbelt and Cooper (2010), and the adoption of structural heave plates as they have been shown to provide added mass by Koh and Cho (2011). The determination of the structure's geometrical parameters to increase the power take-off during operational periods and to increase survivability during unfavourable extreme conditions is discussed.

The hydrodynamic coefficients and wave exciting forces are calculated by WAMIT through a standard 3D linear radiation-diffraction flat panel method. This method assumes potential flow theory which satisfies the Laplace equation in the fluid domain. The linear boundary value problem is formulated for the wave body interactions in incident waves. Green's theorem is then used to formulate the integral equations with unknown velocity potentials on the mean wetted surface area of the body. The body is discretised into panels. There is a constant potential across each panel. This leads to a set of linear simultaneous equations in the unknown potentials.

The software used in this study (WAMIT v7.0) is able to extend the boundary value problem to include bodies where all or part of the body is a free surface. A nonzero oscillatory pressure acts on this surface. This allows the pressure distribution of the free surface, rather than the normal velocity, to be specified. Oscillating water column wave energy devices and air-cushion vehicles are examples where this nonzero oscillatory pressure acting on a free

surface may be implemented. The mathematical grounding and background workings of WAMIT are included in Appendix A – WAMIT Theory. The operational files (input files) are in Appendix B – WAMIT Operational Files.

4.2 Developing a Model in WAMIT

The basis for the OWC model is a free-floating cylinder with a central moonpool generated with the GEOMXACT subroutine within WAMIT. The basic cylinder is composed of three patches (NPATCH=3): the outer surface, the inner surface and the bottom annulus. Specifying the cylinder radius, moonpool radius, cylinder draft, and radius of gyration creates the model within WAMIT. An additional weightless patch (NPATCH=4) is added. This a free pressure surface (FSP) on the moonpool column used to simulate the power take-off damping of an OWC device. Additional information about the structure is required when using NPATCH=4. The user is required to input a mass matrix, damping matrix and stiffness matrix for each degree of freedom. Limiting the additional patch to one degree of freedom, heave, results in a 7x7 matrix for damping and stiffness. Newman (1977) has defined the mass matrix of the structure as equation 4.1.

$$M = \begin{bmatrix} m & 0 & 0 & 0 & mz_G & -my_G \\ 0 & m & 0 & -mz_G & 0 & mx_G \\ 0 & 0 & m & my_G & -mx_G & 0 \\ 0 & -mz_G & my_G & I_{11} & I_{12} & I_{13} \\ mz_G & 0 & -mx_G & I_{21} & I_{22} & I_{23} \\ -my_G & mx_G & 0 & I_{31} & I_{32} & I_{33} \end{bmatrix} \tag{4.1}$$

Here, the mass of the structure can be calculated using:

$$m = \iiint_{V_B} \rho_B \, dV \tag{4.2}$$

The centre of gravity of the structure is needed to determine the inertia tensor and is defined as:

$$x_G = \frac{1}{m} \iiint_{V_B} \rho_B x \, dV \tag{4.3}$$

Lastly, for a uniform cylinder, the inertia tensor is defined as:

$$I_{ij} = \iiint_{V_B} \rho_B \left[x' \cdot x' \delta_{ij} - x_i' x_j' \right] dV$$

$$= \begin{bmatrix} \frac{1}{12} m(3(r_1^2 + r_2^2) + h^2) & 0 & 0 \\ 0 & \frac{1}{12} m(3(r_1^2 + r_2^2) + h^2) & 0 \\ 0 & 0 & \frac{1}{12} m(r_1^2 + r_2^2) \end{bmatrix} \tag{4.4}$$

The model developed for the WAMIT investigation is the same model developed during the numerical example of the structure and oscillating water column sizing in Chapter 3. The model sized in Chapter 3 has an oscillating water column diameter of 10 metres and an outer structure diameter of 10.54 metres. The draft of the structure is 12.3 metres. These dimensions give an oscillating water column with an undamped natural period of approximately 8 seconds. This is seen in Figure 3.7. The structure mass required to give a draft of 12.3 metres is about 110 tonnes. This is calculated using Archimedes principle. A schematic of the model and location of the patches is seen in Figure 4.1.

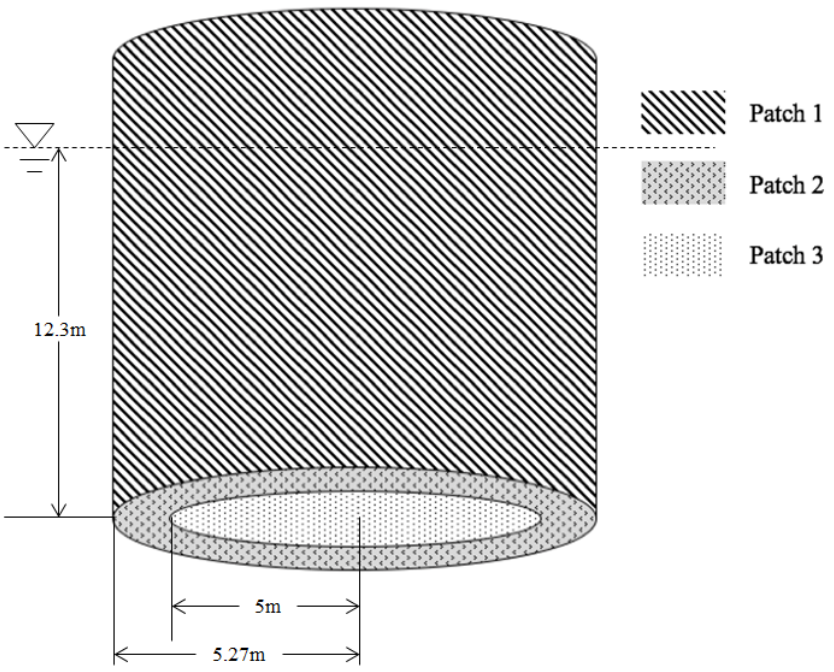

Figure 4.1: WAMIT Model with dimensions and patches

4.3 Panel Size Sensitivity Analysis

WAMIT employs a higher or lower order method to produce results. This research was undertaken using the higher order method. More information on the lower order method is available in Appendix A – WAMIT Theory. The higher order method describes the body by reducing it into patches. These patches are further reduced into panels. Each panel is a continuous surface and is therefore not limited to flat quadrilaterals or triangles as in the lower order method (a complete description of each method is seen Appendix A – WAMIT Theory). The intersection of a cylindrical patch and flat patches is shown in the Figure 4.2 (WAMIT Manual). The blue sections of the patches are the only parts specified by the user. Reflecting the user defined patched on the X and Y-axis of symmetry produces the yellow part of the body.

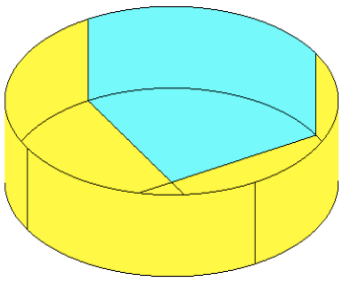

Figure 4.2: Discretisation of a cylinder using patches (WAMIT)

To further improve accuracy, WAMIT reduce the patches into smaller panels and each patch can be composed of a number of panels. Each panel can be described as rectangle in parametric space and as a curved surface in physical space. Each patch of Figure 4.2 has been reduced into four panels. This result of this is seen in Figure 4.3.

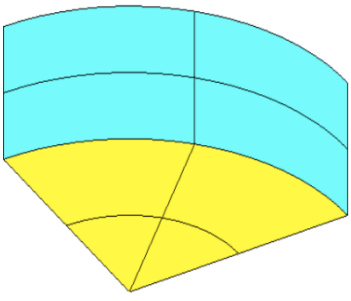

Figure 4.3: Reduction of patches into smaller panels (WAMIT)

Choosing an appropriate maximum panel size to ensure accurate results is most easily achieved by reducing the panel size to the pre-set WAMIT size of 0.1. The unit of the panel size is dependent on the value of ULEN selected by the user. In this study the units are metres. Using the smallest panel size will result in very long computational times for each POTEN run (~days), therefore a balance must be established between accuracy of results and computational time. POTEN is the WAMIT subprogram that solves for radiation and diffraction velocity potentials on the body for the specified modes, frequencies, and wave headings.

To determine an appropriate maximum panel size for the structure sized in Chapter 3, the non-dimensional heave, RAO, structure added mass coefficient, and damping coefficient of the structure are compared for a range of panel sizes. This is seen in Figure 4.4 to 4.7. Panel sizes range from 0.1 m to 40 m. The testing was conducted for wave periods ranging from 0 to 30 seconds at 0.1 second intervals. The added mass coefficient and damping coefficients are defined as:

$$\text{Non-dimensional added mass coefficient: } A_{ij}/m$$

$$\text{Non-dimensional damping coefficient: } \sqrt{B_{ij}/m}$$

Where A_{ij} and B_{ij} are the added mass and damping from WAMIT respectively, and m is the mass of the structure. The added mass coefficient, damping coefficient, structure heave RAO, and water column heave RAO plots were plotted against the wave period. These are seen in Figure 4.4, Figure 4.5, Figure 4.6, and Figure 4.7 respectively.

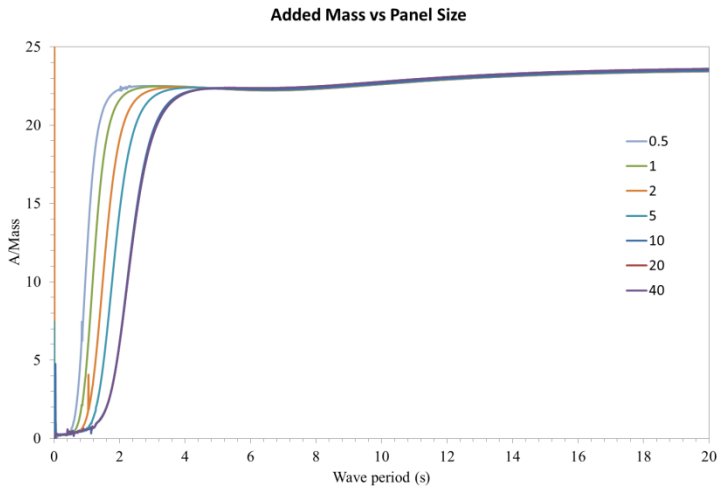

Figure 4.4: Structure added mass for different panel sizes

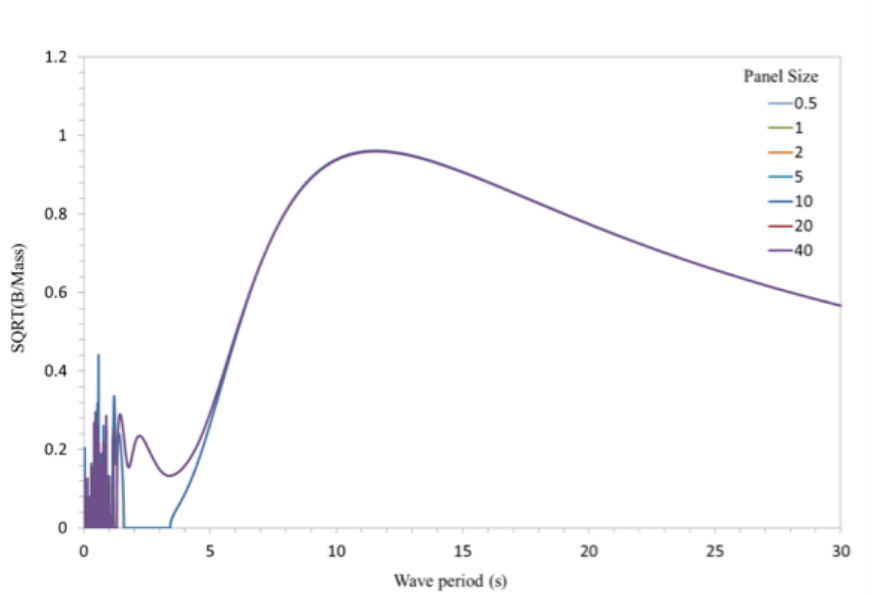

Figure 4.5: Structure heave damping for different panel sizes

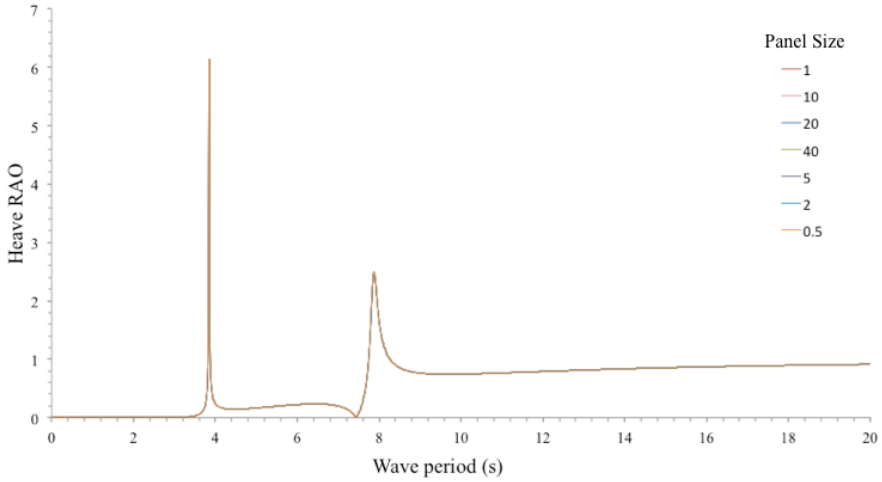

Figure 4.6: Structure heave RAO for different panel sizes

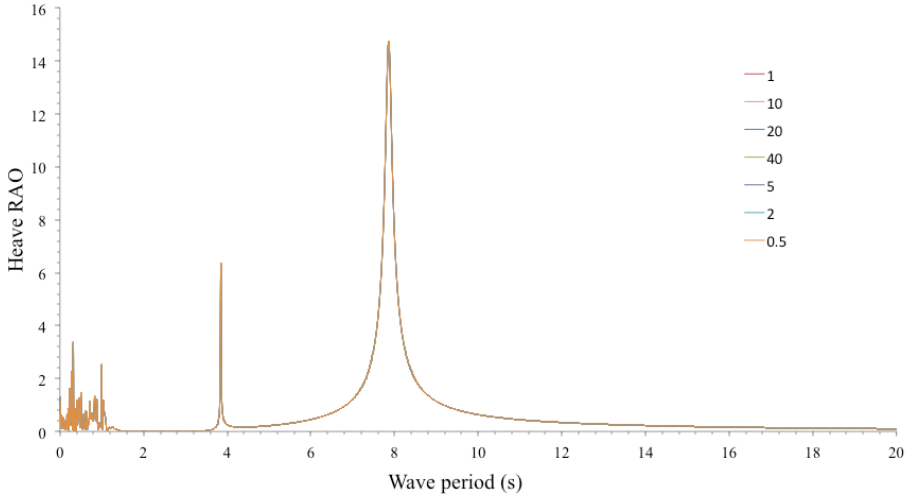

Figure 4.7: Water column heave RAO for different panel sizes

The comparative graphs seen in Figure 4.4 to Figure 4.7 show that there is no practical difference between the panel sizes when comparing the heave, RAO and damping. The added mass in Figure 4.4 does exhibit differences at wave periods less than approximately five seconds when the panel size drops below ten metres. This is expected, as the structure is approximately this size so there will be more than one panel per structure patch; leading to more accurate results at lower wave periods. Further differences are shown when the panel size drops from 5 m to 0.1 m. This difference will not greatly affect the results of WAMIT testing as these smaller wave periods, which are unlikely to be provide enough energy to the system to cause any significant movement.

The heave RAO of the both the water column and structure do not exhibit any significant differences at these smaller wave periods. The added mass and damping for panel sizes (20 m and 40 m) greater than the structure have been shown to be equal. This is likely because the maximum panel size is capped at the size of the structure. WAMIT sees a panel size of 20 m as the same as 40 m if the panel size of 20 m already exceeds the size of the structure. This occurs because WAMIT is run from a text file containing the inputs, hence validation of the input data is not possible.

Ideally, the smallest panel size would be used during the WAMIT analysis as this will produce the most accurate results; however, this will result in very long computational times. Since all panel sizes show convergence, a panel size that produces results in a timely manner yet is still smaller than the structure was chosen. Figure 4.4 to 4.7 have shown that a panel size of five metres is small enough to produce results that do not differ greatly from a panel size 0.1 m but are achievable in a significantly shorter period of time. A panel size of 5 m was used in this investigation.

4.4 System Modification using WAMIT

4.4.1 Heave Added Mass

Stappenbelt and Cooper (2010) concluded that a separation of the natural frequencies of the water column and structure will lead to a larger power capture. The system should be established such that the structure has a lower natural frequency than the oscillating water column. This separation of natural frequencies also allows a phase difference between the structure and water column. Because of the complexities of mooring system stiffness, the structure's natural period is not as easy to express as the water column's natural period. The best method to predict the structure's natural period is to use the generic expression:

$$T_s = 2\pi\sqrt{\frac{m}{k}} \tag{4.5}$$

where m is the mass, and k is the stiffness.

As evident in the above expression, the natural period of the structure can be increased by increasing the mass, or added mass or by decreasing the stiffness of the system within the possible maximum and minimum limits of stiffness achievable in catenary mooring systems. These suggestions are supported by Stappenbelt and Cooper (2010) as viable methods to control the structure's natural period.

It must be noted that increasing the stiffness of the structure is much easier than decreasing it as there exists a lower limit for stiffness; this lower limit will occur when the structure is freely floating. This means that a decrease in the structure's natural period through mooring line tensioning is more viable than increasing the natural period through increasing the mooring line slack. Increasing the structure stiffness to adjust the structure natural period is not ideal, as the optimal structure will have a natural period greater than the oscillating water column's natural period; increasing the structure mass is likely to be the most viable method to attain a separation of natural periods.

On the other hand, care must be taken when increasing the actual mass of the structure. An increase in structure mass will increase the draft of the structure and cause the length of the water column to increase. This will result in a larger natural period of the water column, negating the purpose of the exercise and the separation in natural frequencies will not increase. A viable method to increase the mass of the structure is to use heave plates to

increase the added mass as is often done in the offshore oil and gas industry. An increase in added mass will not increase the draft of the structure and the water column's natural period will remain constant.

Subbulakshmi et al. (2015) have investigated the effect of heave plate geometry on spar platforms. It has been shown that the inclusion of heave plates can have a significant effect on the added mass of the structure. Koh and Cho (2011) have shown that the added mass coefficient of a structure can be increased by a factor of seven without increasing the damping coefficient. Techet (2005) has expressed the relationship between the added mass, mass, and natural period mathematically. Identifying that the mass of the structure in equation 4.5 is actually the sum of the physical mass, m, and the added mass, m_a, the natural period of the structure can be expressed as equation 4.6

$$T = 2\pi \sqrt{\frac{m + m_a}{k}} \tag{4.6}$$

Hence, the natural period of the structure is proportional to the square root of the mass (real and added).

Within WAMIT, the effect of heave plates was simulated by increasing the mass of the structure in heave while keeping it constant in other degrees of freedom. In a practical application these heave plates are usually thin flat discs placed around the structure. The heave mass value corresponds to value 3,3 in the mass matrix seen in equation 4.1. The heave inertia tensor, I_{zz}, will also be modified accordingly. This will not increase the draft of the structure.

The results of this process are seen in the Figure 4.8, Figure 4.9, and Figure 4.10. As the heave mass and heave inertia tensor are increased so do the natural period of the structure. Figure 4.8 to Figure 4.10 plot the structure (RAO3), water column (RAO7), and the water column relative to the structure (RAO7 relative to RAO3) responses against the ratio of the forcing wave period to the oscillating water column natural period. The relativity is obtained by finding the difference between RAO3 and RAO7 (Figure 4.8 and Figure 4.9 respectively). As the heave mass of the structure increases so does the natural period. The extent of the increase is detailed in Figure 4.14. It is important to note that a greater separation between the natural periods results in a larger area below the RAO curve. This larger area represents more movement over a broader range of wave periods and hence a higher chance of a greater

power output; Stappenbelt and Cooper (2010) also show this to be the case. The structure (RAO3) and the water column relative to the structure (RAO7) confirms that an increase in the added mass of the structure can increase the natural period of the structure with little change to the dynamics of the oscillating water column.

Further analysis of the phase angles of each degree of freedom reveals more about the system and design targets. The phase difference between the water column and the adjacent wave falls to zero at values close to the natural period of the oscillating water column and at values that coincide with the natural frequency of the structure. This is seen in Figure 4.11 to Figure 4.13. Wave periods that lie between the natural periods of the water column and structure are shown to cause both the water column and structure to be approximately 170-180 degrees out of phase with the forcing wave. This is not ideal as it will result in a zero phase difference between the structure and water column and will result in very little power extraction (Stappenbelt and Cooper, 2010). The phase difference between the structure and water column is essential for power production. This phase difference can be achieved in undamped systems at wave frequencies less than the structure natural frequency or greater than the oscillating water column natural frequency. This is shown in Figure 4.13.

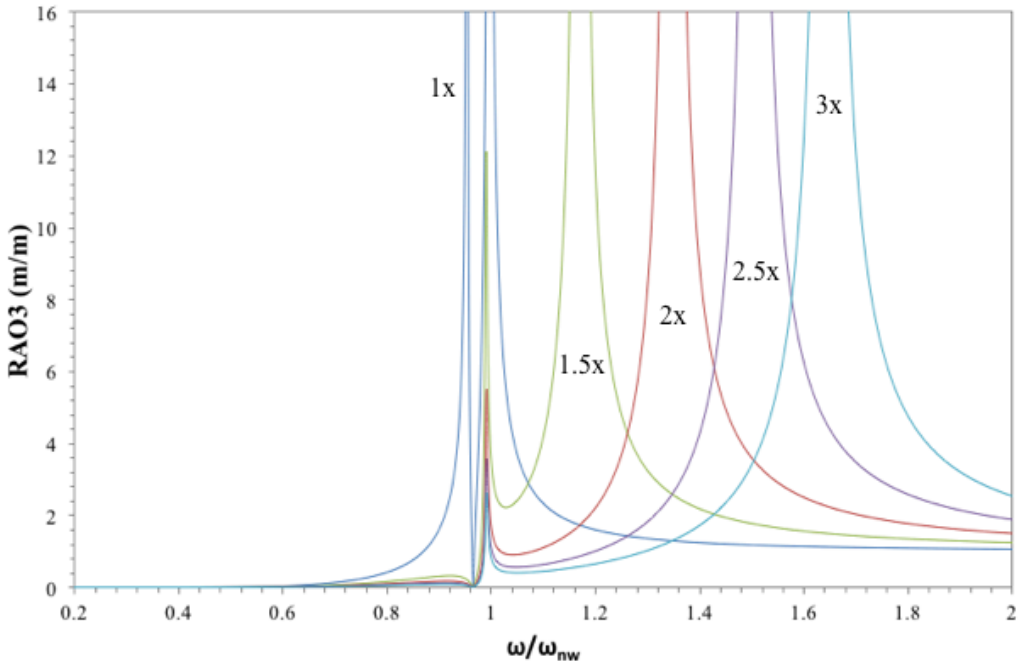

Figure 4.8: Structure RAO at different heave masses

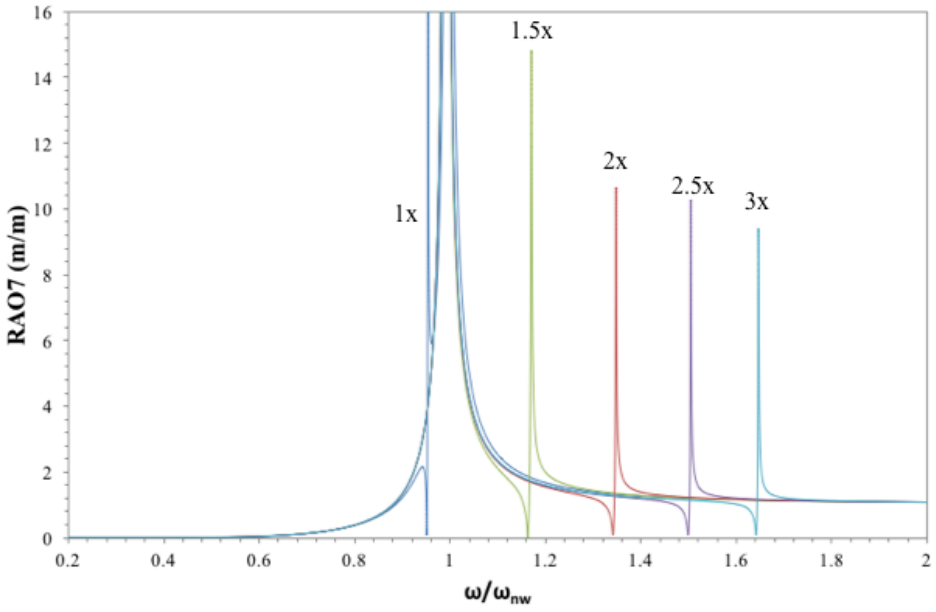

Figure 4.9: Water column RAO at different heave masses

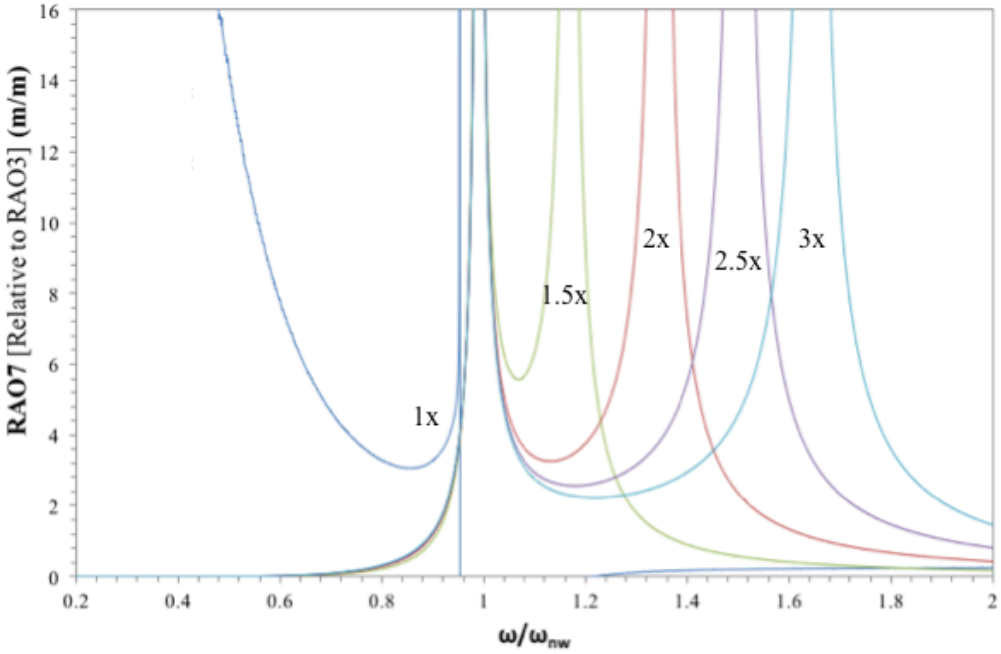

Figure 4.10: Water column RAO relative to structure RAO at different heave masses.

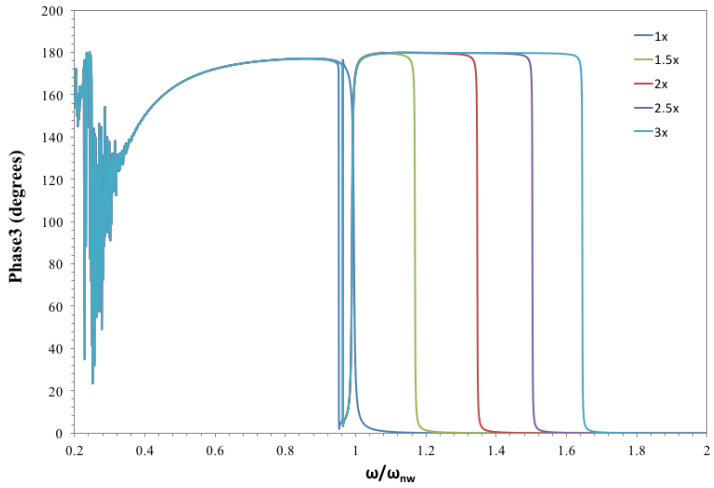

Figure 4.11: Phase angle between the wave and structure at different heave masses

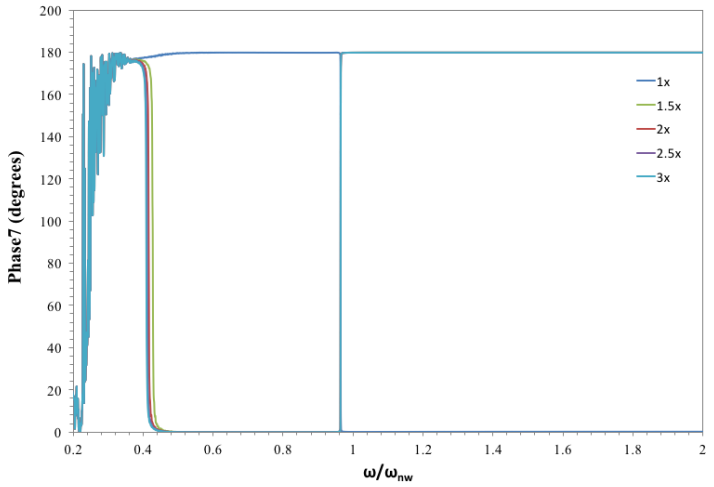

Figure 4.12: Phase angle between the water column and wave at different heave masses

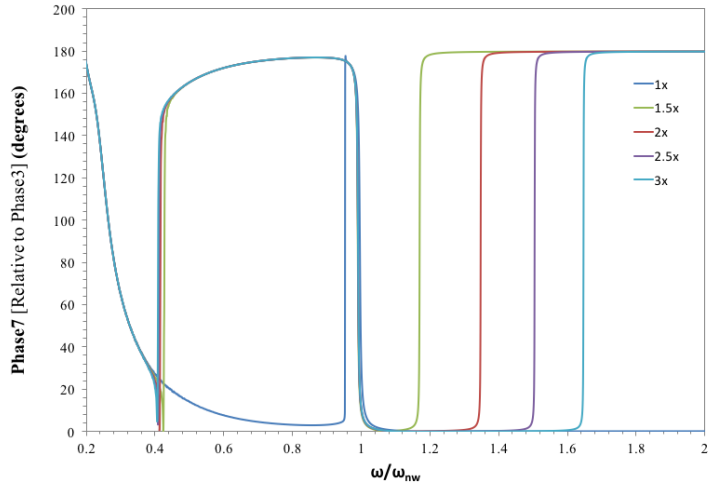

Figure 4.13: Phase angle between the water column and structure at different heave masses.

The information contained in Figure 4.8 to Figure 4.13 can be compressed into two Figures, Figure 4.14, and Figure 4.15. These two figures are produced from the data in Figure 4.8 to Figure 4.13. Figure 4.14 shows that as the added mass of the structure is increased, the natural period of the structure also increases. This increase in the structure natural frequency has little to no effect on the natural frequency of the water column. This is confirmed in Figure 4.15. The water column natural frequency remains approximately constant for different values of added heave mass. The largest decrease is approximately 0.6%. This is small enough to be assumed negligible.

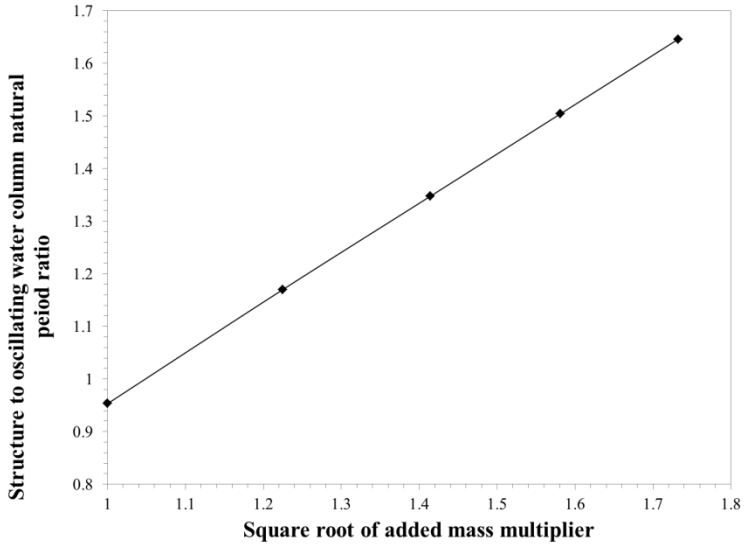

Figure 4.14: How the increase in heave mass affects the percentage increase of the structure's natural period

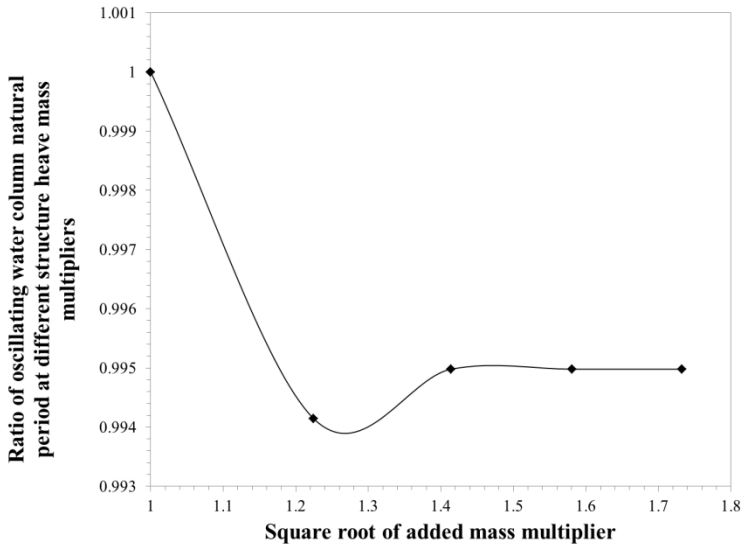

Figure 4.15: The effect on the water column natural period as the structure heave mass in increased.

Figure 4.14 and Figure 4.15 confirm that the natural period of the structure may be altered without changing the natural period of the water column. This conclusion has uses during both the power take-off phase and storm phases where the waves may not be suitable for energy production. If the natural period can be increased to the extent that it falls outside the majority of the storm wave component periods the structure is more likely to survive the extreme conditions. This assumption is based on reduced structural movement at wave periods that are far from the natural period of the structure. Further investigation into this concept was undertaken and is considered in the time domain analysis of Chapter 6. Adjustment of the natural period might be used in conjunction with other methods. Another potential method of control is damping adjustment.

4.4.2 Determining damping values

Structure

The previous conclusions have been drawn from a system that only accounts for radiation damping (WAMIT). This is a large underestimation of the damping expected in practical applications (Tao and Cai, 2004) and additional damping will need to be included in the system. This additional damping will be due to the viscous damping around the structure and the power take-off of the system. Tao and Cai (2004) provided heave viscous ratios, ξ, for spar buoys using heave plates while investigating the effect of heave plates on the natural period of spar buoys. These ratios are with respect to the critical damping of the system. The critical damping of the system can be expressed as a function of the mass, m, added mass, m_a, and excitation frequency:

$$B_r = 2(m + m_a)\omega \tag{4.7}$$

While the viscous damping ratio is expressed as:

$$B_v = \xi B_r \tag{4.8}$$

By using these two equations it is possible to estimate viscous damping values for the structure. Tao and Cai (2004) provide damping ratios for various heave plate setups used to control the natural period of spar buoys in the oil industry. Viscous damping is traditionally non-linear but for vessels with small fluctuations in velocity, such as those found offshore, it can be approximately by a linear value, as was done in Subbulakshmi et al (2015). The average value is approximately 0.02. This value is adopted for this present research.

WAMIT is able to provide the frequency dependent non-dimensional added mass of the structure as described above. This is seen for a forcing period ratio (wave period to oscillating water column natural period) ranging from 0 to 2 (see Figure 4.16). The added mass of the structure will remain constant over the forcing period ratios (>0.4) in which this research interested while the structure geometry remains constant. The added mass over the specified frequency range remains constant at 3000 kg/kg. WAMIT does not allow for frequency dependent viscous damping values but, rather, uses a fixed value. To meet this restraint imposed by WAMIT, the average added mass value of 3000 kg/kg has been used. This restriction also limits the wave angular frequency input value used to determine the critical damping value. A wave angular frequency value corresponding with the median wave period

of the wave period range (8s) was chosen for this computation. WAMIT requires a dimension for the added mass value to be used in the force control file. Using Equation (4.7 it is possible to determine the non-dimensional added mass.

$$A_{ij} = \bar{A}_{ij}\rho L^k \tag{4.9}$$

If i,j = 3,3 then k = 3. Here, L is equal to the length as defined by the ULEN parameter (L=1). The ULEN parameter is a distance measurement used to define the value for gravitation acceleration used during the WAMIT analysis. This allows WAMIT outputs in different systems of measurements. Since 9.81 m/s^2 was the defined value for gravitation acceleration, the ULEN parameter is equal to one. Therefore, the dimensional added mass is equal to

$$A_{ij} = 3000 \cdot 1 = 3{\times}10^3 \text{ kg}$$

In WAMIT, the value for ρ is the ratio of the fluid density to the density of sea water. The use of non-dimensional added mass allows the results to be applicable to fluids other than sea water. In the case of sea water, the value is one because the system is placed in the ocean.

The viscous damping values are shown in Table 4.1. The viscous damping increases with the additional mass of the system. The mass and added mass values in Table 4.1 are the structure mass and added mass.

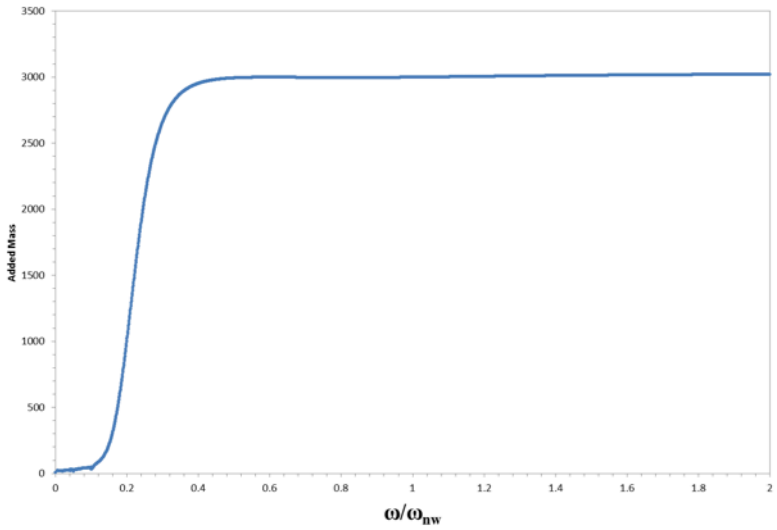

Figure 4.16: Added mass of the structure as a function of the ratio of the forcing frequency to the natural frequency of the water column

Table 4.1: Determination of Viscous Damping

Heave Multiplier	Frequency (Hz)	Added Mass (kg)	Mass (kg)	Total Mass (kg)	Critical Damping (kg/s)	Viscous Damping (kg/s)
1	0.7854	3000	729	3729	3905	78
1.5	0.7854	3000	1094	4094	4287	86
2	0.7854	3000	1485	4485	4697	94
2.5	0.7854	3000	1822	4822	5050	101
3	0.7854	3000	2187	5187	5432	109

To understand the effect of viscous damping, the system was analysed with and without the additional damping value. A system utilizing a 2.5 times increase in added mass has been used because this system conforms to the natural period ratio suggested by Stappenbelt and Cooper (2010). This suggestion was for the structure natural period to be approximately 1.5 times that of the water column natural period.

The effect of the inclusion of viscous damping is significant. The RAOs and phase angles are shown in Figure 4.17 to Figure 4.22. Non-physical (unobtainable values in a real system) RAO values for the structure have been removed by the addition of this viscous damping (see Figure 4.17). The value of RAO3 at forcing period ratios around 1.5 show a sharp decline from ~55 m/m to ~4 m/m. The RAO of the water column has also been changed with the inclusion of viscous damping. This is highlighted in both RAO7 plots (see Figure 4.19 and Figure 4.21). While there still exists non-physical values surrounding the natural period of the water column, the response at wave periods matching the natural period of the structure is significantly reduced and is somewhat uncoupled from the response of the structure. This is highlighted in Figure 4.19 and Figure 4.21 at forcing period ratio values of ~1.5. The phase angle of both RAOs has also been altered. Figure 4.22 suggests that the structure and oscillating water column are no longer always in phase (phase angle of 0°) at wave periods that fall between the oscillating water column (period forcing period ratio equal to 1) and the structure's natural period (forcing period ratio equal to ~1.5). Figure 4.22 also highlights that a large phase difference between the oscillating water column and structure is possible at forcing period ratios less than one. Figure 4.18 and Figure 4.20 suggest that the inclusion of viscous damping reduces the large changes in phase difference at critical forcing period ratios in both the oscillating water column and structure.

In summary, viscous damping has been shown to have a pronounced effect on the motions of water column wave energy devices over wave period likely to be encountered during the operation phase ($0.4<\omega/\omega_{nw}<1.5$) and must be included in the analysis of a wave energy converter system.

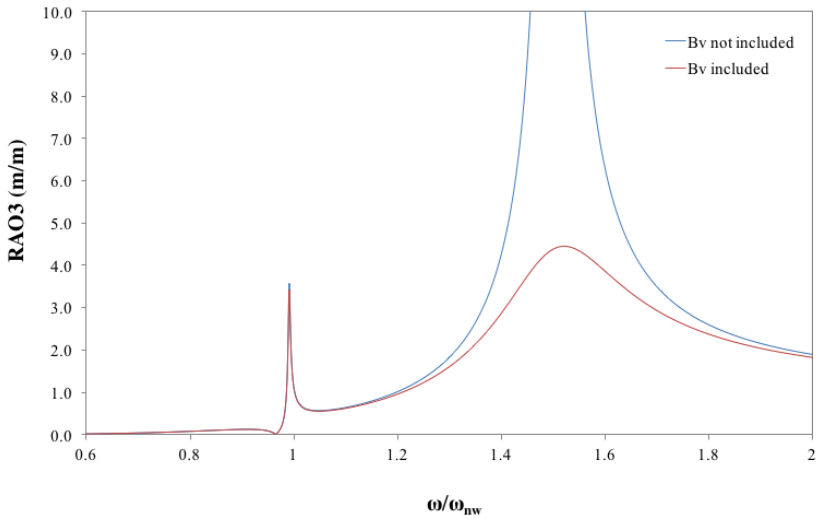

Figure 4.17: Structure heave RAO with and without viscous damping

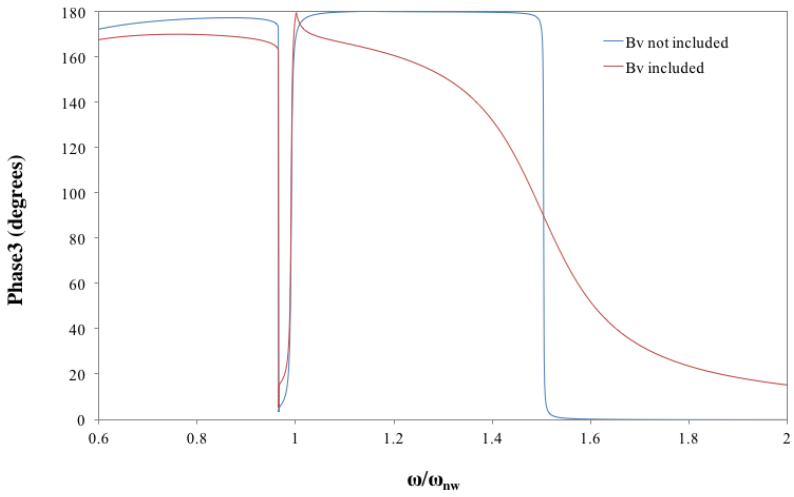

Figure 4.18: Phase angle between the structure and wave with and without viscous damping

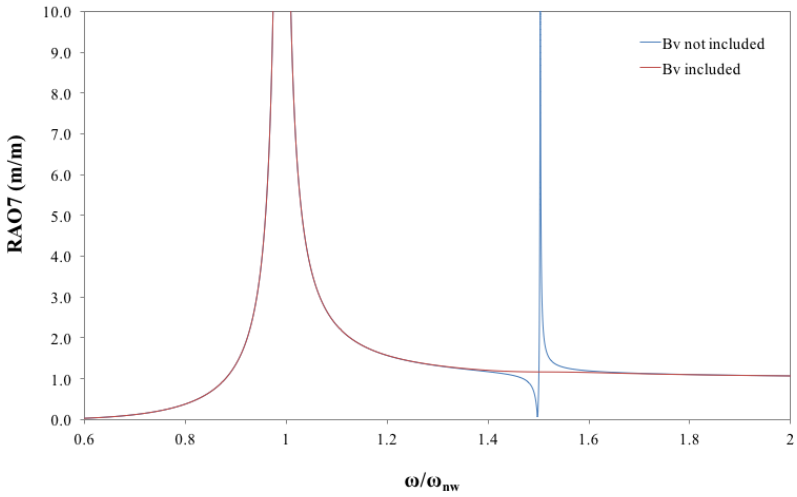

Figure 4.19: Water column heave RAO with and without viscous damping

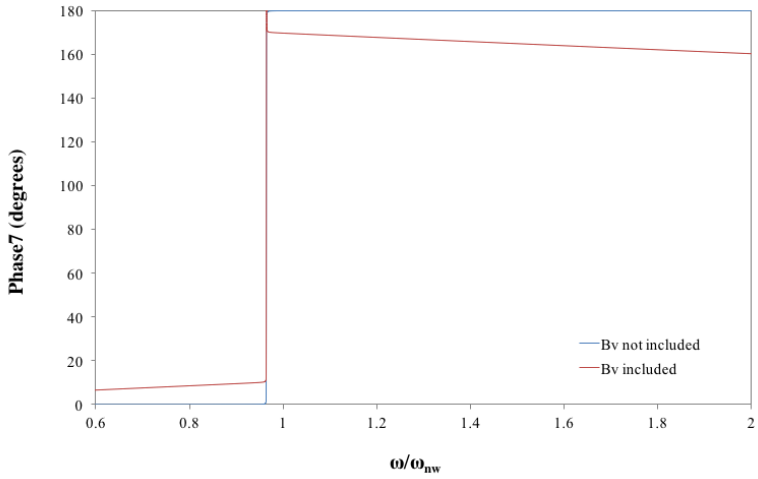

Figure 4.20: Phase angle between the water column and wave with and without viscous damping

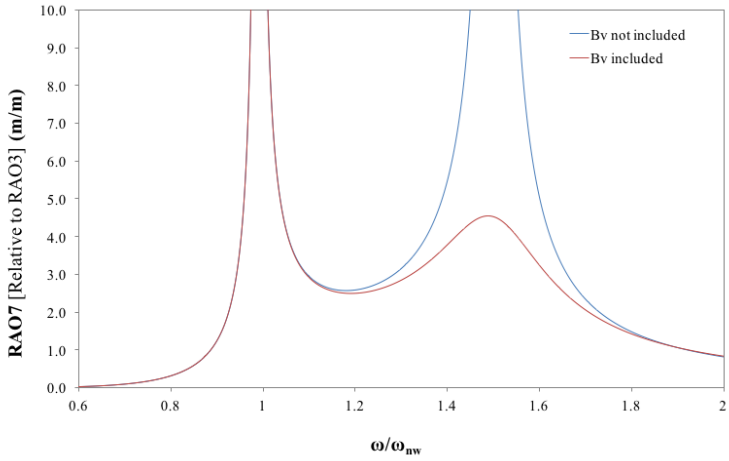

Figure 4.21: Heave RAO of the water column relative to the structure with and without viscous damping

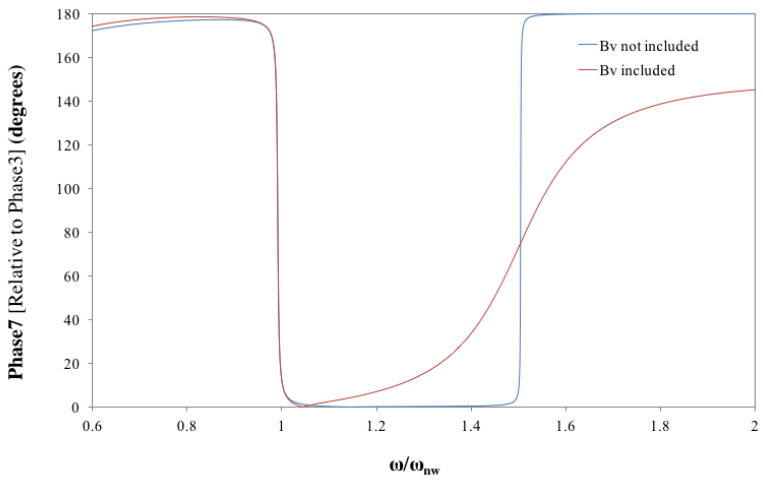

Figure 4.22: Phase angle between the water column and structure with and without viscous damping

The inclusion of viscous damping has removed the non-physical, or unrealistic, RAO values of the structure; however, non-physical values of the water column RAO still remain in the system. This is evident by the large RAO values around a forcing period ratio of one in Figure 4.19 and Figure 4.21.

Water Column

Sheng et al. (2011) and Imai et al. (2011) have both experimentally determined that the maximum practical RAO value experienced by an oscillating water column within a fixed structure is approximately equal to 1.5 and 1 respectively. The practical limitation is a result of the power take-off damping. These two practical maximas for the water column RAO are used as a guideline to determine the applicable free surface patch damping values for patch four in WAMIT. Patch four is the surface area of the oscillating water column. These values were not strictly adhered to because the system investigated is a floating structure rather than a fixed structure seen in the work by Sheng et al. (2011) and Imai et al. (2011). Damping values were gradually increased until the maximum RAO of the OWC was appropriate. Viscous damping of the structure was included in this analysis.

Increasing the damping value of the free surface of the water column (patch four) allows variable power take-off damping values to be simulated. Power take-off removed energy from the system; therefore, it can be simulated by a damping term. The magnitude of power produced will be mostly dependent on the turbine of device. Simulation is done by adjusting the magnitude of value [7,7] in the damping matrix of the force control file (FRC) file in WAMIT (see Appendix A). Each value of the damping matrix refers to a degree of freedom. This value represents the damping due to power take-off. For the sake of simplicity this value

will be called *b77*. Values ranging from 0 to 1200 kg/s were simulated in WAMIT and the results are shown in Figure 4.23 to Figure 4.28. Alcorn (2000) showed that the turbine damping of Wells turbine can be modelled linearly. Alcorn defines the damping as the gradient of the pressure difference versus the airflow through the turbine. Fiorentini (2010) also showed this linear assumption holds up in scale model testing.

An increase in damping values has, as expected, caused a decrease in the heave response of the both the structure (RAO3) and the water column (RAO7). This can be seen in Figure 4.23 and Figure 4.24 respectively. The minimum peak RAO value of the water column is approximately 2. This value occurred when *b77* was just greater than approximately 100 kg/s. This value is approximately 2% of the structure critical damping. An increase in damping from this point resulted in an increase in the peak of oscillating water column RAO. The damping value that coincides with the minimum water column RAO can be called the oscillating water column critical damping value. As the damping increases above the oscillating water column critical value the system starts to behave as a single degree of freedom system rather than a two degrees of freedom system. This transition can be seen between damping values of 200 kg/s and 400 kg/s as shown in Figure 4.23 and Figure 4.24. The resonant peak of the single system (just less than $\omega/\omega_{wc} = 1.12$) does not coincide with either of the water column ($\omega/\omega_{wc} = 1$) or structure ($\omega/\omega_{wc} \approx 1.5$) peaks. At this combined resonant peak there is no phase difference between the water column and structure; the high level of damping is causing the volume of air within the chamber to be fixed. This fixed volume means that a phase difference between the oscillating water column and structure can only arise when the air is compressed. This characteristic may be a useful tool to passively control the motions of the OWC device during unfavourable wave conditions. This will be addressed in Chapter 6. The inclusion of power take-off damping in the system has removed the non-physical values of the water column RAO.

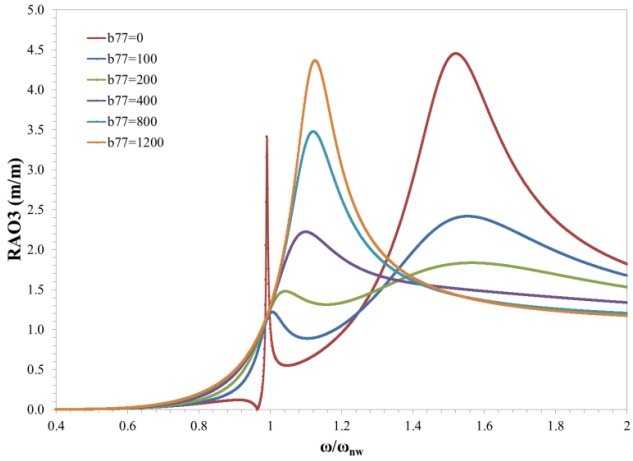

Figure 4.23: Structure response amplitude operator at different levels of power take-off damping

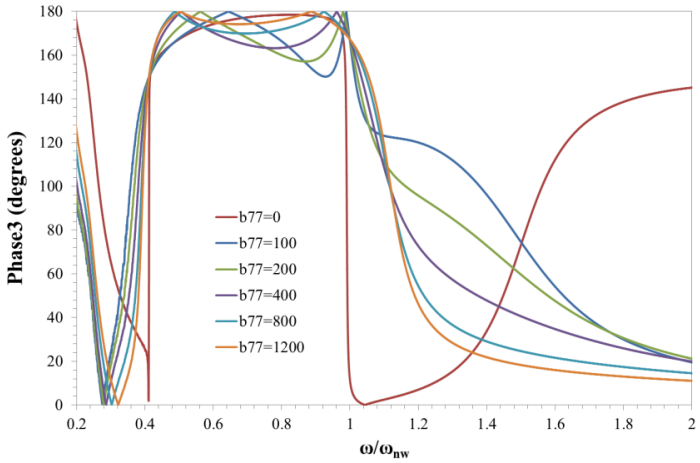

Figure 4.24: Structure phase angle with reference to the forcing wave at different power take-off damping levels.

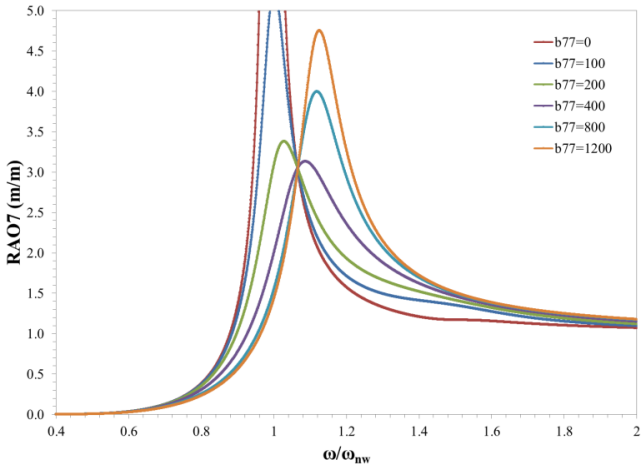

Figure 4.25: Water column response amplitude operator for different levels of power take-off damping

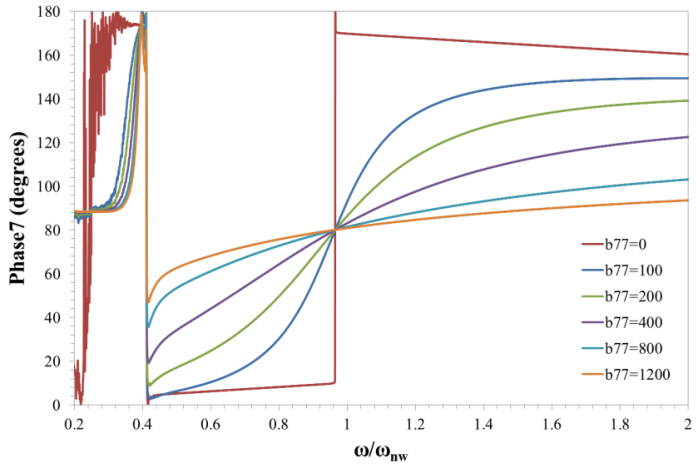

Figure 4.26: Water column phase angle with reference to the forcing wave at different power take-off damping levels.

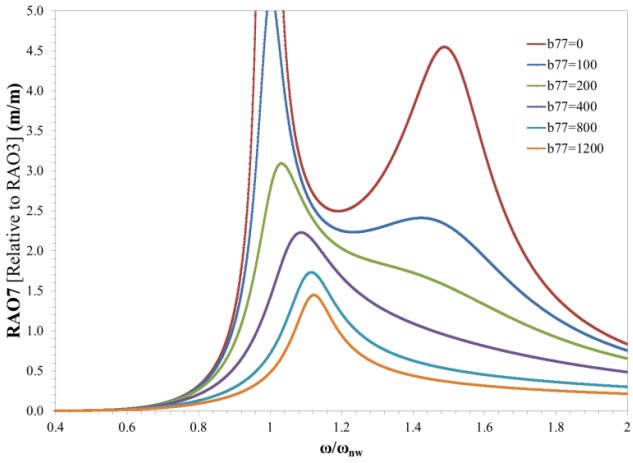

Figure 4.27: Structure heave response amplitude operator with reference to the water column heave response amplitude operator at different damping levels.

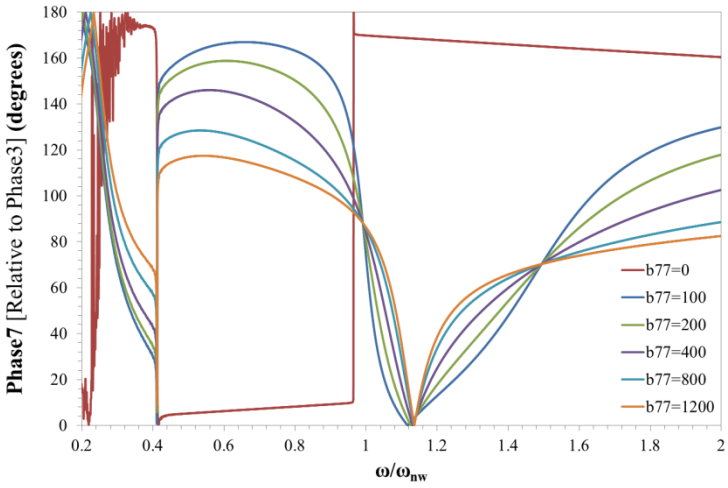

Figure 4.28: Structure phase angle with reference to the water column at different power take-off

damping levels.

An increase in power take-off damping has been shown to reduce the maximum possible phase difference between the structure and water column (see Figure 4.28). The undamped phase difference is seen when $b77 = 0$. At non-zero levels of power take-off damping various system characteristics are highlighted. As the free pressure surface damping value increases so does the phase difference at wave periods that lie between the structure and water column natural periods. Phase differences decrease as free pressure surface damping is increase for wave periods that lie above and below the structure and water column natural periods. Three critical period values also come to light at non-zero power take-off damping values. These are the natural period of the water column, the natural period of the combined system, and the natural period of the floating structure. The phase difference at these values is independent of the damping values.

Figure 4.29 to Figure 4.33 plot the maximum value of the RAO of the structure, the maximum value of the RAO of the oscillating water column, the maximum phase angle between the oscillating water column and structure over a forcing frequency ratios between 0.4 and 0.95, the forcing period ratio value corresponding to the maximum value of the structure RAO, and the forcing period ratio value corresponding to the location (defined here as the value of the wave frequency divided by the oscillating water column natural frequency) of the value of the maximum oscillating water column RAO as functions of the free pressure surface damping, or power take-off damping in a practical setting. These values are determined from the data used to produce Figure 4.23 to Figure 4.28.

Figure 4.29 highlights that there is a damping value that corresponds with the minimum value of the structure RAO. Increasing power take-off damping from zero up to this limit likely causes a reduction in peak value of structure RAO through power take-off; however, power take-off damping values above this limit start to cause the dual degrees of freedom system to behave as one. In a practical case the air cannot escape the system quick enough causing the structure to rise; hence the higher RAO. The damping value corresponding to the low point in the structure heave RAO may be the optimal damping value of the system during wave conditions likely to cause heave motions that may compromise the mooring systems. This is because the structure experiences less heave motion at the damping value than any other value. Figure 4.30 highlights that the maximum value of oscillating water column RAO drops significantly once the power take-off damping is increased. This is expected as the energy of

the system is being removed. Further increases in power take-off damping after the initial drop in the maximum value of the RAO do not lead to any further decreases in the maximum value of the oscillating water column RAO. There is, however, a reduction in the maximum phase angle between the oscillating water column and the floating structure as the free surface, or power take-off, damping is further increased. This can be seen in Figure 4.31. Figure 4.30 and Figure 4.31 highlight that as the power take-off damping is increased beyond the value corresponding to the initial drop in oscillating water column RAO (~100 in Figure 4.30) the oscillating water column RAO is no longer greatly affected but the structure is affected. The maximum value of the structure RAO increases as a results of this larger power take-off damping value and causes the system to merge into a single degree of freedom setup; hence, the reduction in the phase angle between each degree of freedom (Figure 4.31).

Figure 4.32 and Figure 4.33 plot the location of the maximum value of the RAO as a function of the power takeoff damping. With no power take-off damping, the location of the oscillating water column is equal to one, and the location of the structure is equal to 1.5. Figure 4.33 shows that as the power take-off damping increases the location of the maximum value of the RAO of the oscillating water column increases. This means the natural period of the water column is increasing as a result of the power take-off damping. The increase reaches a maximum at around 1.12 which is a 12% increase. Power take-off damping levels are unlikely to reach this high in a practical setting unless the turbine is closed; again, because of the increased structure heave experienced at high power take-off damping levels this is unlikely to occur (Figure 4.29). Practical levels of power take-off damping are likely to occur around the value that corresponds to the minimum structure RAO. At this level of damping the increase in the oscillating water column is much smaller; around 3%. This value will be negligible in random sea states.

Figure 4.34 shows that the structure's natural period behaves differently to the oscillating water column natural period as the power take-off damping is increased. The structure's natural period shows a gradual increase as the power take-off is increased from zero. This increase peaks at approximately 1.6 (a 7% increase) at the power take-off damping level corresponding to the maximum structure RAO value before dropping quickly and remaining constant at approximately 1.12. This constant is the same ratio reached by the oscillating water column and means the two degree of freedom system has merged into a single degree of freedom system.

These results have several implications. There exists an optimal power take-off damping value with regards to dynamics between the oscillating water column and structure. Damping above this value causes the intended separation between the oscillating water column and structure natural periods to be reduced. This reduction leads to a lower phase difference between the two degrees of freedom and a lower maximum RAO of the water column and culminates in a system that produces less power and a structure that experiences unnecessarily large heave values. Too little damping will also cause an increase in structure heave yet capture less power than is available. Both occurrences must be avoided during peak production conditions.

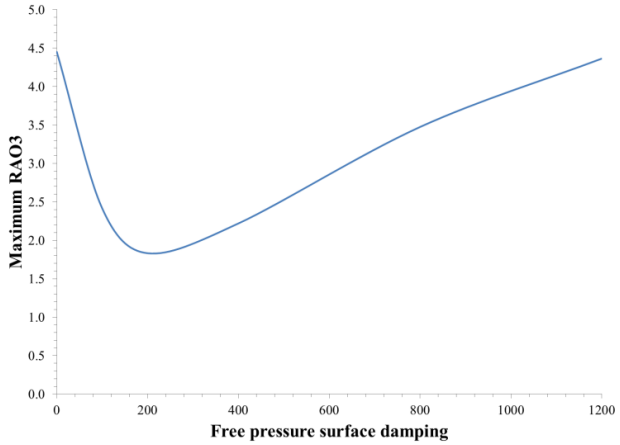

Figure 4.29: The effect of free surface damping on the structure RAO

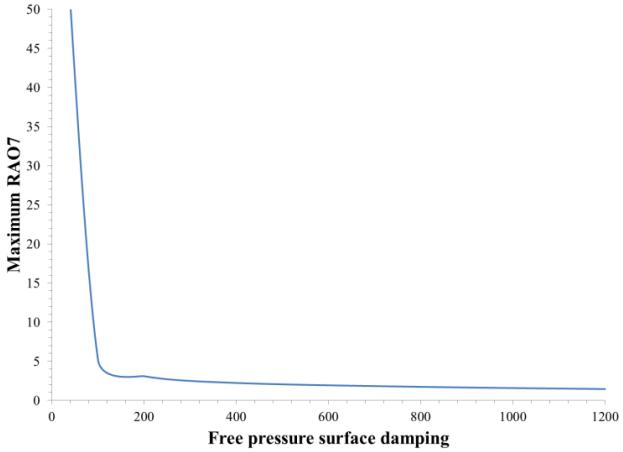

Figure 4.30: The effect of free surface damping on the oscillating water column RAO

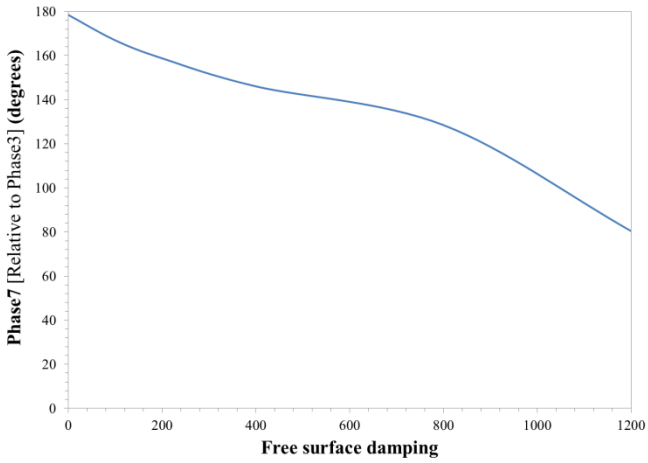

Figure 4.31: The effect of free surface damping on the maximum phase difference between the oscillating water column and structure.

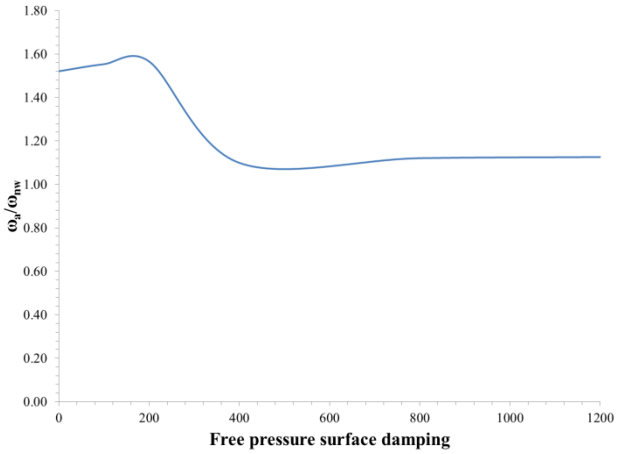

Figure 4.32: The effect of free surface damping on the frequency location of the maximum structure RAO

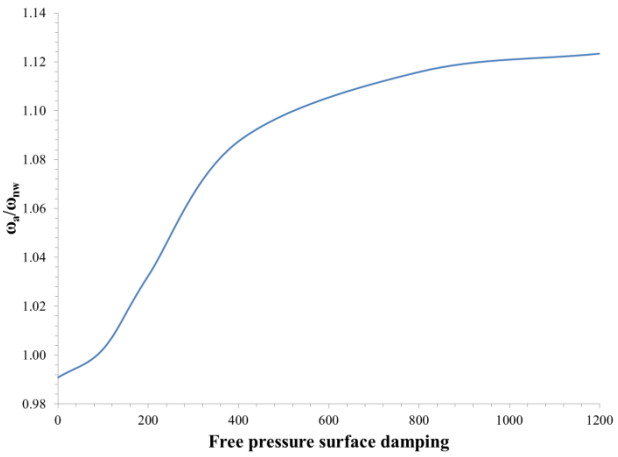

Figure 4.33: The effect of free surface damping on the frequency location of the maximum oscillating water column RAO

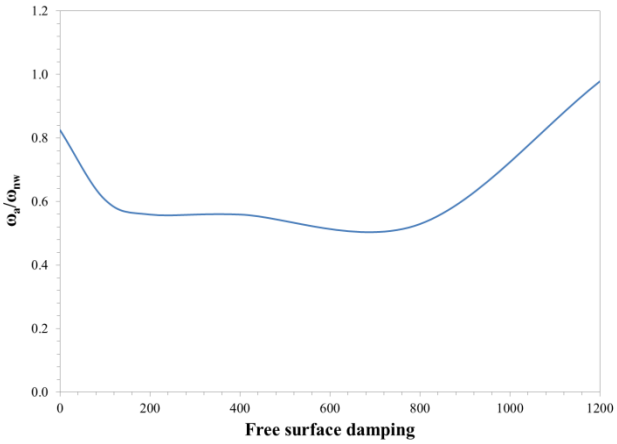

Figure 4.34: The effect of free surface damping on the frequency location of the maximum phase difference between the water column and structure.

The motion of an oscillating water column in a fixed wave energy converter device has been investigated by Kamath et al. (2015). The results for a floating wave energy converter are in agreement with the fixed system investigated by Kamath et al. Through CFD simulations, they determined that the power take-off damping plays a large part in determining the efficiency of the device. The Kamath et al. (2015) and this present study are in agreement; there exists an optimal damping value for a given system. Damping above or below this value will results in a less efficient system. This damping value is equal to approximately 2% of the critical damping for the structure.

4.4.3 Vertical Stiffness

Investigations into the effect of varying vertical and horizontal stiffness values on the structure heave and surge RAOs and on the water column heave RAO was undertaken. Vertical stiffness values ranged from 100 N/m to 1400 N/m and horizontal stiffness values ranged from 100 N/m to 10,000 N/m. These values were chosen as they caused a small but noticeable effect on the RAOs of the structure. These simulations have not taken into account the feasibility of achieving these stiffness values in mooring system but rather to investigate the possible effect of varying stiffness. A feasibility study is conducted in Chapter 6.

The heave RAOs of the structure, water column, and water column relative to the structure are pictured in Figure 4.35, Figure 4.36, and Figure 4.37 respectively. The phase angle response to different vertical stiffness values for the structure, water column, and water column relative to the structure can be seen in Figure 4.38, Figure 4.39, and Figure 4.40 respectively.

A stiffness value corresponds to a peak in the RAOs (Figure 4.35, Figure 4.36, and Figure 4.37). This is likely caused by the stiffness value adjusting the natural frequency of the structure closer to the oscillating water column. Hence a small increase in the maximum value of the RAO. This stiffness value for the structure and the water column are approximately equal to 850 N/m (see Figure 4.35 and Figure 4.36). The stiffness value corresponding to the largest RAO for the relative displacement of the water column with respect to the structure is larger than the previous stiffness values. It is approximately 1200 N/m. A possible reason for the increase in RAOs at specific vertical stiffness values may be that a stiffer structure allows more energy to be transferred to the water column; hence the larger RAO.

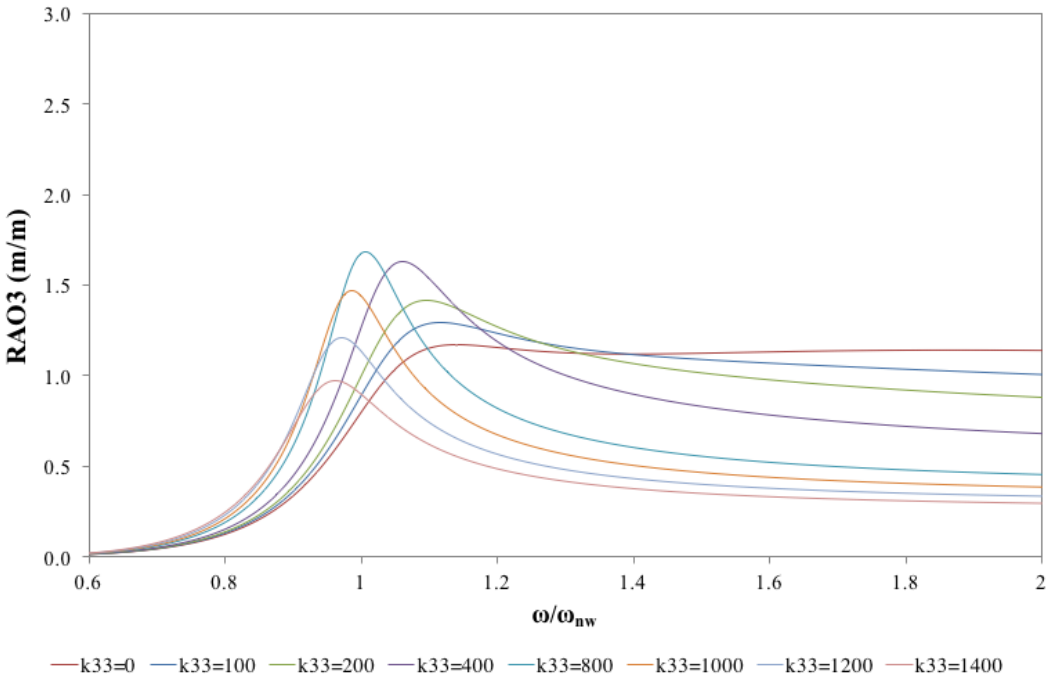

Figure 4.35: Structure heave response at different heave stiffness values

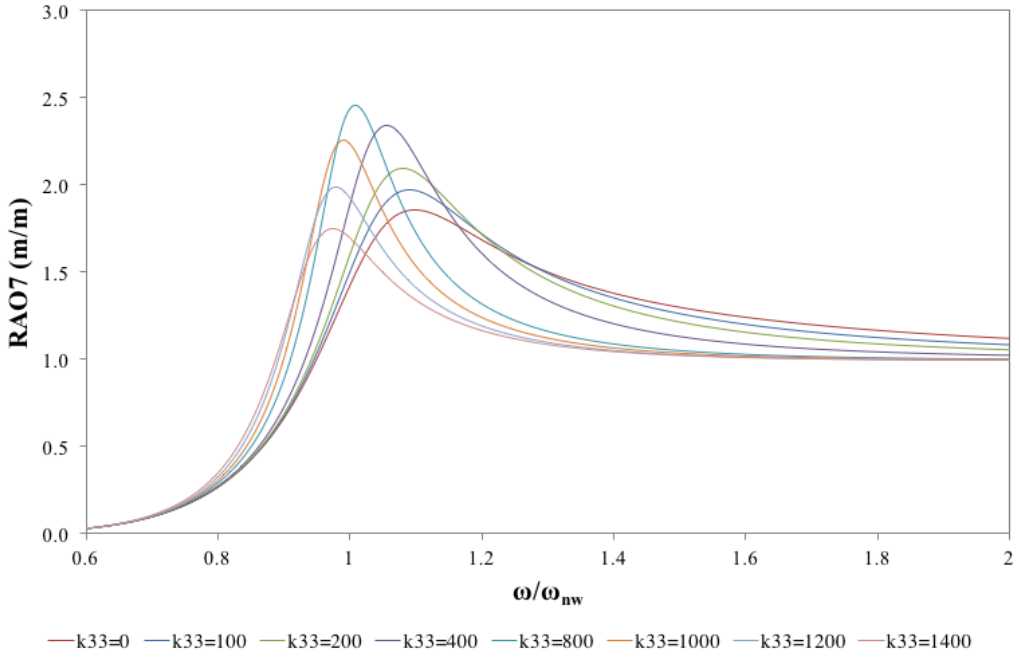

Figure 4.36: Water column heave response at different heave stiffness values

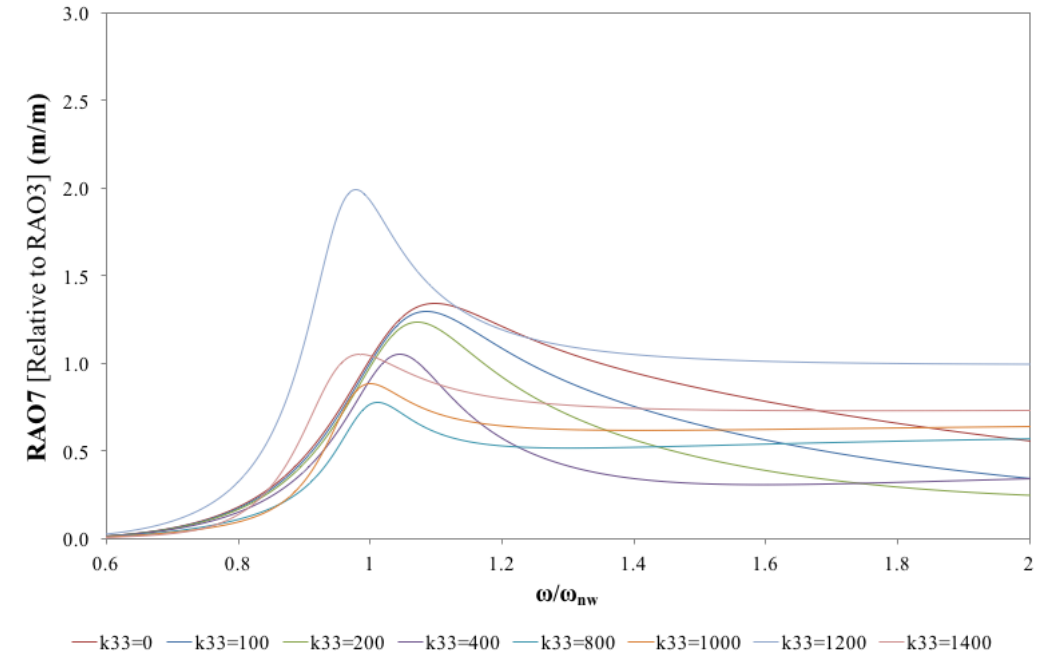

Figure 4.37: Water column heave response with respect to the structure heave response at different heave stiffness values

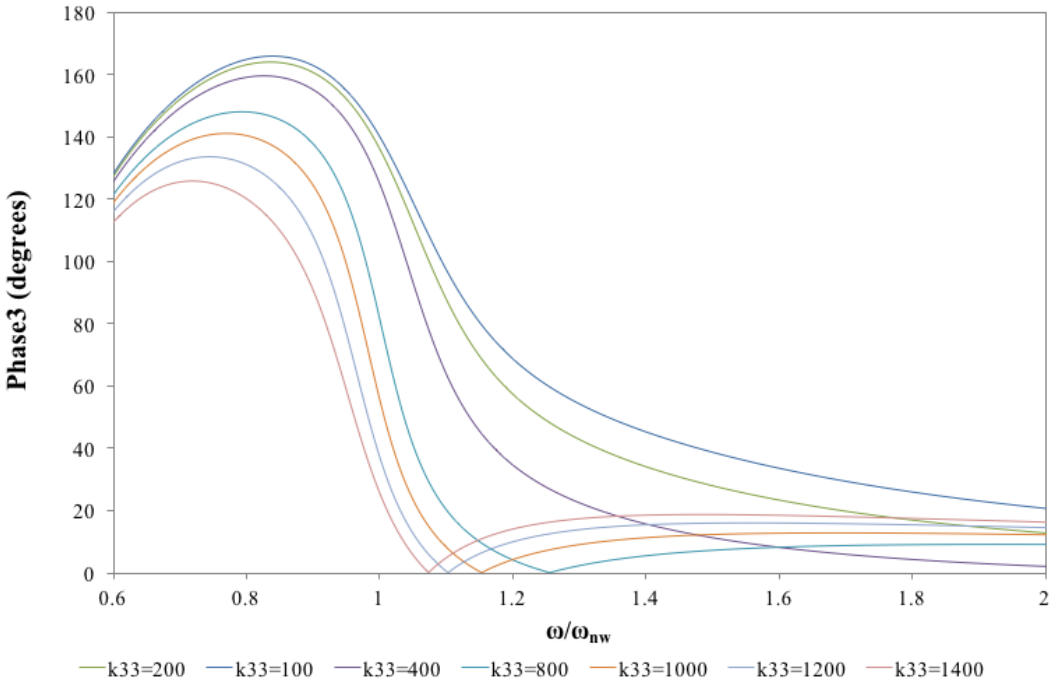

Figure 4.38: Structure phase angle at different vertical stiffness values

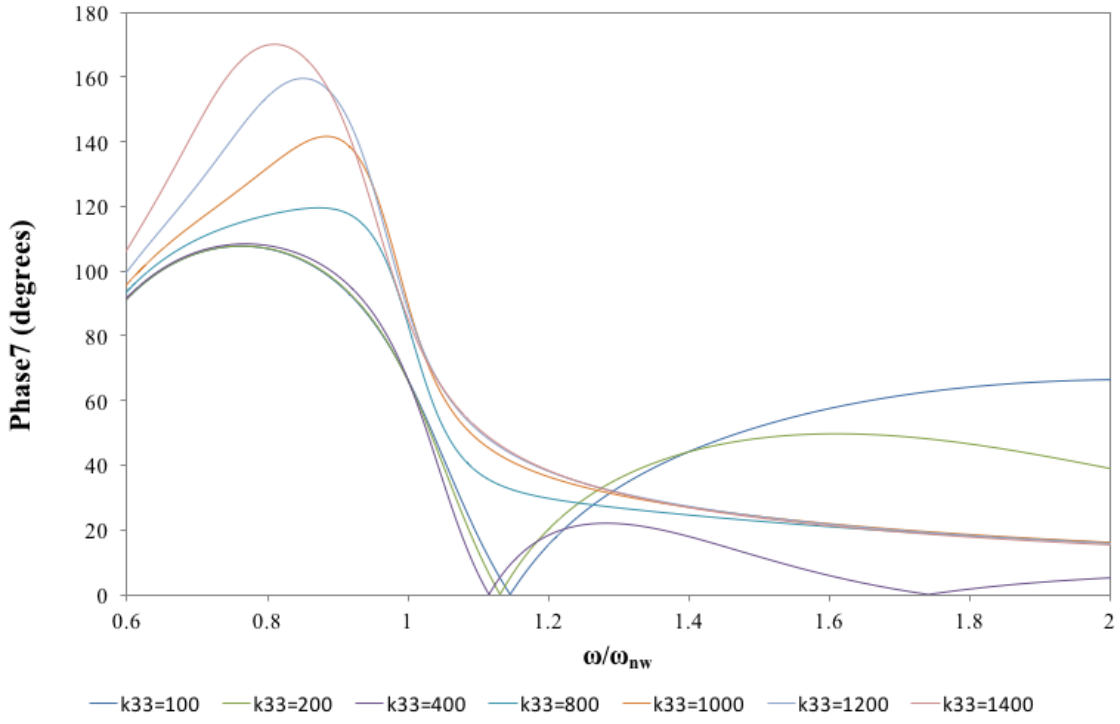

Figure 4.39: Water column phase angle at different vertical stiffness values

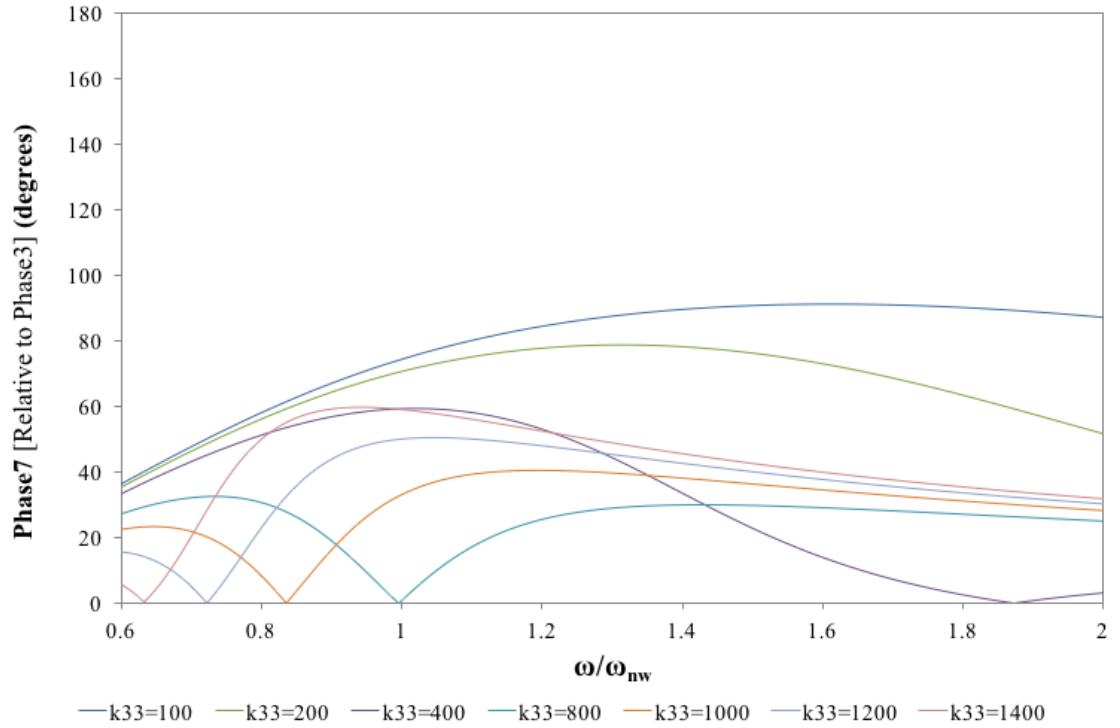

Figure 4.40: Phase difference between the water column and structure at different vertical stiffness values

The effect of vertical stiffness on the system, its RAOs and phase angles, are better displayed in Figure 4.41, Figure 4.42, Figure 4.43, and Figure 4.44. These figures are all plotted as a function of the vertical stiffness ratio. The vertical stiffness ratio is defined as the ratio of the actual stiffness to the stiffness value that corresponds to the minimum value of the RAO of the water column. Figure 4.41 plots the system heave RAOs and Figure 4.42 plots the system phase angles. Figure 4.43 and Figure 4.44 plot the location of the maximum heave value and phase angle respectively as a function of the vertical stiffness ratio. The location is defined as the ratio of the forcing period to the natural period of the water column.

Figure 4.41 and Figure 4.42 highlight a few key characteristics of the system when subjected to different levels of vertical stiffness. There exists a vertical stiffness value that corresponds to a minimum level of water column heave. Values larger than this value show a decrease in the RAO of the structure and the water column relative to the structure. Figure 4.41 shows an increase in the water column RAO above a vertical stiffness ratio of one. However, this RAO is with respect to the wave and not the structure. At values above one, the structure and water column tend towards the same value (that is one). Investigation of the phase angles of the system at different vertical stiffness ratios reveals more details about the behaviour of the system. The minimum value of the phase angle of the water column with respect to the structure occurs at the same stiffness value as the minimum RAO and, hence, the minimum value of this function (see Figure 4.42) occurs at a stiffness ratio value of one. Changes either side of this value lead to an increase in the phase angle of the water column with respect to both the forcing wave and the structure, and a decrease of the structure phase angle with respect to the wave.

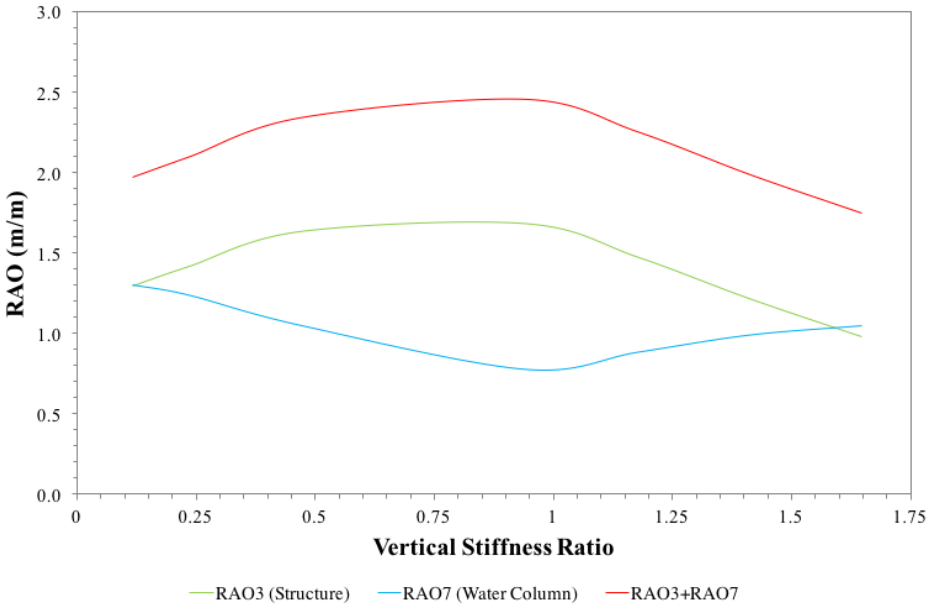

Figure 4.41: System RAOs as a function of the vertical stiffness ratio

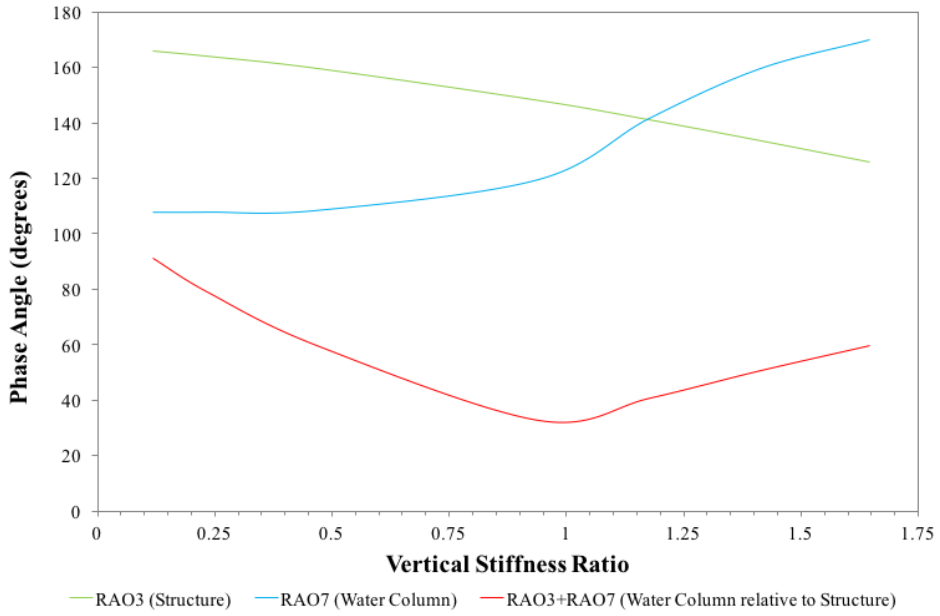

Figure 4.42: System phase angles as a function of the vertical stiffness ratio

Figure 4.43 and Figure 4.44 detail the location of the peak of the RAO and phase angle as a function of the vertical stiffness ratio. Figure 4.43 shows that as the stiffness value is increased, the location of the peak RAO value decreases from approximately 1.1 times the natural period of the water column at a vertical stiffness ratio of 0.1 to 0.98 times the water column natural period at a vertical stiffness ratio of 1.4. This characteristic is repeated for all

RAOs in the system. Figure 4.44 details the location of the peak phase angle as a function of the vertical stiffness ratio. The location for the phase angle between the structure and forcing wave, and the water column and forcing wave, remain much the same across the range of stiffness ratios. The phase angle for the water column with respect to the structure shows a minimum value at a vertical stiffness ratio value of approximately one. The phase angle increases as the vertical stiffness ratio reduces. The phase angle also increases up to a local maximum as the stiffness ratio is increased to approximately 1.2. The phase angle decreases again once the stiffness ratio is increased above 1.2. This implies that using the vertical stiffness of the system can allow an advantageous phase difference between the oscillating water column and structure.

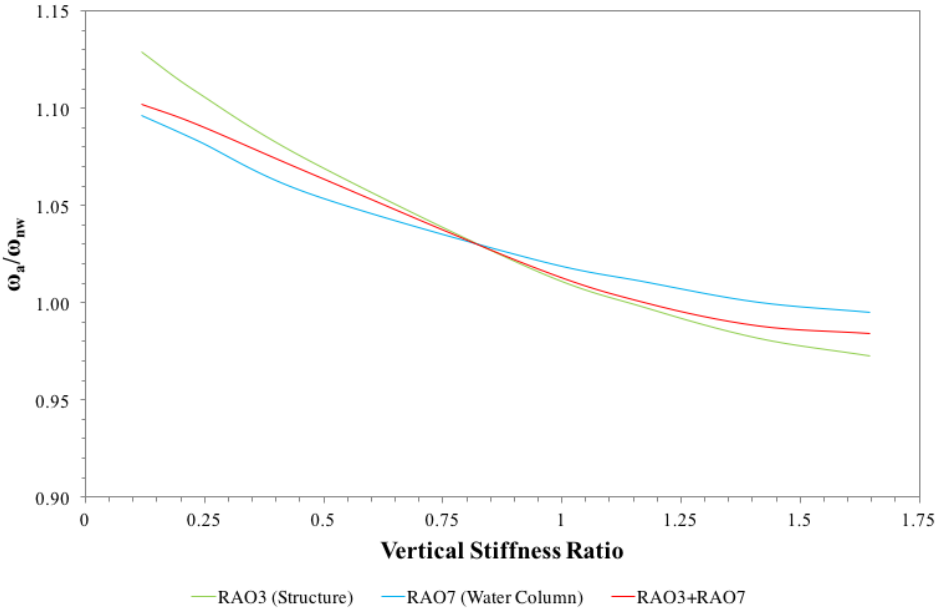

Figure 4.43: Location of the maximum heave RAO (forcing frequency ratio) as a function of the vertical stiffness ratio

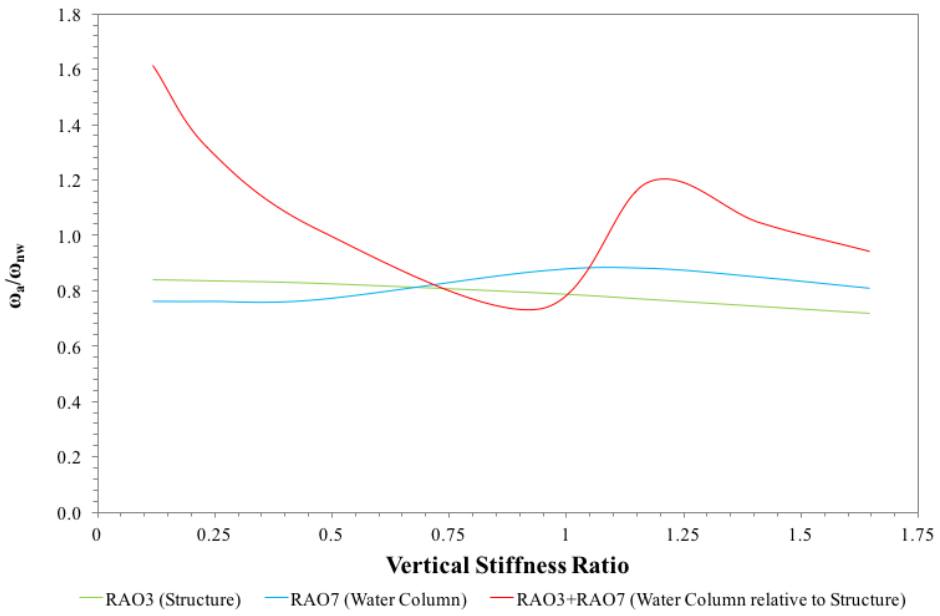

Figure 4.44: Location of the maximum phase angle (forcing frequency ratio) as a function of the vertical stiffness ratio

Specifying a vertical stiffness ratio range is essential to the design of an optimal system. Figure 4.41 and Figure 4.42 highlight that vertical stiffness ratio values less than one are more favourable than values greater than one because the RAO and the phase angle of the water column with respect to the structure is increased. The RAO value remains elevated for vertical stiffness ratio values from approximately 0.4 to 1. Figure 4.43 and Figure 4.44 show that the locations of the peak RAOs and phase angle do not experience much variation (~5%) over the range of vertical stiffness ratios investigated. This small variation is likely to be nullified when the system is placed in a wave spectrum as the variation in the wave spectrum will be greater than this.

4.4.4 Horizontal Stiffness

The surge RAO of the system is not responsible for power production. With this in mind the aim of this investigation was to develop horizontal stiffness guidelines that reduce the surge RAO of the structure. Specifying a vertical stiffness is likely to also cause a horizontal stiffness in the system. The effect of horizontal stiffness on the surge RAO was investigated to ensure large surge RAOs are avoided. The surge analysis was undertaken by adjusting the surge stiffness value in the WAMIT force control file. Various values ranging from 25 N/m to 10,000 N/m were simulated. The vertical stiffness was tested from 100 N/m to 1400 N/m. The surge response (RAO1) was plotted against the forcing frequency ratio and the output can be seen in Figure 4.45.

As the horizontal stiffness is increased, the surge RAO of the system is reduced; however, the forcing period at which the maximum point of the RAO occurs also reduces. This means that as the stiffness of the system increases the RAO of the system at wave periods likely to be experienced, around a forcing frequency ratio of one, actually increases rather than decreases.

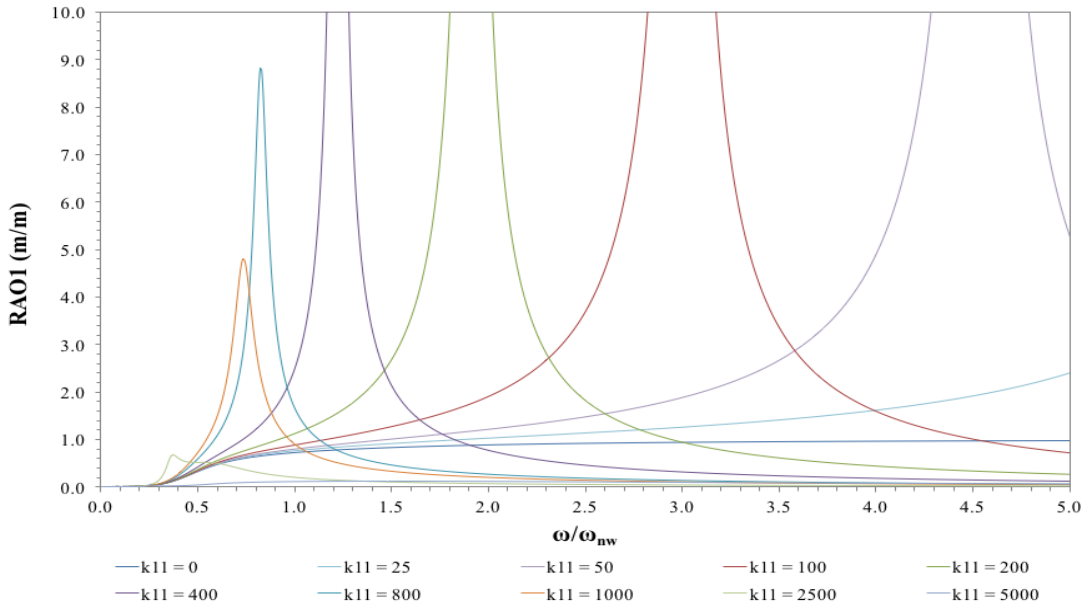

Figure 4.45: Surge response of the structure at various horizontal stiffness values

The effect the horizontal stiffness has on the surge RAO of the structure is seen in Figure 4.46. Figure 4.46 plots the surge of the structure against the horizontal stiffness ratio. The horizontal stiffness ratio, calculated in the same manner as the vertical stiffness ratio, is the horizontal stiffness divided by the value of vertical stiffness that corresponds to the minimum

water column heave RAO. Since the structure stiffness is likely to be provided by the same mooring line, this method allows for a comparison between the optimal vertical and horizontal stiffness of the mooring system. Figure 4.46 has two plotted functions because the surge RAO of the system reduces significantly at higher horizontal stiffness ratios.

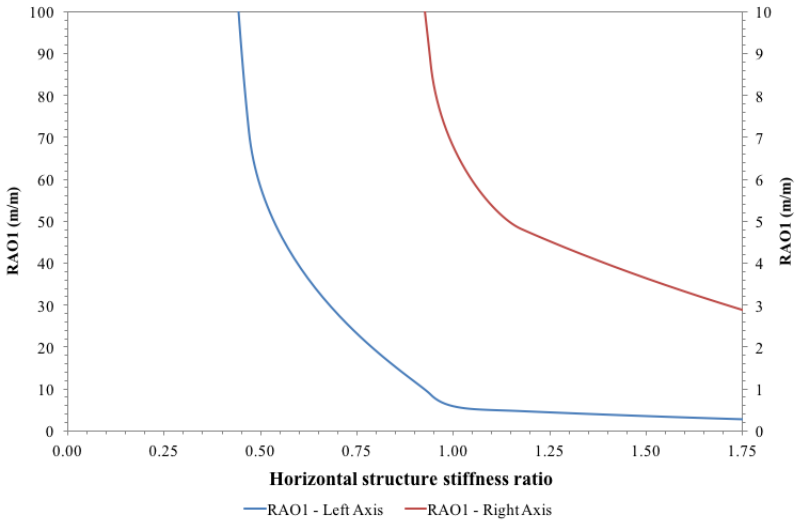

Figure 4.46: Maximum surge RAO as a function of the horizontal stiffness ratio

Further investigation about where the maximum RAO of the system occurs was undertaken and the result is seen in Figure 4.47. Figure 4.47 has also used two functions because of the sharp decrease in the maximum RAO values at larger horizontal structure stiffness ratios. Figure 4.47 provides evidence that the very large RAOs experienced by the structure at low horizontal stiffness ratios are very unlikely to occur as these large surge values only occur at wave forcing periods thirty to forty times that of the water column natural period.

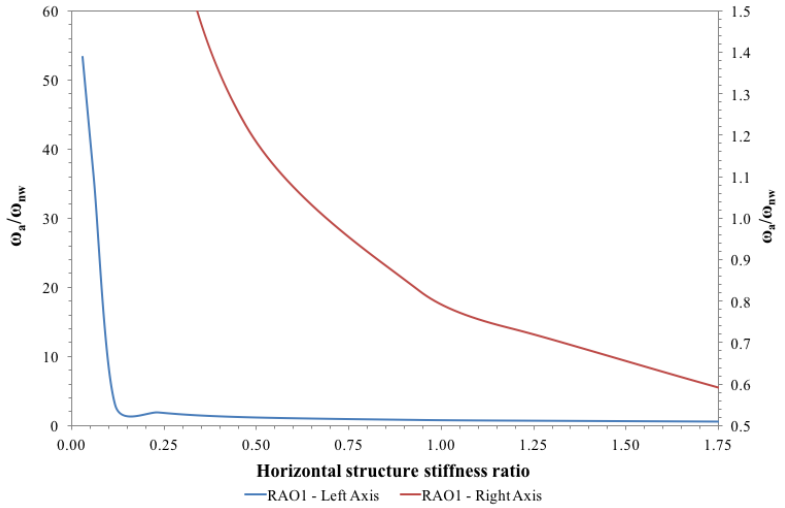

Figure 4.47: Forcing period ratio location of the maximum surge RAO

Figure 4.48 restricts the domain of the function to forcing period ratios between 0.9 and 1.1, and between 0.5 and 1.5. As the horizontal stiffness ratio is increased so does the expected structure surge RAO. This trend continues until the horizontal structure stiffness ratio is approximately one. Once the horizontal structure stiffness ratio increases past one there is a sharp initial drop in the surge RAO followed by a gradual reduction as the stiffness ratio is further increased. Comparison of the difference between the two domain restrictions shows that for sea states with a larger standard deviation in the wave period, larger surge displacements are expected. This characteristic will need to be accounted for during the design phase of the structure.

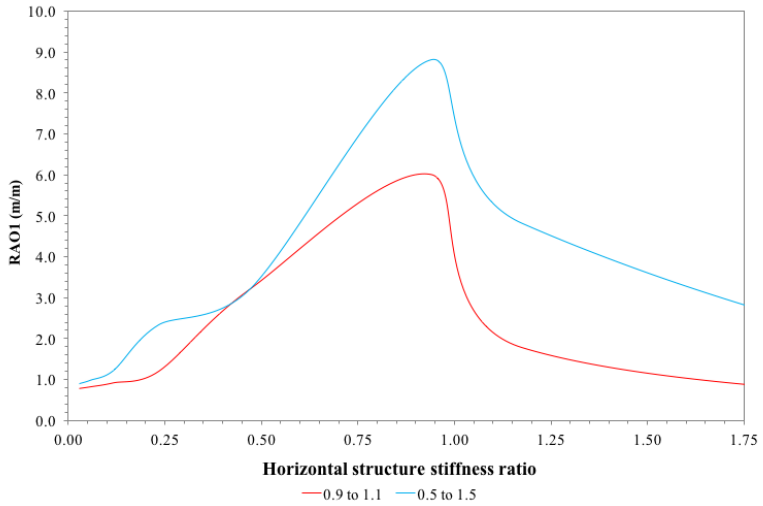

Figure 4.48: structure surge RAO over a restricted forcing period domain as a function of the horizontal stiffness ratio

The surge RAO of the system is not responsible for power production. With this in mind the aim of this investigation was to develop horizontal stiffness guidelines that reduce the surge RAO of the structure. Reduced surge excursion will result in lower mooring forces and a structure with a more robust mooring system. Figure 4.48 highlights that a horizontal structure stiffness ratio less than 0.5 or greater than one is desirable given the mooring system can withstand the increased tension from stiffer mooring lines at higher stiffness ratios.

By combining this conclusion with the conclusion from the investigation into the vertical structure stiffness ratios the ideal mooring system will produce a vertical stiffness ratio of less than one, combined with a horizontal stiffness greater than one. This mooring system will have to be able to withstand the associated mooring tensions from such a setup.

4.5 Chapter Summary

This study makes three recommendations. The first recommendation is that the design target natural period for the water column should be approximately 10% lower than the peak frequency of the waves at the desired installation location. This design target natural period value is approximately equal to the undamped OWC natural period. Wave frequencies corresponding to the undamped OWC natural period produce a sizeable RAO response for the water column relative to the structure and, perhaps more importantly, will allow a phase difference between the movement of the structure and the water column.

The second recommendation is with regards to power take-off damping. It has been shown that varying the power take-off of the system can have a significant effect on the coupled responses of the structure and water column. The phase difference and RAO of the water column relative to the structure can be controlled to a certain extent, and the RAO of the structure can be minimised by adjusting the power take-off damping. Minimising the structure RAO might prove beneficial during unfavourable wave conditions. The results also show that there is a critical level of free surface or power take-off damping. At this critical damping, the heave RAOs and phase angle between the structure and water column are favourable for increased power production. A damping increase above the critical value is likely to result in a system with a lower power production capacity and a greater structure heave response; neither of these is wanted in such a system.

The final recommendation is with respect to the vertical and horizontal stiffness of the system. There exists a vertical stiffness value that corresponds to the maximum RAO of the oscillating water column. This vertical stiffness value has been named the critical stiffness value. The actual vertical and horizontal stiffness divided by the critical value will determine the stiffness ratio. An ideal power production system during favourable operational conditions would have a vertical stiffness ratio of less than one and a horizontal stiffness greater than one. Appropriate horizontal and vertical stiffness values are likely be a product of the mooring system and water plane stiffness; hence, the mooring system must be able to withstand the associated mooring tensions if it is to be used to increase the stiffness of the system.

Chapter 5 Optimisation of the WEC in the Time Domain

5.1 Introduction

This chapter introduces OrcaFlex and the analysis of wave energy converter systems using the fully nonlinear time-domain modelling program. This chapter considers the use of OrcaFlex to use the results obtained through the frequency domain package, WAMIT, and tests the applicability and sensitivity of the frequency domain results in the time domain using sinusoidal waves and wave spectra. This is undertaken through testing in the time domain beginning with sinusoidal waves and then moving on to wave spectra. OrcaFlex was chosen to complete the time domain simulations in this study for four reasons. The first was that the OrcaFlex is able to perform time domain simulations using wave spectra. This is needed to investigate the sensitivity of the conclusions drawn in the frequency domain using WAMIT. The second was due to an existing understanding of the software package. The third reason was that UOW has an ongoing license for the software package. The fourth reason was the very user-friendly graphical user interface. Other suitable packages, such as ARIANE, do exist but did not have the advantages of OrcaFlex.

As highlighted in Chapter 2, there are precedents for the use of WAMIT and OrcaFlex in the offshore renewable energy realm. Two projects have utilized WAMIT and OrcaFlex when testing in the time domain. Rhinefrank (2010) used a combination of WAMIT and OrcaFlex to investigate the feasibility of a novel point absorber wave energy device. Rhinefrank (2011) then used OrcaFlex to investigate a 1:7 scale model of a point absorber wave energy device. This was used for a performance and mooring analysis. To date, there are no known investigations of oscillating water column devices utilising a combination of WAMIT and OrcaFlex.

This chapter first presents the results of the investigation using single sinusoidal waves then the results of the wave spectra investigation. A case study is presented to assess the conclusions of the wave spectra investigation.

5.2 OrcaFlex

OrcaFlex is a finite element analysis program developed by Orcina (Orcina, 2015). OrcaFlex is a leading offshore marine system time domain analysis package. It is used mainly in the offshore oil and gas industry to perform static and dynamic analyses on offshore systems

including risers, moorings, and CALM and SPAR buoys. OrcaFlex also has military applications such as in ship-to-ship replenishments, helicopter landing systems, and floating protection booms and nets. OrcaFlex is also used in the renewable energy sector in applications including wave power systems, offshore wave farm installations, power take-off, and floating wind turbines.

OrcaFlex offers a full time domain solution capable of non-linear implicit and explicit analysis of full coupled vessels and mooring lines. OrcaFlex is able to analyse multi body setups including hydrodynamic coupling, tension, torsion, and bending. A screenshot of the model tested in this chapter can be seen in Figure 5.1.

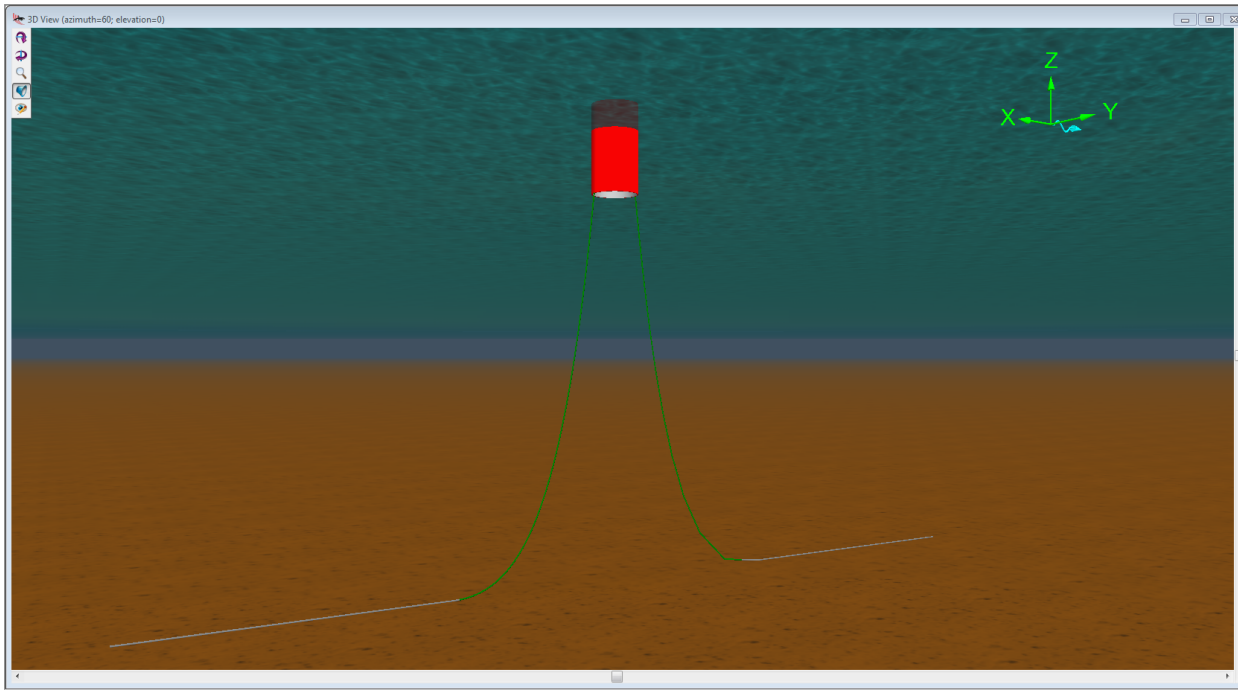

Figure 5.1: OrcaFlex user interface screenshot showing a floating oscillating water column device

OrcaFlex is able to provide a large range of results for every aspect of the model in question. A screenshot of the results selection pane is shown in Figure 5.2. The results used in this chapter include the time history of the heave displacement and velocity of the device and of oscillating water column, the time history of the vertical displacement of the sea, and the spectral density plots of these time history graphs. These results allow an investigation into how the dynamics of the structure affect the power output of the device. Chapter 6 makes use of the statistics regarding the tension in the mooring lines during unfavourable storm conditions.

Figure 5.2 highlights the extent of the simulation results available to the user. The user may select predefined time periods of the time domain results (upper right of Figure 5.2). The user may also select results plotted against results other than time. An example would be the mooring line tension as a function of surge. This option is seen in the left of Figure 5.2.

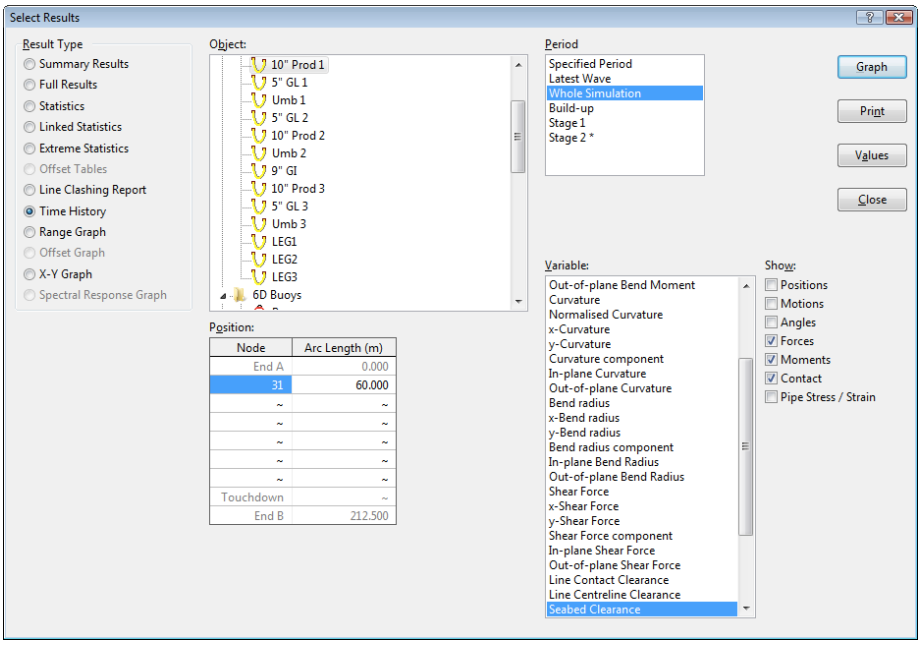

Figure 5.2: OrcaFlex results selection pane screenshot

5.3 Theoretical Understanding of OrcaFlex

5.3.1 Static Analysis

Static analysis is the first stage of analysis when using OrcaFlex. Static analysis serves two purposes. The first is to determine the equilibrium position of the system under all loading conditions. The second is to establish a starting point for dynamic analysis. The loading conditions include typical offshore forces such as weight, buoyancy, mooring forces, wind, current, and hydrodynamic drag. The static analysis consists of a number of iterative stages until equilibrium is established. This iterative process converges to give the static positioning of the components of the system. The iterative process is undertaken in the following steps:

1. The user defines the initial positions of the body and mooring lines. This also defines the initial position of the line ends.

2. The equilibrium position for each line is calculated with the ends of the line fixed.

3. The load is then balanced on each body or line and a new position is estimated.

Steps 1 to 3 are repeated until the out of balance load on each vessel and line is zero. The user may change the tolerance of this final value.

If the iterative process fails to converge the degrees of freedom within the system, the user may limit the tolerance to allow static equilibrium to be reached. This was not needed as all the models in this chapter converged within a short time.

5.3.2 Dynamic Analysis

A description of the dynamic analysis is provided to justify the use of the implicit integration scheme within OrcaFlex. OrcaFlex dynamic analysis in the time domain is a fully nonlinear solution. Each component of the system analysis (such as mass, damping, forces, and location) are evaluated at each time step. The time step integration is undertaken using both implicit and explicit integration. The user specifies the time steps and total run time. The default time step is set at 0.1 seconds. This has been kept constant for analysis in this present study. Both integration methods use a numerical time stepping algorithm to evaluate the loading and position of the vessel and mooring lines at each time interval. The final position at each time interval is then used as the starting position of the vessel and mooring lines for the subsequent time interval. OrcaFlex solves the following equation of motion at each time step.

$$\mathrm{M}(\mathrm{p},\mathrm{a}) + \mathrm{C}(\mathrm{p},\mathrm{v}) + \mathrm{K}(\mathrm{p}) = \mathrm{F}(\mathrm{p},\mathrm{v},\mathrm{t}) \tag{5.1}$$

Where

M(p,a) is the system inertia load

C(p,v) is the system damping load

K(p) is the system stiffness load

F(p,v,t) is the external load

p is the position vector

v is the velocity vector

a is the acceleration vector

t is the simulation time

Explicit integration is undertaken by calculating the forces and moments acting on each body and node rather than on a global scale. This means that simple inversion of a 3x3 or 6x6 matrix will find the solution. Solving for the acceleration by rearranging equation 5.1:

$$\mathrm{M}(\mathrm{p},\mathrm{a}) = \mathrm{F}(\mathrm{p},\mathrm{v},\mathrm{t}) - \mathrm{C}(\mathrm{p},\mathrm{v}) - \mathrm{K}(\mathrm{p}) \tag{5.2}$$

Once the acceleration at a particular time step is known then the velocity and position vectors at the next time (t+1) can be calculated:

$$v_{t+1} = v_t + \mathrm{d}t.\, a_t \tag{5.3}$$

$$p_{t+1} = p_t + \mathrm{d}t.\, v_t \tag{5.4}$$

where d*t* is the time step.

This process is repeated until the user-specified simulation time is completed. Because the body can move a long way in a short period, it is important for dt to be kept as small as possible. The value of dt is determined by balancing the time required for the simulation with the maximum possible time step that still allows convergence.

Implicit integration utilises the generalised-α scheme. This method evaluates the position and velocity vectors at the end of the time step. This method requires an iterative solution, this these much larger time steps are tolerable. The larger time steps often allow for a quicker solution. The simulations used in the present study were run using explicit integration. This method was chosen because it is not susceptible to the inaccuracies encountered during the implicit method when choosing too large a time step.

Dynamic analysis in OrcaFlex consists of multiple stages; the first being the ramping stage. The system forces are slowly introduced in this stage in an effort to reduce the transient response of the system. Orcina set the default time for the ramping stage at eight seconds. The simulations considered in this chapter have kept this value for the transient period. Another reason multiple stages are used is to allow the introduction of changes, and to allow for adjustment to the system at desired time periods (such as a line releasing after ten seconds). The second stage, or testing stage, has been set to last for 10800 seconds or three hours as this is the standard defined by the DNV standards.

5.4 Development of OrcaFlex Models

The structures tested in OrcaFlex were developed from data imported from WAMIT. This data includes the frequency dependent added mass and damping coefficients, the RAOs, and forces acting on the structure and water column. OrcaFlex does not allow data from systems with more than the conventional six degrees of freedom to be imported for one vessel. To overcome this, the system is modelled as two vessels. One vessel will represent the water column and the other will represent the structure. The RAOs for each structure are drawn from the single RAO output from WAMIT, which produces an RAO output for each specified degree of freedom.

The setup includes the regular six degrees of freedom for the structure and the additional heave degree of freedom of the water column giving a total of seven degrees of freedom. To overcome the issue of having seven degrees of freedom the heave RAO of the water column has been removed from the WAMIT RAO output to produce an RAO for only the structure. The removed water column RAO is saved as an additional file. This method allows the coupled dynamics of the system to remain intact despite reducing the system to two vessels rather than one. Each RAO file is imported into OrcaFlex separately and assigned to its respective vessel. This was achieved through the use of an automation macro and the computer software macro.

This validity of this method can be confirmed by comparing the imported RAOs of each vessel in OrcaFlex with the RAOs produced in WAMIT. Both data sets are plotted in Microsoft Excel. While it might seem obvious that the RAOs match, separation of coupled systems may lead to a neglect of some dependent movements, hence this check was undertaken. The heave RAO comparison for the structure and water column is seen in Figure 5.3 and Figure 5.4 respectively, and the phase angle RAO of the structure and water column is seen in Figure 5.5 and Figure 5.6 respectively. Figure 5.3 to 5.6 show that the isolated RAOs in OrcaFlex for each vessel match the combined RAO produced in WAMIT. Each Figure shows a perfect match over the period of tested wave periods. This confirms that the deconstruction of a single vessel system with WAMIT to a dual vessel system in OrcaFlex is possible. Figure 5.3 to 5.6 detail the response of a vessel with a draft of 12.3 metres, a structure diameter of 10.54 metres, and a water column diameter of 10 metres. The natural period of the structure is approximately 11.67 seconds and the natural period of the water column is approximately 8.75 seconds.

These values are slightly higher than the 8 seconds specified in Chapter 4. This is due to the presence of power takeoff damping. The natural period of the structure is within the typical natural periods of real ocean waves. Examples of this are seen in Table 2.6. This system would be target for a sea with an average period of 8.75 seconds. The ratio of the structure to oscillating water column natural period for this model is 1.33.

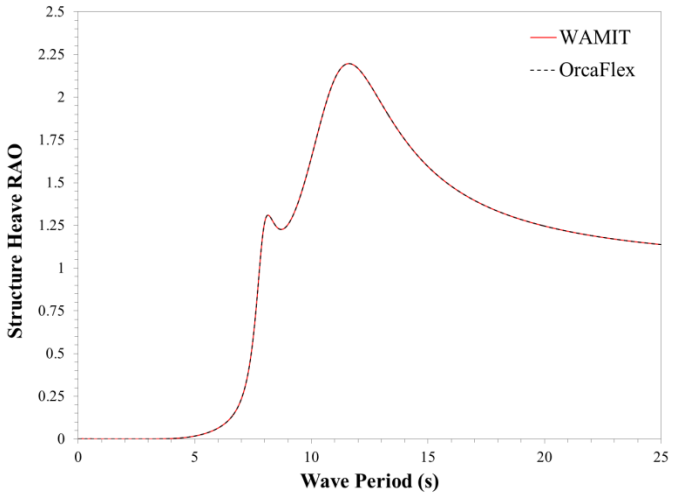

Figure 5.3: WAMIT vs. OrcaFlex heavy RAO comparison for the floating structure

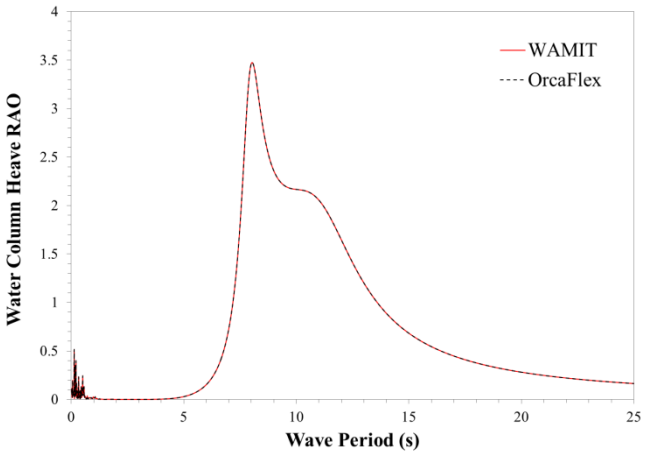

Figure 5.4: WAMIT vs. OrcaFlex heave RAO comparison for the water column

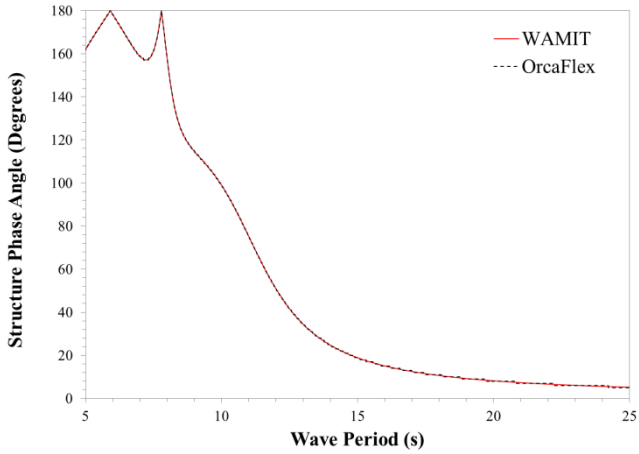

Figure 5.5: WAMIT vs. OrcaFlex phase RAO comparison for the floating structure

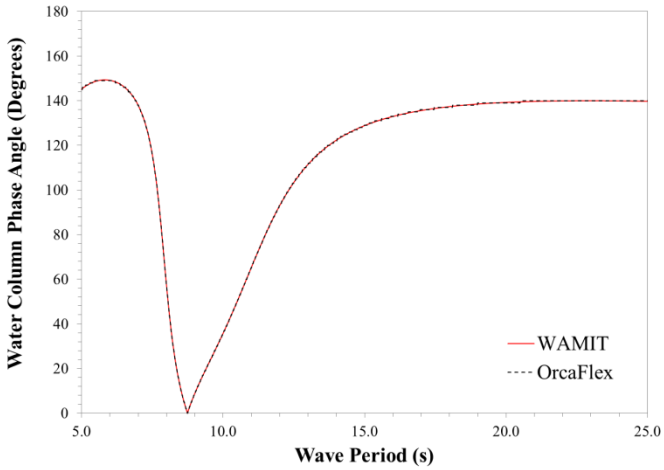

Figure 5.6: WAMIT vs. OrcaFlex phase RAO comparison for the water column

5.5 Method of OrcaFlex Testing

OrcaFlex testing takes models developed in the WAMIT from the frequency domain to the time domain. Testing is undertaken with single sinusoidal waves and with typical wave spectra. The wave spectra will test how the model is expected to perform in a real ocean setting and confirm how sensitive the conclusions drawn in WAMIT are to changes in wave frequencies. This was done to assess whether the frequency domain results from WAMIT are applicable in the time domain when using wave spectra rather than single frequency waves. The initial model established in WAMIT is the optimal operational state model. This model

has been optimised for power output production in a suitable sea state. These calculations were completed in Chapter 3.4.

5.6 Instantaneous Power Production and System Efficiency

The instantaneous power production as a function of time is derived below. This is an extension of the work performed by Sheng et al. (2012) on fixed oscillating water column devices in single sinusoidal waves.

The relative motion and hence velocity of the water column and structure is largely responsible for the production of power within the system. If the heave velocity of the structure with respect to the still water level is denoted as V_{Hs} and the water column heave velocity with respect to the still water level as V_{Hw}, then the relative velocity between the two degrees of freedom is expressed as:

$$V_H = V_{Hs} - V_{Hw} \tag{5.5}$$

This system assumes that the air is incompressible. According to Folley and Whittaker (2005) who have included compressible air in an OWC device, this may lead to a slight overestimate of the power production of this model as the potential additional natural frequency of the system is removed.

This incompressible assumption means that the continuity equation for the airflow holds true. That means that the air moving through the turbine (modelled as an orifice) must be moving at the same flow rate as the air that is initially moved by the water column. This relationship allows the following to hold true:

$$\mathrm{Q(t)} = \mathrm{C_q A_1 V_1(t)} = \mathrm{A_0 V_H(t)} \tag{5.6}$$

where C_q is the flow loss coefficient for the orifice, A_1 is the area of the orifice, V_1 is the velocity of the airflow through the orifice, and A_0 is the area of the water column.

Using Bernoulli's principal, the pressure drop across the orifice can be expressed as:

$$\Delta p(t) = \frac{1}{2}\rho_a V_1^2(t) = \frac{\rho_a}{2C_q^2}\left(\frac{A_0}{A_1}\right)^2 V_H^2(t)\mathrm{Q(t)} = \mathrm{C_q A_1 V_1(t)} = \mathrm{A_0 V_H(t)} \tag{5.7}$$

where ρ_a is the density of air.

This leads to an expression for the power extraction by the orifice as a function of time:

$$P(t) = \Delta p(t) \times Q(t) = \frac{\rho_a A_0}{2C_q^2}\left(\frac{A_0}{A_1}\right)^2 |V_H^3(t)| \tag{5.8}$$

To equate different systems and wave conditions, the power extracted needs to be compared to the power available for extraction. The power available for extraction is equal to the power available in each passing wave and is easily calculated when dealing with sinusoidal waves by integrating the power extracted over one wave and dividing this value by the power of that wave. The energy flux of such a wave is found using (Herbich, 2000):

$$E = \frac{\rho_w g^2}{64\pi} H^2 T \tag{5.9}$$

where H is the wave height, T is the wave period, g is the acceleration due to gravity, and ρ_w is the density of the wave fluid.

The efficiency ratio, η, is determined by dividing equation 5.8 by the energy of the wave calculated using a modified version of equation 5.9. Equation 5.9 has also been weighted by multiplying the average energy per wave by the length of the test period (t_2-t_1) divided by the peak wave period of the wave spectrum in question. This provides the average wave energy available for each wave in a spectrum over a given test period. This means that the power from spectrums with fewer waves in a given period is not underestimated. This equation is seen in equation 5.10.

$$\bar{E} = \frac{\rho_W g^2}{64\pi} H_S^2 T_P \times \frac{t_2 - t_1}{T_p} \tag{5.10}$$

The dimensionless efficiency ratio can then be expressed as:

$$\eta = \frac{\bar{P}}{\bar{E}} = \frac{64\pi}{T_P \rho_W g H_S^2 (t_2 - t_1)} \int_{t_1}^{t_2} P(t)\, dt \tag{5.11}$$

The power production metrics are used to evaluate the system under different wave conditions.

5.7 Operational State Testing

The definition of operational state testing is the testing of the vessel during favourable power production sea conditions. The primary objective of this testing is to determine the optimal system for power production. This optimal device will be determined by efficiency ratios. Characteristics of the device include the sizing of the structure, oscillating water column, and targeted wave frequency. The input file for these simulations is the modified output file from the WAMIT analysis. This file was modified to decouple the responses of the oscillating water column and wave energy device structure.

5.7.1 Regular Sinusoidal Waves

The first stage of time domain testing is to investigate the response of the system to sinusoidal waves. Three wave periods have been investigated. The first was chosen based on the WAMIT analysis conclusion that the wave period should be approximately 10% less than the water column natural period; this wave has a period of 7.875 seconds. The second wave has a period that matches the natural period of the water column (8.75 seconds) and the third wave has a period that matches the natural period of the structure (11.67 seconds). The second and third wave periods have been chosen as these periods coincided with the peaks of the RAO outputs of Chapter 4. All waves have amplitude of 0.5 metres and a wave height of 1.0 metres. This allows extrapolation of the data to waves of varying heights assuming minimal non-linear effects. The time domain history for each vessel and the wave history are produced in OrcaFlex. A heave velocity comparison graph for each vessel is also produced. These results confirm the conclusion from the WAMIT investigation and sheds light on why it may not be best to aim to produce a structure with a water column natural period that matches the forcing period.

5.7.2 Time Domain Response

The time histories of the vessels subjected to single sinusoidal waves are seen in Figure 5.7, Figure 5.8, and Figure 5.9. Figure 5.7 has a forcing period equal to 10% less than the natural period of the water column, Figure 5.8 has a forcing period equal to the natural period of the water column, and Figure 5.9 has a forcing period equal to the natural period of the structure. The phase lag and relative RAO between all three degrees of freedom is of importance here. A favourable phase difference (~90°) between the oscillating water column and structure and

a large oscillating water column and structure heave compared to the wave will likely highlight the setup of the optimal system. A summary of the amplitudes and phase angles are seen in Table 5.1.

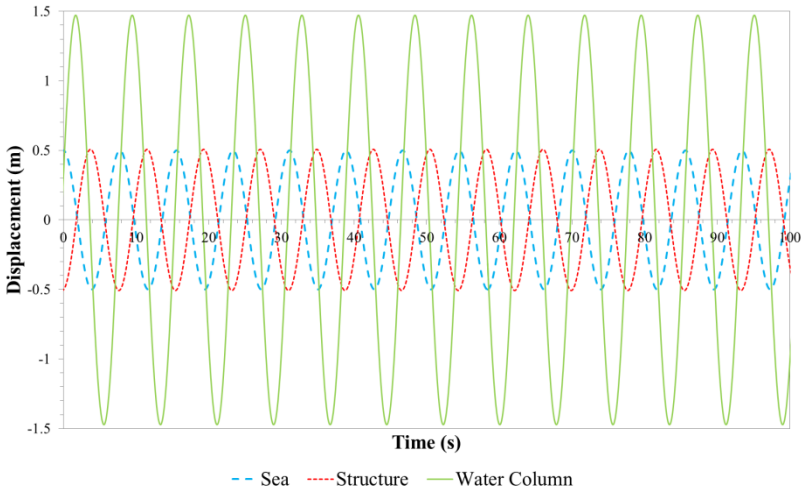

Figure 5.7: Time history for a sinusoidal wave with a period equal to 10% less than the water column natural frequency (T = 7.875s)

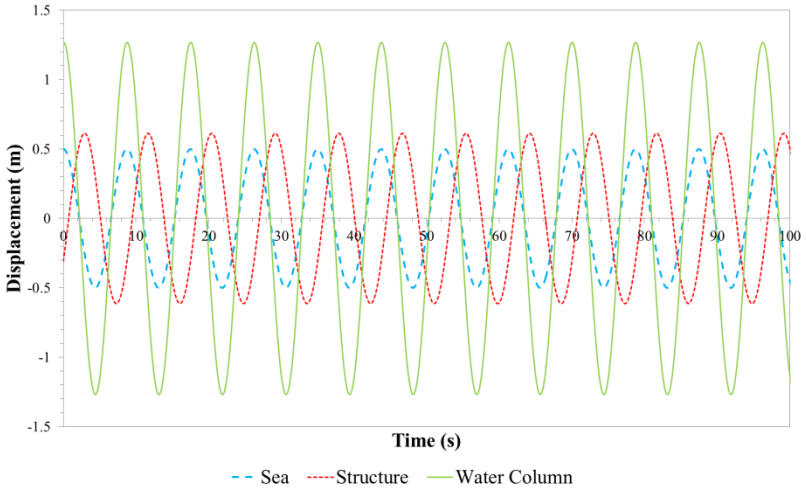

Figure 5.8: Time history for a sinusoidal wave with a period equal to the natural period of the water column (T = 8.75s)

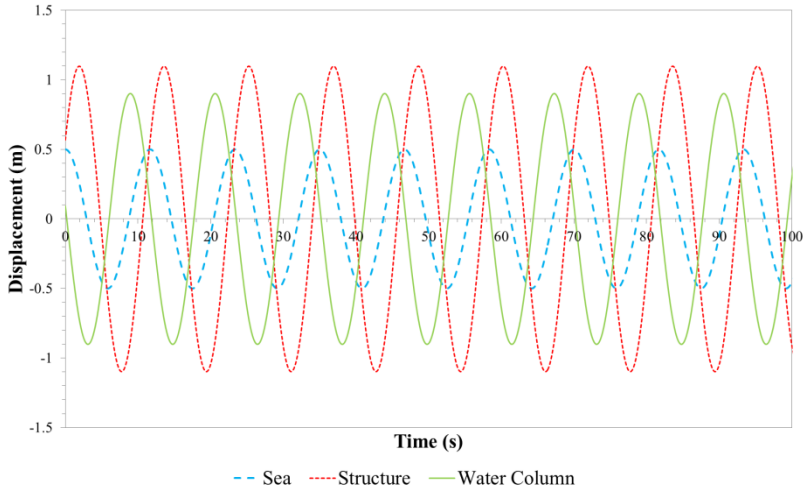

Figure 5.9: Time history for a sinusoidal wave with a period equal to 1.3 times the natural period of the water column which is equal to the natural period of the structure (T = 11.67s)

Table 5.1: Summary of aplitudes and phase angles for a sinusoidal wave analysis

	Amplitude of oscillation			**Phase angle w/ respect to the wave**	
Forcing period ratio	**Sea**	**Structure**	**Water column**	**Structure**	**Water column**
0.9	0.5	0.5	1.5	180	90
1	0.5	0.6	1.25	80	0
1.3	0.5	1.1	0.5	85	45

The heave response of each vessel was greater when the forcing period matched its natural period compared to matching the natural period of the other vessel; however, the response was even greater when the forcing period matched the recommendation from the WAMIT frequency domain analysis (10% below the natural period of the oscillating water column). Figure 5.7 shows that the water column experienced a heave response of approximately three times (1.5 compared to 0.5) the wave height while the structure showed a response approximately equal to the wave height. Also highlighted in this response is the phase difference between the structure, wave, and water column. The water column is approximately ninety degrees out of phase with the structure and the wave while the structure is 180 degrees out of phase with the forcing wave. These phase angles suggest the water column is in resonance with the forcing wave and the structure.

Figure 5.8 also shows a large comparative water column response when the system is subjected to a wave with a forcing period equal to the natural period of the water column.

However, there is no significant phase difference between the water column and forcing wave. There is a phase difference between the structure and wave and also between the structure and oscillating water column. This difference is approximately 80 degrees. There is also an increase in the structure RAO at the forcing frequency. This structure RAO increase and water column decrease without a favourable phase difference will reduce the power output potential of the system.

Figure 5.9 shows that when the natural period of the driving force matches the structure, the heave response of the structure is greatly increased. It is now approximately double the wave height and the response of the water column has been reduced by the same extent as the structure heave has been increased. Despite this unfavourable change in RAOs there is now a phase difference between all three degrees of freedom that is different to that seen in Figure 5.8.

Comparison of each forcing period shows that a forcing period that is approximately 10% less than the water column natural period may be more beneficial for producing a system with greater power output. It may also provide for a system that is more robust in storm conditions when compared to systems subjected to waves with forcing periods equal to the natural period of the water column or structure. This forcing period ratio corresponds to the undamped natural period of the oscillating water column. The responses shown here are in agreement with the expected responses shown in Figure 5.4 to Figure 5.6.

Comparing the difference in heave reponses of each system highlights this fact; the large increase in the structure response at a forcing period of 11.67 seconds is accompanied by only a small decrease in water column repsonse. It may be more beneficial to the integrity of the system to reduce the structure response. This will subject the mooring lines to lower levels of tension at the extreme ends of movement.

5.8 Structure-Column Velocity Functions

This theory was undertaken to develop an understanding how the heave velocity of the structure compares to the heave velocity of the water column and the same point in time. This is done because the difference in these velocities is directly proportional to the power output of the wave energy device. Parametric equations were chosen because they allow a direct comparison without the need for the time variable.

5.8.1 Theory

Further investigation of the relative motion of the water column and structure was conducted. The water column and structure are expected to respond to the sinusoidal wave force in a sinusoidal manner. Hence the OWC (x(t)), and structure (z(t)) time domain responses can be expressed as:

$$x(t) = A\cos(\omega t - \theta) \tag{5.12}$$

$$z(t) = B\cos(\omega t - \phi) \tag{5.13}$$

Where A and B are the amplitudes of oscillation, ω is the wave angular frequency, and θ and ϕ are the phase angles. Differentiating equation 5.12 and equation 5.13 produces the velocities of the oscillating water column and structure as a function of time. These are seen in equation 5.14 and equation 5.15 respectively.

$$v_x(t) = -A\omega\sin(\omega t - \theta) \tag{5.14}$$

$$v_z(t) = -B\omega\sin(\omega t - \phi) \tag{5.15}$$

Plotting the parametric relationship between equation 5.14 and equation 5.15 will produce an ellipse. This function will be referred to as the structure-column velocity function. Investigation into the major and minor axes of these ellipses was undertaken.

A perfect major axis of the structure-column velocity function for the system with respect to power production will be a straight line with a gradient of 135° measured anticlockwise from the positive x-axis (slope of -1) and intercept of zero. This system would have the water column always moving down while the system is always moving up, and vice versa. During this state, the oscillating water column and structure would be 180° out of phase. This state is impossible to reach in a practical setting as such a system would require two driving forces to achieve a 180° phase difference between the two degrees of freedom but systems exhibiting phase differences close to 180° are still achievable.

The worst case for this system, assuming the air is incompressible, is one that produces no power; this would be a major axis as a straight line with a gradient of 45° (slope of +1) and an intercept of zero. If this were the case, then the water column and structure would always be moving at the same speed in the same direction. This setup would have the oscillating water column and structure moving in phase. This will not cause airflow through the turbine

and, so, produce no power. The two functions are plotted in Figure 5.10. The figure is limited to 1.5 because this value is sufficient enough to illustrate the idea.

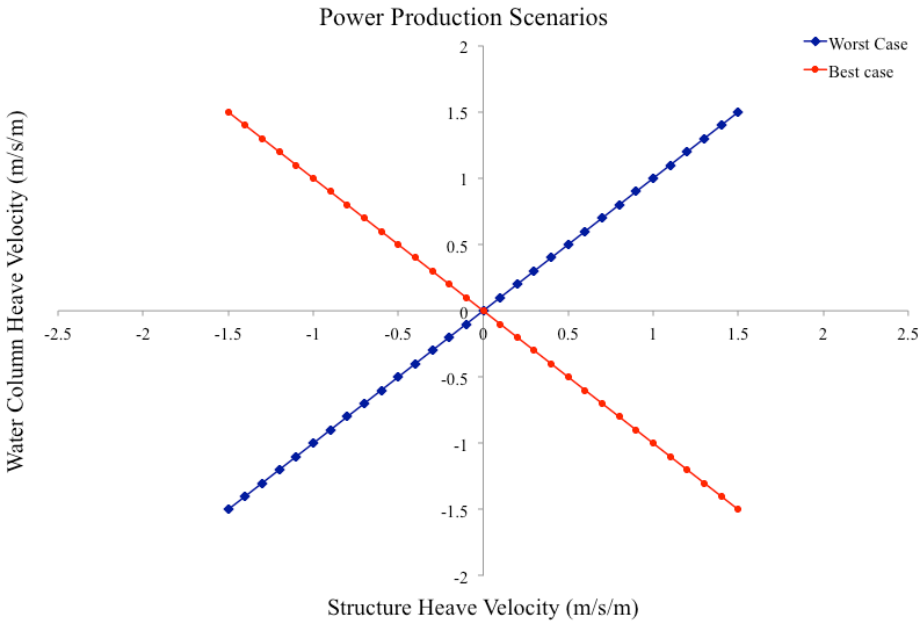

Figure 5.10: Best and worst case functions with respect to power production potential

The greater the length of the function the greater the maximum velocity of the water column and/or structure is. A higher relative velocity will produce more power. The simulations will be used to determine whether the length or gradient of the function has a greater influence and, therefore, is the more useful in predicting power output of an oscillating floating water column wave energy device.

The ideal function for a system with respect to structural integrity would be a vertical line passing through the origin. This will ensure that the water column still maintains movement while the structure remains motionless. A motionless structure and a heaving water column will ensure that air will still be passed through the turbine while keeping the tension on the structure's mooring system as low as possible. The motionless structure would arise from the inherent dynamics of the system rather than through the application of stiffness to the system such as tension legs or taut mooring lines. This would essentially be a fixed oscillating water column wave energy device. This scenario is not ideal for power production because it does not allow an increase in the relative motion between the oscillating water column and structure. These two functions are seen in Figure 5.11. There is no significance to a value of 1.5 in this graph. This value has been chosen to illustrate an idea.

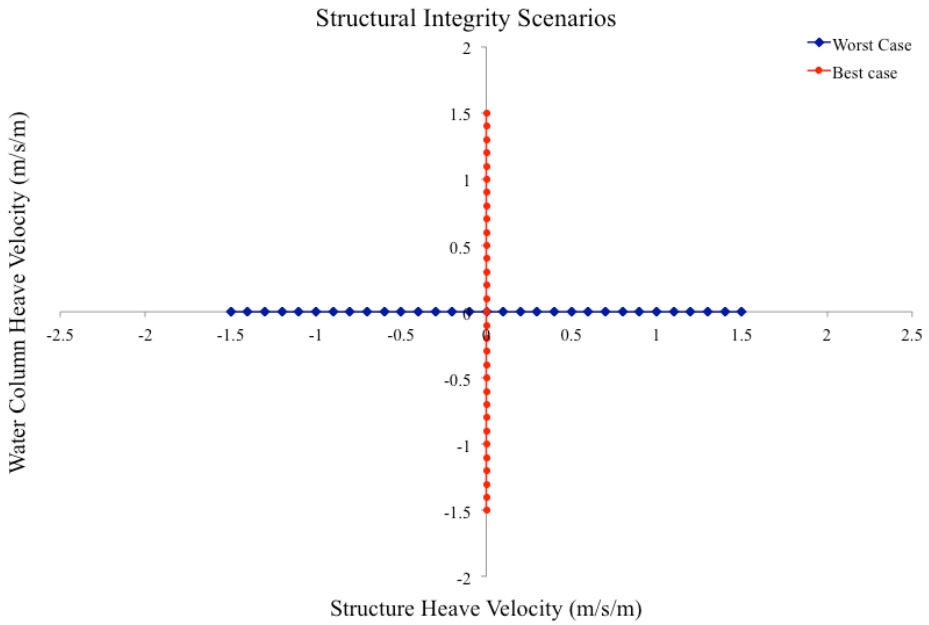

Figure 5.11: Best and worst case functions with respect to structural integrity

Finally, the further the function extends from the origin the greater is the maximum velocity of the water column or structure. A higher velocity will produce more power. The ranking of these parameters with regards to power production potential has yet to be identified. This ranking is determined in this chapter.

The structure-column velocity comparison functions produced in OrcaFlex are not straight lines but rather elliptical in shape (an example is seen in Figure 5.14). These can be characterised by the major (long) and minor (short) axes. Investigation into the effect of the length of the major axis, minor axis, and axes gradients has on the efficiency of the system has been conducted along with the effect the forcing frequency has on the aforementioned parameters.

5.9 Results and Discussion

Further investigation of the aforementioned metrics has been undertaken. Figure 5.12 details the time domain response of the structure (equation 5.12) and oscillating water column (equation 5.13) to a wave with a forcing period equal to the natural period of the water column ($T = T_w$ = 8.75s) and wave amplitude of 0.5 metres. This is the same data as seen in Figure 5.8. Figure 5.13 plots the power production (equation 5.8) of the system in the same time domain. Figure 13 shows how the power extraction of the system varies with time and relative structure and oscillating water column velocities. The power production is maximised when the difference in velocity is the greatest and is zero when the velocities are equal.

The parametric structure-column velocity comparison functions seen in Figure 5.14 are produced from the data in Figure 5.7, Figure 5.8, and Figure 5.9. Figure 5.14 is produced from data collected from different forcing wave periods. The parametric plot is elliptical in shape.

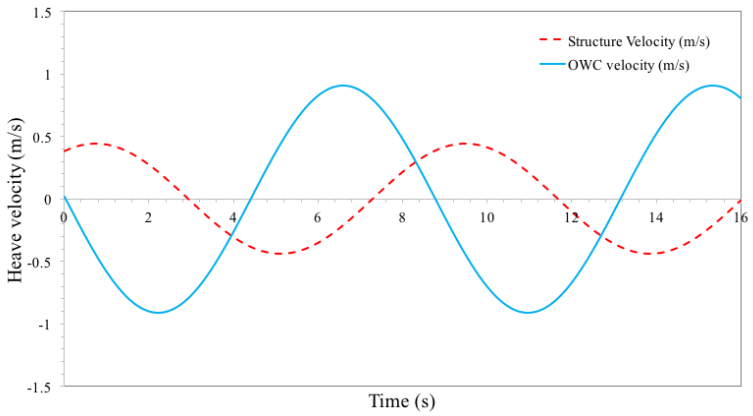

Figure 5.12: Time domain output for *T=Tw*

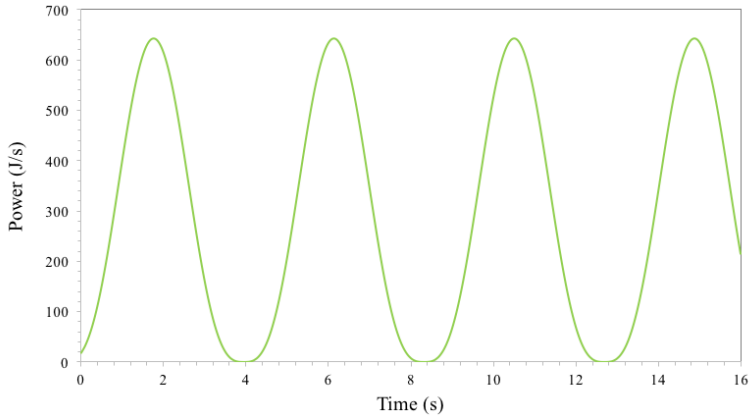

Figure 5.13: Power production of a system at *T=Tw*

These wave periods are expressed as a ratio of the forcing wave period (T) to the natural period of the water column (Tw). These ellipses can be characterised by the major (long) and minor (short) axes. Investigation into the effect of the length of the long axis, short axis, and axes gradients has on the efficiency of the system was conducted along with investigation of the effect the forcing frequency has on the aforementioned parameters.

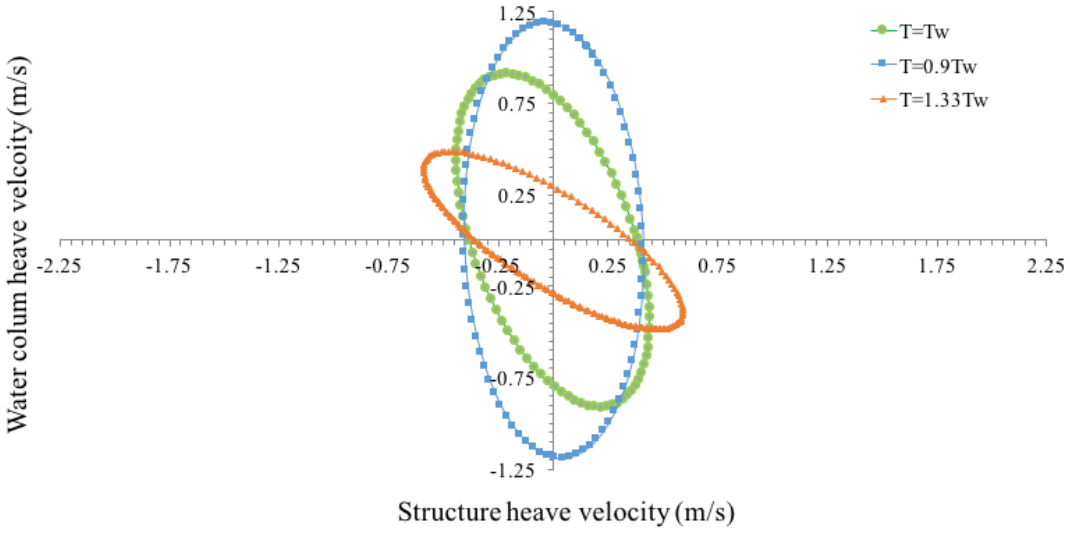

Figure 5.14: Water column heave velocity vs. structure heave velocity for sinusoidal waves with a forcing period ratios of 0.9, 1, and 1.33 and a wave height of 1 metre.

The lengths of the ellipse axes represent the maximum magnitude of the structure and water column heave velocities. The gradient of the major axis gives insight into the relative time difference between the peak of the heave velocities of the structure and water column. Investigation into power output as a function of the gradient of the long axis has also been undertaken in an effort to establish a link between the power output and structure geometry.

Figure 5.15 plots the major and minor axes lengths as a function of system efficiency, η, for the data collected over the range of the tested wave periods. The structure geometry and hence dynamics has been kept constant over all wave periods. Figure 5.15 shows a strong (R^2>0.9) linear correlation between the length of the respective axes of the ellipse and the expected efficiency of the system. The physical interpretation of this is that the larger axis length allows for more chance for a larger difference in heave velocity between the oscillating water column and floating structure regardless of the phase angle between the two oscillating peaks. A greater velocity difference allows more power to be extracted from the system and, hence, a greater system efficiency.

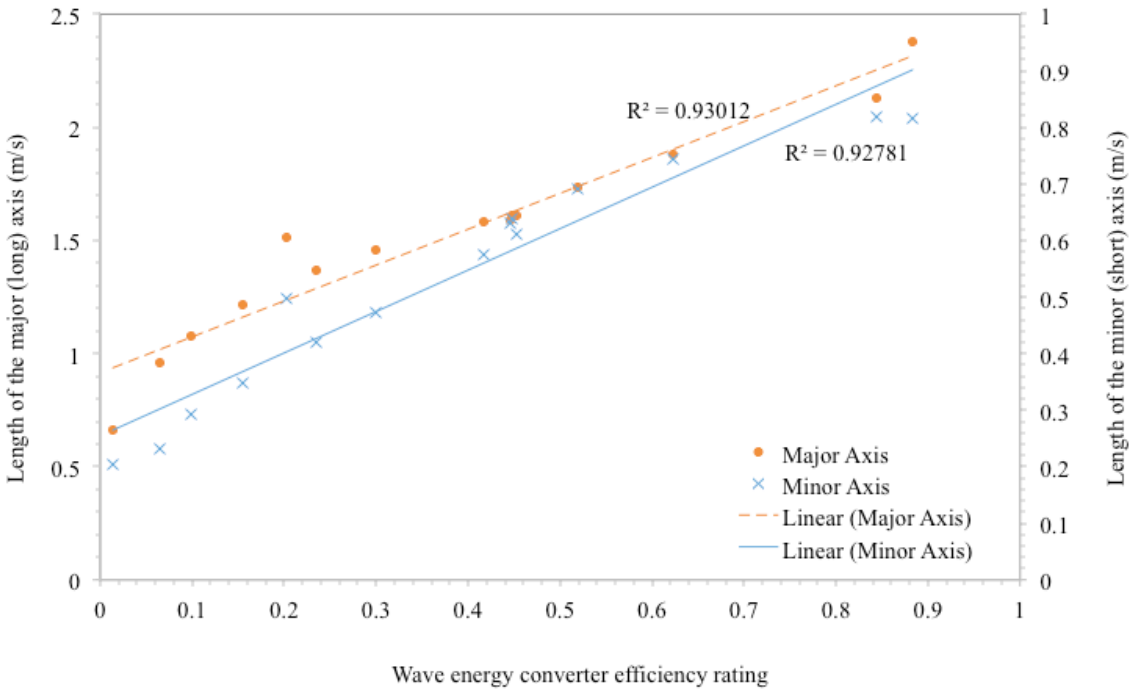

Figure 5.15: Axes length as a function of efficiency▄Efficiency calculated using eq 5.11.

This establishes that increasing the lengths of the axes leads to a linear increase in system efficiency. To understand which forcing frequency provides the greater axes lengths the axis length values have been plotted against the ratio of the forcing frequency to water column natural period. This is seen in Figure 5.16. Figure 5.16 shows a peak in both axes lengths at a forcing frequency ratio of approximately 0.90. Values below this show a sharp decrease in efficiency while values above 0.90 reduce at a slower rate. There is a plateau at approximately 1.30 and this ratio corresponds to the natural period of the structure. These results indicate that forcing frequencies between the water column natural period and the structure natural period will produce the most efficient systems and that the peak in the axis length will occur at a forcing period ratio of 0.9. This is seen in Figure 5.16.

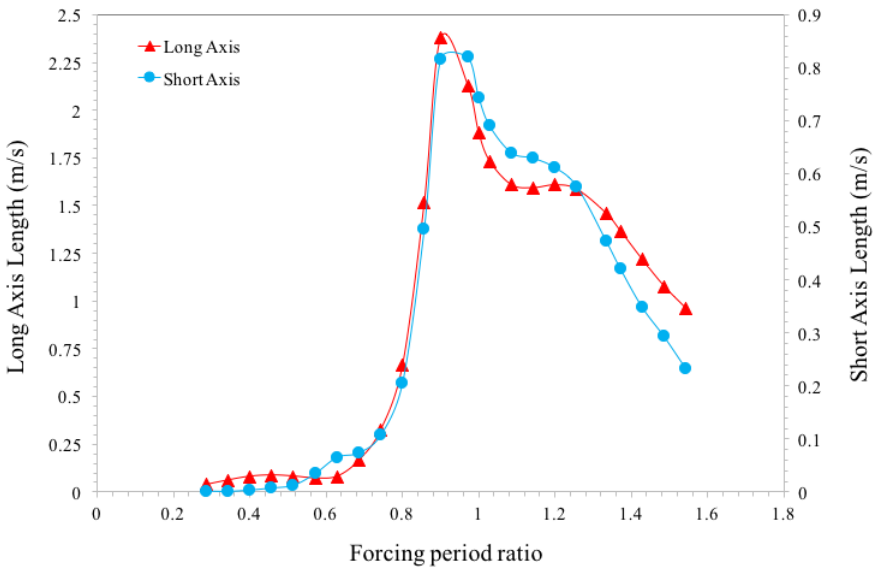

Figure 5.16: Axes lengths as a function of the forcing frequency ratio

The power output as a function of the gradient of the major axis is seen in Figure 5.17. The gradient of the major axis is measured in degrees with anticlockwise being positive and starting at the positive *x*-axis. Larger energy conversions were expected at gradients equal to 135° (slope of -1); however' a gradient of approximately 92° correlated to a higher energy conversion efficiency in this study. Gradient values less than approximately 92° show a sharp decline in system efficiency while gradient values greater than this show a drop in system efficiency to approximately 50% until a gradient of approximately 140°. Gradient increases above 140° show a gradual decline is system efficiency. Figure 5.17 suggests that an ellipse with a vertical (~90°) major, and hence a horizontal (~0°) minor, axis may lead to a more efficient system.

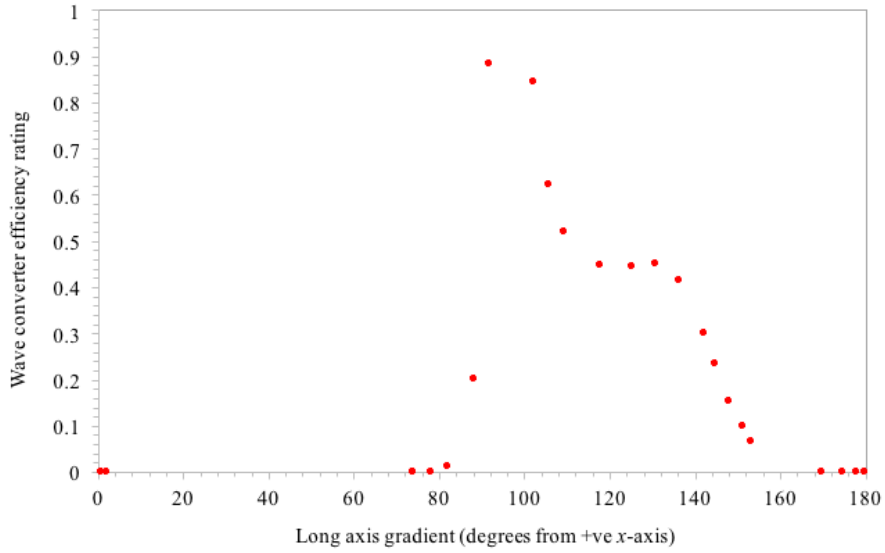

Figure 5.17: Wave energy converter efficiency as a function of the gradient of the long axis

Figure 5.18 plots the major axis length and the major axis gradient as a function of the efficiency of the system.

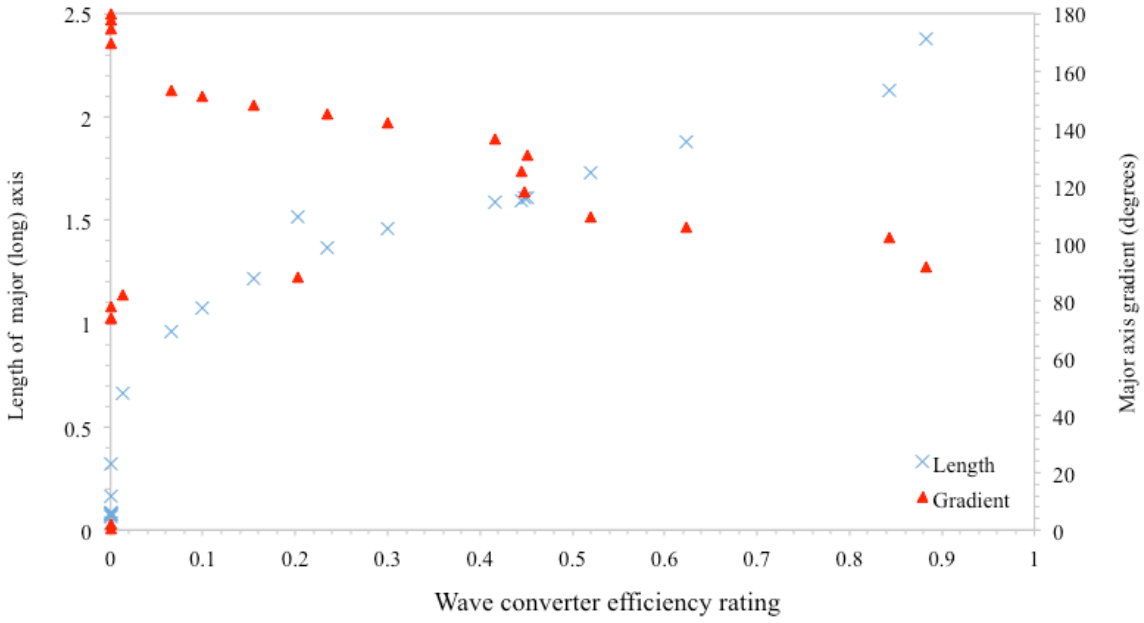

Figure 5.18: Efficiency as a function of major axis length and major axis gradient

Figure 5.18 shows that the optimal gradients occur at the maximum axis lengths. It cannot be concluded that the gradient of the axis has any bearing on the efficiency of the system or whether it is simply a function of the axis lengths. The data suggests that the axis length is the determining factor in system efficiency. This suggestion arises from the data in Figure 5.15.

Figure 5.15 suggests that larger major and minor axes will produce more power. The axis relative length is dictated by the proximity of the oscillating water column natural period to the forcing period of the wave. This inturn is dictated by the structure draft and inner diameter.

A thought experiment comparing a system with a major axis gradient of 90° and minor axis gradient of 0° will resolve this issue. This system could occur if there was not sufficient separation between the natural frequencies of the water column and the difference between the major and minor axis of an ellipse is the length. The larger axis is deemed the major and the smaller axis the minor. Take a system with a fixed minor axis length and major axis fractionally bigger than the minor axis. This system will have a major axis gradient of approximately 90°. Figure 5.18 suggests this is the optimal system. However, if this system is altered so that the major axis is now fractionally smaller than the minor axis the axes would effectively be swapped, producing a system with a major axis that has a gradient of 0°. Figure 5.15 suggests that the efficiency of the system would remain relatively constant given the lengths of both the major and minor axes also remain nearly constant. This leads to the conclusion that the gradient of the major and/or minor axis is not a key indicator of performance but is rather a characteristic of the ratio between the axis lengths.

5.10 Case Study

The conclusions regarding axis length and major axis gradients are tested using the model developed and detailed in Chapter 4. Comparing the plots in Figure 5.14 shows that matching the forcing period to the natural period of the vessel will result in a higher maximum velocity of that vessel. Key aspects of these three plots are compared using the axes of the ellipse.

The length of the major axis of the ellipse will serve as the design/performance indicator tool. The lengths are calculated by using the extreme points of the structure and water column velocity as the inputs to Pythagoras's theorem. The higher this value, the higher the potential for the relative velocity between the water column and structure to be high (given there is phase difference between the two). The lengths for the ellipses of Figure 5.14 are seen in Table 5.2.

Table 5.2: Major and minor axis lengths (m/s) at different forcing period ratios

Forcing period ratio	Major (long) axis length	Minor (short) axis length
0.9	2.040	1.709
1	1.622	1.513
1.3	1.421	0.5100

Using this metric, it is evident that matching the forcing wave period to a value 10% less than the water column natural period produces a more favourable system than the two alternatives because this system exhibits the largest axis lengths of the forcing periods tested. This result is in agreement with Figure 5.15. The wave with a forcing period ratio of 0.9 produces a system with a larger water column peak velocity, a smaller structure peak velocity, and more points where the structure velocity and water column velocity are opposite in magnitude. This leads to the conclusion that the system will be able to produce more power while ensuring a reduction in mooring line stress.

The power extraction for each wave sinusoidal wave is established by using the data points seen in Figure 5.14. These data points are from the data in Figure 5.7, Figure 5.8, and Figure 5.9. The absolute value of the power produced in each system as a function of time is seen in Figure 5.19.

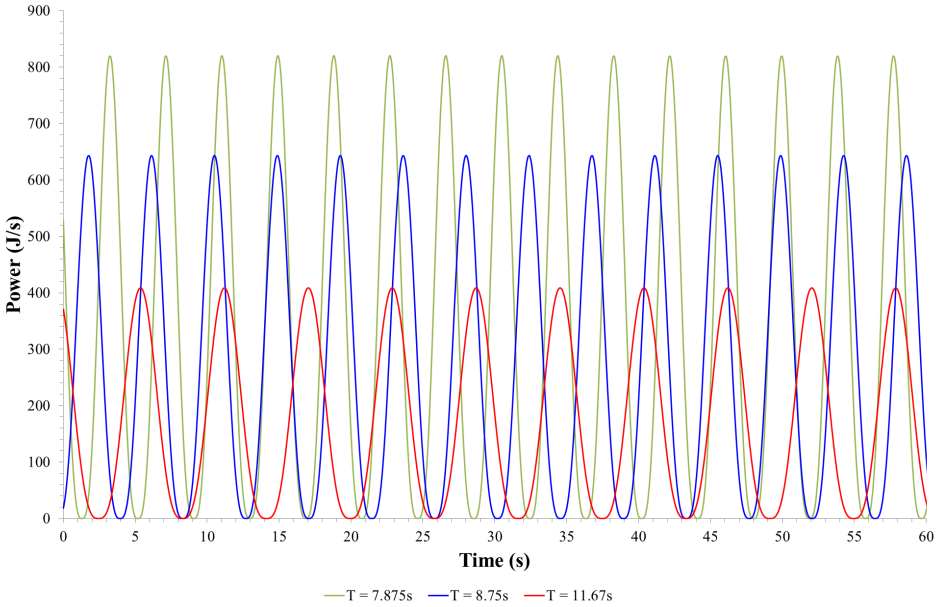

Figure 5.19: Power production as a function of time for each sinusoidal wave

By using the metrics established at the beginning of this chapter (equation 5.11), this power production graph can be quantified. The sinusoidal wave with a period of 7.875 seconds (forcing period ratio equal to 0.9) has an efficiency ratio of 0.8837, the wave with a period of 8.75 seconds (forcing period ratio equal to 1.0) was found to have an efficiency ratio of 0.6243 while the sinusoidal wave with a period of 11.67 seconds (forcing period ratio equal to 1.3) was found to have an efficiency ratio of 0.2973. These efficiency ratios confirm that greater power production is possible without maximum structure heave and occurs when the forcing period is equal to approximately 10% less than the natural period of the water column rather than at the natural period of the water column or structure (as suggested during the WAMIT analysis) and through investigation of the structure-heave velocity comparison function.

An FFT of each power production curve produced in the time domain for waves with periods ranging from 2.5 seconds (period ratio of 0.29) to 13.5 seconds (period ratio of 1.54) has been undertaken. This has been done to develop and envelope of the power production as a function of forcing wave periods. These waves all have a wave height of 1.0 meter. This has been undertaken to develop the power production envelope over a range of wave periods. This has been done to determine the wave period that corresponds to the highest power output. The power production as a function of wave period is seen in Figure 5.20. The different colours shown in Figure 5.20 correspond to the different period ratios tested.

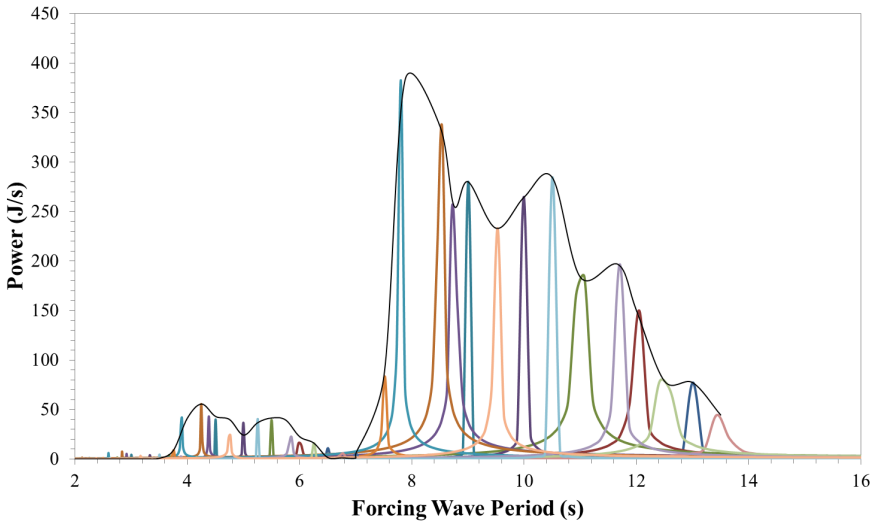

Figure 5.20: Power production as a function of forcing wave period with 1.0m wave height.

The peaks correspond to the various forcing periods of the forcing wave. Each wave produced a peak at the period of that wave. The black line is the envelope of the FFT outputs. Figure 5.21 plots this separately.

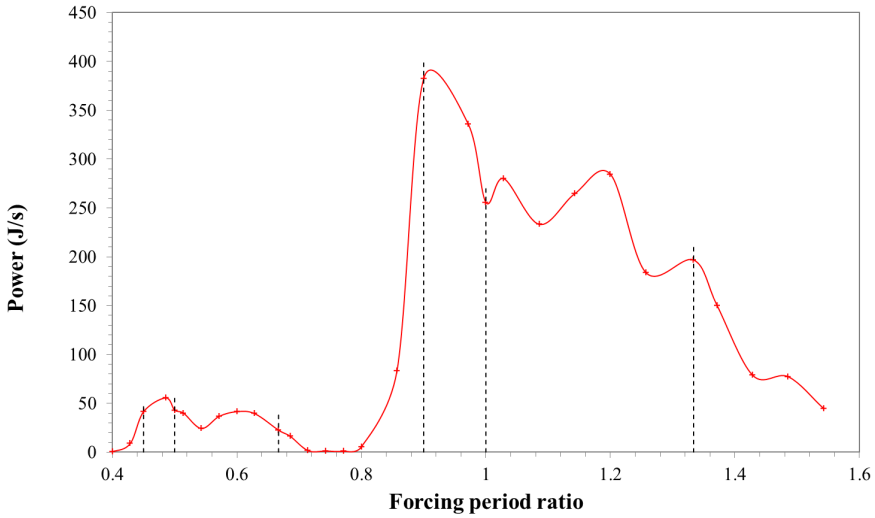

Figure 5.21: FFT envelope function

Figure 5.21 details the FFT envelope of the power output as a function of the forcing period ratio (wave period divided by oscillating water column natural period) rather than the absolute value of the forcing wave period. Additional vertical dotted lines indicate the key ratio values of 0.9, 1, and 1.33. These lines have also been plotted in the secondary power production area (period ratio <0.8) at values corresponding to half the ratio values. Figure 5.21 confirms the results from the axis investigation. That is that the optimum forcing period ratio is equal to 0.9 when using single sinusoidal waves. The maximum power production value is produced when the axis of the structure-velocity curve is maximised. This occurs

when single sinusoidal waves with a forcing period ratio of 0.9 are used. Figure 5.21 also confirms that forcing period ratios that lie between the value corresponding to 90% of the natural period of the oscillating water column (period ratio of 0.9) and the natural period of the structure (forcing period ratio of 1.33) produce more power than values falling either side of these limits. Figure 5.22 and Figure 5.23 plot the major and minor axis lengths against the power FFT envelope respectively. The power FFT envelope shows close agreement with both the axis lengths. This confirms that axis length is a valid indicator for performance for an oscillating water column wave energy converter.

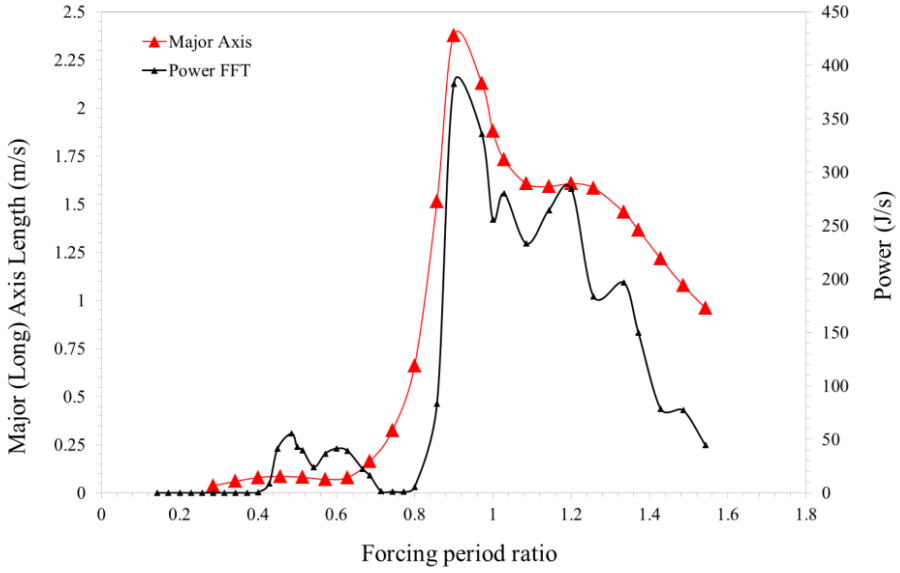

Figure 5.22: Major axis length and power production as a function of forcing period ratio

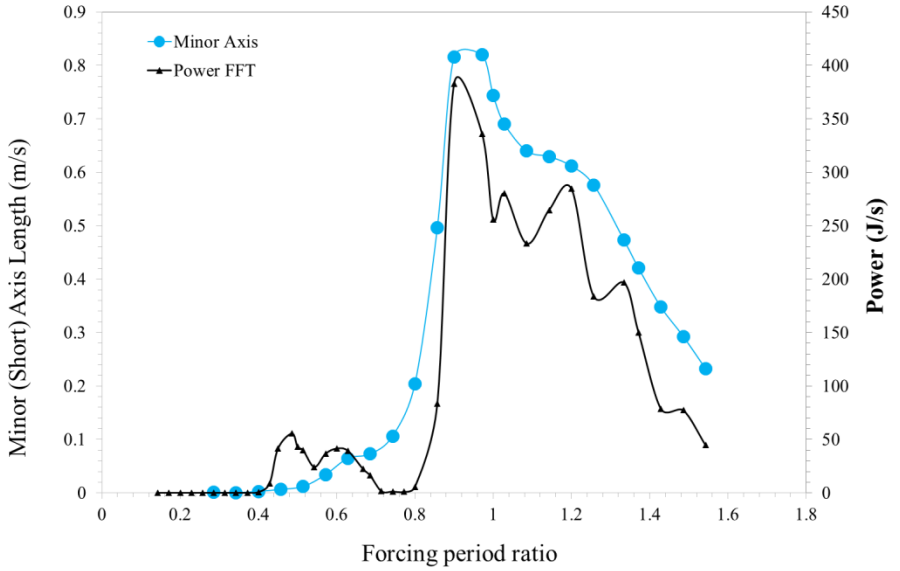

Figure 5.23: Minor axis length and power production as a function of forcing period ratio

5.11 Single Sinusoidal Wave Analysis Summary

This investigation has shown that the conclusions drawn in the frequency domain of WAMIT hold true in the time domain of OrcaFlex when investigating single frequency waves. Further investigation into the power output of the system was also conducted. The conclusions drawn from this investigation support the conclusion drawn from other aspects of the investigation. They also validate the metrics used to evaluate the suitability and opportunity for power production of the system when working in the frequency domain.

This heave velocity study has shown a strong linear relation between the power output of a floating oscillating water column wave energy device and the length of the long axis of the ellipse relating the heave velocity of the structure to the heave velocity of the water column. Therefore, the length of the long and short axes of the ellipse can be used as an indicator for potential OWC power production capabilities rather than using the expected heave of the structure or water column with respect to the forcing wave.

These theoretically derived results suggest that there is no discernible link between the gradient of the long axis of the ellipse and the power output production despite common sense suggesting a greater velocity differential in such a system. Using OrcaFlex, this investigation has shown that the magnitude of the relative velocity of the structure with respect to the oscillating water column or vice-versa is the key indicator of power output rather than a difference in displacement between either. This study has also highlighted that resonance between the structure and wave is not a key parameter for optimal power output as was outlined in the literature review.

Further investigation into the sensitivity of these conclusions to changes in wave frequency is needed to give an estimate on how such a system would behave in a practical setting. The next section of this chapter explores the response of the system to various wave spectra.

5.12 Wave Spectra

The current OrcaFlex model has been subjected to three wave spectra. The three spectra are ISSC spectra. The equation for this spectrum is shown in Chapter 3. These spectra are representative of wave conditions likely to be used during power production periods. The three spectra have a peak enhancement factor of one and a peak wave period corresponding to a value 10% less than the water column natural period (7.875s), the water column natural period (8.75s), and structure natural period (11.67s) respectively.

A time history, spectral density, and velocity differential graph for each wave spectrum has been produced. Analysis of these first three wave spectra is again used to test the conclusion that it is better to design a system with the water column natural period rather than the structure natural period matching the ocean waves, and to determine the sensitivity of the conclusions drawn when testing with single sinusoidal waves. This will also be used to determine the ideal operational state of the system. These wave spectra will be used to test the conclusions drawn from the single sinusoidal analysis testing. Wave spectra testing is necessary because the device will be subjected to this type of loading in a practical setting.

5.12.1 Time Domain Output

Figure 5.24, Figure 5.25 and Figure 5.26 detail the time domain response history of the ISSC wave spectra. Each test was run for 10800 seconds, or three hours. A random but consistent three-minute period (180 seconds) time period has been plotted. This has been done to allow the differences in phases to be observed. Plotting the full test would result in an unreadable graph. Figure 5.24 details the time domain response to a wave spectrum with a peak period of 7.875 seconds; this is equal to 90% of the water column natural period. Figure 5.25 details the time domain response to wave spectrum with a peak period of 8.75 seconds; this corresponds to the natural period of the water column. Figure 5.26 details the time domain response to a wave spectrum with a peak period of 11.67 seconds; this is approximately 1.33 times the natural period of the water column and is equal to the natural period of the structure. Because of the random nature of wave spectra it is difficult to quantify the response of the structure and water column from just the time domain output. To overcome this, the spectral density functions for each spectrum and the response of each vessel have been produced. Comparison of the spectral density functions will give a better insight into the extent and location of the heave motion of the vessels.

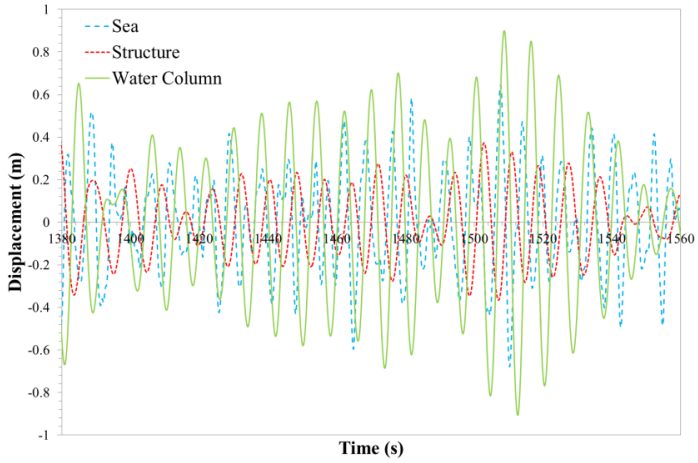

Figure 5.24: Time history for a ISSC wave spectrum with a 1m significant wave height and a peak wave period of 7.875s.

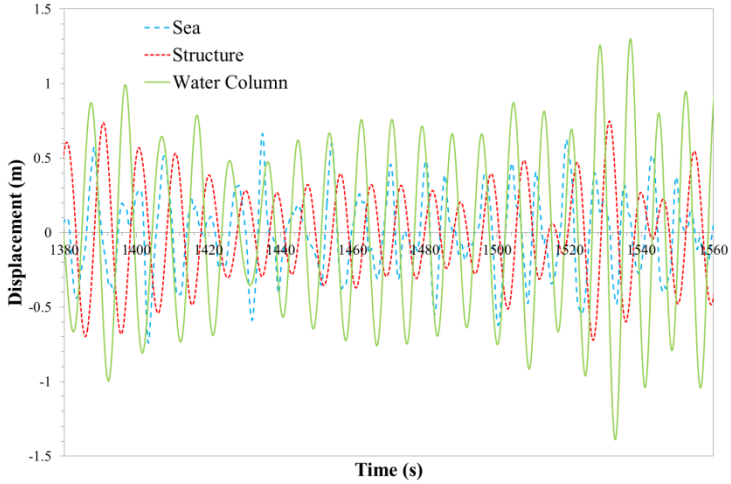

Figure 5.25: Time history for a ISSC wave spectrum with a 1m significant wave height and a peak wave period of 8.75s.

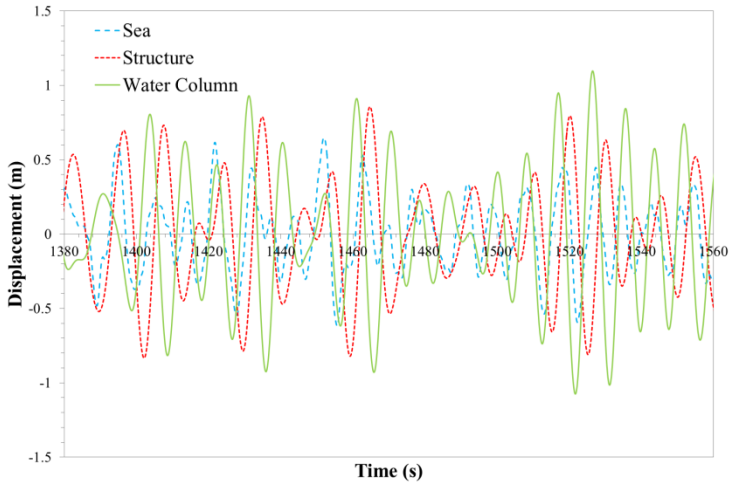

Figure 5.26: Time history for a ISSC wave spectrum with a 1m significant wave height and a peak wave period of 11.67s.

5.12.2 Structure-Column Velocity Functions

Investigating the relative velocity of the water column and structure for each wave spectrum can further support the conclusion reached from the single sinusoidal investigation. Figure 5.27, Figure 5.28, and Figure 5.29 correspond to the wave spectrum with a peak wave period of 7.875 seconds (period ratio of 0.9), 8.75 seconds (period ratio of 1.0) and 11.67 seconds (period ratio of 1.3) respectively. Because of the irregular nature of a wave spectrum, these relative velocity graphs are not regular like those produced by a regular single sinusoidal wave. The structure-column heave velocity functions have been quantified differently in this investigation because of the irregular nature of wave spectra. Using the maximum points on the functions could lead to an over estimation of the power production potential because a single optimal wave within a large spectrum could produce such an over estimation. To overcome this, the standard deviations of the structure and water column heave velocities have been used to quantify the length of the ellipse axis. The statistical data for each structure-heave velocity plot is seen in Table 5.3.

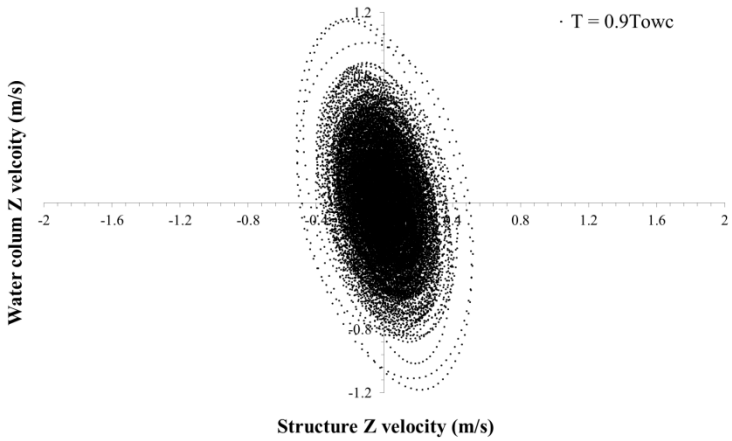

Figure 5.27: Water column heave velocity vs. structure heave velocity for an ISSC wave spectrum with a 1m significant wave height and a peak wave period of 8.75s.

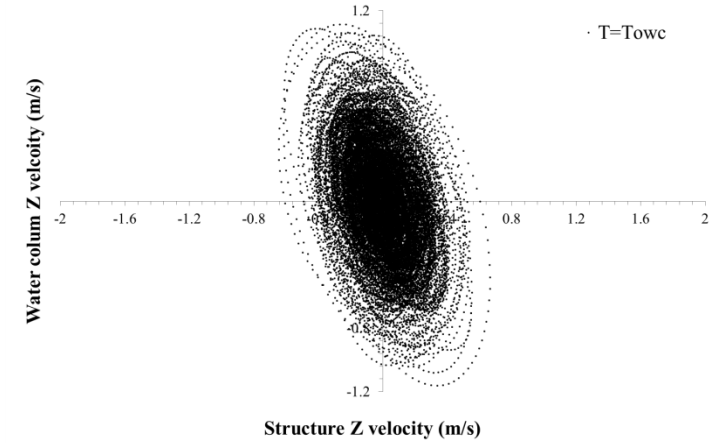

Figure 5.28: Water column heave velocity vs. structure heave velocity for an ISSC wave spectrum with a 1m significant wave height and a peak wave period of 8.75.

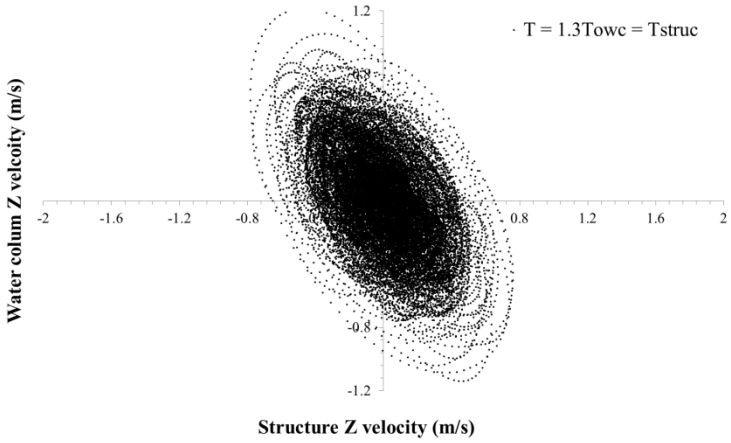

Figure 5.29: Water column heave velocity vs. structure heave velocity for an ISSC wave spectrum with a 1m significant wave height and a peak wave period of 11.67s.

Table 5.3: Statistical Summary of Velocity Comparison Graphs

Tp (s)	Vessel	Min	Max	Standard Dev.	Mean	Mode
7.875	Structure	-0.514	0.521	0.1421	-5.1×10^{-5}	0.1074
	Water Column	-1.183	1.159	0.3128	0.00027	-0.4201
8.75	Structure	-0.6436	0.6669	0.1756	5.28×10^{-5}	-0.1856
	Water Column	-1.1639	1.1123	0.344	-0.00018	0.5204
11.67	Structure	-0.7826	0.7623	0.2304	7.78×10^{-5}	-0.4338
	Water Column	-1.1405	1.2147	0.3156	-8.13×10^{-5}	-0.1842

The irregular nature of the wave spectra causes an irregular response in both the oscillating water column and the structure and, because of this, quantification of the response is difficult.

Despite this, trends in the responses do exist. The structure heave velocity increases with an increase in peak wave periods of the ISSC spectrum. The largest structure velocity occurs when the peak wave period of the spectrum coincides with the natural period of the structure. This is highlighted in Table 5.2, where the structure heave velocity maximum value increases from 0.5210 to 0.6669 and then again to 0.7623 as the peak wave period moves from 7.875 seconds to 8.75 seconds and then to 11.67 seconds respectively. The standard deviation also increases as the peak wave period moves closer to the natural period of the structure. This also holds true for the oscillating water column standard deviation but not for the maximum value.

The oscillating water column standard deviation value at a peak wave period of 90% of the natural period is equal to 0.3128. It increases to 0.3440 when the peak wave period coincides with the water column natural period and then decreases to 0.3156 when the peak wave period is 1.3 times the natural period of the water column. The oscillating water column, however, does not undergo as significant a change as the structure does as the peak wave period changes. This system is in agreement with the trends established by the sinusoidal wave analysis.

The length of the major and minor axes of the ellipse fitting the structure-water column heave velocity function does not seem to produce as clear a result during wave spectra as it does with single sinusoidal waves. Axis lengths for the three tested peak wave periods are seen in Table 5. The major axis length is calculated using the standard deviation for each wave and minor axis length is calculated from observation of Figures 26, 27, and 28.

Table 5.4: Wave spectra major and minor axis lengths

Tp (s)	Major Axis Length (m/s/m)	Minor Axis Length (m/s/m)
7.875	0.6872	1.8456
8.75	0.7724	2.1565
11.67	0.7816	1.0426

5.12.3 Power Extraction

The power extraction for each wave spectrum is established by using the data points for the structure and oscillating water column heave at 0.1-second intervals produced during the OrcaFlex analysis. The calculations used are outlined in section 1.3. The absolute value of the power as a function of time over a one-minute period is seen in Figure 5.30.

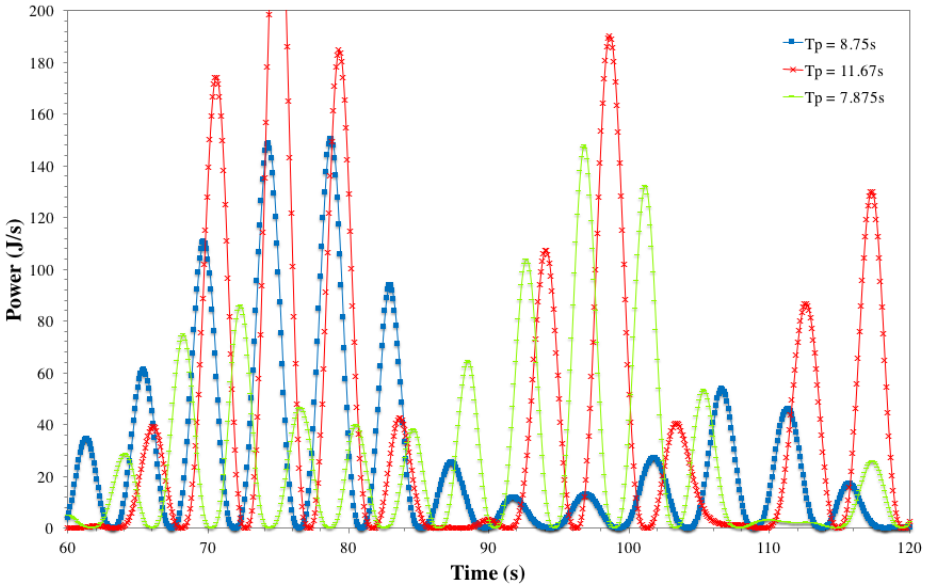

Figure 5.30: Power production as a function of time for each wave spectrum

Figure 5.31 plots the spectral density function of the power output. Figure 5.31 is produced by performing an FFT on the time domain power output data seen in Figure 5.30. MATLAB is used to perform the FFT on the first 16384 (2^{14}) data points. The FFT output is plotted with the theoretical wave spectrum for each wave spectrum investigated. The FFT of the power curve at a wave period ratio of 1.33 is the largest of three investigated curves. This is followed by the wave period ratio of 1.00 and then 0.90.

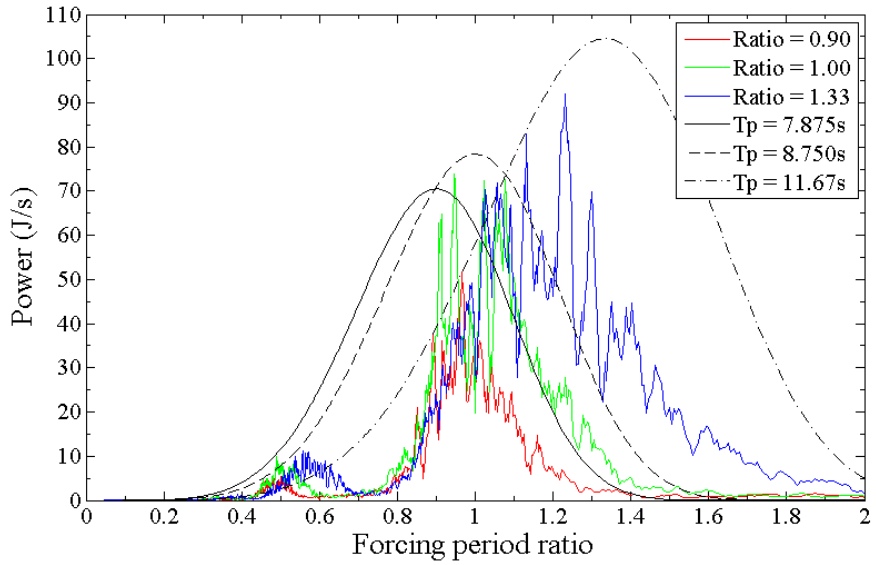

Figure 5.31: ISSC wave spectra power production FFT as a function of forcing period ratio

These results are because there is more power in a wave with a larger peak wave period. Using the metrics established in section 5.6, these power productions FFT graphs can be normalised and quantified. The spectrum with a peak wave period of 7.875 seconds, this corresponds to a forcing period equal to 0.9 times the water column natural period, has an efficiency ratio of 0.0857. The spectrum with a peak wave period of 8.75 seconds (equal to the natural period of the water column) has an efficiency ratio of 0.120. The spectrum with a peak period of 11.67 seconds (equal to the structure natural period and 1.3 times the natural period of the oscillating water column) has an efficiency ratio of 0.1140. These efficiency ratios were calculated using equation 5.11. They confirm that more efficient power production is possible without maximum structure heave experienced at forcing periods equal to that of the structure. This also confirms that, with appropriate separation of the water column and structure natural periods, the development of a system that is able to produce power while also reducing the structure movements is possible.

The results from the wave spectra investigation differ from the sinusoidal wave investigation. When the system is subjected to a spectrum with a peak wave period that corresponds to 0.9 times the water column, it produces a less efficient device than when subjected to a spectrum with a peak wave period equal to the water column natural period or the structure natural period. This disagreement in results probably stems from a combination the shape of the function relating the forcing period ratio to the axis lengths (Figure 5.16, repeated here for convenience) and the shape of the wave spectrum.

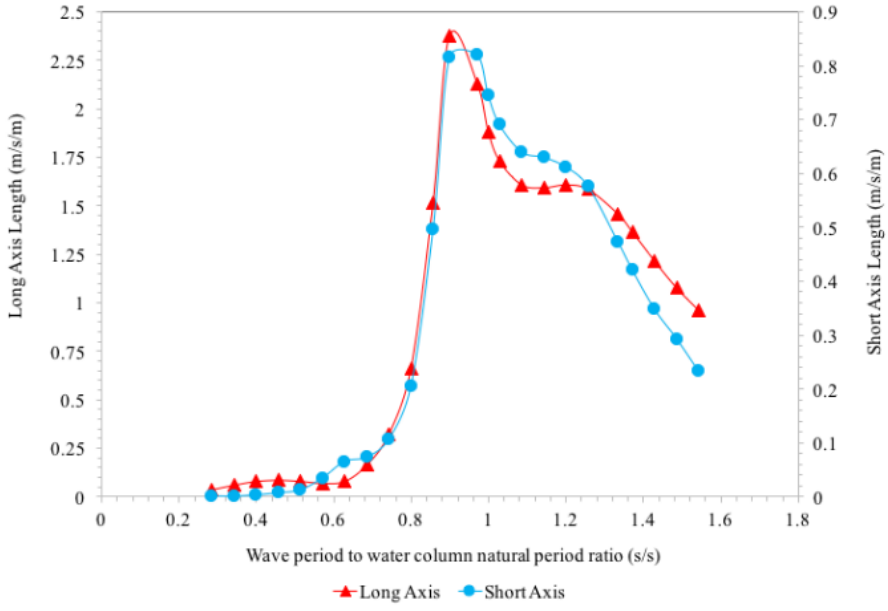

Figure 5.16: Axes lengths as a function of the forcing frequency ratio

Figure 5.16 shows a sharp decline in axis lengths, and hence power production, at forcing period ratios less than 0.9. This, coupled with the spread nature of a wave spectrum, will cause many wave periods to produce forcing period ratios less than 0.9. Wave spectra with higher peak wave periods produce higher values of forcing period ratios; hence, there is a higher chance a majority of the individual waves within the spectrum fall within the optimal power production forcing period ratio range. This range is from approximately 90% of the water column natural period to the structure natural period. This is explained graphically in Figure 5.32. Here the ISSC spectrum tested has been plotted over the data of Figure 5.16. Figure 4.32 shows that more of the ISSC spectra with a peak wave period ratio of 0.9 falls outside of the optimal forcing period ratio range compared with the ISSC spectrum with a peak wave period ratio of 1.0 or 1.3.

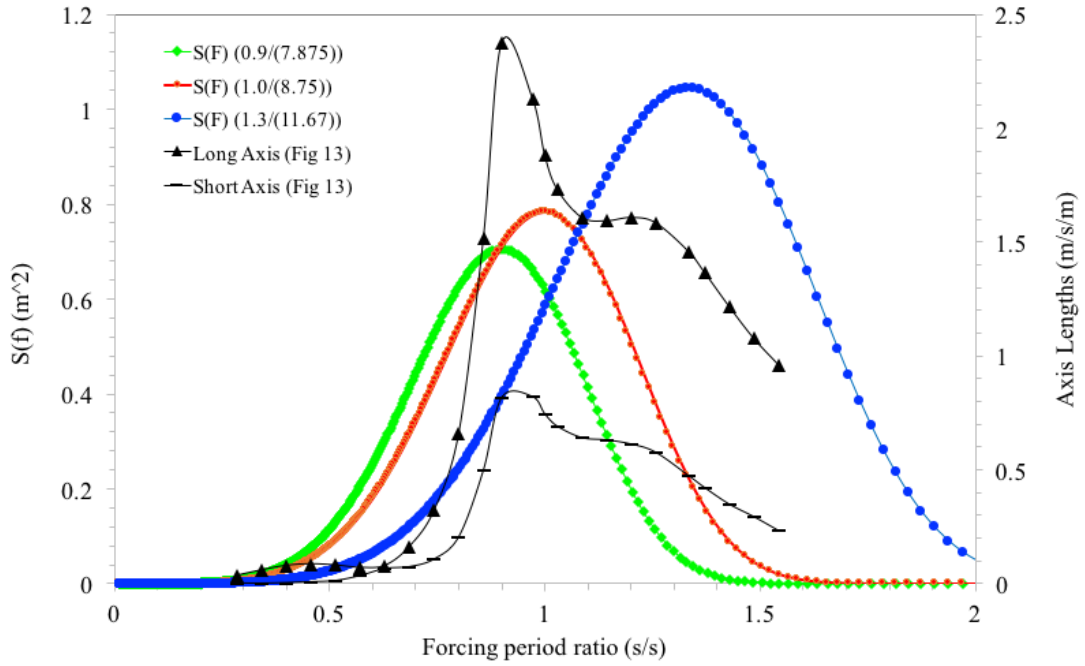

Figure 5.32: ISSC wave spectra overlaid with Fig 5.16

5.13 Chapter Summary

It has been shown that the conclusions drawn from WAMIT in the frequency domain and with single sinusoidal waves in the time domain with OrcaFlex are mostly applicable to systems subjected to wave spectra. Frequency domain results suggest that a target period for the forcing waves should be approximately 90% of the value of the water column natural frequency; however, the nature of the spread of wave spectra moves this target forcing period to be equal to the natural period of the water column as more energy falls within the higher energy capture range of the device.

The results have indicated that this system is somewhat sensitive to small changes in wave periods if these changes mean the forcing period ratio falls below 1.0. This is shown in the steep drop off of expected power output at values less than 1.0 in Figure 5.16. Changes in the peak wave period resulting in a forcing ratio greater than 1.0, but less than the ratio of the structure natural period to the oscillating water column natural period, have little effect on the power output potential of the system because the power output remains elevated between these two values. This is also seen in Figure 5.16.

It has been shown that a compliant oscillating water column wave energy device is able to produce power without large movements in the heave of the structure. This could potentially ensure structural integrity of the mooring system during this operational phase if the water column natural period is matched to the peak wave period of the surrounding sea state. More investigation in the feasibility of this with respect to mooring line integrity is undertaken in Chapter 6.

Furthermore, for these conclusions to be true the separation of the natural frequencies of the water column and structure must be ensured. It is recommended to use the guidelines suggested by Stappenbelt and Cooper (2010) who suggest that the structure should have a natural period of approximately 1.5 times the water column. Without this separation it is not possible to target only the natural period of the structure without also targeting the natural period of the oscillating water column.

Chapter 6 Optimising Survivability in DNV Defined Survival Conditions

6.1 Introduction

A wave energy converter device is only feasible if it can withstand unfavourable storm conditions and produce power during favourable conditions. The survivability of the device is almost entirely dependent on structural integrity of the mooring system (Bedard et al. 2005). The mooring system represents approximately 5% of the capital costs of a farm of oscillating water column devices (Carbon Trust, 2011). Care must be taken to ensure this mooring system is not over designed. An overdesigned system is likely to incur costs similar to the cost of the losses associated with an under designed system (Harnois et al. 2015). This chapter investigates the effectiveness of the oscillating water column device developed in Chapter 4 and Chapter 5 in storm conditions. The device will be subjected to various 100-year storms from around the world. The device developed in Chapter 5 is designed in such a way that power production is the paramount objective. This means that the system dynamics are setup in a manner that enhances the device and water column motions that produce the most efficient system during the mean sea conditions at a particular location.

Storm conditions at any location provide extremes of the mean conditions. From a structural standpoint, the feasibility of the system dynamics established to optimise power production during these extreme conditions must be assessed. In the absence of a proposed location for the device this chapter will look at a range of potential 100-year events for different parts of the globe. These locations are not locations suggested for installation but rather provide a holistic overview of the conditions that are practically possible.

The 100-year events are modelled by the JONSWAP spectrum. The parameters for this spectrum are taken from DNV-OS-301. JONSWAP spectra have been used to model random wave patterns when investigating offshore wind turbines in the North Sea (Ponce de León, Bettencourt, and Kjerstad, 2011; Brommundt et al. 2012) and during ultimate limit state analysis of offshore wind turbines in the Mediterranean Sea (Benassai et al. 2014). It is possible that choosing an installation location will not only be based on the prevalence of waves optimal for the operational state but also locations with storm conditions that are likely

to be survived. To highlight this, different locations were tested. The parameters from DNV-OS-E301 are seen in Table 6.1.

Two locations were chosen to gain an insight into storm conditions and the response of the wave energy device. The Norwegian Sea and the West Africa (swell) represent the highest and lowest sea conditions defined by DNV-OS-301. The same metrics developed in the operational state analysis in Chapter 5 are used to assess the feasibility of the system in these storm conditions. These storm conditions have been chosen as they provide a good representation of the spectra found in Table 6.1. Ultimate limit state analysis in the offshore industry is often undertaken with such wave spectra.

A better oscillating water column wave energy device will be able to withstand storm conditions and produce power during optimal conditions without changing too many aspects of the design. The aspects include mooring line tension, power take-off damping and altering the heave mass of the structure. With this in mind, the feasibility of the system shown in the operational state section of this chapter in surviving a storm is tested.

This chapter considers the feasibility of the tuning mechanisms discussed in Chapter 2 and investigated in the frequency domain in Chapter 4 and in the time domain in Chapter 5. These tuning mechanisms are adjustment of the heave mass, adjustment of the structure stiffness, and adjustment of the power take-off damping. Each storm swell is investigated to determine the feasibility of the tuning mechanism. The feasibility is judged on the peak surge and heave displacements of the structure, the peak mooring line tensions, and the average heave displacement. The time domain outputs and spectral density functions serve as the principal outputs of the investigation. The time domain outputs are developed through implicit integration using OrcaFlex. The wave train developed from the JONSWAP spectrum for each storm serves as the force input for the system. This random wave train is developed through a method previously outlined in Chapter 3. All simulations are run for a time period of three hours. This time period is the period specified in DNV-OS-301. The chapter first presents the results of these investigations and then discusses their meaning and implications.

This unaltered system is one that has an oscillating water column natural period that matches the mean sea state, a structure natural period that is approximately 1.5 times the oscillating water column natural period, and is optimally damped. Such a system is likely to have heave plates deployed to increase the natural period of the structure without increasing the mass of

the structure. This 'unaltered' system is the system developed for the mean sea conditions. Hence, it is unaltered during storm conditions.

6.2 Wave Spectra used during analysis

The 100-year storm conditions were used for the wave spectra tested. The Norwegian Sea and West Africa (Swell) have been selected. The defining characteristics for each storm are seen in Table 6.1. The entire suite of DNV defined storm conditions are presented to give context to the selected storms.

Table 6.1: DNV OS E-301 100-Year Storm and 10-Year Current Guidance Values (DNV-OS-E301, 2010)

Location	H_S (m)	T_P (s)	γ*	U_W (1-hr. avg.) (m/s)	U_C (m/s)
Norwegian Sea	16.5	17.0-19.0	2	37	0.9
Northern North Sea	15	15.5-17.5	2	40.5	1.5
North Sea	14	15.0-17.0	2	34	0.55
Gulf of Mexico (GOM)	11.9	14.2	3	41.4	1.98
West Africa (swell)	3.6-4.1	15.5-16.0	1	16	0.9-1.85
West Africa (squalls)	2.0-2.7	7.0-7.6	1	22.0-30.0	1.6
Brazil	8	13	2	35	1.6
South China Sea (non-Typhoon)	7.3	11.1	3	28.6	0.85
South China Sea (Typhoon)	13.6	15.1	3	56.3	2.05

Each wave spectrum is defined by the significant wave height, peak wave period and peak enhancement factor. The definition of each factor is as follows (Sarpkaya, T., & Isaacson, M. (1981):

- Significant wave height: The average height of the highest one third of the waves in the spectrum.
- Peak wave period: For the single waves that compose the spectrum this is the wave period that occurs most often.
- Peak enhancement factor: A scalar that determines the magnitude of the spectrum at the peak wave period. A larger value means more waves are concentrated around the peak wave period.

Norwegian Sea

The first 100-year storm spectrum tested is for the Norwegian Sea. The significant wave height of this storm is 16.5 metres. The peak wave period is from 17 to 19 seconds (2.71 to 3.02 rad/s). The average value of 18 seconds (2.86 rad/s) has been used in this study. The

Norwegian Sea has a JONSWAP peak enhancement factor of 1.9. This spectrum is seen in Figure 6.1. A wind speed of 37 m/s and a current of 0.9 m/s have been included. The wind and current are both acting in the same direction as the wave force.

West Africa (Swell)

The West Africa (Swell) 100-year storm is described by a significant wave height between 3.6 and 4.1 metres (the value of 3.85 metres has been used in OrcaFlex). The peak wave period is between 15.5 and 16 seconds (a value of 15.75 seconds (0.42 rad/second) has been used). The peak enhancement factor is 1.0. This spectrum can also be seen in Figure 6.1. A wind speed of 16 m/s and a current of 1.85 m/s have been included. The wind and current are both acting in the same direction as the wave force.

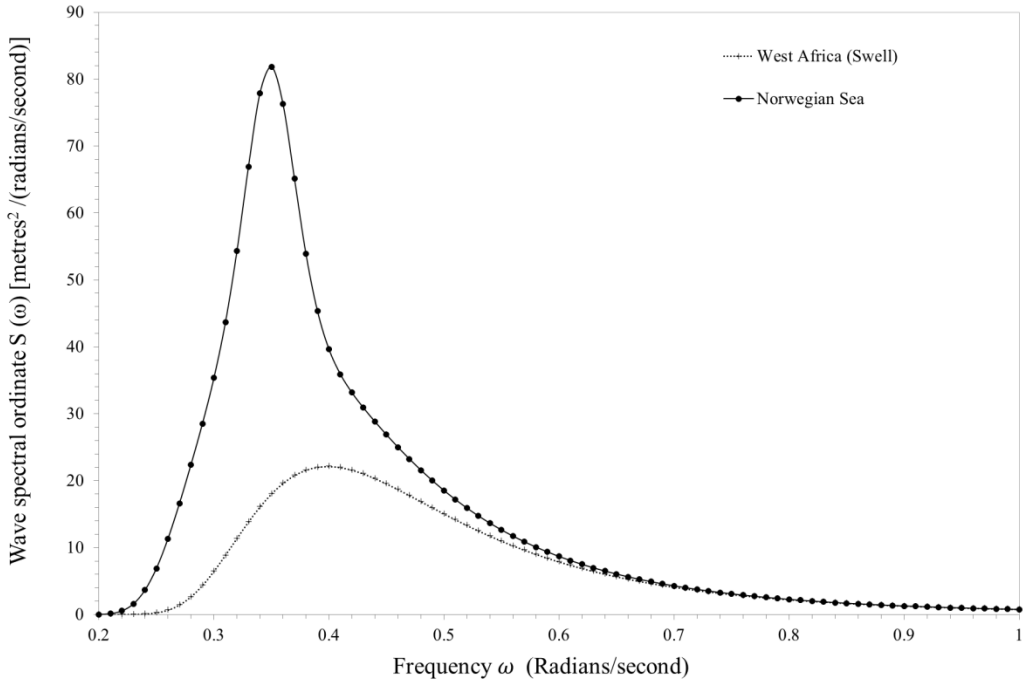

Figure 6.1: Frequency spectra of each storm swell

These two storm spectra were chosen as they provided samples of the ranges of 100-year events in DNV-OS-301. These events were also characterised by parameters that allowed the unfavourable conditions tested to be different enough to the favourable conditions established in Chapter 4 and Chapter 5.

These spectra differ slightly from the wave spectra typically found along the east coast of Australia. The significant wave height and average peak wave period for a 100-year event along the east coast of Australia is 3.95 metres and 14.97 seconds respectively. This has been

calculated from the data in Table 6.2. This is most similar to the 100-year event in West Africa. The wave spectra characteristics for the east coast of Australia are seen in Table 6.2. Each spectrum is plotted in Figure 6.2. Because of this similarity, the wave conditions for West Africa will still be used. This is because these conditions are defined by DNV-OS-301 and the Australian conditions are not.

Table 6.2: Wave Statistics from various Australian Locations

Location	Brisbane	Byron Bay	Coffs Harbour	Crody Head	Sydney	Botany Bay	Port Kembla	Batemans Bay	Eden	Average
Data Range	1976-2009	1976-2009	1976-2009	1985-2009	1987-2009	1971-200-	1974-2009	1986-2009	1978-2009	-
Effective record (yrs)	28.5	24.3	28.5	20.7	19	34	30.6	21.2	26.6	25.93
Signifcant wave height (m)										
Mean	1.63	1.66	1.58	1.61	1.63	1.6	1.58	1.43	1.64	1.6
Median	1.47	1.5	1.43	1.46	1.46	1.43	1.43	1.3	1.52	1.44
10% exceedence	2.57	2.59	2.44	2.48	2.55	2.54	2.47	2.22	2.43	2.48
1% exceedence	4.04	3.93	3.85	3.94	4.19	4.17	3.94	3.57	3.93	3.95
Maximum	7.36	7.64	7.37	7.35	8.43	8.86	8.43	7.19	7.14	7.75
Variance	0.51	0.48	0.44	0.46	0.54	0.55	0.48	0.39	0.42	0.47
Peak wave period (s)										
Mean	9.32	9.59	9.58	9.71	9.72	9.82	9.57	9.36	9.41	9.56
Median	9.31	9.5	9.5	9.5	9.77	9.38	9.5	9.5	9.5	9.5
10% exceedence	12.14	12.2	12.2	12.2	12.5	11.98	12.23	12.2	12.2	12.21
1% exceedence	14.67	15.1	15.1	15.1	15.1	14.38	15.1	15.1	15.1	14.97
Maximum	19.17	19.7	19.79	19.79	20	23.65	19.7	19.7	19.69	20.13
Variance	4.75	4.92	4.99	5.12	5.57	5.24	5.17	5.17	5.46	5.15

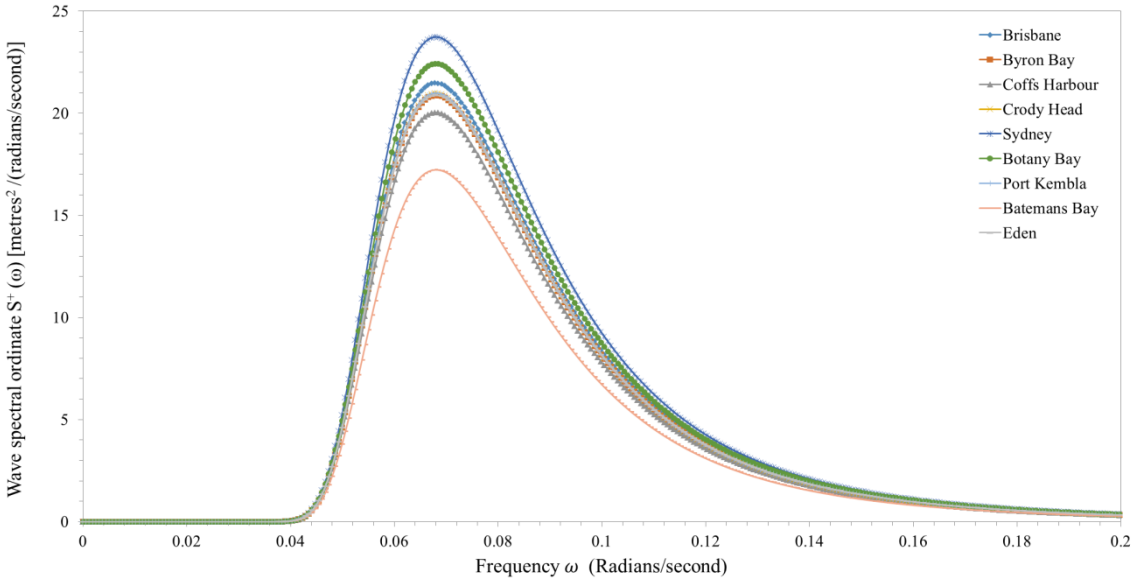

Figure 6.2: 1% exceedance storm spectra for Australia's east coast

6.3 Physical Model Description and Justification

The systems used for analysis in OrcaFlex are the systems developed in the frequency domain using WAMIT. Each system is composed of two vessels. The first vessel is the floating structure and the second is the oscillating water column. This has been done to circumvent the OrcaFlex limitation of six degrees of freedom per vessel. The coupling between the structure and oscillating water column has been maintained during this separation of the RAOs. This is confirmed in Section 5.4.

Mooring lines have been attached to the structure to investigate the effect of tuning mechanisms on the peak mooring line tension. Two mooring lines have been used. One mooring line is attached to the front of the vessel (heading of 0 degrees) and one to the back of the vessel (heading of 180 degrees). The use of two mooring lines is justified, the structure does not experience any sway movement due to the intentional alignment of the wave force, current, and wind. The forces have been aligned because peak mooring line tension is of concern; aligning the forces causes the greatest combined force on the vessel and hence the mooring line. The addition of mooring lines does not alter the movements of the structure because the RAO of the structure is defined with the inclusion of mooring lines. This situation presents the worst-case scenario for a moored system. The mooring lines are catenary in shape. They are 160 metres long in a depth of 100 metres. A wire schematic is seen in Figure 6.3 and a three-dimensional rendering is seen in Figure 6.4. The mooring lines are beneath the seabed in Figure 6.3 because the system has not undergone a static analysis yet.

The attachment of mooring lines or the mooring line type chosen in OrcaFlex does not alter the response of the structure or oscillating water column. They simply allow the tensions in mooring lines at the particular displacements to be determined. This will allow the maximum mooring line tensions to be found during the simulations. Any mooring line effects are included in the WAMIT input data. Hence, investigation into mooring line setups, material types, anchor points, etc. has not been undertaken in this section of the thesis.

No failure criteria were set for the mooring lines. They were assumed to be infinitely strong. This has allowed the tension is the lines to be measured without stopping the simulation due to a failure.

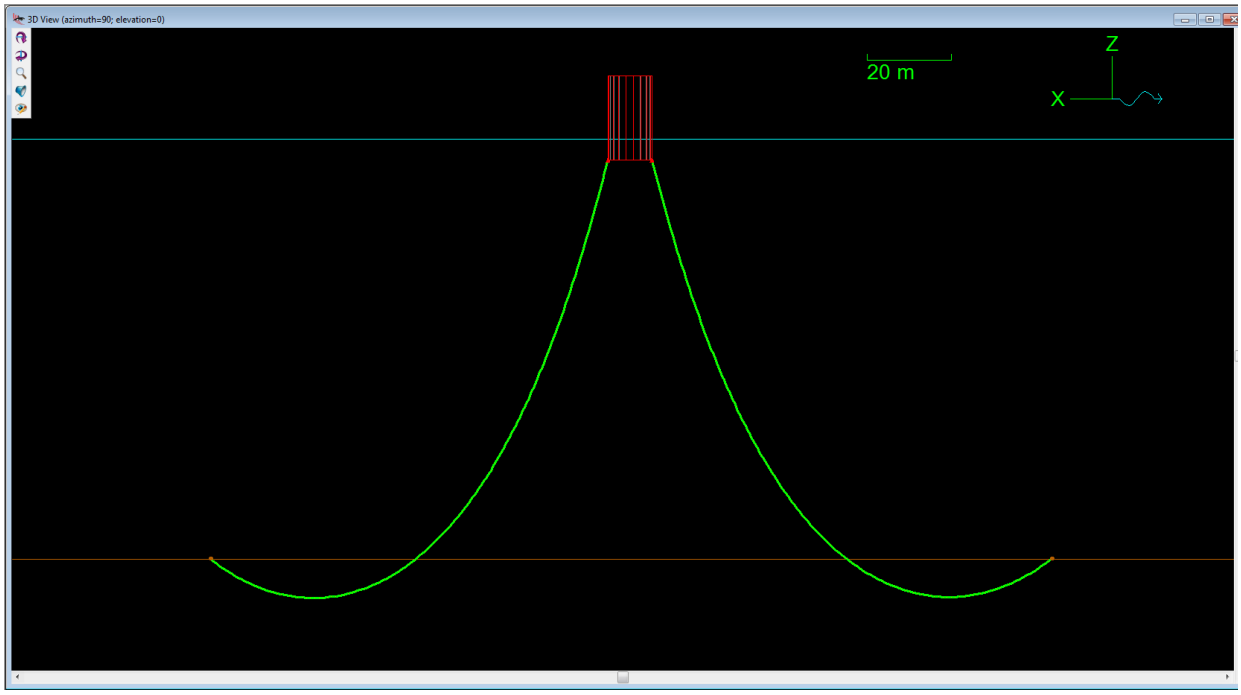

Figure 6.3: Wire drawing of moored OrcaFlex model before finding the equilibrium point

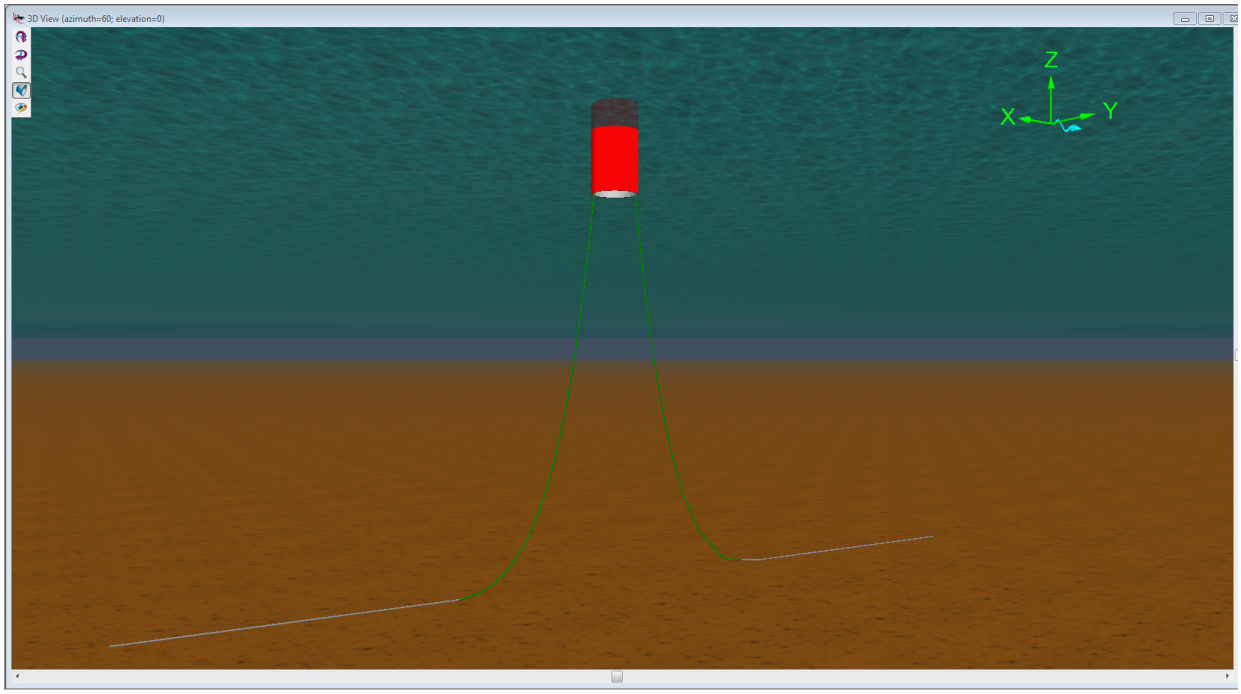

Figure 6.4: 3D rendering of moored OrcaFlex model at equilibrium

6.4 Extreme Value Determination

The maximum likely mooring line tensions, peak surge displacements, and peak heave displacements were calculated using Weibull Distribution. The Weibull distribution is fitted using the maximum likelihood method. A mathematical background to this method can be seen in Coles (2001). The Weibull distribution has historically been used in the marine industry and for failure analysis in many other engineering disciplines. This method of determining global maximum of mooring line tension is in accordance with DNV-OS-301. The Weibull distribution of global maxima may be written as:

$$F(x) = e^{\left\{-\left(\frac{x-\gamma}{a}\right)^{\beta}\right\}}$$

An example of the global maxima extraction from a time domain output can be seen in Figure 6.5.

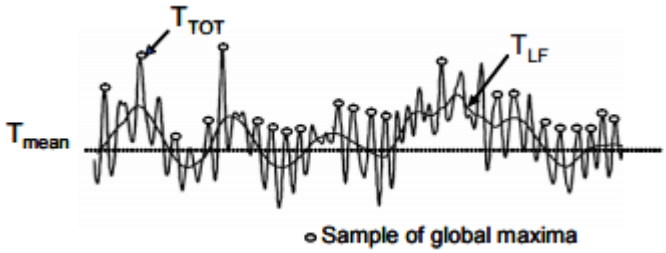

Figure 6.5: Global maxima and low frequency tensions in a mooring line

All simulations were run for a time of three hours as DNV-OS-301 requires the three hour maximum tension value to be reported. The Weibull distribution analysis provides the three hour return level for the upper tail of effective tension in the mooring line and the 95% confidence interval for this value.

The peak mooring line tensions will be a function of the peak heave and peak surge displacement of the vessel. The greater the displacement, the greater the mooring tension.

Because the area of the structure's surfaces perpendicular to the waves, current, and wind are the same, the peak surge displacement will be a function of the physical wave characteristics, the wind speed, and the current. Changing the surge RAO will require changing the shape of the structure. A reduction in surge is likely to warrant a slender structure. This is unlikely to occur as the structure shape is defined by the mean sea conditions at the installation site. Hence, to reduce the peak mooring tension the peak heave displacement should be

minimised. The surge RAO from WAMIT is seen in Figure 6.6. For this structure, the peak surge displacement will be equal to approximately the peak wave height of the spectrum.

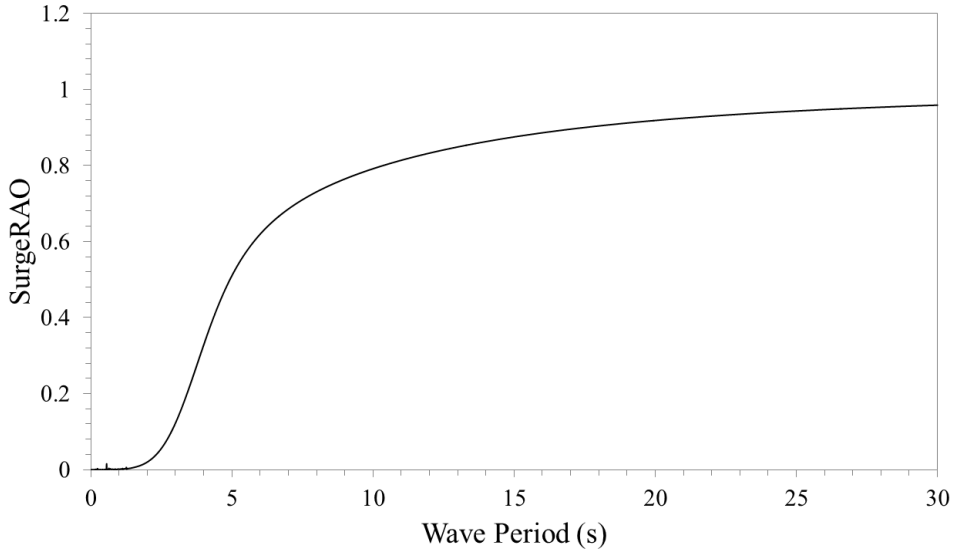

Figure 6.6: Surge RAO for structure tested.

6.5 Tuning Mechanisms Used

The same tuning mechanisms were used in all storm conditions despite the potential for them not to be optimised for each sea state. This means the determination of sea state characteristics (mean and 100 year events) are likely to define an installation location. Modifications to the system include altering the power takeoff damping, heave mass, and stiffness. A summary of each tuning mechanism is seen in Table 6.3. Combinations of these modifications are also possible. The RAOs in this section were produced with WAMIT. The tuning mechanisms are further explained in the coming sections of this thesis. All modifications are made to the input files of the WAMIT analysis. An example of these files is seen in Appendix B – WAMIT Operational Files.

Table 6.3: Summary of tuning mechanisms used in this investigation

Tuning mechanism	Description
Heave mass reduction	This tuning mechanism reduces the heave mass of the structure. This reduction in the heave mass reduced the added mass and therefore reduces the natural period of the structure
Power takeoff damping increase	This tuning mechanism increases the power takeoff damping and hence the overall damping of the structure. This increase in damping causes a slight reduction of the RAO and also a reduction in the natural period of the structure.
Stiffness increase	This tuning mechanism increases the vertical stiffness of the structure. This increase causes an decrease in the natural period of the structure.

6.5.1 Untuned device with respect to the storm swell

This device is the one developed to produce power from the mean sea state of the chosen installation site. This system has optimal power take-off damping, a heave mass (real plus added) and stiffness (water plane and mooring line) that produces a natural period equal to approximately 1.5 times the oscillating water column natural period, and a oscillating water column that is sized so that the natural period matches the mean peak wave period of the site. The RAO of the structure of this structure is seen in Figure 6.7. This is the system developed from the results of Chapter 5 of this thesis.

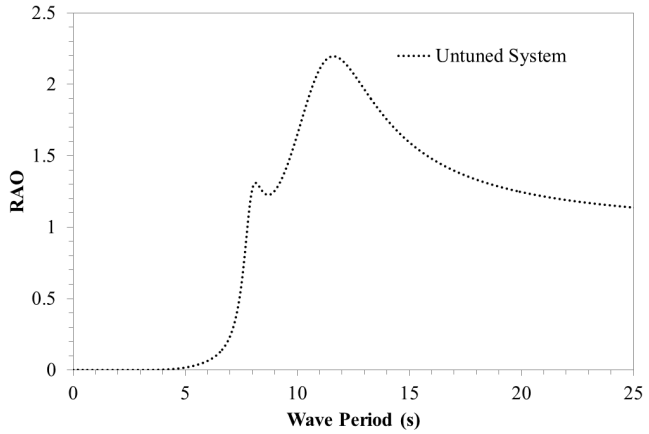

Figure 6.7: RAO of the untuned structure.

6.5.2 Heave Mass Reduction

The first alteration is to reduce the artificially increased heave mass used during the operational state. The heave mass has been reduced to the actual heave mass of the system which is 2.5 times less than the optimal heave mass. This is achievable through a reduction in added mass. The easiest way to achieve this will be with a change in structure geometry or a withdrawal of heave plates. A reduction in heave mass will move the structure natural period from a value (11.67 seconds) roughly equal to 1.33 times the natural period of the oscillating water column to a value (8.75 seconds) roughly equal to the oscillating water column. The RAO of this system along with the untuned system is seen in Figure 6.8. The large peak is likely to cause increase displacement in the structure when subjected to wave periods corresponding to the period at which the peak occurs. Care must be taken to ensure this wave period is outside of the expected wave periods for the storm.

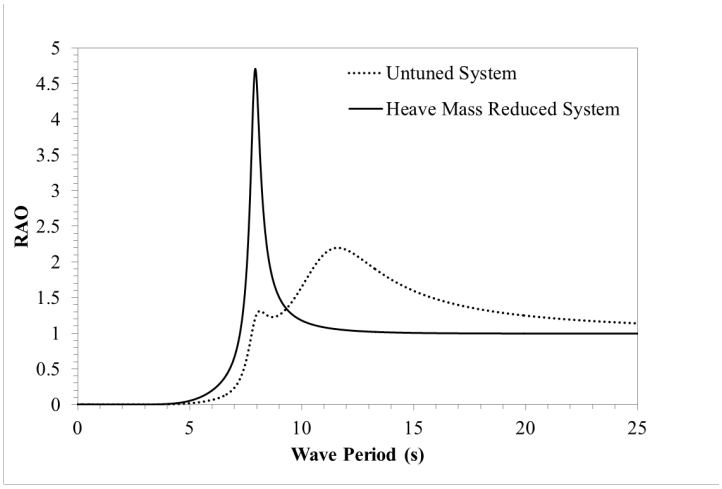

Figure 6.8: RAO of the system tuned with a decrease in heave mass and the untuned system.

6.5.3 Power Take-off Damping Increase

Investigation into the effect of power take-off damping on the heave response of the system is undertaken in the same manner as the investigation into the heave mass reduction. For this investigation, the heave mass has been kept at 2.5 times the actual heave mass of the system. This is the same mass as that established in the system that is optimized for power take-off during suitable conditions (Chapter 5). The power take-off damping established during the optimized phase has been doubled for this investigation. Based on the results of the testing with WAMIT in the frequency domain, the maximum RAO of the oscillating water column is expected to reduce while the maximum RAO of the structure is expected to slightly increase.

The RAO of this system, along with the untuned system (see section 6.5.1), is seen in Figure 6.9.

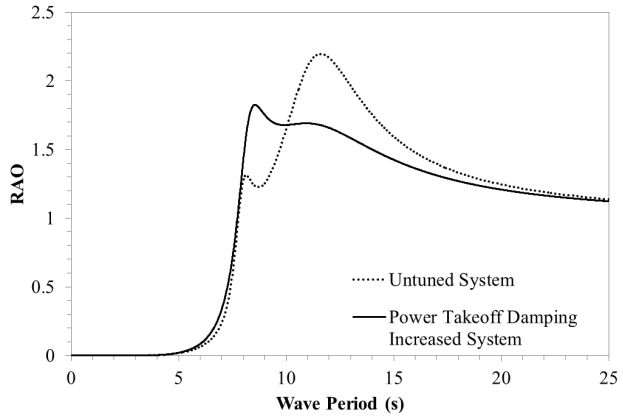

Figure 6.9: RAO of the system tuned with an increase in power take-off damping and the untuned system.

6.5.4 Stiffness Increase

Increasing the stiffness of the system will reduce the natural period of the structure. The most viable way to do this will be to increase the tension in the mooring lines by reducing mooring line length. The extent to which this method can be implemented will be reliant on what mooring line materials are available and the maximum expected excursion of the structure. These adjustments will be different for every installation location because the structure will experience different heave responses for different wave spectra. Feasible stiffness values have not been determined in this analysis but are explored later in the chapter.

Method

To increase the stiffness of the system within WAMIT the user is required to specify a heave stiffness value. This stiffness value will be an external stiffness parameter that is placed on the system. The origin of this stiffness is up to the user but will mostly likely come from a change to the mooring system. The stiffness of the system then becomes the inherent water plane stiffness plus the additional external stiffness. Simply attaching taught mooring lines to the vessel in OrcaFlex would not produce a stiffer system as OrcaFlex only reads the WAMIT RAOs. Utilising taught mooring lines would allow the force in each mooring line to be calculated. This value can then be used to determine an applicable setup to reduce the device motions in a practical setting.

WAMIT does not explicitly specify the water plane stiffness of the system and this makes estimating an appropriate external stiffness value difficult. To overcome this problem, the structure RAO and value of the natural period without any external stiffness damping has been compared to structure RAOs and natural periods with different stiffness parameters. This means that the external stiffness value is essentially picked at random and the effect on the RAO studied. This relationship can be expressed mathematically; the structure natural period (period value that corresponds to the peak of the RAO) is proportional to the square root of the ratio of the structure mass (M) to total stiffness (K). In the case where there is no additional external stiffness, the total stiffness is equal to the water plane stiffness (K_i):

$$T_1 = \sqrt{\frac{M}{K_i}} \tag{6.1}$$

If the additional external stiffness (from a mooring system) (K_e) is imposed onto the system then then the total stiffness is equal to the sum of the water plane and external system:

$$K_T = K_e + K_i \tag{6.2}$$

Since the absolute value of the water plane stiffness used by WAMIT is unknown, it can be expressed as a function of the applied external stiffness:

$$K_i = \alpha K_e \tag{6.3}$$

where α is the stiffness scalar.

This relationship can now be substituted into equation 6.1 to produce a solvable equation when the stiffness scalar is greater than zero:

$$T_2 = \sqrt{\frac{M}{K_e(\alpha + 1)}} \tag{6.4}$$

Assuming the mass is constant and dividing equation 6.1 by equation 6.4, the relationship between the structure natural period before and after the addition of external damping can be found:

$$\frac{T_1^2}{T_2^2} = \frac{\alpha + 1}{\alpha} \tag{6.5}$$

Solving equation 6.5 for the stiffness scalar produces:

$$\alpha = \frac{T_2^2}{T_1^2 - T_2^2} \tag{6.6}$$

Selecting different values of external stiffness and comparing the natural period of the structure with and without this stiffness value will allow the user to determine the value of the stiffness scalar using equation 6.6. Once the value of the stiffness scalar is known then equation 6.3 can be used to determine the value of the water plane stiffness.

This method was implemented until a stiffness scalar of one was found. This means that the external stiffness is equal to the internal stiffness leading to a system that has a stiffness value double that of the original system. The RAOs with and without the external stiffness parameter are seen in Figure 6.10. The structure with internal stiffness only is the structure tuned for power production. This system was then imported into OrcaFlex to determine how viable this method is to combat increased structure movement during storm conditions.

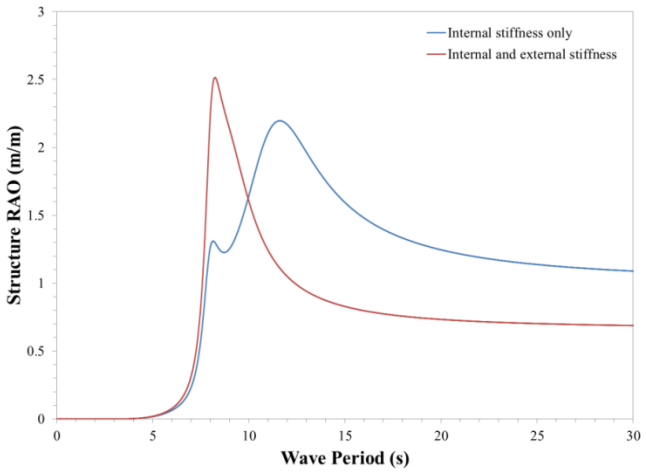

Figure 6.10: Comparison of the structure RAO with and without external damping.

6.5.5 Combination of Heave Mass Reduction and Power Take-off Damping Increase

It was hypothesised that changing the power take-off damping to reduce the oscillating water column heave in conjunction with a heave mass reduction may also reduce the structure heave during storm conditions. This was hypothesised because the structure and oscillating water column motions are coupled and an increase in power take-off damping above the optimal damping level was shown to cause a decrease in the heave response of the oscillating water column during the WAMIT analysis. To test this hypothesis, the heave mass established in the isolation testing of the heave mass reduction was coupled with a power take-off damping value double that of the value used to produce the optimal operational state system. This setup showed that a large reduction in the heave of the system is possible. The RAO of this system along with the untuned system is seen in Figure 6.11.

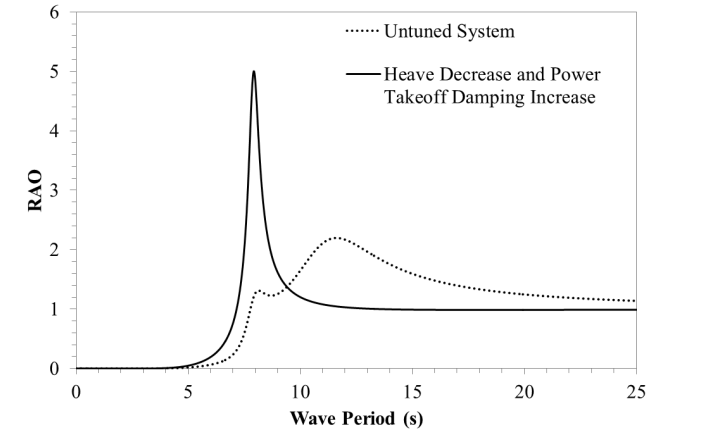

Figure 6.11: RAO of the system tuned with a decrease in heave mass and an increase in power take-off damping, and the untuned system.

This combination of alterations to the system has caused the peak of the RAO to move from a value of 12 second to a value of approximately 8 seconds. The RAO of the untuned system shows two distinct peaks. One from the water column natural period and one from the structure natural period. These two peaks lead to a RAO that is more spread than the tuned system where the water column natural period and the structure natural period are aligned. The narrow banded RAO of the tuned system could be advantageous if the entire band can be avoided by the forcing period of the ocean waves.

6.5.6 Combination of Stiffness Increase and Power Takne-off Damping Increase

The increase in both these parameters is kept constant with the increase chosen during investigation of these parameters in isolation. The added external stiffness is equal to the internal stiffness and the power take-off damping is double that of the optimal value. During the isolation testing, the increased stiffness reduced the structure natural period and the increase power take-off damping reduced both the oscillating water column and structure heave motion. Because of the coupled motions of the oscillating water column and structure, these two alterations are expected to produce favourable results when combined. The RAO of this system along with the untuned system is seen in Figure 6.12

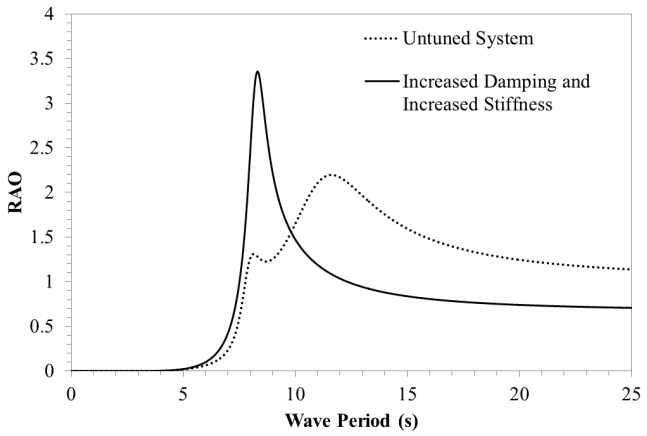

Figure 6.12: RAO of the system tuned with an increase in power take-off damping and stiffness, and the untuned system.

6.5.7 Combination of Heave Mass Reduction and Stiffness Increase

Reducing the heave mass and increasing the structure stiffness will both lead to a reduction in the structure natural periods. This combination is expected to produce favourable results given the conclusions drawn when each alteration was tested in isolation. The magnitude of heave reduction and stiffness increase is kept constant with the values established in separate testing. A large reduction in structure natural period is expected to move the natural period to a value outside the range over which the majority of the ocean wave periods lie. This is confirmed in Figure 6.13. Figure 6.13 shows the structure heave RAO from WAMIT. The peak value of the RAO now lies at a period value of approximately 8 seconds. This is a 50% reduction in the value established in the system during its operational state.

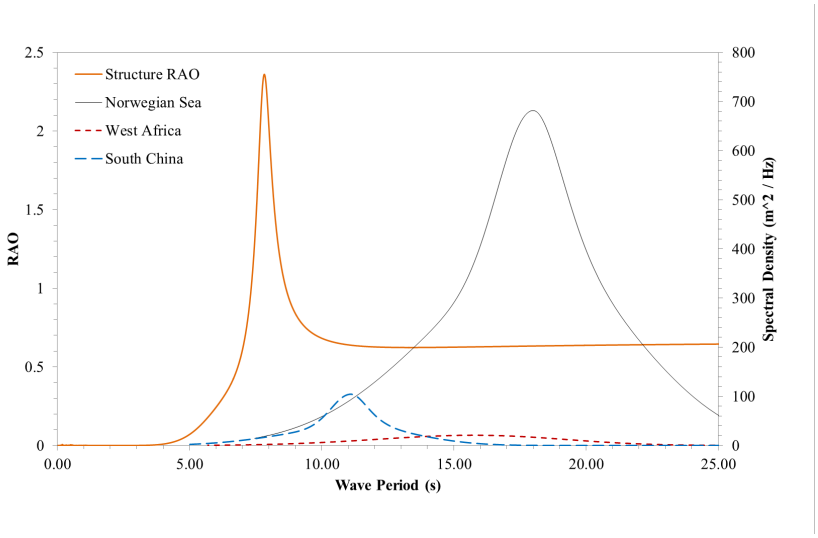

Figure 6.13: Structure RAO vs sea state spectral density functions

Combination of all Tuning Mechanisms

6.5.8 Combination of Heave Mass Reduction, Power Take-off Damping Increase, and Stiffness Increase

The final investigation into system alterations is to investigate the effect of combining all three alterations into a single system. The testing used the previously established alterations; 2.5 times reduction in heave mass, introducing an external stiffness value equal to the internal stiffness of the system, and doubling the optimal power take-off damping value. The RAO of this system, along with the untuned system, is seen in Figure 6.14.

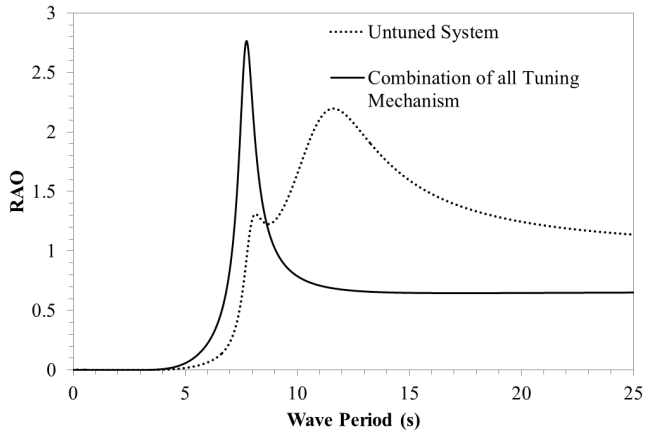

Figure 6.14: RAO of the system tuned with a decrease in heave mass, an increase in stiffness, and an increase in power take-off damping, and the untuned system.

6.6 Spectral Density Functions

Spectral density functions are the results of a Fast Fourier transform of the time domain output. The spectral density functions of the sea states tested are plotted against the theoretical sea spectrum. This is seen in Figure 6.15. Both storm spectra show close agreement with the theoretical plots. These are slightly different because the simulation time needs to be run for an infinite period of time before convergence will occur. This is not feasible. The spectral density functions will allow a better understanding of how the structure and oscillating water column are expected to behave in a particular sea state.

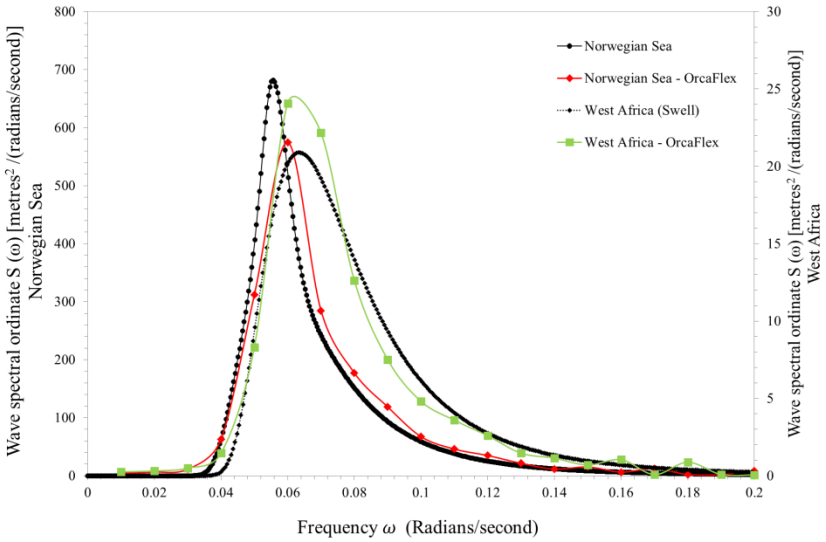

Figure 6.15: Theoretical vs actual storm spectra

Since the spectral density functions essentially describe the power at each frequency component, integration of the function between any two points will determine the power (or an indication of the power available) between those two points (Norton, 1989). The total area under the spectral density curve is known as the zeroth moment. This can be fined mathematically as:

$$m_o = \int_{f-\infty}^{f\infty} S_f \times d_f \tag{6.7}$$

The zeroth moment can be used to express the significant wave height, or significant displacement of the wave, structure, and oscillating water column. The significant height is calculated as:

$$H_{sig} = 4\sqrt{m_o} \tag{6.8}$$

The significant wave height is measured from trough to crest; hence the significant heave displacement above the mean sea level is approximately half the significant wave height:

$$D_{sig} = 2\sqrt{m_o} \tag{6.9}$$

This means that a smaller spectral density peak will mean the structure experiences a smaller average displacement. A smaller average displacement likely means a smaller peak displacement. Comparison between the vessel movements and the storm spectrum will allow comparisons between storm spectra to be completed.

6.7 Results of the Norwegian Sea Analysis

The first 100-year event simulated in OcraFlex is the event from the Norwegian Sea. As outlined earlier, this sea state has a peak wave period of 18 seconds, a significant wave height of 16.5 metres, a 0.9 m/s current, and a one hour average wind speed of 37 m/s. The wind speed and current are acting in the same direction as the wave. This will produce the highest force on the system. All simulations were run for a period of three hours.

6.7.1 Time Domain Output

Untuned System

The time domain output for the untuned system in the 100-year event for the Norwegian Sea is seen in Figure 6.16. The time domain figures show a small section of the total simulation to allow the movements to be seen clearly. Plotting all data points will result in graph that is unreadable.

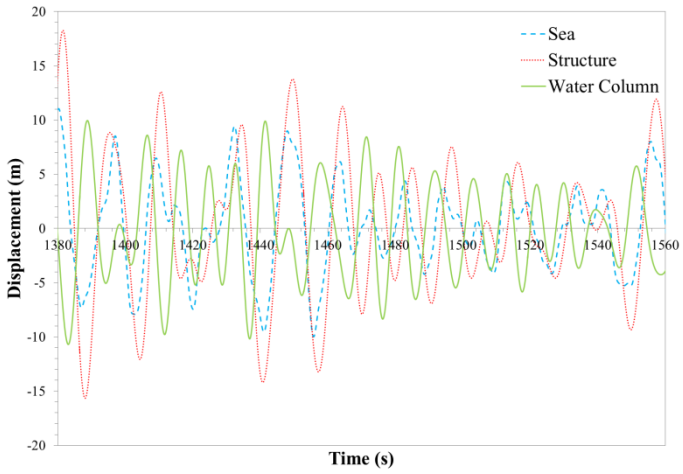

Figure 6.16: Time domain response for the 100-year storm in the Norwegian Sea for an untuned System

Figure 6.16 shows the response to the 1-in-100 year Norwegian Sea storm. It shows a structure that appears to be in phase with similar amplitude to the forcing wave. The oscillating water column appears to be oscillating at approximately double the frequency of the wave. The peak structure and oscillating water column motions exceed the peak wave height. The peak heave expected by the structure during this testing period was 20.43 metres with an upper limit of 23.59 metres. The maximum sea state was 16.65 metres with an upper limit of 17.81 metres. The peak surge value for the structure was equal to 11.68 metres with an upper limit of 13.85 metres. The peak mooring line tension in Line 1 was 4373 kN with an

upper limit of 5441 kN. The peak mooring line tension in Line 2 was 1524 kN with an upper limit of 1778 kN.

Heave Mass Reduction

Figure 6.17 details the time domain response to the Norwegian Sea 100-year storm conditions.

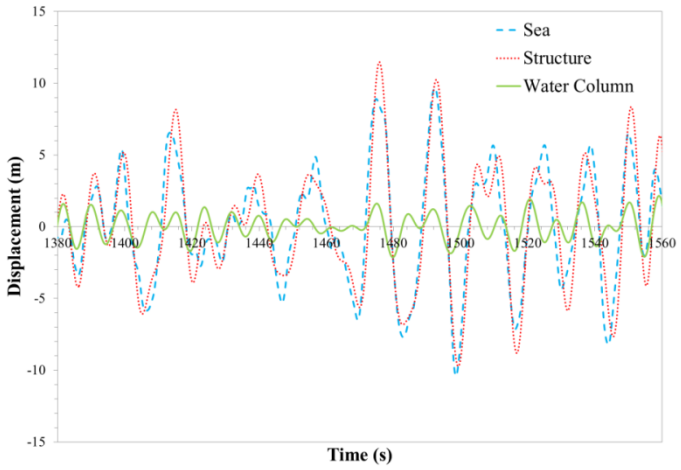

Figure 6.17: Time domain response for the 100-year storm in the Norwegian Sea for a system with reduced heave mass.

Figure 6.17 shows the response to the 1-in-100 year Norwegian Sea storm of the system with a reduced heave mass. It shows a structure that appears to be in phase with nearly equal amplitude to the forcing wave. The oscillating water column appears to be oscillating at approximately double the frequency of the forcing wave with little to no amplitude. The peak structure heave displacement appears to be equal to the peak wave height. The peak structure heave displacement expected during this testing period was 14.28 metres with an upper limit of 14.51 metres. The maximum sea state was 16.65 metres with an upper limit of 17.81 metres. The peak surge value for the structure was equal to 11.68 metres with an upper limit of 13.85 metres. The peak mooring line tension in Line 1 was 1782 kN with an upper limit of 2047 kN. The peak mooring line tension in Line 2 was 1367 kN with an upper limit of 1586 kN.

Power Take-off Damping Increase

The time domain response to the Norwegian Sea 100-year storm of the system with increased power take-off damping is seen in Figure 6.18.

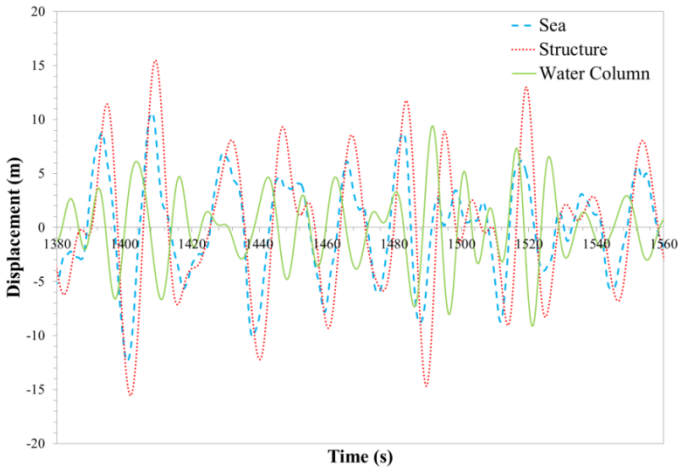

Figure 6.18: Time domain response for the 100-year storm in the Norwegian Sea for a system with increased power take-off damping

The domain output for this tuning mechanism shows the structure and wave moving approximately in phase with a small difference in heave amplitude. The structure appears to be experiencing slightly more heave than the wave height. The oscillating water column looks to be oscillating slightly out of phase with both the wave and structure. The amplitude of oscillation is smaller than both the structure and wave. The peak structure heave displacement expected during this testing period was 18.76 metres with an upper limit of 22.14 metres. The maximum sea state was 16.65 metres with an upper limit of 17.81 metres. The peak surge value for the structure was equal to 11.68 metres with an upper limit of 13.85 metres. The peak mooring line tension in Line 1 was 3114 kN with an upper limit of 3766 kN. The peak mooring line tension in Line 2 was 1244 kN with an upper limit of 1441 kN.

Stiffness Increase

The time domain response to the Norwegian Sea 100-year storm of the system with increased stiffness is seen in Figure 6.19.

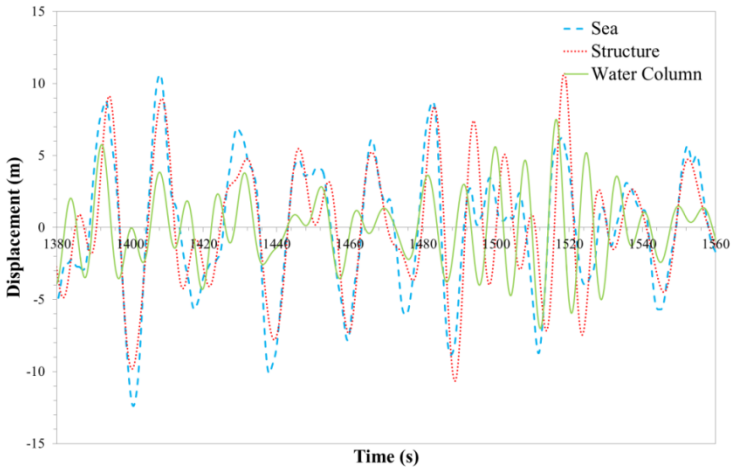

Figure 6.19: Time domain response of the stiffened system for the 100-year storm in the Norwegian Sea for a system with increased stiffness.

The time domain output for the structure with an increase in stiffness is very similar to the time domain output for the structure with a decrease in heave added mass (Figure 6.17). The oscillating water column shows greater heave in this system than the system seen in Figure 6.17. The structure output similarities are expected as an increase in system stiffness and decrease in added mass both have the same effect on the natural period of the structure. The peak structure heave displacement expected during this testing period was 14.06 metres with an upper limit of 16.35 metres. The maximum sea state was 16.65 metres with an upper limit of 17.81 metres. The peak surge value for the structure was equal to 11.68 metres with an upper limit of 13.85 metres. The peak mooring line tension in Line 1 was 1519 kN with an upper limit of 1776 kN. The peak mooring line tension in Line 2 was 1037 kN with an upper limit of 1218 kN.

Combination of Heave Mass Reduction and Power Take-off Damping Increase

The time domain output for the system subjected to a combination of a heave mass reduction and increase in power take-off damping (to double the optimal value) is seen in Figure 6.20

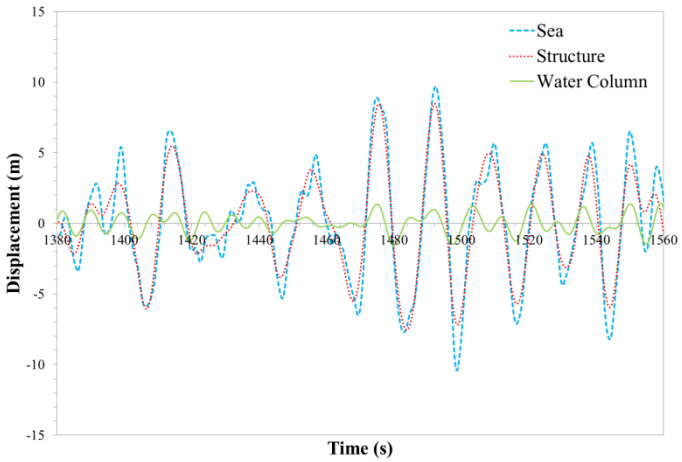

Figure 6.20: Time domain response for the 100-year storm in the Norwegian Sea for a system with an increase in power take-off damping and reduction in heave mass.

Viewing the time domain output of the system against the three storm spectra shows an immediate reduction in the structure heave compared to the untuned system. The structure is tending to move in phase and with equal heave to the wave while the oscillating water column experiences very little motion. This is most likely because of the increased damping provided by the larger power output value. The peak structure heave displacement expected during this testing period was 17.51 metres with an upper limit of 21.71 metres. The maximum sea state was 16.65 metres with an upper limit of 17.81 metres. The peak surge value for the structure was equal to 11.68 metres with an upper limit of 13.85 metres. The peak mooring line tension in Line 1 was 2847 kN with an upper limit of 3489 kN. The peak mooring line tension in Line 2 was 1757 kN with an upper limit of 2110 kN.

Combination of Stiffness Increase and Power Take-off Damping Increase

The time domain output for the system subjected to a combination of a stiffness increase (double the water plane stiffness) and increase in power take-off damping (to double the optimal value) is seen in Figure 6.21

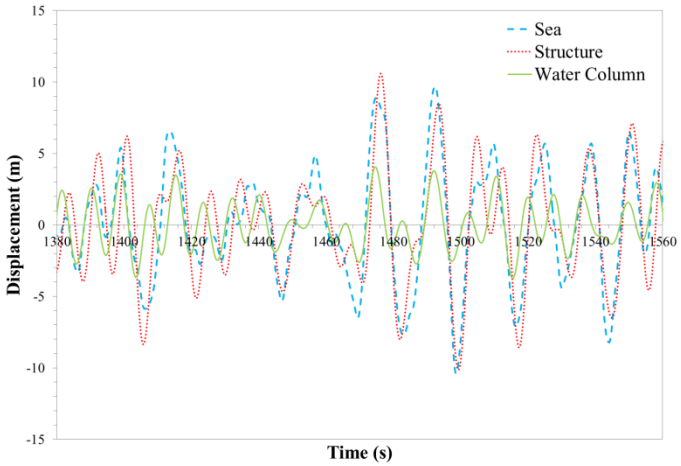

Figure 6.21: Time domain response for the 100-year storm in the Norwegian Sea for a system with an increase in power take-off damping and an increase in system stiffness.

The structure appears to be moving in phase with the wave and with equal amplitude of oscillation. The oscillating water column appears to be oscillating out of phase with both the structure and wave. The oscillating water column amplitude of oscillation is approximately half the value experienced by the wave and structure. The peak structure heave displacement expected during this testing period was 14.80 metres with an upper limit of 20.91 metres. The maximum sea state was 16.65 metres with an upper limit of 17.81 metres. The peak surge value for the structure was equal to 11.68 metres with an upper limit of 14.52 metres. The peak mooring line tension in Line 1 was 1768 kN with an upper limit of 2040 kN. The peak mooring line tension in Line 2 was 1237 kN with an upper limit of 1454 kN.

Combination of Heave Mass Reduction and Stiffness Increase

The time domain output for the system subjected to an increase in stiffness and a decrease in heave mass is seen in Figure 6.22

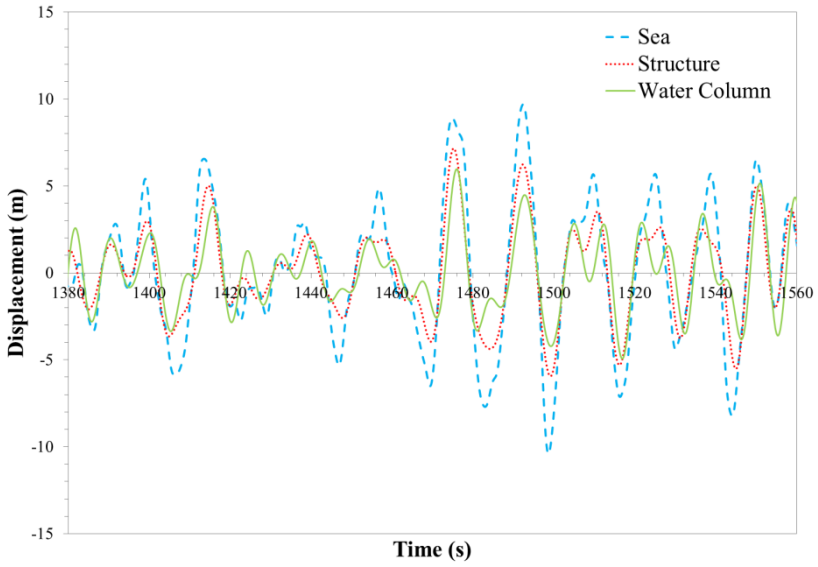

Figure 6.22: Time domain response for the 100-year storm in the Norwegian Sea system with an increase in stiffness and a decrease in heave mass.

The structure and oscillating water column both appear to be moving in phase with the wave but both at a lower amplitude of oscillation. This implies that the natural period of the structure and oscillating water column are far removed from the peak wave period of the storm. The peak structure heave displacement expected during this testing period was 8.619 metres with an upper limit of 8.728 metres. The maximum sea state was 16.65 metres with an upper limit of 17.81 metres. The peak surge value for the structure was equal to 11.88 metres with an upper limit of 14.52 metres. The peak mooring line tension in Line 1 was 711.3 kN with an upper limit of 801.8 kN. The peak mooring line tension in Line 2 was 812.1 kN with an upper limit of 989.0 kN.

Combination of all Tuning Mechanisms

The time domain output of the system subjected to all three tuning mechanisms is seen in Figure 6.23

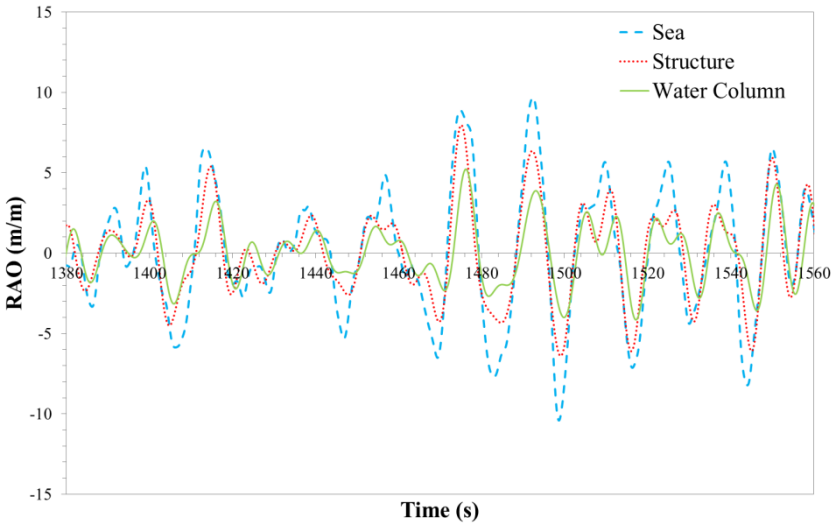

Figure 6.23: Time domain response for the 100-year storm in the Norwegian Sea with a decreased heave mass, increased power take-off damping, and increased stiffness.

This response shows a setup where the structure and oscillating water column are once again in phase with the wave but experience less amplitude of oscillation. This implies that the natural period of the structure and oscillating water column are far removed from the peak wave period of the storm. The peak structure heave displacement expected during this testing period was 9.189 metres with an upper limit of 10.93 metres. The maximum sea state was 16.65 metres with an upper limit of 17.81 metres. The peak surge value for the structure was equal to 11.88 metres with an upper limit of 14.52 metres. The peak mooring line tension in Line 1 was 794 kN with an upper limit of 893.5 kN. The peak mooring line tension in Line 2 was 880.0 kN with an upper limit of 1034 kN.

6.7.2 Spectral Density Functions of Responses from OrcaFlex Time Histories

The results displayed in section 6.7.2 are summarised and in Table 6.4 in section 6.8.2. The results are analysed and the implications of each tuning method is also discussed in section 6.8.2.

Untuned System

The spectral density functions of time domain response of the untuned system is seen in Figure 6.24.

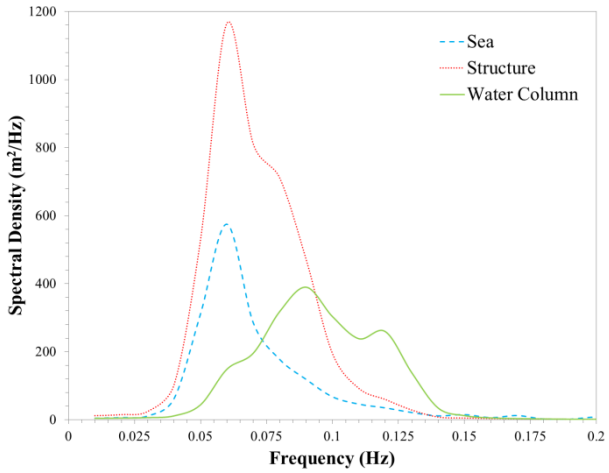

Figure 6.24: Spectral density function of the response to the Norwegian Sea 100-year storm of an untuned system.

The relative magnitudes and locations of the function peaks give insight into how the system is behaving. The structure is experiencing significant heave at wave periods equal to the peak wave period of the storm spectrum. The oscillating water column shows that an increased heave is occurring at values that are equal to its natural frequency. The integration of each function produces a value that is indicative of the power of each. The integral value for the wave is equal to 19.22 m^2, for the structure it is equal to 38.52 m^2, and for the oscillating water column it is equal to 16.30 m^2.

Heave Mass Reduction

The spectral density function for the system with a decreased heave mass subjected to the 100 year Norwegian Sea storm is seen in Figure 6.25.

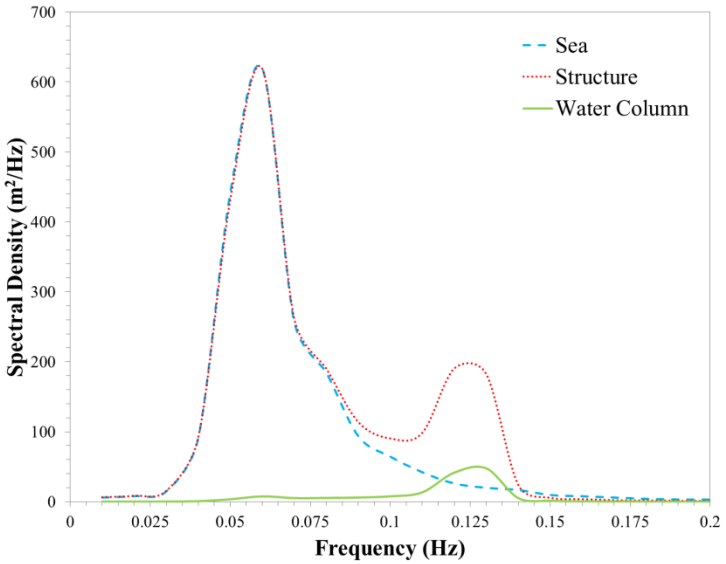

Figure 6.25: Spectral density function of the response to the Norwegian Sea 100-year storm of a system with a reduced heave mass.

The increase in structural values corresponding to the peak wave frequency of the storm have been nullified. Figure 6.25 shows a system where the structure and wave functions are nearly identical at frequency values most often experienced during the wave spectrum. The oscillating water column is still showing a peak at values corresponding to its natural frequency. This is causing an increased motion of the structure around these values because of the coupled nature of the system. The integral value for the wave is equal to 19.38 m^2, for the structure it is equal to 23.53 m^2, and for the oscillating water column it is equal to 1.476 m^2.

Power Take-off Damping Increase

The spectral density function for the system with an increased power take-off damping double the optimal damping level subjected to the 100 year Norwegian Sea storm is seen in Figure 6.26.

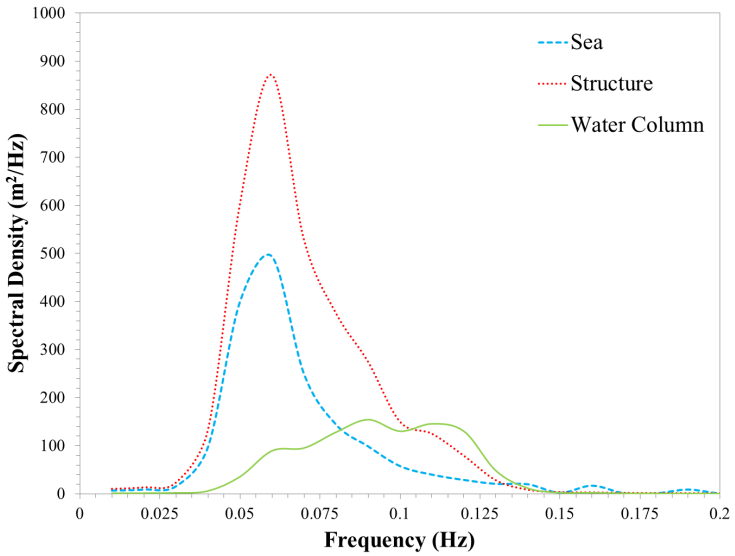

Figure 6.26: Spectral density function of the response to the Norwegian Sea 100-year storm of a system with increased power take-off damping.

The spectral density function seen in Figure 6.26 shows a structure with a much larger peak than the wave or oscillating water column. The oscillating water column function appears to be somewhat muted with no distinct peak. The maximum level of the oscillating water column function occurs at wave frequencies that sit well away from the peak wave frequency. The integral value for the wave is equal to 19.36 m^2, for the structure it is equal to 36.48 m^2, and for the oscillating water column it is equal to 10.38 m^2.

Stiffness Increase

The spectral density function for the system with an increased stiffness level subjected to the 100 year Norwegian Sea storm is seen in Figure 6.27.

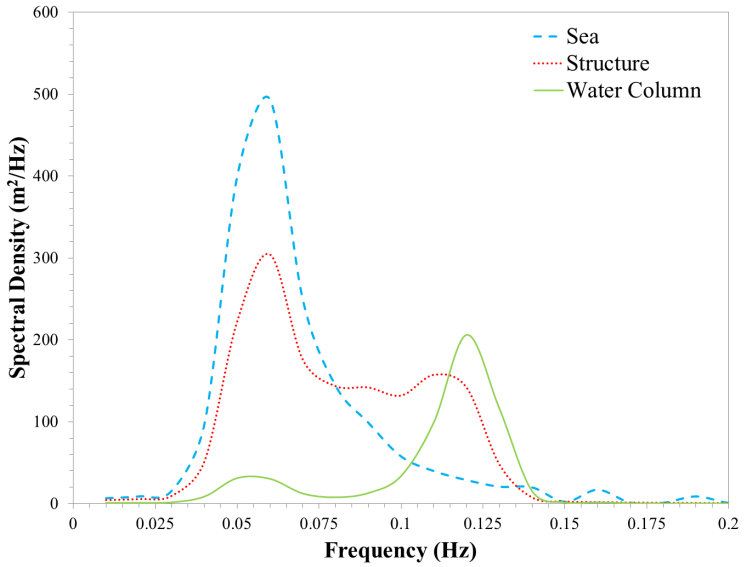

Figure 6.27: Spectral density function of the stiffened system in response to the Norwegian Sea 100-year storm.

The spectral density functions seen in Figure 6.27 show a significantly smaller value for the peak of the structure function. This peak is still occurring at values corresponding to the peak wave frequency value. The oscillating water column is showing a distinct peak at a value corresponding to its natural frequency. This is causing the structure function to remain elevated between the peak wave frequency and oscillating water column natural frequency. The integral value for the wave is equal to 19.38 m^2, for the structure it is equal to 16.98 m^2, and for the oscillating water column it is equal to 6.021 m^2.

Combination of Heave Mass Reduction and Power Take-off Damping Increase

Figure 6.28 details the spectral density functions of the system subjected to a decrease in heave mass and increase in power take-off damping.

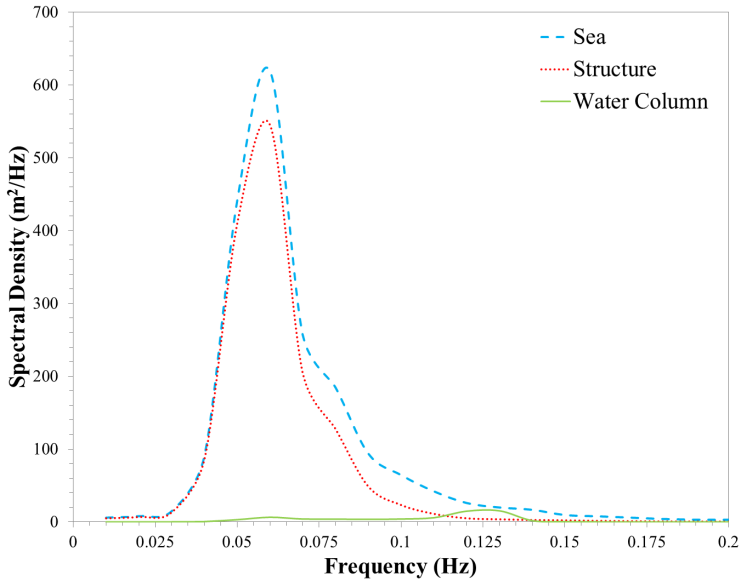

Figure 6.28: Spectral density function of the response to the Norwegian Sea 100-year storm with an increase in power take-off damping and a decrease in heave mass.

A combination of increased power take-off damping and decreased heave mass has produced a system with a structure function that has a lower peak level than the wave. The wave and structure both peak at the same frequency. The oscillating water column motion seems to have been severely dampened. The peak value is still occurring at a frequency value corresponding to its natural frequency. This motion does not appear to be causing any additional structural movement. The integral value for the wave is equal to 19.38 m^2, for the structure it is equal to 15.08 m^2, and for the oscillating water column it is equal to 0.6487 m^2.

Combination of Stiffness Increase and Power Take-off Damping Increase

Figure 6.29 details the spectral density functions for the system with increased stiffness and increased power take-off damping.

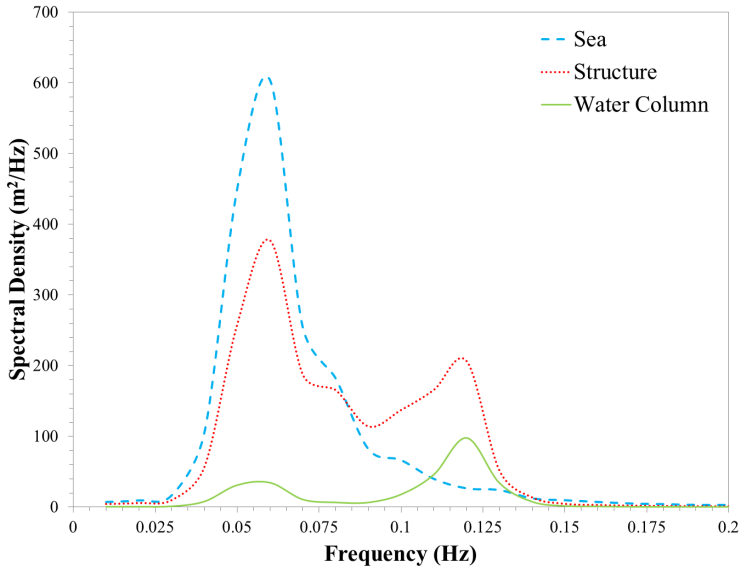

Figure 6.29: Spectral density function of the response to the Norwegian Sea 100-year storm of a system with increased stiffness and increased power take-off damping.

Figure 6.29 appears to be a combination of the results of each tuning mechanism used in isolation. The structure function peak is less than the wave function peak but is still occurring at the same frequency value. The oscillating water column shows a distinct peak at its natural frequency. This increase is accompanied by an increase in the structure function at this natural frequency. The increase in oscillating water column peak at its natural frequency is likely to be caused by the increase in structure stiffness. The increase in damping is causing the structure to be elevated at this frequency value. The integral value for the wave is equal to 19.36 m^2, for the structure it is equal to 17.83 m^2, and for the oscillating water column it is equal to 3.093 m^2.

Combination of Heave Mass Reduction and Stiffness Increase

Figure 6.30 details the spectral density response of the structure with increased stiffness and decreased heave mass.

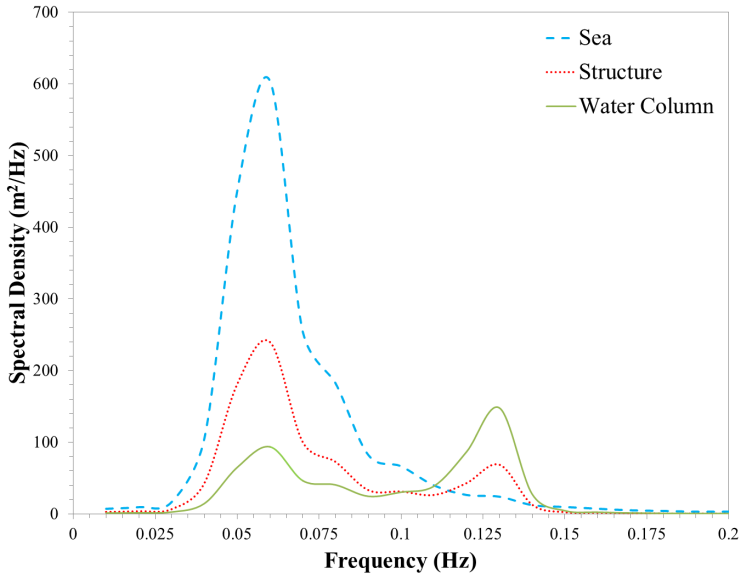

Figure 6.30: Spectral density function of the response to the Norwegian Sea 100-year storm of a system with decreased heave mass and increased stiffness.

Figure 6.30 shows a structural function with a peak significantly less than the wave peak. The two peaks are aligned at the peak wave frequency of the storm. The oscillating water column is showing a distinct peak at a value corresponding to its natural frequency. The oscillating water column peak is accompanied by a peak in the structure function at the natural frequency of the oscillating water column; however, the oscillating water column peak is roughly twice as high as the structure peak. This increase in oscillating water column peak is caused by the increase in structure stiffness. The integral value for the wave is equal to 19.36 m^2, for the structure it is equal to 8.787 m^2, and for the oscillating water column it is equal to 6.378 m^2.

Combination of all Tuning Mechanisms

Figure 6.31 details the spectral density function of the system tuned with a combination of a reduction in heave mass, an increase in stiffness, and an increase in power take-off damping.

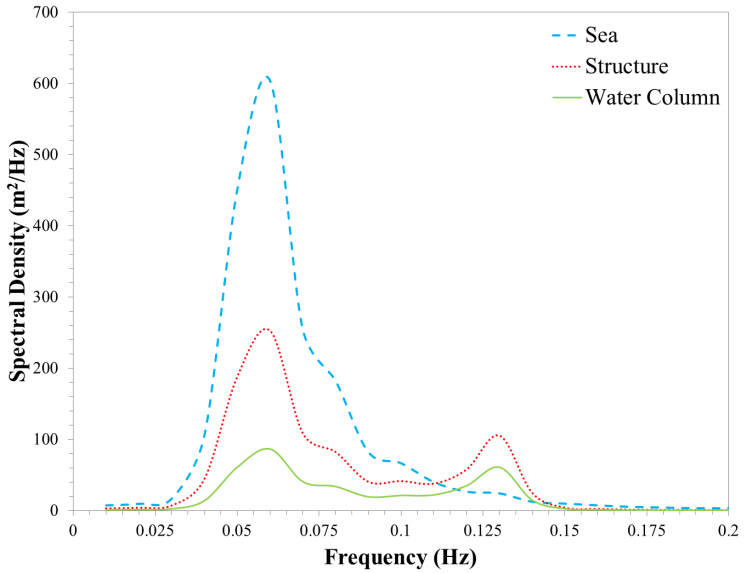

Figure 6.31: Spectral density function of the response to the Norwegian Sea 100-year storm of a system with an increase in power take-off damping, increase in stiffness, and a decrease in heave mass.

The spectral density functions in Figure 6.31 show the peak of the structure function is significantly less than the peak of the wave function. These two peaks are aligned at a value corresponding to the peak wave frequency of the storm. The oscillating water column shows two distinct peaks. The first occurs at a value equal to the peak wave frequency of the storm and the second occurs at its natural frequency. The second peak is accompanied by a secondary structure peak. The reason for the oscillating water column peak at its natural frequency is the increased structure stiffness. The structure is experiencing a higher peak at this frequency value because the power take-off damping is increased. The integral value for the wave is equal to 19.38 m^2, for the structure it is equal to 10.13 m^2, and for the oscillating water column it is equal to 4.220 m^2.

6.8 Discussion of the Norwegian Sea Analysis Results

6.8.1 Time Domain Analysis Results

The peak displacements for all tuning mechanisms and the peak mooring line tensions in line 1 and line 2 are shown in Table 6.4

Table 6.4: Peak displacement values for all storm spectra and all tuning mechanisms

	Norwegian Storm					
	Wave (m)	Heave (m)	Ratio	Surge (m)	Line 1 (kN)	Line 2 (kN)
No tuning	16.65	20.43	1.227	11.68	4373	1524
Heave reduction	16.65	14.28	0.8577	11.68	1782	1367
Damping increase	16.65	18.76	1.1267	11.68	3114	1244
Stiffness increase	16.65	14.04	0.8432	11.68	1519	1037
Heave + Damping	16.65	17.51	1.0517	11.68	2847	1757
Stiffness + Damping	16.65	14.8	0.8889	11.68	1768	1237
Heave + Stiffness	16.65	8.619	0.5177	11.68	711.3	812.1
All three	16.65	9.189	0.5519	11.68	794	880

*Ratio is defined at the heave peak displacement divided by the wave peak displacement

The combination of tuning mechanism results on the peak displacement values from Table 6.4 has been graphed in Figure 6.32. The smaller the peak displacement of the structure, the more likely the system is to survive during unfavourable storm conditions. While the absolute reduction is likely to be a key design parameter, the effect of tuning mechanisms are better understood if the ratio of the peak structure displacement to the wave peak displacement is shown. A value of 1 means that the structure is experiencing a peak displacement equal to the peak wave height of the storm, a value less than 1 indicates that the peak displacement of the structure is less than the peak wave height of the storm, and a value greater than 1 indicates the opposite.

All tuning mechanisms used in isolation and all combinations of tuning mechanism have shown to decrease the heave peak displacement and the mooring line tension in the leading (heading of 0 degrees) mooring line. The surge displacement of the structure has remained constant across all tuning mechanisms. This was expected as the tuning mechanisms all influence the heave RAO of the structure rather than the surge RAO.

From the isolation testing, the increase in system stiffness has been shown to cause the greatest reduction in mooring line tensions and heave displacement of the structure. The peak

heave displacement ratio is 0.8432 and the mooring line tension of line 1 has dropped from 4373 kN in the untuned system to 1519 kN in the tuned system. A reduction in the heave mass has also shown promising results when used in isolation. The peak heave displacement ratio is 0.8577. This has caused the mooring line peak tension to drop from 4737 kN in the untuned system to 1782 kN in the tuned system.

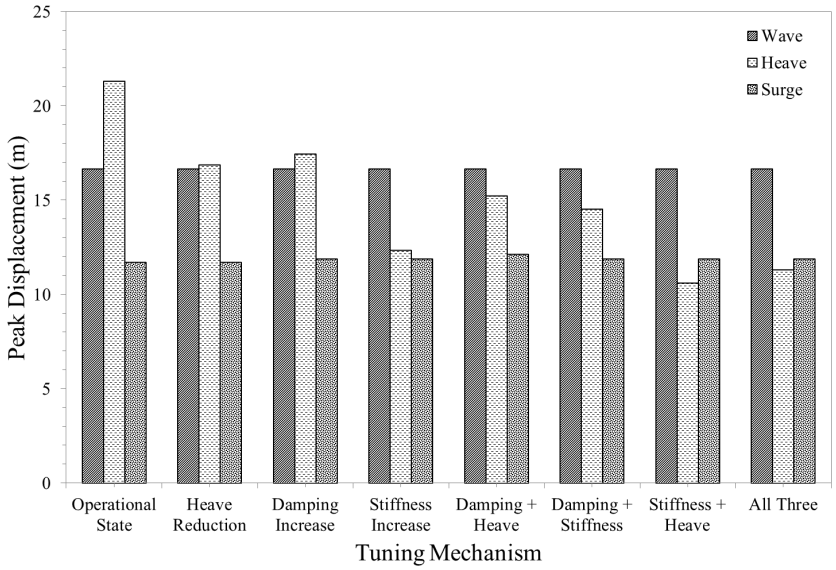

Figure 6.32: Peak displacements of the wave and structure heave and surge motion during the 1-in-100 year Norwegian Sea storm.

An increase in power take-off damping has not performed as well as an increase in stiffness or a decrease in heave mass when used in isolation. The peak displacement ratio is 1.127. This small reduction has caused the peak line tension in line 1 to drop from 4737 kN in the untuned system to 3114 kN in the tuned system.

The combinations of tuning mechanisms performed better than any mechanism used in isolation except for an increase in system stiffness. A combination of a heave mass reduction and an increase in system stiffness has reduced the peak displacement ratio to 0.5177. This has caused a considerable drop in the peak tension of mooring line 1. The tension has reduced from a value of 4737 kN in the untuned system to a value of 711.3 kN in the tuned system. The other combinations have shown little to no benefit over any of the isolated test results. The combination of all three mechanisms shows a greater peak displacement ratio (0.5519) than when only using an increase in stiffness and damping. With this increase, there is an associated increase in peak mooring line tension in line 1 (794 kN). These results suggest that utilising an increase in power take-off damping above the optimal damping value is unlikely

to produce a system with lower peak displacements and hence lower peak mooring line tensions. Figure 6.33 graphically illustrates the last two columns of Table 6.4

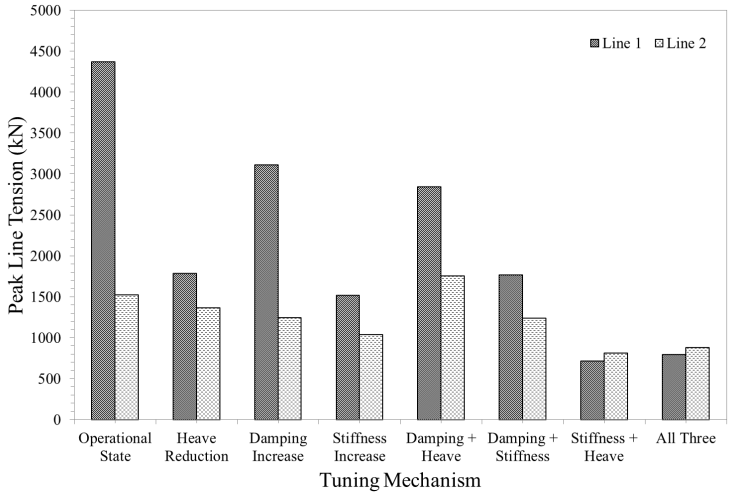

Figure 6.33: Peak line tension in Line 1 and Line 2 during the 1-in-100 year Nowegian Sea storm.

6.8.2 Spectral Density Analysis Results

The spectral density integral values are summarised in Table 6.5. The ratio of the significant displacements has also been calculated. These are shown in the last three columns of the table.

Table 6.5: Spectral density integral values for the 1-in-100 year Norwgian Sea storm

	Norwegian Storm								
	Sea		Structure		OWC		Structure/Sea	OWC/Sea	OWC/Structure
Tuning mechanism	m_0 (m^2)	D_{sig} (m)	m_0 (m^2)	D_{sig} (m)	m_0 (m^2)	D_{sig} (m)			
No tuning	19.22	8.769	38.52	12.41	16.3	8.075	1.415	0.9209	0.6506
Heave reduction	19.38	8.805	23.53	9.701	1.476	2.429	1.102	0.2759	0.2504
Damping increase	19.36	8.8	36.48	12.08	10.38	6.444	1.373	0.7322	0.5334
Stiffness increase	19.38	8.805	16.98	8.241	6.021	4.908	0.936	0.5574	0.5955
Heave + Damping	19.38	8.805	15.08	7.767	0.6487	1.611	0.8821	0.183	0.2074
Stiffness + Damping	19.36	8.8	17.83	8.445	3.093	3.517	0.9597	0.3997	0.4165
Heave + Stiffness	19.36	8.8	8.787	5.929	6.378	5.051	0.6737	0.574	0.852
All three	19.36	8.8	10.13	6.366	4.22	4.109	0.7234	0.4669	0.6454

The ratios of the integral values from Table 6.5 are graphed in Figure 6.34. The graph includes all isolation testing and all combinations of the isolated alterations. The smaller the value the more likely the system is to survive an unfavourable storm period. The zeroth moment values and significant displacement values have been plotted for each tuning mechanism.

Figure 6.34: Integral value ratios for each tuning mechanism

As touched on before, the integral values give an indication of the heave motion of the device, oscillating water column, and wave. The integral value for the wave is approximately equal for all tested states. This is expected as the time domain wave is drawn from the same spectrum. If this spectrum is left to run for long enough it will converge to the theoretical

spectrum defined by the JONSWAP equation. The equal values obtained suggest that this time period (3 hours) is sufficient to be able to compare results from different sea states.

The ratio of the integral values has been calculated for ease of comparison. A value of 1 suggests the numerator of the ratio is experiencing more heave motion over the duration of the testing period than the denominator. The first column of the results in Figure 6.34 is the structure divided by the wave, the second column is the oscillating water column divided by the wave, and the third column is the structure divided by the oscillating water column. The most important ratio with respect to system survivability is the structure to wave ratio. A ratio value larger than 1 suggests that the expected peak displacement is likely to be greater than the wave peak displacement; while a value smaller than one suggests the opposite. The results from the spectral density analysis conform to the results from the time domain analysis regarding peak displacement and peak mooring line tension. A drop in the integral ratio is indicative of a drop in the peak mooring line tension.

The results from the isolation testing and combination testing confirm the conclusions regarding the best performing tuning mechanisms. An increase in stiffness used in isolation (D_{sig} = 8.241 m) is slightly better than a decrease in heave mass (D_{sig} = 9.701 m) which is substantially better than only increasing the power take-off damping to double the optimal value (D_{sig} = 12.08 m). Damping increases combined with a decrease in heave (D_{sig} = 7.767 m) or an increase in stiffness (D_{sig} = 8.445 m) or a combination of both (D_{sig} = 6.366 m) does not perform as well as a combination of heave mass decrease and stiffness increase (D_{sig} = 5.929 m).

6.9 Results of the West Africa Storm Analysis

The second 100-year event simulated in OcraFlex is the event from the sea located off West Africa. As outlined earlier, this sea state has a peak wave period of 15.75 seconds, a significant wave height of 3.85 metres, a 1.85 m/s current, and a one-hour average wind speed of 16 m/s. The wind speed and current are acting in the same direction as the wave. This will produce the highest force on the system.

6.9.1 Time Domain Output

Untuned System

The time domain output for the untuned system in the 100 year event for the sea off West Africa is seen in Figure 6.35. The time domain figures show a small section of the total simulation to allow the movements to be seen clearly. Plotting all data points would result in a graph that is unreadable.

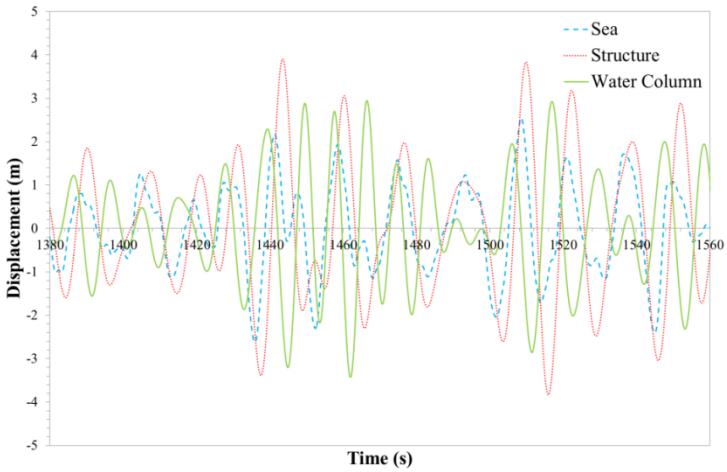

Figure 6.35: Time domain response for the 100-year storm off West Africa (swell) of an untuned system.

Figure 6.35 shows a structure and oscillating water column with large heave compared to the wave. The structure and oscillating water column appear to be out of phase with the wave. The peak structure and oscillating water column motions exceed the peak wave height. The peak heave expected by the structure during this testing period was 5.821 metres with an upper limit of 7.318 metres. The maximum sea state was 3.970 metres with an upper limit of 4.221 metres. The peak surge value for the structure was equal to 3.219 metres with an upper limit of 4.554 metres. The peak mooring line tension in Line 1 was 366.6 kN with an upper limit of 406.5 kN. The peak mooring line tension in Line 2 was 112.4 kN with an upper limit of 117.8 kN.

Heave Mass Reduction

Figure 6.36 details the time domain response to the West Africa 100-year storm conditions for a system tuned with a reduction in heave mass.

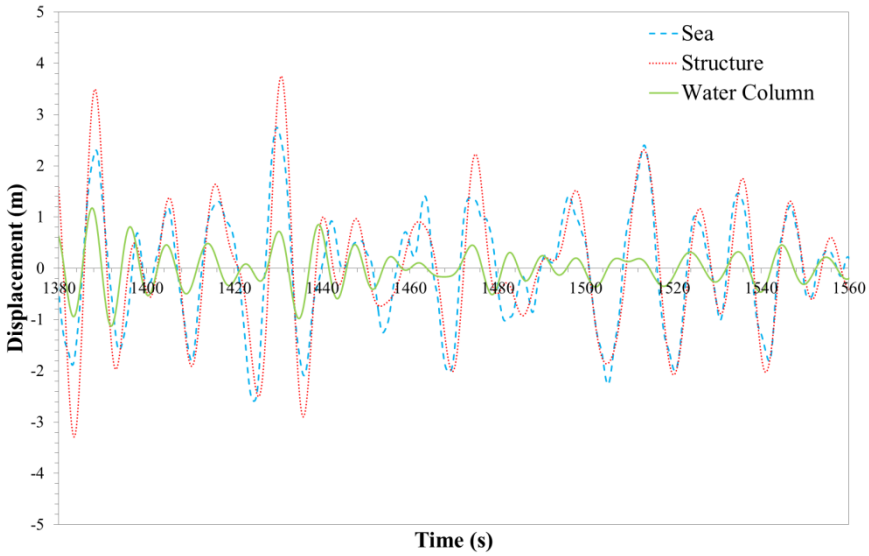

Figure 6.36: Time domain response for the 100-year storm off West Africa (swell) of a system with a reduction in heave mass.

The system shows a structure that is moving in phase with the wave. The amplitude of the structure is usually greater than or equal to that of the wave. The oscillating water column appears to be oscillating at double the rate of the structure and wave and with significantly smaller amplitude. The peak heave expected during this testing period by the structure was 4.386 metres with an upper limit of 5.319 metres. The maximum sea state was 3.970 metres with an upper limit of 4.221 metres. The peak surge value for the structure was equal to 3.219 metres with an upper limit of 4.554 metres. The peak mooring line tension in Line 1 was 309.2 kN with an upper limit of 333.8 kN. The peak mooring line tension in Line 2 was 121.9 kN with an upper limit of 151.3 kN.

Power Take-off Damping Increase

Figure 6.37 details the time domain response of the system with increased heave mass to the 100 year event in the sea off West Africa

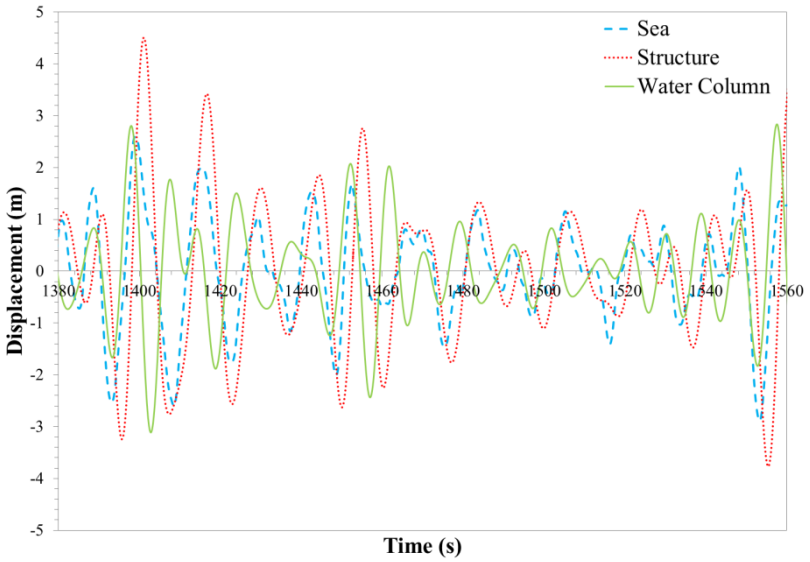

Figure 6.37 Time domain response for the 100-year storm off West Africa (swell) of a system with an increase in power take-off damping

The system shows a structure that is moving roughly in phase with the wave with an amplitude generally greater than that of the wave. The oscillating water column is moving out of phase with the structure and is experiencing about the same amplitude as the wave amplitude. The peak heave expected by the structure during this testing period was 5.232 metres with an upper limit of 6.107 metres. The maximum sea state was 3.970 metres with an upper limit of 4.221 metres. The peak mooring line tension in Line 1 was 361.9 kN with an upper limit of 394.4 kN. The peak mooring line tension in Line 2 was 266.6 kN with an upper limit of 271.6 kN.

Stiffness Increase

Figure 6.38 details the time domain response of the system with increased stiffness to the 100 year event in the sea off West Africa

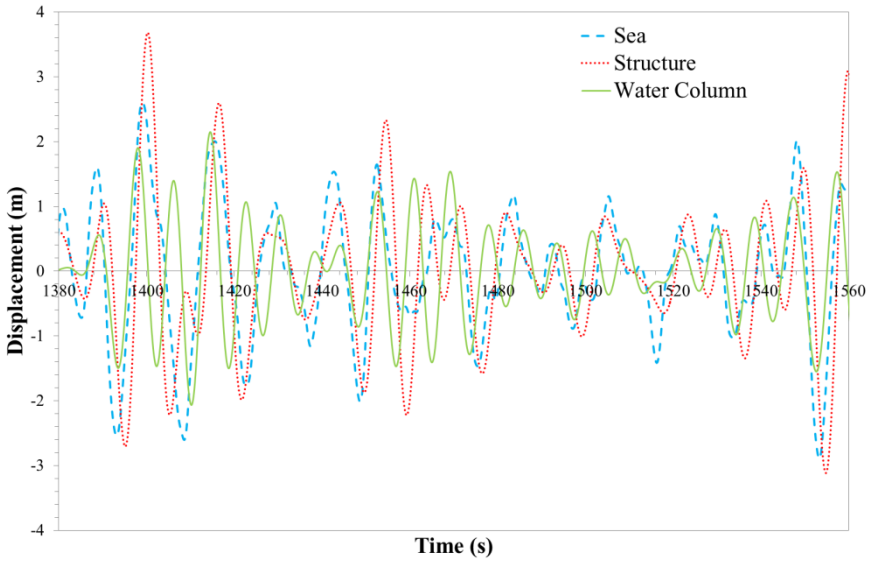

Figure 6.38: Time domain response for the 100-year storm off West Africa (swell) of a system with an increase in stiffness

This system shows a structure that is moving in phase with the wave. The structure experiences time periods where the displacement peak is both greater and less than the wave peak displacement. The oscillating water column appears to be moving roughly in phase with the wave at times and out of phase at other times. The peak heave expected by the structure during this testing period was 4.083 metres with an upper limit of 4.532 metres. The maximum sea state was 3.970 metres with an upper limit of 4.221 metres. The peak surge value for the structure was equal to 3.219 metres with an upper limit of 4.554 metres. The peak mooring line tension in Line 1 was 321.6 kN with an upper limit of 370.2 kN. The peak mooring line tension in Line 2 was 111.3 kN with an upper limit of 117.8 kN.

Combination of Heave Mass Reduction and Power Take-off Damping Increase

Figure 6.39 details the time domain response of the structure tuned with a decrease in heave mass and an increase in power take-off damping.

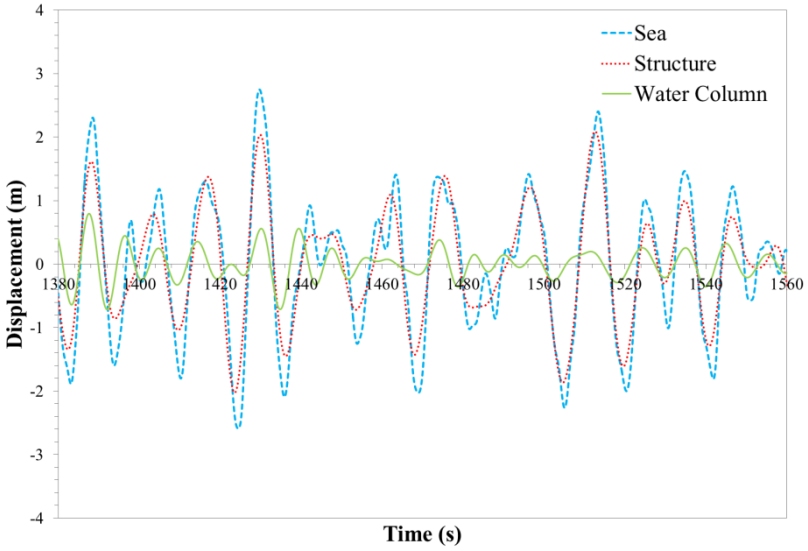

Figure 6.39: Time domain response for the 100-year storm off West Africa (swell) of a system with an increase in power take-off damping and a decrease in heave mass.

The heave time domain output shows the structure is moving mostly in phase with the wave. The structure is lower amplitude than the wave. The oscillating water column seems to be oscillating at a faster rate than both the wave and structure. The oscillating water column amplitude is much smaller than both the wave and structure. The peak heave expected by the structure during this testing period was 4.364 metres with an upper limit of 4.696 metres. The maximum sea state was 3.970 metres with an upper limit of 4.221 metres. The peak surge value for the structure was equal to 3.219 metres with an upper limit of 4.554 metres. The peak mooring line tension in Line 1 was 330.7 kN with an upper limit of 361.4 kN. The peak mooring line tension in Line 2 was 108.9 kN with an upper limit of 112.9 kN.

Combination of Stiffness Increase and Power Take-off Damping Increase

Figure 6.40 details the heave time domain response for a structure tuned with an increase in stiffness and an increase in power take-off damping subjected to the 1-in-100 year storm spectra off West Africa.

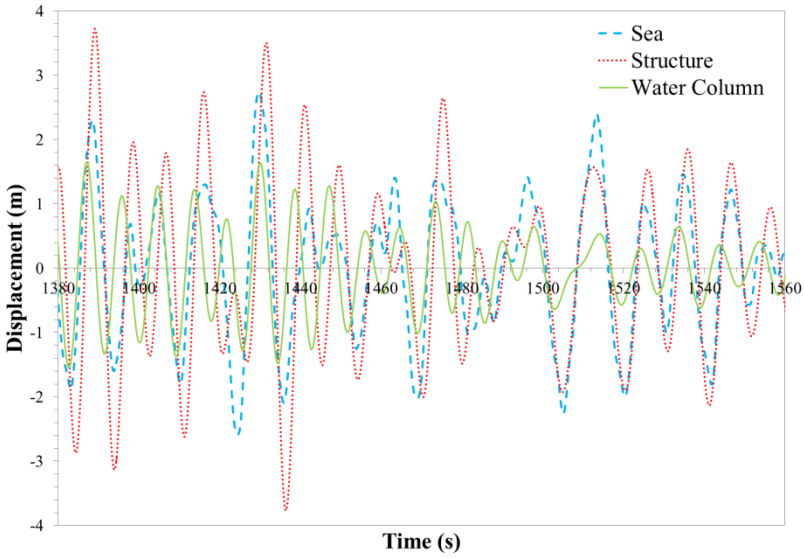

Figure 6.40: Time domain response for the 100-year storm off West Africa (swell) of a system with an increase in stiffness and an increase in power take-off damping.

The heave time domain output shows the structure is moving mostly in phase with the wave. The structure is experiencing greater amplitude than the wave. The oscillating water column seems to be oscillating approximately in phase with the structure and the wave. The oscillating water column amplitude is half the wave and structure amplitude. The peak heave expected by the structure during this testing period was 4.340 metres with an upper limit of 4.965 metres. The maximum sea state was 3.970 metres with an upper limit of 4.221 metres. The peak surge value for the structure was equal to 3.219 metres with an upper limit of 4.554 metres. The peak mooring line tension in Line 1 was 324.5 kN with an upper limit of 365.9 kN. The peak mooring line tension in Line 2 was 114.7 kN with an upper limit of 126.4 kN.

Combination of Heave Mass Reduction and Stiffness Increase

Figure 6.41 details the heave time domain response of the structure tuned with a heave mass reduction and stiffness increase subjected to the 1-in-100 year storm spectrum off West Africa.

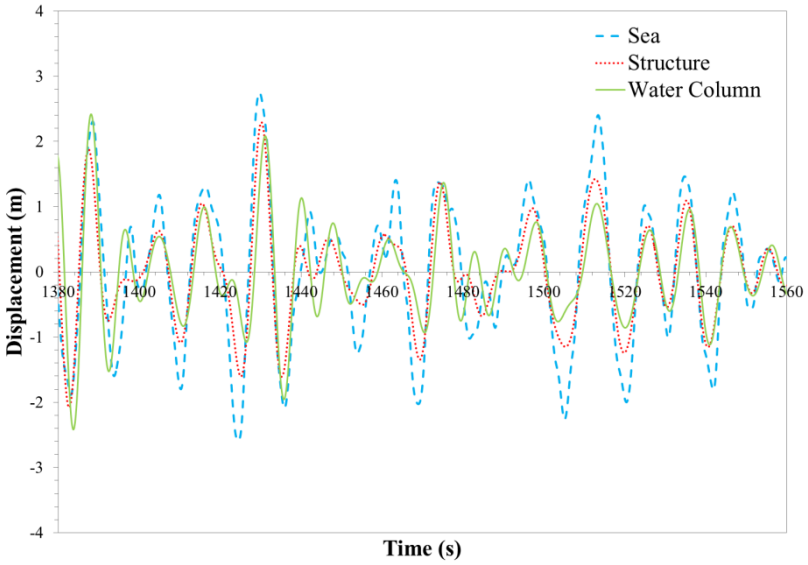

Figure 6.41: Time domain response for the 100-year storm off West Africa (swell) of a system with an increase in stiffness and a decrease in heave mass

The heave time domain output shows the structure is moving in phase with the wave. The structure is experiencing slightly smaller amplitude than the wave. The oscillating water column seems to be oscillating approximately in phase with the structure and the wave. The oscillating water column amplitude is approximately equal to the wave and structure amplitude. The peak heave expected by the structure during this testing period was 2.514 metres with an upper limit of 2.801 metres. The maximum sea state was 3.970 metres with an upper limit of 4.221 metres.. The peak surge value for the structure was equal to 3.219 metres with an upper limit of 4.554 metres. The peak mooring line tension in Line 1 was 233.9 kN with an upper limit of 238.3 kN. The peak mooring line tension in Line 2 was 102.9 kN with an upper limit of 106.1 kN.

Combination of all Tuning Mechanisms

Figure 6.42 details the heave time domain response of the structure tuned with a decrease in heave mass, an increase in stiffness, and an increase in power take-off damping

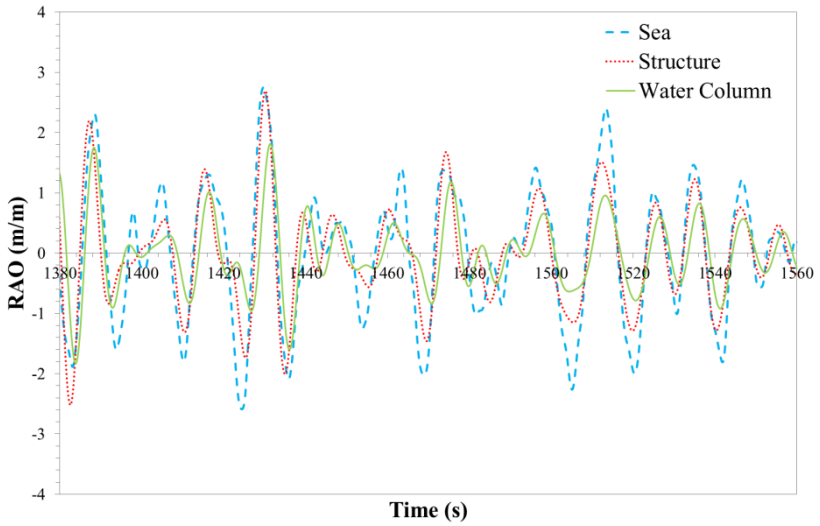

Figure 6.42: Time domain response for the 100-year storm off West Africa (swell) of a system with an increase in stiffness, decrease in heave mass, and an increase in power take-off damping.

The heave time domain output shows the structure is moving in phase with the wave. The structure is experiencing slightly smaller amplitude than the wave. The oscillating water column seems to be oscillating approximately in phase with the structure and the wave. The oscillating water column amplitude is approximately equal to the wave and structure amplitude, and at times may be slightly less. The peak heave expected by the structure during this testing period was 2.952 metres with an upper limit of 3.783 metres. The maximum sea state was 3.970 metres with an upper limit of 4.221 metres. The peak surge value for the structure was equal to 3.219 metres with an upper limit of 4.554 metres. The peak mooring line tension in Line 1 was 241.3 kN with an upper limit of 258.7 kN. The peak mooring line tension in Line 2 was 107.0 kN with an upper limit of 110.6 kN.

6.9.2 Spectral Density Functions

The results displayed in section 6.7.2 are summarised and in Table 6.6 in section 6.10.2. The results are analysed and the implications of each tuning method is also discussed in section 6.10.2.

Untuned System

Figure 6.43 details the spectral density functions of the untuned system subjected to the 100 year event off West Africa

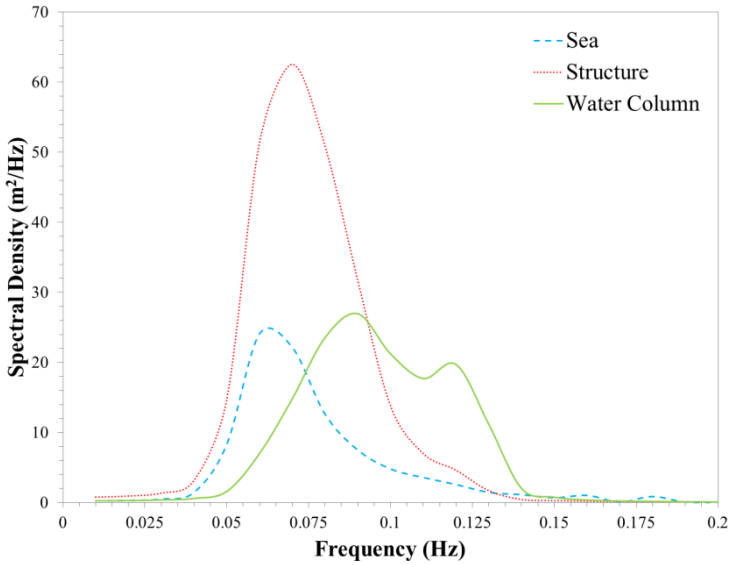

Figure 6.43: Spectral density function of the response to the West Africa (swell) 100-year storm of an untuned system

The structure function is significantly larger than both the oscillating water column and wave function. The structure function seems to create an envelope that contains both the wave peak and the oscillating water column peak. The oscillating water column exhibits two peaks. The first and largest peak falls at a frequency period between the natural period of the structure and oscillating water column. The second peak coincides with its natural period. The integration of each function produces a value that is indicative of the power of each. The integral value for the wave is equal to 0.9106 m^2, the structure is equal to 2.516 m^2, and the oscillating water column is equal to 1.924 m^2.

Heave Mass Reduction

Figure 6.44 details the spectral density functions of the system tuned with decreased heave mass subjected to the 100 year event off West Africa

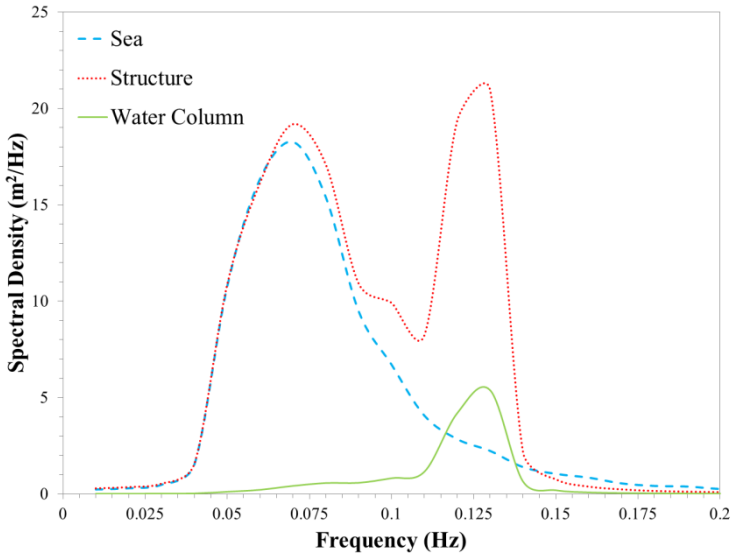

Figure 6.44: Spectral density function of the response to the West Africa (swell) 100-year storm of a system with a decrease in heave mass

The structure function in Figure 6.44 is closely aligned with the wave function at wave frequencies close to the peak wave frequency of the sea spectrum. The structure function peaks higher than the wave at a frequency that matches the natural frequency of the oscillating water column. The oscillating water column function also peaks at this value. This behaviour is attributed to a combination of a reduction in heave mass moving the structure natural period away from the prevalent wave periods of the storm; hence the structure peak aligning with the wave peak, and the coupled nature of the structure and oscillating water column. The integration of each function produces a value that is indicative of the power of each. The integral value for the wave is equal to 0.9517 m^2, for the structure it is equal to 1.403 m^2, and for the oscillating water column it is equal to 0.1472 m^2.

Power Take-off Damping Increase

Figure 6.45 details the spectral density functions of the system tuned with increased power take-off damping subjected to the 100 year event off West Africa

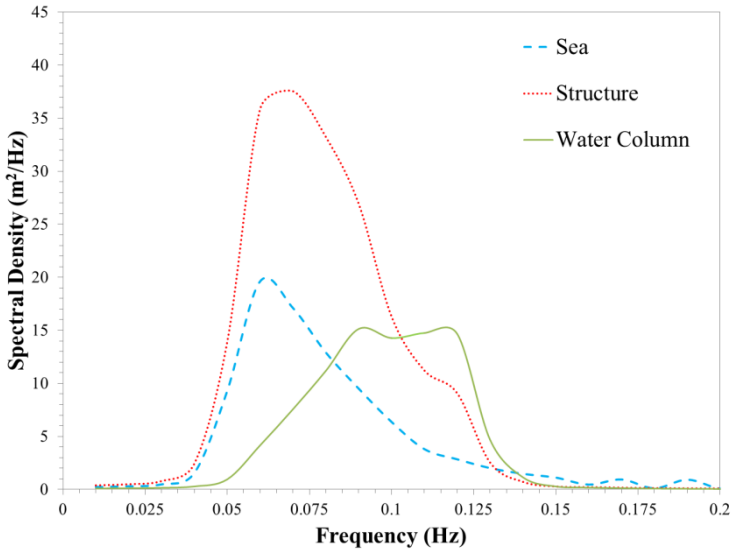

Figure 6.45: Spectral density function of the response to the West Africa (swell) 100-year storm of a system with an increase in power take-off damping.

Figure 6.45 shows the structure peak is significantly higher than the wave and oscillating water column peaks. The structure peak is occurring at the peak wave frequency of the storm. The increased power take-off damping has somewhat uncoupled the structure and oscillating water column movements. The structure is no longer experiencing a peak that aligns with the oscillating water column peak. The oscillating water column peak is located at its natural frequency but is elevated from a frequency value approximately half way between the structure natural frequency and the oscillating water column natural frequency. The integration of each function produces a value that is indicative of the power of each. The integral value for the wave is equal to 0.9542 m^2, for the structure it is equal to 2.034 m^2, and for the oscillating water column it is equal to 0.9361 m^2.

Stiffness Increase

Figure 6.46 details the spectral density functions of the system tuned with increased stiffness subjected to the 100 year event off West Africa

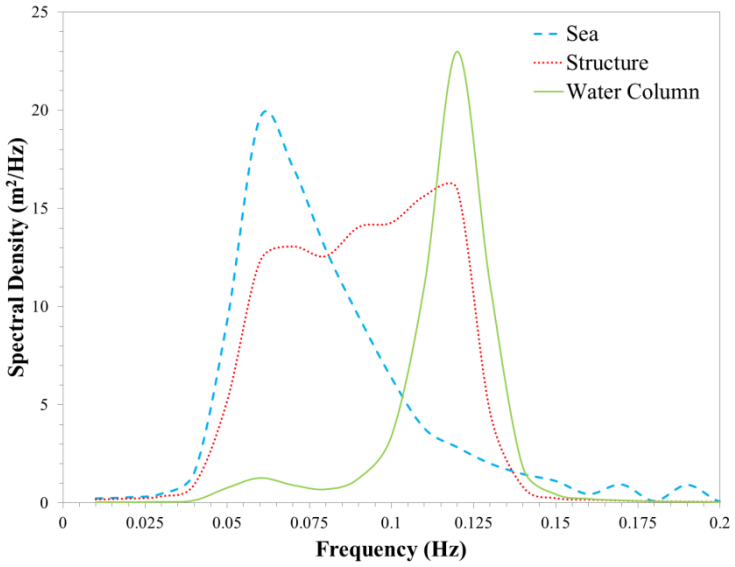

Figure 6.46: Spectral density function of the response to the West Africa (swell) 100-year storm of a system with an increase in stiffness

Figure 6.46 shows the structure function has reduced to a value below the wave peak at the peak wave frequency of the storm. This is mostly likely attributed to a reduction in the heave RAO at frequencies values surrounding the peak frequency. The structure function, however, shows a large peak around the peak of the oscillating water column function. This is most likely due to the coupled nature of the system. The oscillating water column function shows a significantly large peak with the system stiffness increased. This large peak is likely due to the oscillating water column stiffness being less than the structure stiffness and hence more relative movement it now possible. The integration of each function produces a value that is indicative of the power of each. The integral value for the wave is equal to 0.9517 m^2, for the structure it is equal to 1.142 m^2, and for the oscillating water column it is equal to 0.5738 m^2.

Combination of Heave Mass Reduction and Power Take-off Damping Increase

Figure 6.47 details the spectral density functions of the system tuned with increased power take-off damping and decreased heave mass subjected to the 100 year event off West Africa.

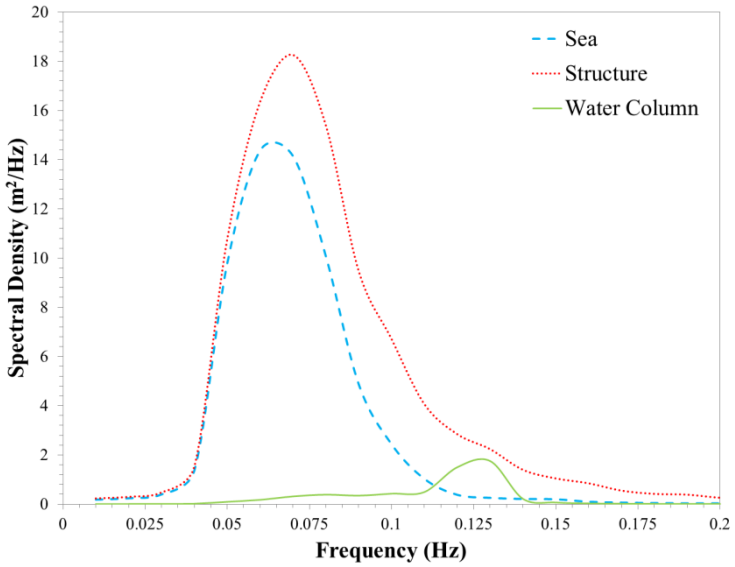

Figure 6.47: Spectral density function of the response to the West Africa (swell) 100-year storm of a system with an increase in power take-off damping and decrease in heave mass.

The structural function peak is greater than the wave peak. The structure function peak is occurring at a frequency value slightly greater than the peak wave frequency for the wave spectrum. This peak value is greater than the peak value of the system tuned with only a heave mass reduction. This suggests the increase in power take-off damping is causing an increase in structure heave. The oscillating water column is exhibiting a small peak at a frequency value equal to its natural period. There is no associated structure peak at this frequency value. This is likely because of the increased damping reducing the coupling effect between the structure and oscillating water column. The integration of each function produces a value that is indicative of the power of each. The integral value for the wave is equal to 0.9517 m^2, for the structure it is equal to 0.6064 m^2, and for the oscillating water column it is equal to 0.0594 m^2.

Combination of Stiffness Increase and Power Take-off Damping Increase

Figure 6.48 details the spectral density functions of the system tuned with increased power take-off damping and an increase in stiffness subjected to the 100 year event off West Africa.

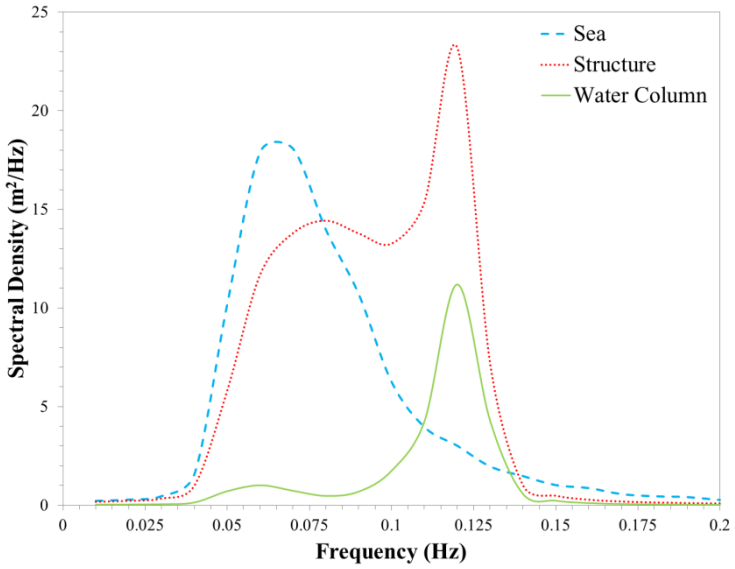

Figure 6.48: Spectral density function of the response to the West Africa (swell) 100-year storm of a system with an increase in power take-off damping and increase in stiffness.

This system shows a reduction in the structure peak at frequencies equal to the peak wave frequency of the storm spectrum. The system peak is now less than the wave peak. The oscillating water column is showing a distinct peak at its natural frequency. This distinct peak is associated with the increase in structure stiffness. The increased structure peak at this frequency is most likely caused by the closer alignment of the structure natural frequency and the wave natural period. This closer alignment is due to the increase in stiffness causing an increase in the natural frequency of the structure. The integration of each function produces a value that is indicative of the power of each. The integral value for the wave is equal to 0.9542 m^2, for the structure it is equal to 1.236 m^2, and for the oscillating water column it is equal to 0.2666 m^2.

Combination of Heave Mass Reduction and Stiffness Increase

Figure 6.49 details the spectral density functions of the system tuned with increased stiffness and a decrease in heave mass subjected to the 100 year event off West Africa.

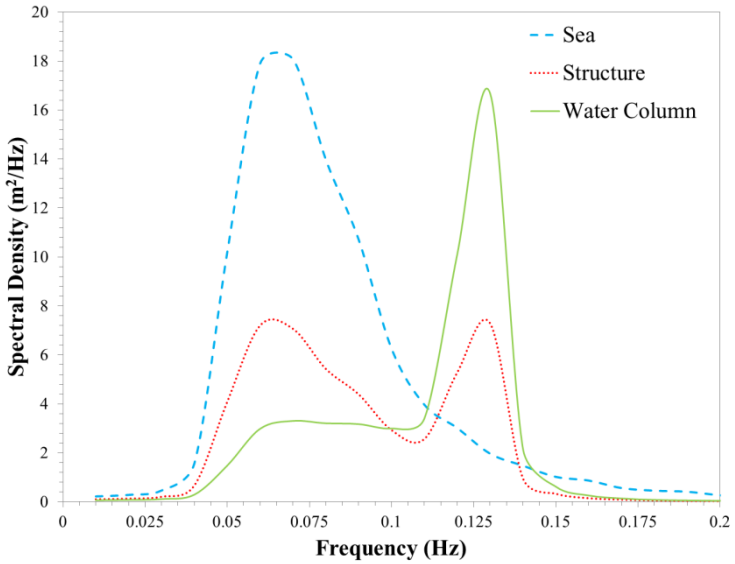

Figure 6.49: Spectral density function of the response to the West Africa (swell) 100-year storm of a system with an increase in stiffness and a decrease in heave mass.

The structure function shows a large reduction in the peak value at wave frequencies around the peak wave frequency of the storm. This peak value is significantly smaller than the peak wave value. The structure shows a second distinct peak of similar magnitude at a frequency equal to the oscillating water column natural frequency. The oscillating water column also exhibits a large peak at this frequency value. The coupled nature of the system and a smaller (optimal power production) value of power take-off damping are causing the structure to experience significant heave around this frequency value. The increase in the oscillating water column peak value is attributed to the increased stiffness in the structure. The integration of each function produces a value that is indicative of the power of each. The integral value for the wave is equal to 0.9542 m^2, for the structure it is equal to 0.4933 m^2, and for the oscillating water column it is equal to 0.5170 m^2.

Combination of all Tuning Mechanisms

Figure 6.50 details the spectral density functions of the system tuned with increased stiffness, increased power take-off damping, and a decrease in heave mass subjected to the 100 year event off West Africa.

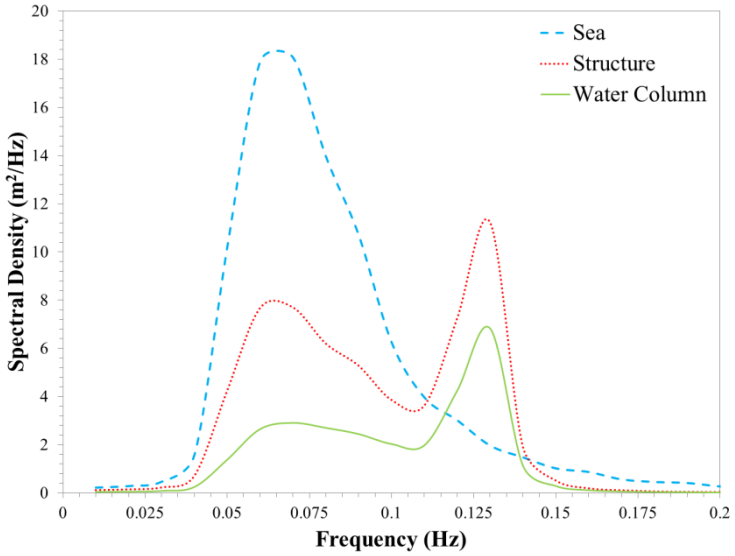

Figure 6.50: Spectral density function of the response to the West Africa (swell) 100-year storm of a system with an increase in stiffness and a decrease in heave mass and an increase in power take-off damping.

The functions of this system exhibit much of the same behaviour as those of the system subjected to only an increase in stiffness and a decrease in heave mass. This system differs at frequency values equal to the oscillating water column natural period. The increase in power take-off damping is causing the water column peak to reduce and structure peak to increase. This is likely to lead to a greater peak displacement of the structure at frequencies around this value. The integration of each function produces a value that is indicative of the power of each. The integral value for the wave is equal to 0.9542 m^2, for the structure it is equal to 0.6155 m^2, and for the oscillating water column it is equal to 0.2952 m^2.

6.10 Discussion of the West Africa Analysis Results

6.10.1 Time Domain Analysis Results

The peak displacements for all tuning mechanisms and the peak mooring line tensions in line 1 and line 2 are listed in Table 6.6. The peak displacements and peak mooring line tensions experienced during the West Africa storm spectrum are all less than those experienced during the Norwegian Sea spectrum.

Table 6.6: Peak displacement values for all tuning mechanisms subjected to the 100 year West Africa storm spectrum.

	West Africa					
	Wave (m)	Heave (m)	Ratio	Surge (m)	Line 1 (kN)	Line 2 (kN)
No tuning	3.967	5.401	1.362	3.219	366.6	112.4
Heave reduction	3.967	4.386	1.105	3.219	309.2	121.9
Damping increase	3.967	5.232	1.319	3.219	353.8	109.2
Stiffness increase	3.967	4.083	1.029	3.219	321.6	111.3
Heave + Damping	3.967	4.364	1.1	3.219	330.7	108.9
Stiffness + Damping	3.967	4.34	1.094	3.219	324.5	114.7
Heave + Stiffness	3.967	2.514	0.6337	3.219	223.9	102.9
All three	3.967	2.952	0.744	3.219	241.3	107

*Ratio is defined at the heave peak displacement divided by the wave peak displacement

The combination of tuning mechanism results on the peak displacement values Table 6.6 are graphed in Figure 6.51. The smaller the peak displacement of the structure, the more likely the system is to survive during unfavourable storm conditions. While the absolute reduction is likely to be a key design parameter, the effect of tuning mechanisms are better understood if the ratio of the peak structure displacement to the wave peak displacement is shown. A value of 1 means that the structure is experiencing a peak displacement equal to the peak wave height of the storm, a value less than 1 indicates that the peak wave height of the structure is less than the peak wave height of the storm, and a value greater than 1 indicates the opposite.

All tuning mechanisms used in isolation and all combinations of tuning mechanism decrease the heave peak displacement and the mooring line tension in the leading (heading of 0 degrees) mooring line. The surge displacement of the structure has remained constant across all tuning mechanisms. This was expected as the tuning mechanisms all influence the heave RAO of the structure rather than the surge RAO.

The isolation testing shows that the decrease in heave mass causes the greatest reduction in mooring line tensions and heave displacement of the structure. The peak heave displacement ratio is 1.1055 and the mooring line tension of line 1 has dropped from 366.6 kN in the untuned system, and to 309.2 kN in the tuned system. This is significant at 5%. An increase in system stiffness also shows promising results when used in isolation. The peak heave displacement ratio (1.029) was actually less than the value found for the system tuned with a decrease in heave mass. This has caused the mooring line peak tension to drop from 366.6 kN in the untuned system to 321.6 kN in the tuned system. This reduction is not significant at 5%. The mooring line tension is greater in this system despite the lower peak heave displacement. The different (12 kN) may be negligible given the confidence interval of each value.

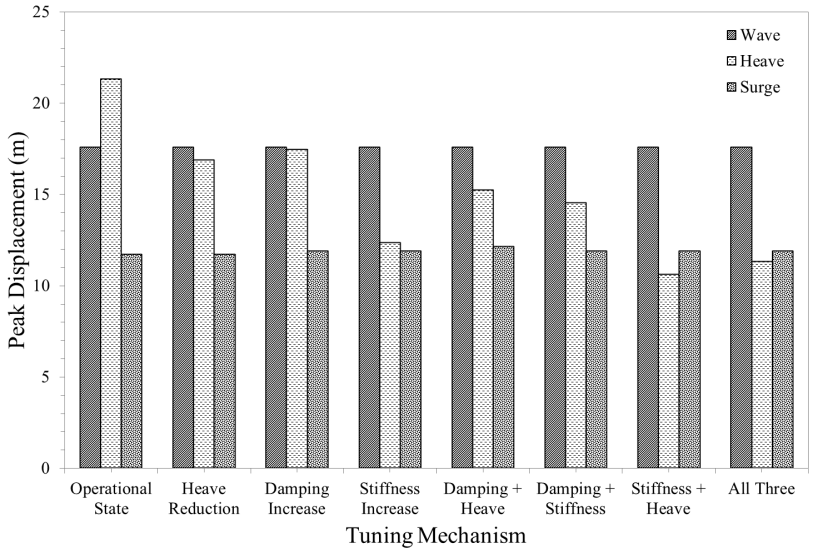

Figure 6.51: Peak displacements of the wave and structure heave and surge motion during the 1-in-100 year West African storm.

An increase in power take-off damping has not performed as well as an increase in stiffness or a decrease in heave mass when used in isolation. The peak displacement ratio is 1.479. This small reduction from the untuned system ratio of 1.319 has caused the peak line tension in line 1 to drop from 366.6 kN to 353.8 kN. There is no significant difference at 5% between these two values as the upper level of the system with increased damping is 396.3 kN. This is greater than the average level of tension in the untuned system.

The combinations of tuning mechanisms performed better than any mechanism used in isolation except for the combination of a heave decrease and damping increase, and a stiffness increase and damping increase. A combination of a heave mass reduction and an increase in system stiffness has performed the best overall. This combination has reduced the

peak displacement ratio to 0.6337. This has caused a considerable (significant at 5%) drop in the peak tension of mooring line 1. The tension has reduced from a value of 366.6 kN in the untuned system to a value of 223.9 kN in the tuned system. The other combinations show little to no advantage over any of isolated testing results. The combination of all three mechanisms shows a greater peak displacement ratio (0.7440) than when only using an increase in stiffness and damping. With this increase there is an associated increase (significant at 5%) in peak mooring line tension in line 1. The peak mooring line tension was found to be 241.3 kN. These results show that utilising an increase in power take-off damping above the optimal damping value is unlikely to produce a system with lower peak displacements and hence lower peak mooring line tensions. Figure 6.52 graphically illustrates the last two columns of Table 6.6.

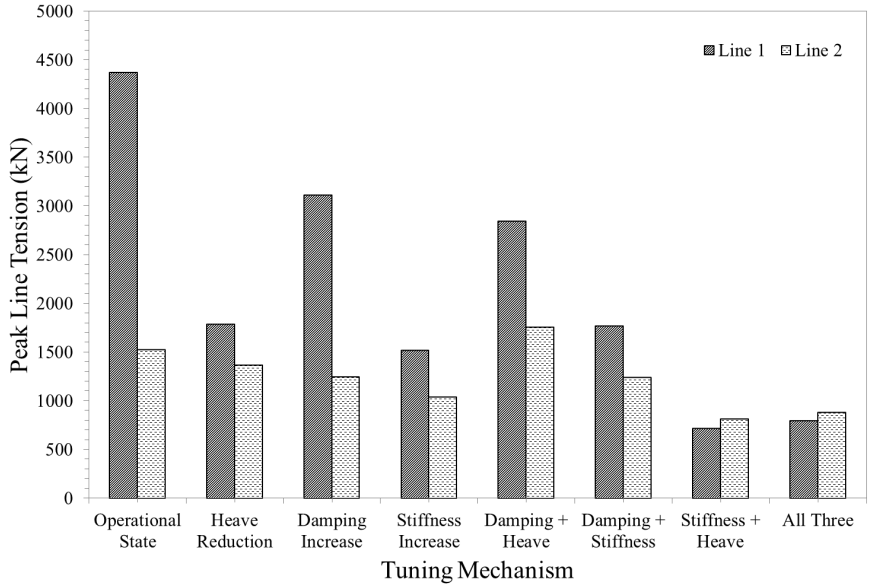

Figure 6.52: Peak line tension in Line 1 and Line 2 during the 1-in-100 year West African storm.

6.10.2 Spectral Density Analysis Results

The spectral density integral values are summarised in Table 6.7

Table 6.7: Spectral density integral values for the 1-in-100 year West Africa storm

	West Africa								
	Sea		Structure		OWC		Structure/Sea	OWC/Sea	OWC/Structur
Tuning mechanism	m_o (m^2)	D_{sig} (m)	m_o (m^2)	D_{sig} (m)	m_o (m^2)	D_{sig} (m)			
No tuning	0.9106	1.909	2.516	3.172	1.924	2.774	1.662	1.454	0.8746
Heave reduction	0.9517	1.951	1.403	2.369	0.1472	0.7673	1.214	0.393	0.3239
Damping increase	0.9542	1.954	2.034	2.852	0.9361	1.935	1.46	0.99	0.6784
Stiffness increase	0.9517	1.951	1.142	2.137	0.5738	1.515	1.095	0.776	0.7088
Heave + Damping	0.9517	1.951	0.6064	1.557	0.0594	0.4874	0.798	0.25	0.313
Stiffness + Damping	0.9542	1.954	1.236	2.224	0.2666	1.033	1.138	0.529	0.4644
Heave + Stiffness	0.9542	1.954	0.4933	1.405	0.517	1.438	0.719	0.736	1.0237
All three	0.9542	1.954	0.6155	1.569	0.2952	1.087	0.803	0.556	0.6925

The ratios of the integral value from Table 6.7 are graphed in Figure 6.53. This includes all isolation testing and all combinations of the isolated alterations. The smaller the value the more likely the system is to survive an unfavourable storm period. The zeroth moment values and significant displacement values have been plotted for each tuning mechanism. The ratio of the significant displacements has also been calculated. These are shown in the last three columns of the table.

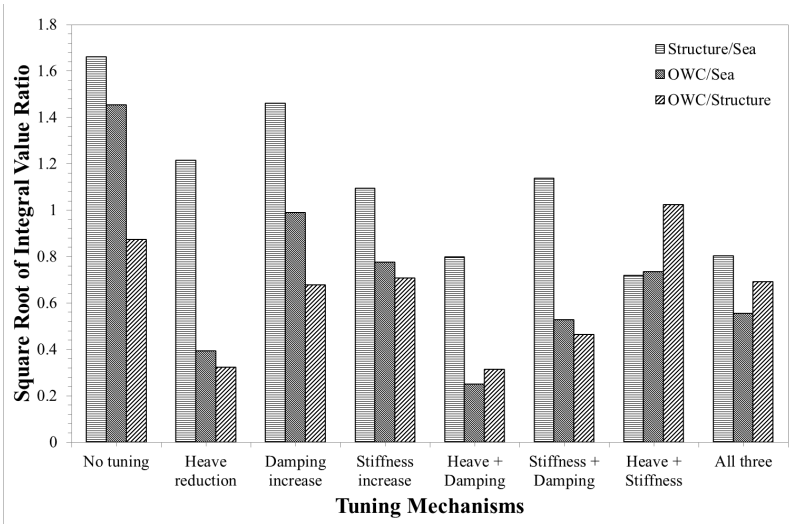

Figure 6.53: Integral value ratios for each tuning mechanism

As touched on before, the integral values give an indication of the heave motion of the device, oscillating water column, and wave. The integral value for the wave is approximately equal in all tested states. This is expected as the time domain wave is drawn from the same spectrum. If this spectrum is left to run for long enough it will converge to the theoretical spectrum defined by the JONSWAP equation. The equal values obtained suggest that this time period (3 hours) is sufficient to be able to compare results from different sea states.

The ratio of the integral values has been calculated for ease of comparison. A ratio of one suggests the numerator of the ratio is experiencing more heave motion over the duration of the testing period than the denominator. The first column of the results in Figure 6.53 is the structure divided by the wave, the second column is the oscillating water column divided by the wave, and the third column is the structure divided by the oscillating water column. The most important ratio with respect to system survivability is the structure to wave ratio. A ratio greater than 1 suggests that the expected peak displacement is likely to be greater than the wave peak displacement; a ratio less than 1 suggests the opposite. The results from the spectral density analysis conform to the results from the time domain analysis regarding peak displacement and peak mooring line tension. A drop in the integral ratio is indicative of a drop in the peak mooring line tension.

The results from the isolation testing and combination testing confirm the conclusions regarding the best performing tuning mechanisms. An increase in stiffness used in isolation (D_{sig} = 2.137m) is slightly better than a decrease in heave mass (D_{sig} = 2.369m) which is substantially better than only increasing the power take-off damping to double the optimal value (D_{sig} = 2.852m). Damping increases combined with a decrease in heave (D_{sig} = 1.557m) or an increase in stiffness (D_{sig} = 2.224m) or a combination of both (D_{sig} = 0.6155) does not perform as well as a combination of heave mass decrease and stiffness increase (D_{sig} = 0.5170m).

6.11 Discussion of Result Trends

6.11.1 Heave Mass Reduction

On the broad scale, a reduction in heave mass works well to reduce the peak heave displacement, peak mooring line tension, and spectral density function integral value. The reduction in heave mass reduces the heave natural period of the structure by a factor of approximately 1.58. The heave natural period reduced from 11.67 seconds to 7.38 seconds. The difference between the tuned natural period and the storm spectrum peak wave period is indicative of the effectiveness of the tuning mechanism. The Norwegian Sea spectrum had a peak wave period of 18 seconds; approximately 2.4 times the natural period of the structure. This was larger than the West Africa spectrum (2.1 times the natural period of the structure). This larger difference between the peak wave period and natural period of the structure gave the largest decrease in the peak line tension in both storm conditions.

The decrease in structure heave mass did not alter the motions of the oscillating water column to any significant extent. Decrease in structure heave mass has the potential to cause increased structure movement around the oscillating water column natural frequency. This effect is seen in all spectral density functions of the system tuned with only a decrease in heave mass. This increase in structure motion due to the oscillating water column is due to the coupled nature of the system.

These two results highlight key characteristics of a sea state in which a reduction in heave mass can be used to ensure the feasibility of an oscillating water column wave energy device. The peak wave period of the storm should be such that it is a sufficient distance from the greatest or smallest structure natural period achievable through heave mass damping alteration. A distance of at least two times in either direction is desirable as this value provides a significant (at 5%) reduction in mooring line tensions. The second key characteristic is that the peak wave period of the storm should be sufficiently different from the natural period of the oscillating water column to avoid an increase in the movement of the structure that is a consequence of an increase oscillating water column movement. Since the oscillating water column is designed to have a natural period equal to the mean period of the sea state, the storm spectrum peak wave period should be sufficiently different to the mean peak wave period. If the peak wave period of the storm spectrum is larger than the mean wave period of the installation location then it should be approximately twice as large as the

mean period. This value assumes that the structure natural period can be reduced to a value equal to the oscillating water column natural period.

6.11.2 Stiffness Increase

An increase in system heave stiffness works in much the same way that a decrease in heave mass does. They both reduce the structure natural period by the square root of the relative change. This system was tested with a stiffness value twice that of the water plane stiffness. This means that the natural period was reduced by a factor of approximately 1.4. This caused the structure natural period to reduce from 11.67 seconds to approximately 8.3 seconds. A decrease in system stiffness is likely to have the same effect on the increase in structure natural period. There is, however, an upper limit to a decrease in system stiffness. The stiffness cannot be less than the stiffness of a freely floating structure. The largest difference between the structure natural period and the peak wave period resulted in the largest percentage decrease in the peak mooring line tension of line 1. This occurred during the Norwegian Sea storm spectrum.

Unlike the decrease in heave mass, the increase in stiffness did alter the motions of the oscillating water column. The increased stiffness of the system means that more movement is experienced in the water column as the 'spring' in this system is easier to compress than the one in the structure. This has the potential to cause increased structure movement around the oscillating water column natural frequency. This effect is seen in all spectral density functions of the system tuned with only an increase in structure stiffness. This phenomenon working alongside the increase structure motion, which is due to being coupled with the oscillating water column, may cause large structure displacements at wave periods equal to the oscillating water column natural period.

These results suggest than an increase in stiffness may not be as successful in reducing the structure peak displacements, and hence peak mooring line tensions, as a decrease in heave mass if the peak wave period of the unfavourable conditions is similar to the oscillating water column natural period. The requirement to have the 100 year event peak period at least double or at a maximum of half the mean peak wave period, should allow this additional structure movement at wave period values close to the oscillating water column natural period to be avoided. Coupling between the reduction in heave mass tuning mechanism and

the increase in stuffiness tuning mechanism may be beneficial if the structure natural period cannot be altered enough using only a change in heave mass.

6.11.3 Power Take-off Damping Increase

An increase in power take-off damping does not have any direct effect on the natural period of the structure or oscillating water column. However, increasing the power take-off damping causes the two separate heave motions to combine into one. This produces a system with a natural period at some value between the structure and oscillating water column. Despite this movement of the natural period being in the right direction, this movement of the natural period of the structure is not as extensive as the movement of the natural period through changing either the heave mass or stiffness of the structure.

An increase in power take-off damping to a value that is double that of the optimal damping value causes the water column motions to reduce. This is likely to be due to the increase in damping causing the air column to become fixed; hence the water column motions are only allowed by the compressibility of the air within the chamber. The results of this tuning mechanism show that it uncouples the structure and oscillating water column motions to a certain extent. This may be useful if the system is such that the structure and oscillating water column natural period align and the peak wave frequency of the storm is not equal to the natural period of the water column. This setup is highly unlikely to be applied because the adjustment of the heave mass is a superior tuning mechanism.

It is not recommended to use the adjustment of power take-off damping in an effort to reduce the peak heave displacement, and hence peak mooring line tensions, of a floating oscillating water column wave energy device.

6.12 Tuning Mechanism Feasibility

The feasibility of the reduction in heave mass and an increase in stiffness is assessed. The feasibility of an increase in power take-off damping is not assessed because this tuning mechanism is unlikely to be used.

6.12.1 Heave Mass Increase

Subbulakshmi et al. (2015) have investigated the effect of heave plate geometry and the number of heave plates on spar platforms. It has been shown that the inclusion of heave plates can have a significant effect on the added mass of the structure. Koh and Cho (2011) have shown that the added mass coefficient of a structure can be increased by a factor of seven without increasing the damping coefficient.

With this in mind, adjustment of the heave natural period through the use of heave plates seems plausible. Since the introduction of heave plates increases the heave mass of the structure, the structure will have to begin with a relatively low heave mass. A low heave mass value will be a value that allows the structure to float deep enough to give the oscillating water column the required draft. This is easy achievable during the design. This design is likely to be a smooth vertical cylinder. The heave plates will be required to be able to be retracted and deployed in response to changing sea conditions. The technical characteristics of such a system will require further research.

6.12.2 Stiffness Increase

Further investigation into the effect of system stiffness increases through mooring line manipulation was investigated using OrcaFlex. The most viable way to increase system stiffness will be to reduce the slack in the mooring line through retraction of the line. This creates a shorter line that may experience higher levels of mooring line tension. To test this, the operational state system (no tuning) was subjected to the ideal wave conditions (peak wave period matching the oscillating water column natural period) with different mooring line lengths. The tensions were then measured and compared. The mooring line lengths tested were 130 m, 140 m, 145 m, 150 m, 160 m, and 170 m. A setup containing all mooring lines is shown in Figure 6.54. The mooring line analyses were conducted individually rather than all at once as Figure 6.54 suggests.

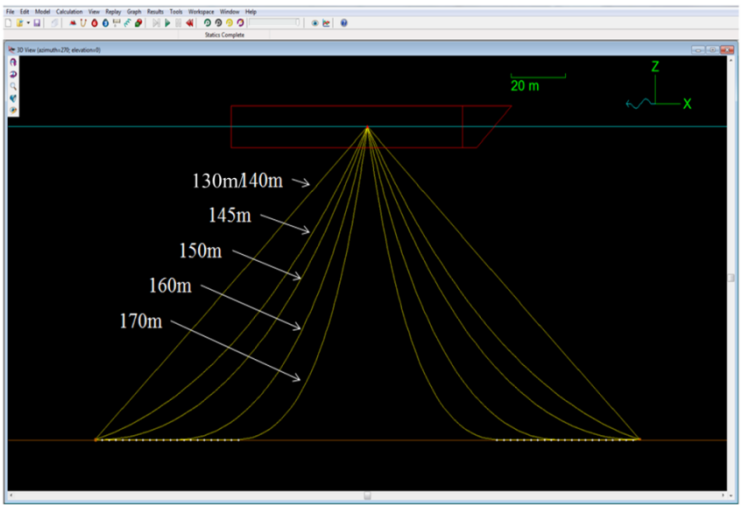

Figure 6.54: Mooring line length analysis setup at 100m depth

The mooring line tensions for line 1 and line 2 are seen in Table 6.8. Here the three hour return level for the upper tail of the weibull distribution is returned. There is a 5% change the mooring line tension will exceed this value over a three hour simulation.

Table 6.8: Mooring line length analysis results

Operational State	3 hour return level for upper tail											
	Line 1 (kN)						Line 2 (kN)					
System State	**130 m**	**140 m**	**145 m**	**150 m**	**160 m**	**170 m**	**130 m**	**140 m**	**145 m**	**150 m**	**160 m**	**170 m**
Ratio = 1.3	68505	14088	246.0	155.9	125.4	108.3	65515	11416	201.2	149.0	123.0	106.3
Ratio = 1.0	66421	12053	218.2	149.8	121.3	106.7	63960	9495	192.5	147.0	121.1	105.9
Ratio = 0.9	65066	10568	199.5	146.9	119.7	106.2	63849	9452	190.6	144.7	119.3	105.3

These results are graphed in Figure 6.55 and Figure 6.56. A logarithmic scale has been used because of the large increase in mooring line tensions for the 130 m and 140 m lines. These large mooring line tensions are due to the prestress in the line caused by stretching the mooring line from 130 m or 140 m to the shortest distance between the vessel and anchor point (141 m).

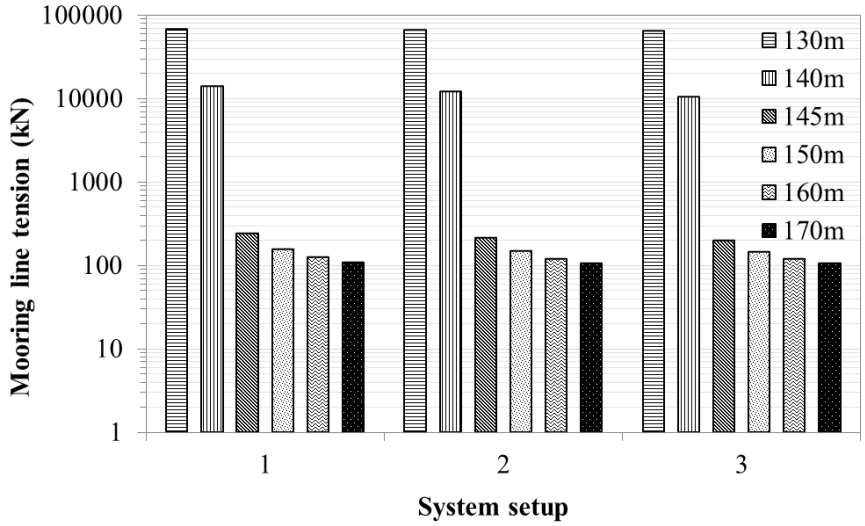

Figure 6.55: Mooring line tensions in Line 1 at different line lengths

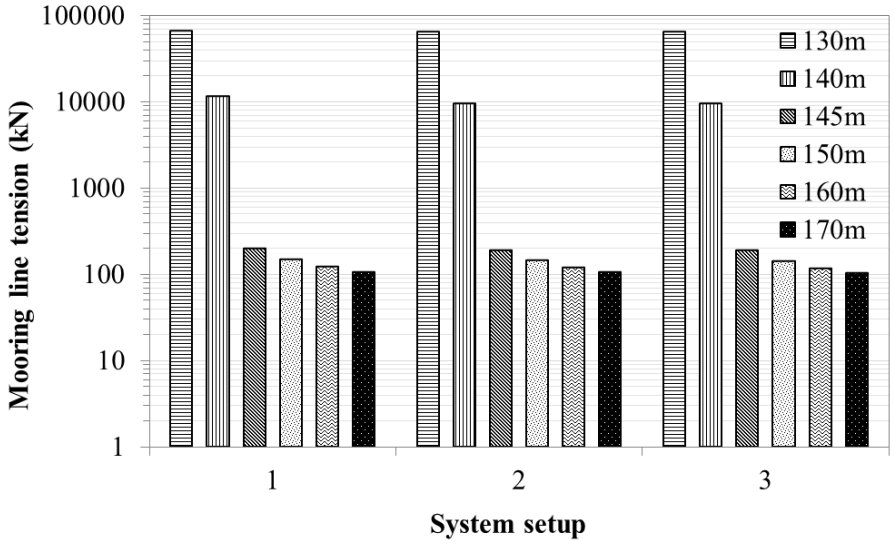

Figure 6.56: Mooring line tensions in Line 2 at different line lengths

If the results from the 130 m and 140 m mooring lines are ignored then the effect of decreasing the mooring line lengths from 170 m to 145 m is a gradual increase in mooring line tensions. The tensions experienced due to this decrease in line length are unlikely to cause any significant concern about exceeding the maximum permissible tensions. However, the change in length is unlikely to cause any significant increase in system stiffness because the mooring lines are still catenary in shape rather than taught. A taught system would resemble an offshore system similar to that of a tensioned leg system. This is the case when the mooring lines are reduced to 140 m and then again to 130 m. The shortest distance between the anchor point of the mooring line and the attachment point to the vessel is approximately 141 m. This means that the mooring lines will be taught at any point in which the vessel experiences a positive heave or surge movement. This setup produces a very large

maximum tension in the mooring lines with values up to 100 times that experienced when the mooring lines behave as a catenary system. This investigation shows that increasing the stiffness of the system through mooring line tensioning is unlikely to be a viable method because the large increase in mooring line tensions created by the system is now, effectively, a tensioned leg system.

These results show that the mooring system is unlikely to be used for anything other than keeping the wave energy device on station. The mooring system must be designed in such a way that the peak mooring line tension does not exceed the maximum tensile strength of the mooring lines. The maximum tension will be a function of the peak surge and heave of the device.

6.13 Mooring System Feasibility

Mooring system selection will be mostly limited to selecting the appropriate chain size. The chain size will determine the maximum allowable tension in the lines. The mooring line length will be stipulated by the combination of the expected peak surge and heave displacements. The mooring line should be long enough that it does not cause the line to be tensioned at peak displacement.

Chain manufacturer Scana Ramnas (1990; 1995) provide the following expressions for the properties of mooring line chains. If the nominal bar diameter of the chain is *D* then the following apply.

$$\text{Mass per metre (M)} = 19.90D^2 \text{ te/m (studless) or } 21.90D^2 \text{ te/m (studlink)}$$

$$\text{E} = 5.44 \text{ x } 10^7 \text{ kN/m}^2 \text{ (studless) or } 6.40 \text{ x } 10^7 \text{ kN/m}^2 \text{ (studlink)}$$

$$\text{Minimum breaking load } = \text{c} \cdot D^2 \cdot (44 - 80D) \text{ kN}$$

Where c is a grade-dependent constant, given in the catalogue data as Grade 2: 1.37 x 10^4, Grade 3: 1.96 x 10^4, ORQ: 2.11 x 10^4, R4 - 2.74 x 10^4.

Ramnas has also provided the mooring line breaking and proofing loads for the lines they manufacture. These are seen in Table 6.9: Ranmas mooring line proof and breaking loads. This table lists the breaking loads for various types of mooring lines offered by Ranmas. The largest mooring line on offer has a breaking load of 29,915 kN. This is far in excess of the peak mooring line tension experienced during any storm spectrum tested in this study if the

mooring lines remain in a catenary shape. This breaking load is not in excess of the mooring line tensions found during the mooring line analysis results seen in Table 6.8 for catenary lines but is greater for taut lines. The 130 metre long mooring line experienced roughly double the breaking load of the strongest mooring line available. This result suggests that tensioning mooring lines to increase stiffness is not viable with the current mooring chains available. This, in turn, suggests that using tuning mechanisms to reduce the heave displacement and, hence, peak mooring line tensions will allow a smaller mooring line to be used. This could lead to a more cost effective system. A total cost analysis has not been undertaken.

Table 6.9: Ramnas mooring line proof and breaking loads

Test Load	Break Load						Proof Load										Weight	
Grade	ORQ	R3	R3S	R4	R4S	R5	ORQ	R3	R3S Stud	R3S Stud-less	R4 Stud	R4 Stud-less	R4S Stud	R4S Stud-less	R5 Stud	R5 Stud-less		
C-factor	0,0211	0,0223	0,0249	0,0274	0,0304	0,032	0,014	0,0156	0,018	0,0174	0,0216	0,0192	0,024	0,0213	0,0251	0,0223	Stud	Stud-less
mm																	kg/m	
76	4621	4884	5454	6001	6658	7009	3066	3417	3942	3811	4731	4205	5257	4665	5498	4884	126	116
78	4847	5123	5720	6295	6984	7351	3216	3584	4135	3997	4962	4411	5514	4893	5766	5123	133	122
81	5194	5490	6130	6745	7484	7877	3446	3840	4431	4283	5317	4726	5908	5243	6179	5490	144	131
84	5550	5866	6550	7208	7997	8418	3683	4104	4735	4577	5682	5051	6313	5603	6602	5866	155	141
87	5916	6252	6981	7682	8523	8971	3925	4374	5046	4878	6056	5383	6729	5972	7037	6252	166	151
90	6289	6647	7422	8167	9062	9539	4173	4650	5365	5187	6439	5723	7154	6349	7482	6647	177	162
92	6544	6916	7722	8497	9428	9924	4342	4838	5582	5396	6699	5954	7443	6606	7784	6916	185	169
95	6932	7326	8180	9001	9987	10512	4599	5125	5913	5716	7096	6307	7884	6997	8246	7326	198	181
97	7195	7604	8490	9343	10366	10911	4774	5319	6138	5933	7365	6547	8184	7263	8559	7604	206	188
100	7596	8028	8964	9864	10944	11520	5040	5616	6480	6264	7776	6912	8640	7668	9036	8028	219	200
102	7868	8315	9285	10217	11336	11932	5220	5817	6712	6488	8054	7159	8949	7942	9359	8315	228	208
105	8282	8753	9773	10754	11932	12560	5495	6123	7065	6829	8478	7536	9420	8360	9851	8753	241	221
107	8561	9048	10103	11118	12335	12984	5681	6330	7304	7060	8764	7790	9738	8643	10184	9048	251	229
111	9130	9650	10775	11856	13154	13847	6058	6750	7789	7529	9347	8308	10385	9217	10861	9650	270	246
114	9565	10109	11287	12420	13780	14506	6346	7071	8159	7887	9791	8703	10879	9655	11378	10109	285	260
117	10005	10574	11807	12993	14415	15174	6639	7397	8535	8251	10242	9104	11380	10100	11902	10574	300	274
120	10452	11047	12334	13573	15059	15852	6935	7728	8916	8619	10700	9511	11889	10551	12434	11047	315	288
122	10753	11365	12690	13964	15493	16308	7135	7950	9173	8868	11008	9785	12231	10855	12792	11365	326	298
124	11057	11686	13048	14358	15930	16768	7336	8175	9432	9118	11319	10061	12576	11161	13153	11686	337	308
127	11516	12171	13591	14955	16592	17466	7641	8515	9824	9497	11789	10479	13099	11626	13700	12171	353	323
130	11981	12663	14139	15559	17262	18171	7950	8858	10221	9880	12265	10903	13628	12095	14253	12663	370	338
132	12294	12993	14508	15965	17713	18645	8157	9089	10488	10138	12585	11187	13984	12411	14625	12993	382	348
137	13085	13829	15441	16992	18852	19844	8682	9674	11162	10790	13395	11906	14883	13209	15565	13829	411	375
142	13887	14677	16388	18033	20008	21061	9214	10267	11847	11452	14216	12637	15796	14019	16520	14677	442	403
147	14700	15536	17347	19089	21179	22294	9753	10868	12540	12122	15048	13376	16720	14839	17487	15536	473	432
152	15522	16405	18317	20156	22363	23540	10299	11476	13241	12800	15890	14124	17655	15669	18464	16405	506	462
157	16352	17282	19297	21234	23559	24799	10850	12089	13949	13484	16739	14879	18599	16507	19452	17282	540	493
162	17188	18166	20284	22320	24764	26068	11405	12708	14663	14174	17596	15641	19551	17351	20447	18166	575	525
167	18030	19056	21278	23414	25977	27345	11963	13330	15381	14869	18458	16407	20508	18201	21448	19056	611	558
172	18876	19950	22276	24513	27196	28628	12525	13956	16103	15566	19324	17177	21471	19055	22455	19950	648	592
177	19725	20847	23278	25615	28420	29915	13088	14584	16827	16267	20193	17949	22437	19912	23465	20847	686	627

6.14 Installation Location Guidelines

6.14.1 Wave Period Based Selection

It has been suggested that the peak wave period of the storm spectrum should be at least two times greater than the structure natural period to increase the chance of survival. Chapter 3 also suggested that the optimal system setup will be one which has a structure natural period approximately one and half times greater than the oscillating water column natural period. Chapter 5 determined that the oscillating water column natural period should be matched with the mean sea state of the installation location. These relationships allow the installation location to be selected based on the peak wave period of the mean and 100 year event wave conditions. It also allows the effect of tuning mechanisms on the sea state selection to be determined.

If the system is not subjected to tuning then the peak wave period of the 100-year storm must be equal to double the structure natural period, which is equal to 1.5 times the oscillating water column natural period. This means that the 100-year event peak wave period must be equal to or greater than three times the mean sea state peak wave period. All tuning mechanisms showed that the structure generally experiences increased heave when the oscillating water column experiences heave. This means that peak storm wave periods around the oscillating water column natural period must be avoided. Because of the spectrum nature of wave conditions, a general guideline peak wave period 20% either side of the oscillating water column, or mean sea state, peak wave period must be avoided. These two guidelines, based on period selection only, provide the sea states where an untuned system may operate effectively and be expected to survive a 100-year event. This area is shaded green in Figure 6.57. Figure 6.57 is a matrix that provides guidance on the optimal relationship between the mean peak wave period and peak wave period of the storm (1-in-100 year) conditions. Different parts of the matrix are shaded depending on the ratio of these two wave periods. The left and bottom horizontal axis are the wave periods measured in seconds. The right and top vertical axis are the corresponding wave periods in radians per second.

Utilising heave plates to reduce the natural period of the structure can increase the number of installation locations. If the natural period of the structure is reduced until it is equal to even less than the natural period of the water column (~85%), as seen in the heave mass reduction investigation, to the natural period of the oscillating water column then locations with peak

wave periods greater than or equal to 1.75 times the mean peak wave period can be utilised. This value is equal to approximately double the ratio of the new structure natural period to the oscillating water column natural period. This area is shaded blue in selection matrix seen in Figure 6.57.

The last part of the selection matrix is the yellow area. This area is the combination of mean and 100 year sea states that is accessible if the heave mass of the structure is increased so that it remains at least twice the peak wave period of the unfavourable storm conditions. This tuning mechanism will take the natural period of the structure from approximately 1.5 times the natural period of the oscillating water column to a value at least three times greater.

This selection matric highlights the effect of using only heave mass changes on the installation locations. The total number of locations has increased significantly.

This selection matrix fails to stipulate the increases in heave mass needed to achieve the required natural period. This stipulation is difficult to state because it will require the initial natural period of the device and the peak wave period of the 100 year event of the installation site to be known. This will vary from installation location to installation location as this value depends on the size of the structure and the size of the structure depends on the mean sea state peak wave period.

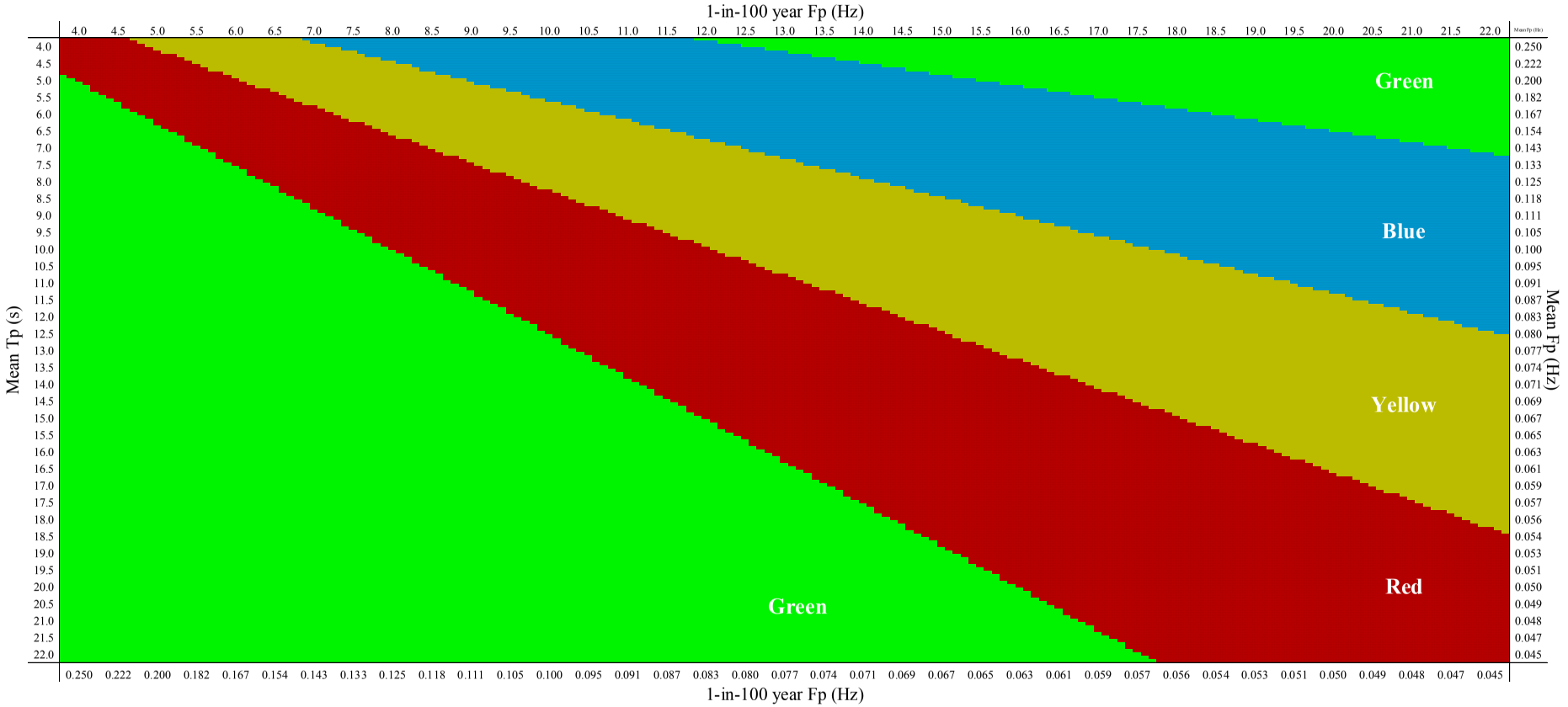

Green: Structure = Sea states which need no tuning
Blue: Sea states which need a decrease structure heave mass to move the structure natural period equal to the oscillating water column natural period.
Orange: Sea states which need an increase in structure heave mass to move the structure natural period to twice the osillating water column natural period.
Red: Sea states which are not optimal despite all tuning mechanisms

Figure 6.57: Site selection matrix based on peak wave periods alone

6.14.2 Significant Wave Height Based Selection

A selection matrix based on the ratio of the significant wave height during the unfavourable storm conditions to the mean significant wave height is also possible. This is seen in Figure 6.58. The reasoning behind this selection matrix is that the surge and heave of the device, and hence peak surge and peak heave, will be proportional to the wave height in any given sea state. The peak surge and peak heave will be directly responsible for the peak mooring line tension. If the peak surge and heave are minimised, then so will the mooring line tensions. This is evident in the peak mooring line tensions experienced during each storm spectrum. The largest mooring line tensions were experienced in the Norwegian Sea spectrum. The sea states had significant wave heights of 16.5 metres. The West Africa storm spectrum has a significant wave height of 3.85 metres.

Figure 6.58 shows a matrix with the mean sea state significant wave height on the vertical axis and the significant wave height of the 100-year event on the horizontal axis. The redder the matrix the larger the difference between the significant wave height of the mean sea state and the 100-year event sea state. This larger difference means that the wave energy device is likely to require a larger tuning effect to survive the unfavourable conditions.

The difference between the mean and peak wave height along the east coast of Australia pairs favourably with this selection matrix. The largest difference between the mean wave height and wave height with a 1% chance of exceeded is approximately 2.6 metres. This is seen in Table 6.2.

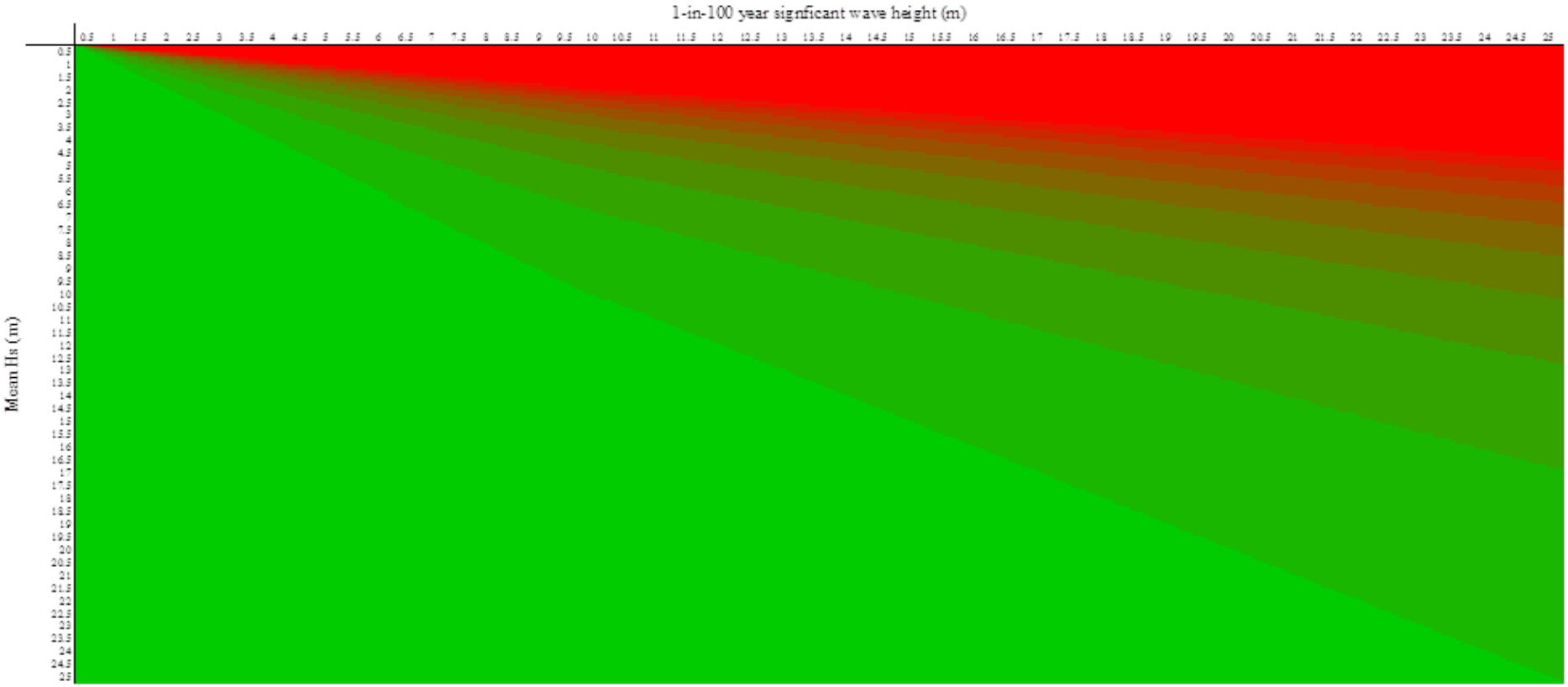

Figure 6.58: Selection matrix for significant wave height based selection

6.15 Chapter Summary

This chapter has examined the effect of system tuning mechanisms on the survivability of a floating oscillating water column wave energy converter. Time domain responses with the peak heave and peak surge displacement, peak mooring line tensions, and spectral density functions have been used to quantify system responses in the time domain to various JONSWAP 1-in-100 year storm spectra. The results from the spectral density function analysis are able to accurately predict the relative magnitudes of mooring line tensions. This was confirmed through a mooring line tensions analysis.

The spectral density function and mooring line tension analysis highlight that the need for tuning mechanisms to ensure the survivability of the system is directly proportional to the magnitude of the change between the operational sea state and the 1-in-100 year storm sea state. This means that the closer the peak wave period of the 1-in-100 year storm is to the peak wave period of the average sea state, the greater the need for tuning mechanisms to ensure device integrity. The key parameters affecting the system behaviour are the peak spectral density value of the storm spectrum compared the peak of the operational state (mean sea state design) system, the value of the peak wave period of the storm compared to the natural period of the structure, and the ratio of the significant wave height of the 100-year event to the mean significant wave height of the installation location.

The most viable tuning mechanism is a reduction in heave mass. The increase in power take-off damping proved to be ineffective and the increase in system stiffness show that the increases in mooring line tensions are unlikely to be practical. An investigation into a mooring system that will increase the overall heave stiffness highlights that such a system is likely to experience mooring line tensions far in excess of the maximum permissible tensions of mooring lines. Despite showing promise as a viable tuning mechanism during the WAMIT analysis, an increase in system power take-off is not recommended. This mechanism is able to shift the natural period of the structure but the subsequent increased heave of the structure offsets this reduction in natural periods.

The results presented in this chapter sheds more light on the ideal location for an oscillating water column wave energy converter. Previously, it was established that the site should be one with favourable operational conditions (mean conditions) but this study now shows that the 1-in-100 year storm conditions would ideally provide conditions with as small an increase in significant wave height, hence peak spectral density value, and as large an increase in peak

wave period as possible. A combination of these two characteristics will allow for a system that is not in need of a very large change in natural period (hence only a small reduction or increase to the heave added mass) and that will not experience a large change in heave during storm conditions. This smaller heave will ensure the mooring lines do not move into a tensioned system but rather stay in a catenary setup. Such a location is likely to be sheltered from areas of large fetch; the east coast of Australia is such a place.

Chapter 7 Experimental Analysis of a Water Column and Structure Heave Velocity Relationship

7.1 Introduction

The objective of this chapter is to investigate whether the conclusions and trends of numerical analysis in Chapter 5 and also published by Stanham et al. (2016) (Appendix E) regarding the axis lengths can be replicated experimentally. This chapter analyses whether the parametric ellipse relating the structure heave velocity to the water column heave velocity and also the ideal forcing period ratio of such a system are able to be reproduced experimentally. This chapter concludes that the trends established in Chapter 5 can be produced experimentally in a two-dimensional wave tank. This experimental work was published in the Australian Journal of Mechanical Engineering in September 2017. It is located in Appendix F.

7.2 Experimental Methodology

The basic mass-spring-damper model outlined by Stappenbelt and Cooper (2009) was recreated experimentally by Bayoumi et al. (2014). The model used by Bayoumi will be used as the basis for the model used for the experimental testing undertaken in this chapter. The model used in this chapter has been altered to fit the tank dimensions. Bayoumi et al. (2014) confirmed that such a model is a valid experimental setup. Bayoumi et al. (2014) conducted the measurement of system characteristics such as damping, stiffness, and mass in an effort to validate the model.

7.2.1 Turbine damping and power production

An orifice above the water column formed the turbine damping parameter modelled as a linear value in WAMIT in Chapter 4, 5 and 6. To simplify the model, the air is assumed to be incompressible. This assumption is valid as the pressure difference is in the range of 0.2-0.3 kPa. This difference is considered negligible when compared to the atmospheric pressure of 101.325 kPa. The turbine damping is assumed to be linear; hence the relationship of the airflow through the orifice and the pressure difference is taken to be linear as shown by Alcorn (2000). The relationship between the pressure difference and airflow can be derived as follows. Figure 7.1 is used to define the directions of motion. The x variable represents the

oscillating water column displacement from the still water level and the z variable represents the structure displacement from the still water level.

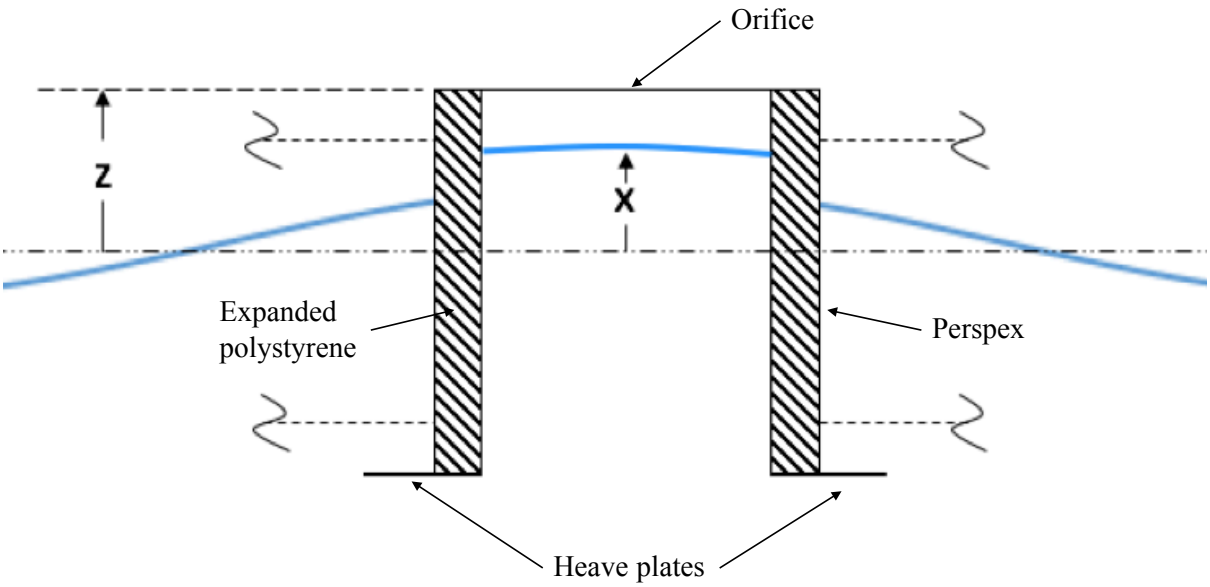

Figure 7.1: Water column schematic

The airflow rate through the orifice, Q, can be expressed as a function of the velocity of the air through the orifice, V_a, and the oscillating water column plan area, A_c:

$$Q = V_a A_c \tag{7.1}$$

This can be expressed as a derivative of the function of the relative displacement between the oscillating water column and the floating structure ($x_r = z - x$) (see Fig. 1):

$$Q = \frac{d(z-x)}{dt} A_c = A_c \dot{x}_r \tag{7.2}$$

Expressing this in terms of the pressure difference, Δp, the density of air, ρ, and the orifice area, A_o and a correction factor/orifice coefficient, K_o.

$$Q = K_o A_o \sqrt{\frac{2\Delta p}{\rho}} \tag{7.3}$$

Arranging for the pressure difference:

$$\Delta p = \left(\frac{Q}{K_o A_a}\right)^2 \frac{\rho}{2} \tag{7.4}$$

The pressure difference relationship may be used to derive the turbine damping value. Damping is defined as a function of the vertical force, F, and oscillating water column velocity, v_c:

$$B = \frac{F}{v_c} = \frac{\Delta p A_c}{Q/A_c} \tag{7.5}$$

Substituting Δp from Eqn. 4 we get:

$$B = \frac{Q\rho A_c^2}{2K_o^2 A_o^2} \tag{7.6}$$

Expressing the damping value as a function of the oscillating water column velocity leads to the final expression for turbine damping:

$$B = \frac{\rho A_c^3}{2K_o^2 A_o^2} |\dot{x}_r| \tag{7.7}$$

Measuring the pressure differential and relative velocity of the oscillating water column the turbine damping can be determined.

7.2.2 Experimental Description

Model

The model consists of a floating Perspex box, mooring lines and an aluminium frame. The dimensions of the model are seen in Table 7.1. The Perspex is 7mm thick.

Table 7.1: Model parameters (internal dimensions)

Parameter	Value
Width (mm)	935
Height (mm)	500
Length (mm)	500
Mass (kg)	13.8
Structure bottom surface area (no heave plates) (mm^2)	106,750
Heave plate surface area (mm^2)	100,000
Oscillating water column surface area (mm^2)	360,750
Orifice diameter (mm)	200, 100, 50
OWC/Chamber width (mm)	925
OWC/Chamber length (mm)	380
Measured OWC Natural Period (s)	1.54
Measured Structure Natural Period (s)	2.10

The Perspex box is lined with expanded polystyrene. This has been done to increase the buoyancy of the device and to also provide a surface area for the heave force to act upon. The two dimensional aspect of the testing has been taken into consideration by only placing foam inserts on the front and rear elevations of the model. A rectangular shape has been chosen to reduce the transverse reflections. These reflections have been further reduced by extending the width of the model to 95% of the width of the tank. A photograph of the model moored to the frame placed in the testing tank is seen in Figure 7.2.

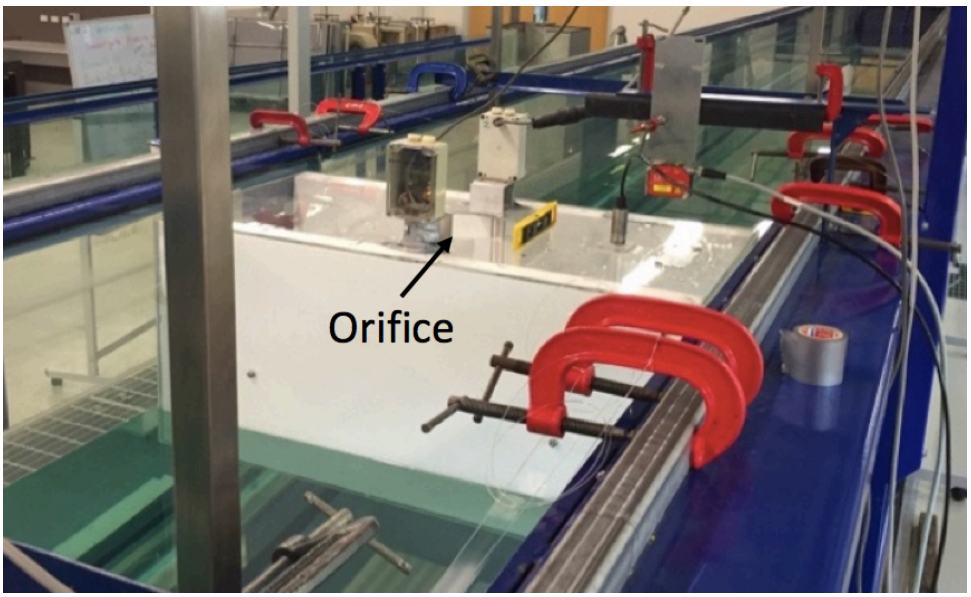

Figure 7.2: Model in wave tank

The model is held in location through a mooring system similar to that used by Fiorentini (2010). This system consists of four lines connected to the front of the model and four to the back. The top set of mooring lines are attached 50 mm from the vertical edge and 50 mm from the top of the model (Refer to Figure 7.4). The bottom set of mooring lines is attached 50 mm from the vertical edge and 50 mm above the bottom of the model. The moorings lines are attached to an aluminium frame that is also placed in the wave tank. The frame has a width of 900 mm and length of 2550 mm. This geometry gives the mooring lines a length of approximately 1025 mm. The frame attachments can be moved vertically to adjust for different draft values if the weight of the structure is increased. This will allow the mooring lines to be horizontal at the structure's point of equilibrium.

The structure has been fitted with two heave plates (100mm by 500 mm), one at the front and one at the back bottom edge. These heave plates are made of aluminium. The addition of the heave plates has allowed in increase in the structure bottom surface area without adding any significant mass to the system, hence the water column length has not been altered. This has

been done to increase the natural heave period of the structure so the ratio of the structure natural period to water column natural period is within the guidelines established by Stappenbelt and Cooper (2009). The guidelines suggest that the structure natural period should be approximately 1.5 times the water column natural period. A photograph of one of the installed heave plates is seen in Figure 7.3.

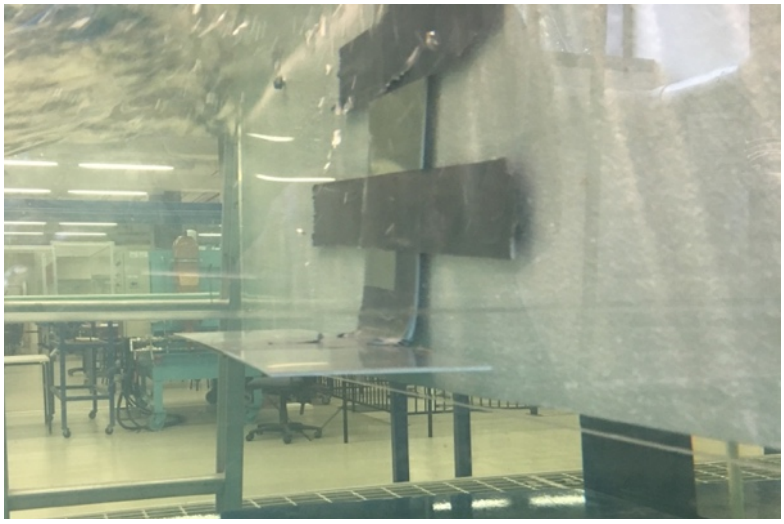

Figure 7.3: Photograph of the front heave plate

Dimensioned images of the structure are seen in Figure 7.4.

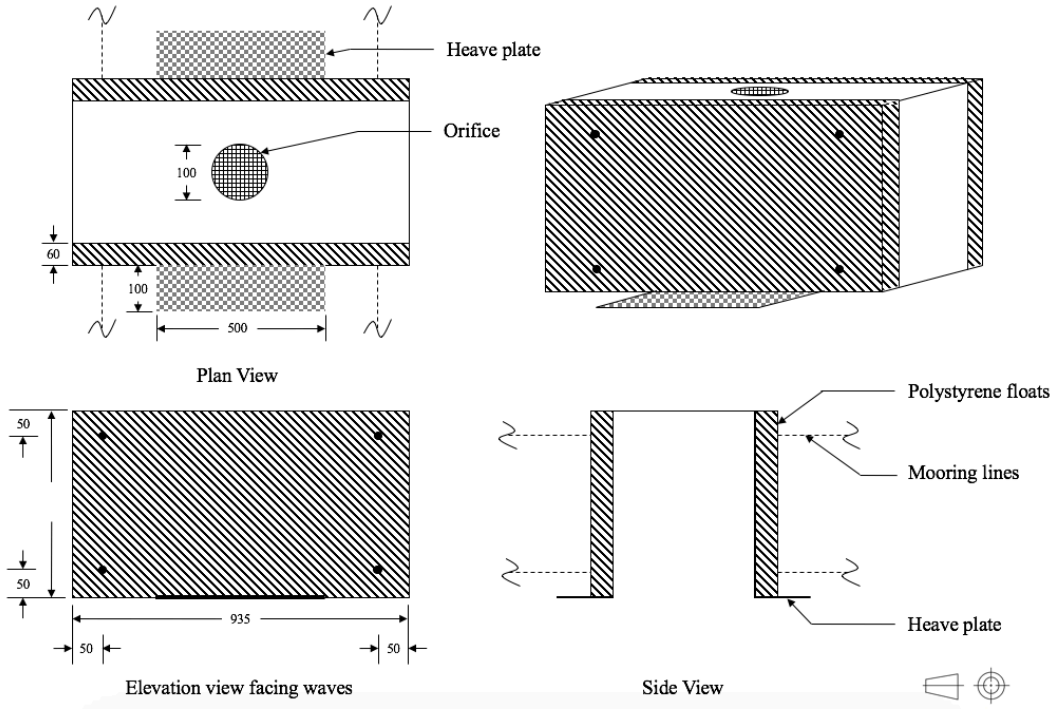

Figure 7.4: Model drawing (not to scale)

Data collection equipment

Two wave probes have been installed within the model chamber, one at the front face and one at the back face. Two probes have been used to determine whether significant sloshing occurs within the chamber. This problem was not encountered during testing. These wave probes have been used to determine the heave displacement of the water column. A pressure sensor has been installed at the top of the model, half way between the orifice and short edge. The pressure sensor was used to measure the pressure differential between the chamber and the atmosphere. A laser sensor has tracked the heave displacement of the structure at a point in the middle of the top surface. These measurement tools and their installation location are shown in Figure 7.5. The wave height is set as an input to the wave maker software.

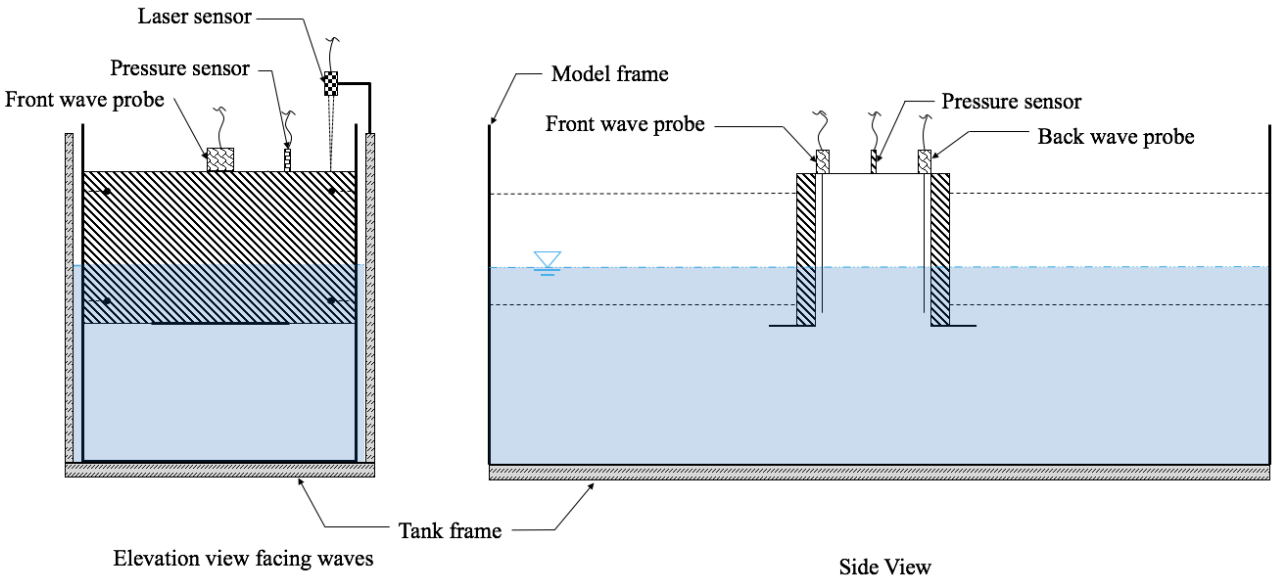

Figure 7.5: Measurement tools installation locations

Testing method

The model has been tested with single sinusoidal waves ranging from a frequency of 0.2 hertz to 1 hertz at 0.05 Hz intervals; at a wave amplitude of 40 millimetres. These wave characteristics were selected on the wave maker software. The simulations were run until the output voltages were repeating, this usually lasted around 40 seconds. Care was taken to avoid long running times because the flat face of the model caused reflected waves to eventually disrupt the incoming sinusoidal waves. The data was collected with LabView and processed in Microsoft Excel.

The natural period of the structure and water column were determined from the resulting RAO plots developed from this frequency sweep. The water column natural period was determined to be approximately 1.54 seconds and the structure natural period was determined to be 2.10 seconds. This produces a period ratio of 1.36. This is similar to that used in the numerical analysis (1.38) in Chapter 5.

Orifice damping linearization

Linearisation of the orifice damping is essential because theoretical programs such as WAMIT and OrcaFlex used in the numerical analysis published in Stanham et al. (2016) and Chapter 5 of this thesis utilise a linear damping value during calculations. Fiorentini (2010) showed that the introduction of layers of nylon mesh of gauge 1 mm over the orifice was able to linearise the orifice damping. Fiorentini (2010) found that three layers of nylon mesh produced a sufficiently linear system. This conclusion has been tested on the model used in this chapter.

The damping of the orifice is equal to the gradient of the function relating chamber pressure to the airflow rate (an example of such a plot if seen in Figure 7.7) through the orifice multiplied by the cross-sectional area of the water column. To achieve this plot, the structure has been oscillated by hand. The displacements of the water column and chamber pressure readings were collected as functions of time. The water column displacement was then used to calculate the water column velocity. Assuming the air is incompressible, the water column volume and velocity displacement should equal the air volume displacement and velocity. This has been undertaken for the 100 millimetre diameter orifice. The plot is seen in Figure 7.7.

7.3 Results and Discussion

The basic mass-spring-damper model outlined by Stappenbelt and Cooper (2009) was recreated experimentally by Bayoumi et al. (2014). The model used by Bayoumi will be used as the basis for the model used for the experimental testing undertaken in this chapter. Due to the work done by Bayoumi et al. (2014) in confirming such a model is a valid experimental setup, measurement of system characteristics such as damping, stiffness, and mass in an effort to validate the model is not essential to the conclusions of this chapter because this chapter aims to validate the conclusions regarding the parametric equations of velocity established in Chapter 5.

7.3.1 Basic behaviour

The data used during this experimental study was collected from time series plots created at difference wave periods. An example of such a plot is seen in Figure 7.6. This figure shows the amplitude of the floating structure and oscillating water column when subjected to a wave train with a period of two seconds and an amplitude of 0.04 m.

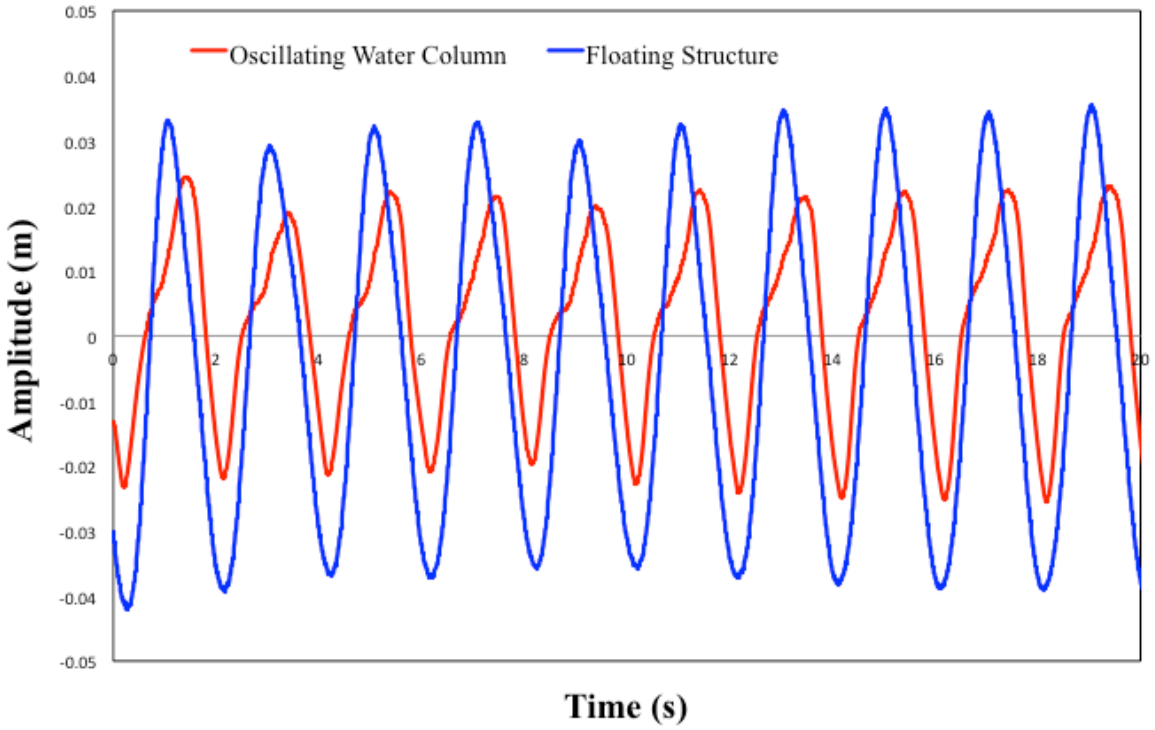

Figure 7.6: Floating structure and oscillating water column time series plot

Figure 7.7 shows good linearity (R^2 = 0.92271) between the airflow rate and chamber pressure. Using the gradient of the line of best fit the water column surface area the power takeoff damping can be estimated to be 6.68 N.s/m. This value is used to determine the power out of the system in this chapter.

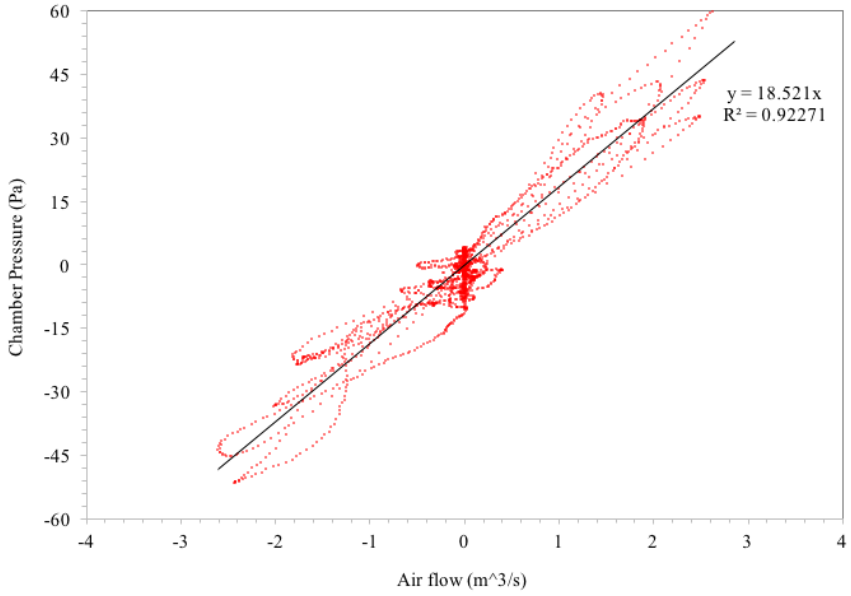

Figure 7.7: Chamber pressure as a function of air flow rate through the 100mm orifice

7.3.2 Measuring the RAOs

The structure and water column response amplitude operators were produced by plotting the ratio of the maximum amplitude value to the wave amplitude against the period of the forcing wave. This output is seen in Figure 7.8. The RAO of each component shows two resonant peaks. This is expected in such a system and is also seen in the work done by Stappenbelt and Cooper (2009), in the numerical analysis by Stanham et al. (2016) and the results in Chapter 5 of this thesis.

The resonant peak at approximately 1.54 seconds corresponds to the water column natural period and the resonant peak at approximately 2.10 seconds corresponds to the structure natural period. The ratio of these natural periods is 1.36. This is similar to that used in the numerical analysis (1.33) in Chapter 5 (page 110).

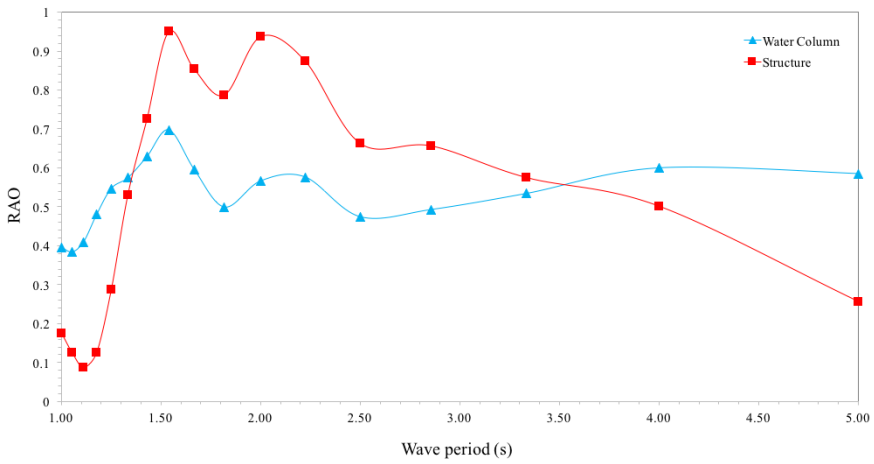

Figure 7.8: Water column and structure response amplitude operators

7.3.3 Parametric Function Analysis

Figure 7.9 details the structure-water column heave velocity data collected for a wave period of 1.54 seconds (0.65 Hz), and also for a wave period of 2.00 seconds (0.5 Hz). A wave with a period of two seconds has been chosen, because this value is the closest value to the structure natural period that the wave maker was able to produce. These two wave periods roughly correspond to the natural period of the water column and structure respectively. The physical interpretation of this parametric plot can be summarised as the instantaneous heave velocity of the structure and water column at the same individual points in time. A graphical representation of this can be seen in the numerical analysis (Stanham et al. (2016)) and also in Chapter 5 of this thesis.

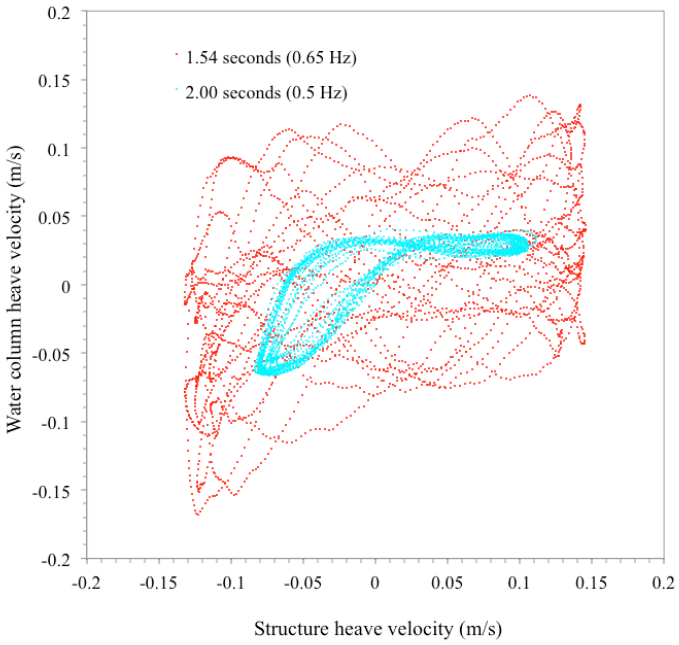

Figure 7.9: Structure-water column parametric plot for a wave of 1.54 seconds (0.65 Hz) and 2.00 seconds (0.50 Hz)

The experimental data does not resemble a typical ellipse like that seen in the numerical analysis of Chapter 5. The reason of this is unclear but may be due to the build up of reflected waves within the tank as a result of the flat front surface of the model. An example how the extent of the parametric plot was quantified is seen in Figure 7.10. Figure 7.10 shows the parametric curve corresponding to the data collected at a wave period of 1.54 seconds (0.65 Hz). This corresponds with the oscillating water column natural period; hence this is a forcing period ratio equal to one.

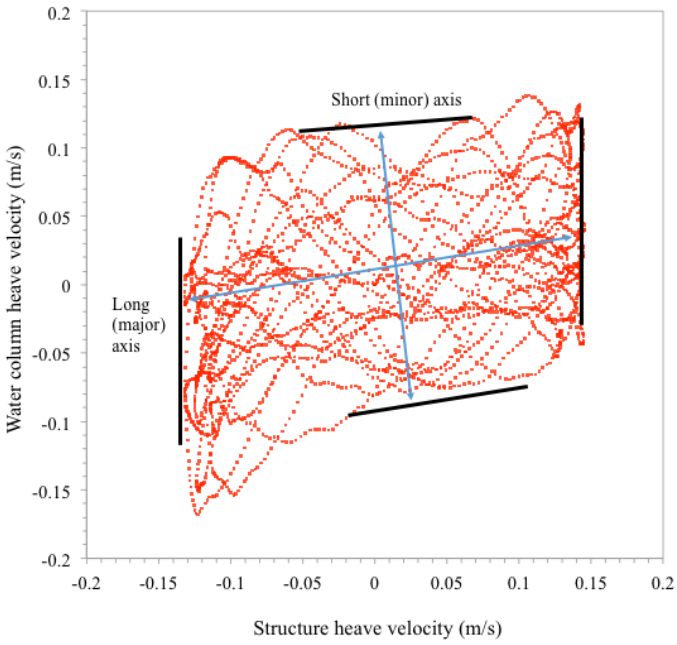

Figure 7.10: Determining extent of the parametric function for data collected from a wave with period of 1.54 seconds (0.65 Hz).

7.3.4 Power production

The power production as a function of the major (long) axis length is seen in Figure 7.11 and power production of the minor (short) axis length is seen in Figure 7.12. There exists a weak linear relationship for the experimental data compared to the stronger linear relationship seen in the numerical analysis Chapter 5. This may be due to the high degree of reflected waves in the tank due to the flat face of the model. This caused irregularities in the forcing waves with lower wave periods (<2.00 seconds). This reflected waves were observed but not measured. The experimental simulation was stopped when the forcing wave no longer resembled a sinusoidal pattern.

This experimental setup showed a greater linear trend between the power production and the short axis (Figure 7.12) length ($R^2 = 0.73$) than the long axis (Figure 7.11) length ($R^2 = 0.44$), however both the long axis length ($P = 0.0039$) and short axis length ($P = 0.000012$) have were determined to have a statistically significant linear relationship with the power production of the model at the 1% level of significance. This weak linear trend may be attributed to inconsistencies on the experimental setup. Such inconsistencies could arise from the mooring line setup, the degree of wave reflection variation at different wave frequencies,

and also the non-linear power takeoff damping. This is seen in the deviation of the damping values from the linear line of fit in Figure 7.7.

The derived data from the experiments in Figure 7.11 and Figure 7.12 show some data points that lie outside the expected trends of the data. These points lie at power output levels significantly higher than the majority of the data points. In Figure 7.11 these include the point corresponding to a power output of ~70 J at an axis length of ~0.275m/s, and the points at a power output of ~10 J at an axis length of ~0.15m/s. In Figure 7.12 the expected points are seen at a power output of ~40 J at an axis length of ~0.28m/s and a power output of ~70 J at an axis length of 0.27m/s. These points of higher power output are the points derived from data collected at forcing periods equal to 1.67 seconds and 1.54 seconds. The exact reason for these large outliers is unknown. These outliers and lower statistical fits can be caused by a combination of increased variability in the model behaviour due to reflected waves, irregular mooring line tensions and the data measurement devices themselves.

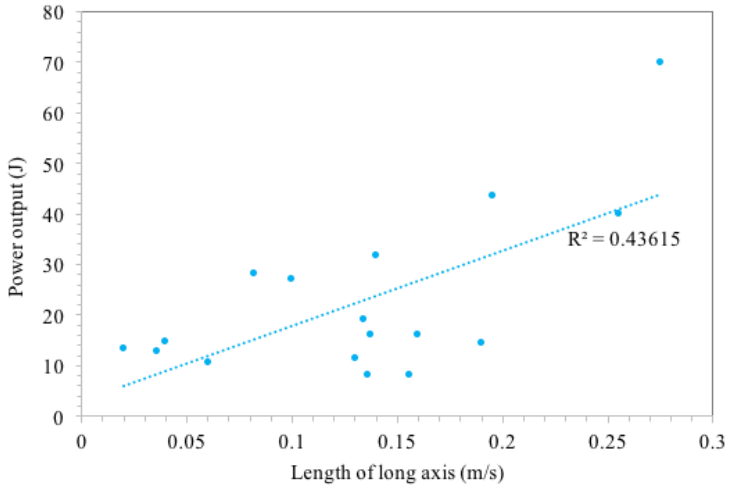

Figure 7.11: Power production as a function of the major (long) axis length

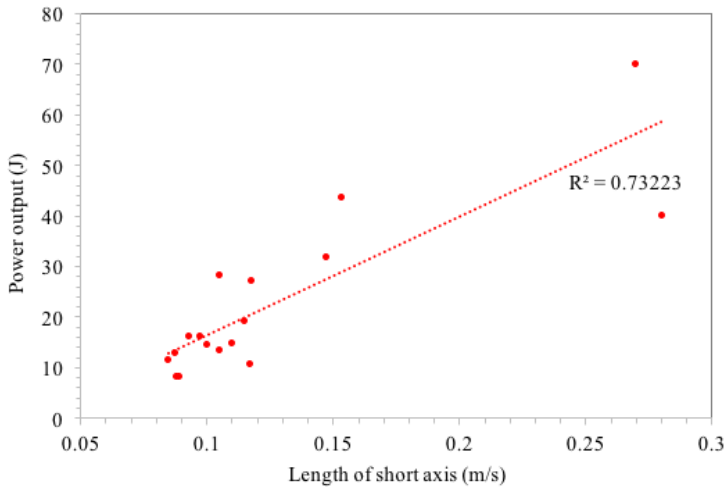

Figure 7.12: Power production as a function of the minor (short) axis length

7.3.5 Location of increased parametric plot extent

The change in axis length of the parametric plot with respect to the natural period of the water column was undertaken, this is seen in Figure 7.13. The peak of the extent lies at a value close to that of the water column natural period (ratio = 1) and stays elevated around the natural period of the structure (ratio = 1.36). This means that the system is able to produce more power when the water column natural period is matched to the forcing period of the wave and the dynamics of the system are such that the structure natural period is larger than water column natural period. This data is in agreement with the work of Stappenbelt and Cooper (2010), Bayoumi et al. (2014), and the numerical analysis in Chapter 5 (Figure 5.16).

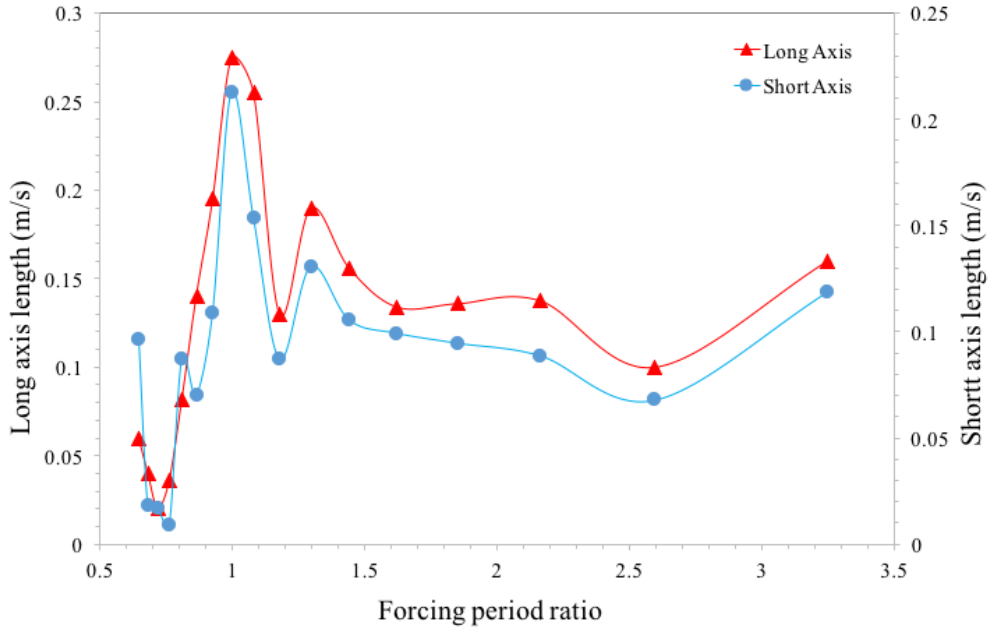

Figure 7.13 : Axis length as a function of the ratio of the forcing period to the water column natural period

7.3.6 Axis gradient

Investigation into the relationship between the gradient of the major (long) axis and the power production was also undertaken experimentally. The results showed little to no link between the long axis gradient and the expected power production. The data set corresponding to this analysis is seen in Figure 7.14. Figure 7.14 plots the power output as a function of the gradient of the major axis. The gradient is measure in degrees anticlockwise from the positive *x*-axis. The short axis gradient is approximately perpendicular to the long axis, hence the random nature of the results remains and the graph has not been plotted.

The experimental data, much the same as the theoretical data in the numerical analysis of Chapter 5 showed that a large phase difference between the water column heave velocity and the structure heave velocity (gradient of close to 135 degrees meaning the heave velocities are 180 degrees out of phase) is not essential to power production in a floating wave energy converter and cannot be attributed to the length of either the major or minor axis but is rather just a characteristic of the system setup at a particular forcing period. This is evident in the experimental analysis due to the lack of a large power output value corresponding to a gradient of 135° in Figure 7.14.

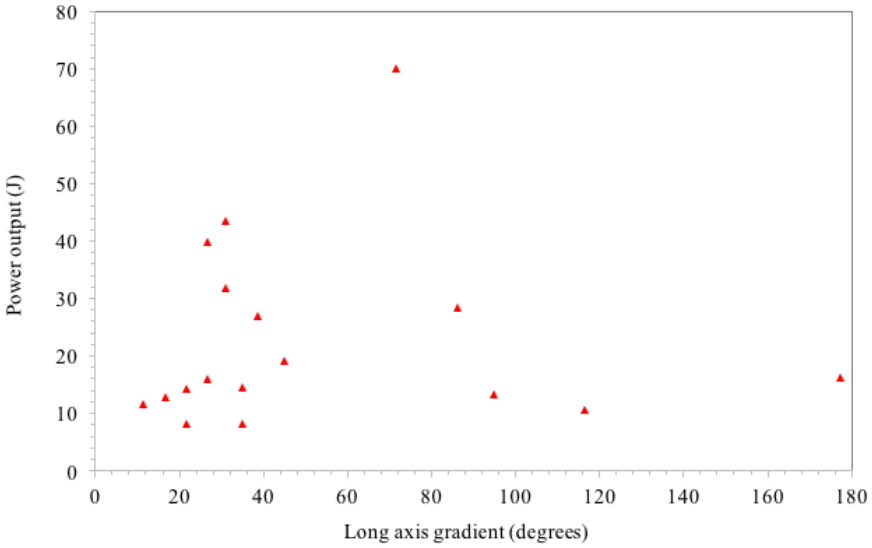

Figure 7.14: Experimental power output as a function of the gradient of the long axis

7.3.7 Phase Averaging

Phase averaging allows the average of all the wave phases to be better compared. It essentially compares the average behaviour of the device and oscillating water column over the tested period. Phase averaging is done by recording the amplitude of the wave at each point of oscillation. This is done for each cycle and plotted between 0 and 360 degrees. Phase averaging the data to produce velocity plots across one wave cycle further supports the conclusions drawn in this experimental study and the results seen in Chapter 5. Figure 7.15, Figure 7.16, Figure 7.17 plots the absolute heave velocity of the oscillating water column and the heave velocity of the floating structure against the phase of each oscillation. Figure 7.15 is produced with a forcing frequency of 0.65 Hz, Figure 7.16 with 0.5 Hz, and Figure 7.17 with 0.4 Hz. Figure 7.17 has been included here as an example of phase averaged data that does not align with either the oscillating water column natural period or the structure natural period.

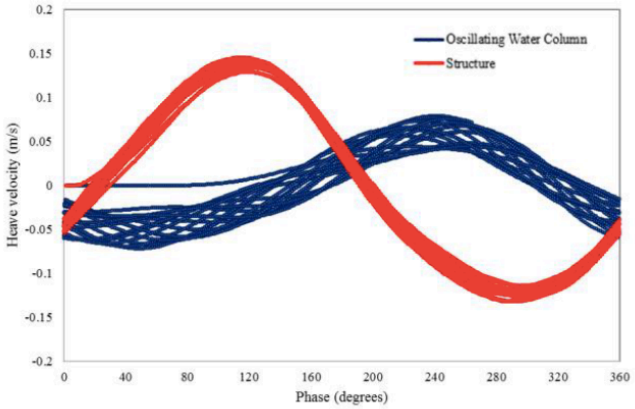

Figure 7.15: Phase averaged heave velocity with a forcing frequency of 0.65 Hz (forcing period ratio of 1)

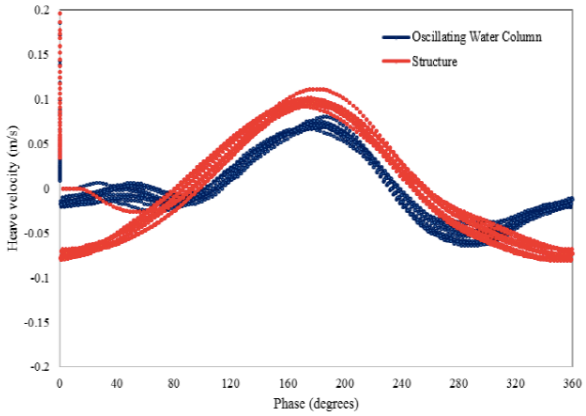

Figure 7.16: Phase averaged heave velocity with a forcing frequency of 0.5 Hz (forcing period ratio of 1.3)

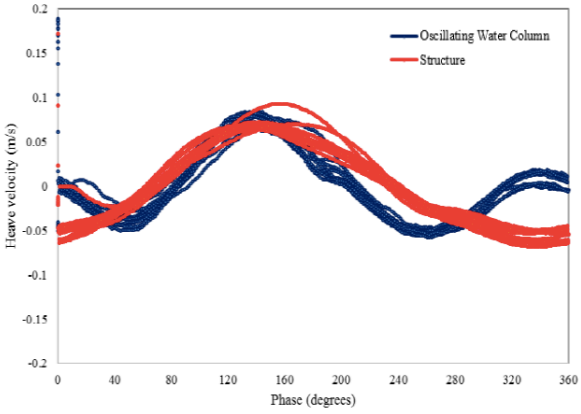

Figure 7.17: Phase averaged heave velocity with a forcing frequency of 0.4 Hz (forcing period ratio of 1.6)

Comparison of Figure 7.15 to Figure 7.17 shows that the larger velocity differential is seen at forcing period ratios corresponding to the oscillating water column natural period (Figure

7.15), then the structure natural period (Figure 7.16), and finally values that do not align with either natural period (Figure 7.17). Figure 7.15 to Figure 7.17 supports the data shown in Figure 7.13. A higher velocity difference leads to longer elliptical axis lengths hence, a higher expected power outputs at those respective forcing periods. This is seen numerically in Chapter 5 in Figure 5.16. This conclusion is supported in Figure 7.11 and Figure 7.12.

7.4 Discussion of results trends

The experimental data does not resemble a typical ellipse like that seen in the numerical analysis seen in Chapter 5 and Stanham et al. (2016). It is believed that this is caused by the irregular waves produced due to a mixture of constructive and deconstructive interference from reflected waves at low wave period. Data collected at higher wave periods (>2s) is much smoother because these waves are able to pass through the system with little reflection. This effect is seen by comparing the plots in Figure 7.9.

Despite this, this study has shown that the relationship between both the major and minor axis length and power output in an oscillating water column wave energy device and the how the length of the major and minor axes changes with forcing period ratios produced experimentally in a two dimensional wave tank can be reproduced numerically with WAMIT and OrcaFlex in the numerical analysis in Chapter 5 (Figure 5.15). The experimental analyses have shown a scattered linear trend between the power output of a floating oscillating water column wave energy device and the length of the long axis of the ellipse relating the heave velocity of the structure to the heave velocity of the water column. These results of the experimental and numerical investigations are seen side by side in Figure 7.18.

Comparison the experimental and numerical results shown in Figure 7.18 is hard because the numerical simulations were not run on a structure of comparable size. Figure 7.19 has been plotted to overcome this difficulty. This has been done so a comparison between the different sizes systems studied in the numerical investigation in Chapter 5 and the experimental work detailed in this chapter. The experimental work and the numerical work differ in sizing because the numerical investigation was aimed at sizing an oscillating water column wave energy device for actual locations along Australia's eastern coastline. These real world wave periods of approximately 8-12 seconds required a much larger device that that possible to test in the laboratory. Due to this the axis lengths of the numerical study are an order of magnitude higher than those seen in the experimental study. Figure 7.19 is produced by plotting the ratios of each the variable as a fraction of the largest measurement for that such variable; hence values lie between zero and one. Experimental data is taken from Figure 7.11 and Figure 7.12 and numerical data is taken from Figure 5.15.

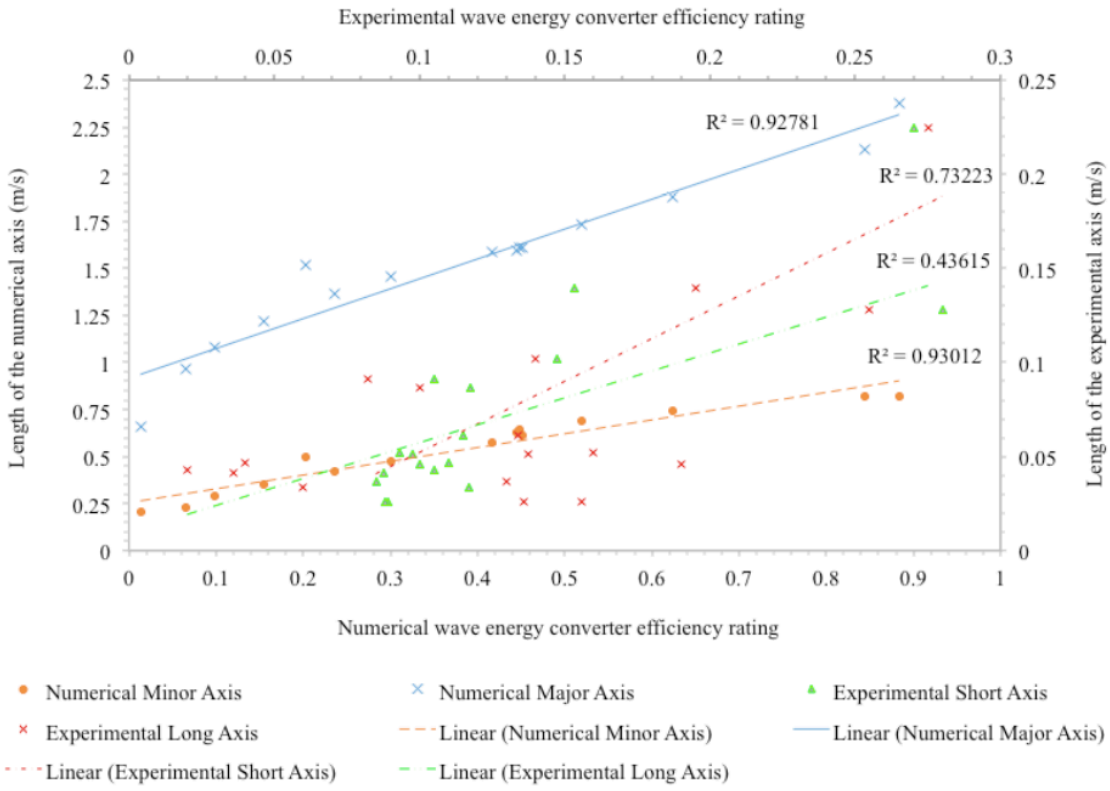

Figure 7.18: Comparison of experimental and numerical investigations

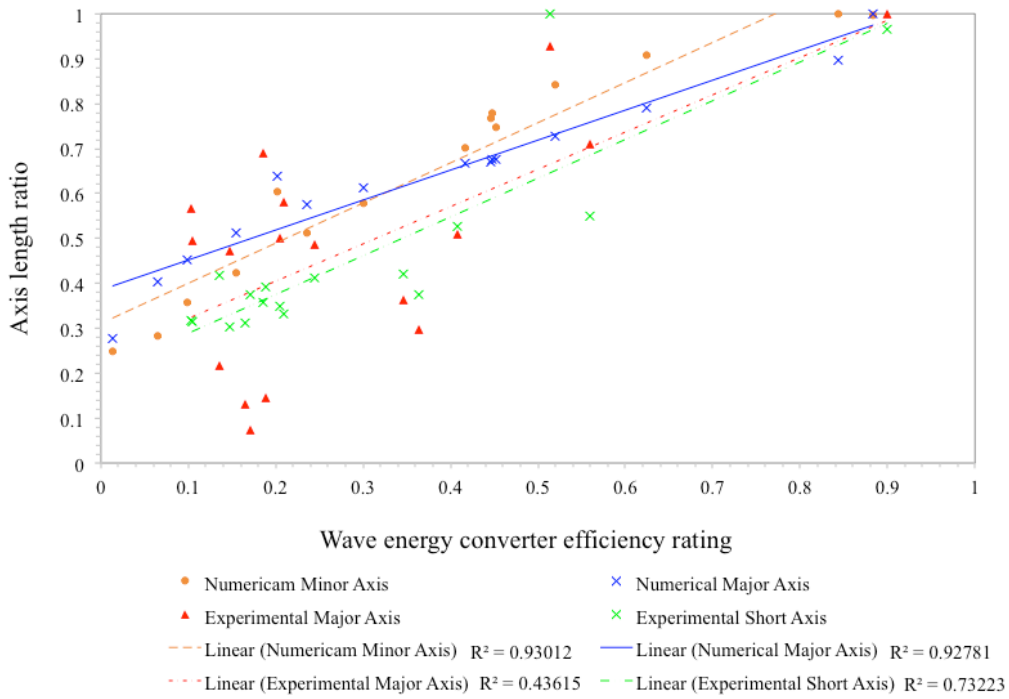

Figure 7.19: Normalised comparison of experimental and numerical investigations

The axis length ratios are ratios of the axis length for a given efficiency ratio over the largest axis length recorded. This allows comparison between the system where the axis length may be different due to different wave amplitudes and periods. The normalised power output ratio of the experimental results has been achieved by multiplying the power ratio of the numerical values by the largest power ratio (0.9) of the numerical results. This value has been chosen as a work around to the energy lost due to the nature of the experimental setup.

The length of the long and short axis of the ellipse, or rather the extent (essentially the magnitude of the velocities) of the parametric plot relating the structure heave velocity to the oscillating water column heave velocity, can be used as an indicator for potential OWC power production capabilities rather than the expected heave of the structure or water column with respect to the forcing wave. The maximum axis lengths have been shown to occur at a forcing period equal to the natural period of the water column. The lengths have also shown to be longer (but not maximised) when subjected to waves with forcing periods corresponding to the natural period of the structure. The axis length, and hence power output, remains elevated between these two points. With this in mind a separation between the natural period of the structure and water column is beneficial for power production in a floating oscillating water column wave energy converter.

The numerical and experimental analysis suggests that there is no discernable link between the gradient of the long axis of the ellipse and the power output production. This is also confirmed through the thought experiment seen in the numerical analysis of Chapter 5.

Further research is needed into how the natural period ratio of the structure to the water column affects the axis lengths. It would be useful to determine if there is an upper limit of this ratio or if further separation shows a continued increase in axis length and hence power production. This information will allow the designer to set the system up in such a way that the axis length is maximised in any given sea conditions. This will allow the most efficient system to be developed.

7.5 Chapter Summary

This chapter has presented experimental work of the numerical investigation into the axis length analysis of Chapter 5. This chapter detailed the two-dimensional model using during the testing, the testing procedure, and the accompanying data analysis. The trends shown in the data analysis are similar to those show in Chapter 5; a longer axis length is indicative of a greater power output. The experimental work was in agreement with the numerical work on which forcing period ratios produce the greatest axis lengths. Both investigations determined that the greatest axis length is achieved at a forcing period ratio of one (wave period equal to the oscillating water column natural period). Both investigations showed that axis lengths are greater at forcing period ration that lie between the oscillating water column natural period and the structure natural period than at forcing periods less than the natural period of the oscillating water column or at forcing periods greater than the structure natural period.

The differences in the data, especially the efficiency of the systems, of the experimental work and the numerical work can likely be attributed to energy lost in experimental setup. As outlined previously, the experiment was highly subjected to reflected waves due to the two-dimensional nature of the setup.

Overall, the results confirm that peak productions are achieved if the natural period of the structure is at least 1.3 times that of the water column and when the water column resonates with the waves.

Chapter 8 Answering the Research Questions, A Review and Discussion

8.1 Introduction

This study considered a number of questions that are asked in section 1.5 on page 6. These questions were proposed at the conclusion of the literature (Chapter 2). This present chapter brings together the results from Chapters 3 to 6, answers the questions and provides an overview of the results and the research undertaken. Chapter 8 presents each question again and then answers it. In answering these questions, the study provides a roadmap for the design of a tuneable oscillating water column wave energy device. The design roadmap can be simply stated in six steps:

1. Confirmation that installation location conditions are within the feasible design guidelines.

2. Design/sizing of the oscillating water column for maximum power takeoff.

3. Design/sizing of the structure.

4. Design/sizing of a heave plate system.

5. Design/sizing and selection of mooring lines.

6. Verification of structural dynamics.

These six steps are expanded in the design flow chart shown in Figure 8.1. The questions posed in Chapter 1 and answered in Chapters 3 to 6 provide the framework for the chart.

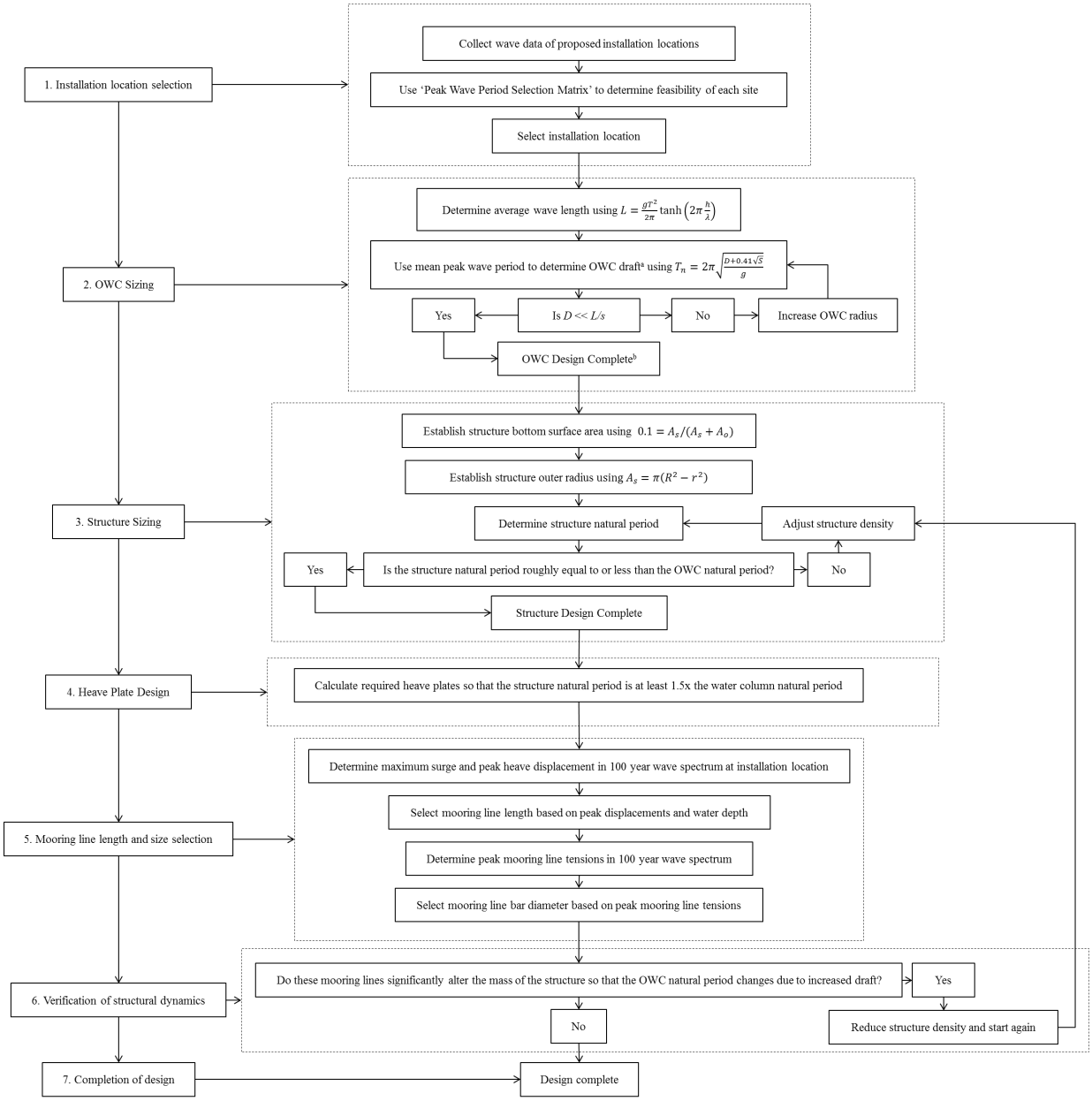

a – The draft will be equal to the oscillating water column length in a bottom open oscillating water column device. In a backward bent duct *D* will be equal to the total duct length rather than the draft.

b - This completion assumes the oscillating water column natural period matches the installation site mean peak wave period at optimal power takeoff damping. This method will slightly underestimate the oscillating water column natural period. This is not a cause for concern because the increase is minimal and actually broadens the power takeoff spectrum.

Figure 8.1: Oscillating water column wave energy device design flow chart.

8.2 Research Questions and Discussion

8.2.1 Current design methodologies

This study began by exploring the current offshore design methodologies and parameters. These design methodologies are generally employed in the oil and gas industry, hence are specifically tailored to such applications. The questions proposed in this section of the research were as follows:

What are the current offshore floating vessel design methodologies and parameters?

The literature review in Chapter 2 outlines the current offshore vessel design methodologies and design parameters. The current design methodologies are heavily codified. The two main codes used are the DNV codes and the RPI codes. Traditional offshore vessels are usually designed for use in the oil and gas industry and are employed in areas of significant hydrocarbon deposits. To ensure that they stay on station and that the riser does not rupture, oil and gas industry vessels are required to experience as little motion as possible by avoiding most of the wave energy rather than capturing it. This leads to a design methodology that ensures the structural dynamics lend themselves to this goal. This means that the structure natural period is selected to fall well outside the wave periods encountered. An example of this is seen in Figure 2.8 on page 25. All RAOs shown experience minimal (=<1) heave at common wave periods (8-12 seconds). The natural periods of all structures are greater than 20 seconds. Mooring lines are selected to ensure the device does not drift off station. The mooring lines are not considered in the structural dynamics of the traditional offshore vessel.

What are the current motion-dependent floating wave energy converter design methodologies and parameters?

Current design methodology for floating wave energy converters often has the installation site with the highest energy density. This is highlighted by Bernhoff et al. (2006) and Iglesias and Carballo (2011). This thesis argues that while these locations do present the highest power concentration, they are also the areas most likely to present storm conditions that such a device cannot withstand. This is evident by comparing the wave energy to the peak wave period and significant wave height in on page 23. This work demonstrates that a device can be tuned to operate efficiently in less energy dense locations and that the device can be tuned to survive the storm conditions (which are typically less extreme) at these locations. Chapter

2 presents numerous potential benefits to developing a wave energy converter to operate in calm sea states. These include:

- Easier to predict wave characteristics.
- Lower chance of unfavourable conditions.
- Lower periods of 'down' time because of unfavourable operating conditions.
- Longer periods of consistent conditions.

The current motion-dependent floating wave energy converters are usually designed in accordance with the DNV standards. Chapter 2 addresses the shortcomings with this design methodology. These can be summarised as:

- Little to no emphasis on the possible effect of the mooring lines on the structural and oscillating water column dynamics.
- Factors of safety that are too demanding considering little to no environmental risk and no risk to human life.
- The standards have only one design goal; to keep the structure as still as possible.

How applicable are traditional design methodologies and parameters to motion-dependent wave energy converter design and operation?

It was concluded in Chapter 2 that the current design methodologies and parameters are not entirely applicable to oscillating water column wave energy converters because the primary objectives are different. The traditional vessel is designed to remain motionless during all sea conditions. The floating oscillating water column device is required to experience motion during the mean sea states and experience minimal motion during the unfavourable sea states. The reasoning behind the design methodologies and parameters employed in the traditional offshore industry is reversed when investigating the design of an oscillating water column wave energy device. Rather than designing a structure with a natural period at least twice the wave period (guidelines for a spar buoy from DNV-OS-301, seen in Table 2.1 on page 24) in an effort to reduce movement, the structure should be designed to increase heave motion in the mean sea state that allows the oscillating water column to experience increased heave motion. This present study does, however, make use of the tuning mechanism employed in

the traditional offshore industry. Chapter 2 (section 2.4.1, page 27) discusses the possible use of heave plates on an oscillating water column wave energy device as a tuning mechanism to both increase power output during favourable conditions and to increase survivability during unfavourable conditions.

What is the most feasible design methodology and hence requirements of a motion-dependent wave energy converter system?

Chapter 2 argues that the existing design methodology can be reversed when designing a structure that requires motion to operate. The existing design methodology can be applied to the floating oscillating water column device when trying to ensure it survives unfavourable storm conditions. The standard design methodology used in the offshore oil and gas industry is to only use mooring lines to keep the vessel on station (DNV-OS-301). This study proposes the use, or at least consideration, of the effect of the mooring system on the structure dynamics when designing a floating oscillating water column wave energy device. It concludes that the use of the mooring system to improve structural dynamics (increased heave in mean conditions and reduced heave in storm conditions) is not as effective as changing the heave added mass of the structure. This conclusion is seen in Chapter 4 where the heave mass increase is shown to significantly increase the structure natural period. This increase is shown to increase the range over which power can be captured in Chapter 5. Chapter 6 shows that controlling the structure natural period through heave mass changes can reduce the peak displacement and peak mooring line tension during two DNV defined 1-in-100 year storm events. This combination of results confirms that tuning through heave mass changes is able to produce a system that can achieve two goals; be more efficient in mean conditions and more structurally robust in unfavourable conditions, without compromising either.

8.2.2 Operational stage wave energy converter moorings

The following questions were asked so that the optimal design with regards to system efficiency from a mean sea state could be determined. The starting point for this study was determined through a literature review of existing designs. Most notable design influences are Stappenbelt and Cooper (2010) who provided the initial sizing starting point, and Koh and Cho (2011) who provide details regarding the sizing of heave plates.

Can a system be developed that allows the vessel to experience increased motion from first order wave loading?

The operational state of a floating oscillating water column wave energy device is investigated numerically in Chapter 4 using WAMIT and Chapter 5 using OrcaFlex and experiementally in Chapter 7. It was determined that a larger velocity differential between the oscillating water column and structure was a better indicator for power output than the expected heave of the structure or the phase and angle between the structure heave velocity and the oscillating water column heave velocity. These results are seen in section 5.9 on pages 121 to 125. Figure 5.15 on page 123 provides evidence that the greater the velocity differential the greater the efficiency of the system. This work is supported by a case study seen in section 5.10 starting on page 127. Further support to this work is seen experimentally in Figure 7.11 and Figure 7.12 on page 230.

Chapter 5 considers the effect of the ratio of the forcing period to the natural period of the oscillating water column. It was determined that when using singular sinusoidal waves the optimal forcing period is approximately 90% of the oscillating water column natural period. This value corresponds to the undamped natural period of the oscillating water column. This conclusion was tested using wave spectra (section 5.12 starting on page 132). It was determined that using wave spectra with a peak wave period equal to the damped oscillating water column natural period produced a system with a higher efficiency than using wave spectra with a peak wave period equal to 90% of the damped oscillating water column natural period. This is because there is a sharp decline in the power output of the system when subjected to wave periods below 90% of the damped oscillating water column natural period. This relationship is highlighted for single sinusoidal waves in Figure 5.16 on page 124 and for wave spectra in Figure 5.31 on page 137 and concluded that the oscillating water column

of the wave energy device should have a damped natural period equal to the mean sea state peak wave period.

The following provides guidelines for the most efficient system given a fixed sea state.

The oscillating water column must have a natural period equal to the mean peak wave period of the sea state. This is achieved by ensuring the oscillating water column draft and oscillating water column surface area are correctly sized. The mathematical relationship governing this sizing is:

$$T_n = 2\pi \sqrt{\frac{D + 0.41\sqrt{S}}{g}} \tag{8.1}$$

where D is the structure draft of a bottom open oscillating water column device (and hence oscillating water column length) and S is the water column surface area.

Note: This relationship does not include the effects of power take-off damping. It serves as a starting point for design. The natural period of the oscillating water column at optimal power take-off damping is likely to be 5% to 10% larger than this value. This damping value can be thought of as an artificial increase in the mass of the oscillating water column; hence the increase in natural period. This effect is seen by comparing the device sized for an eight second wave in section 3.3 on page 54 with its RAO found using WAMIT in Figure 4.25 on page 85 with different power take-off damping values. The natural period has increased from 8 seconds to approximately 8.75 seconds at optimal damping. The exact increase will be dependent on the value of the optimal power take-off damping.

Care must be taken to ensure the draft of the oscillating water column is sufficiently smaller than the estimated average wavelength. The effect of too big an oscillating water column length is highlighted in section 3.2.1 starting on page 45. The greater the draft the smaller the radius of orbit of the water particles encountered. This means that wave attenuation is reduced at increasing depths and so is the possible heave motion of the oscillating water column. This is visualised in Figure 3.1 on page 47. This design stage is illustrated in Figure 8.2.

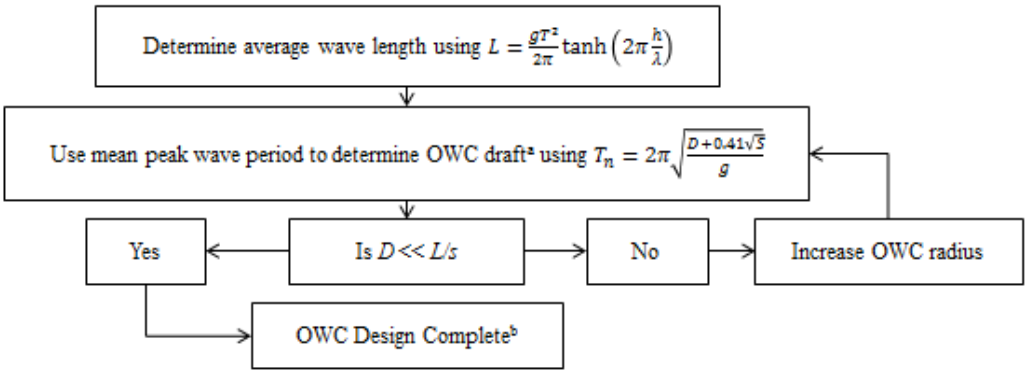

Figure 8.2: Oscillating water column design flow chart

a – The draft will be equal to the oscillating water column length in a bottom open oscillating water column device. In a backward bent duct *D* will be equal to the total duct length rather than the draft.

b - This completion assumes the oscillating water column natural period matches the installation site mean peak wave period at optimal power take-off damping. This method will slightly underestimate the oscillating water column natural period. This is not a cause for concern because the increase is minimal and actually broadens the power take-off spectrum.

If the required draft is not sufficiently smaller than the average wavelength then the surface area of the oscillating water column must be increased. This increase in oscillating water column surface area will allow the natural period to remain constant after a reduction in draft. This is because the natural period of the oscillating water column is a function of both the draft and surface area. Hence, if the draft is reduced the surface area must be increased to keep the natural period constant.

The structural dynamics of the system can be established such that the heave velocity differential between the oscillating water column and structure from first order wave loading can be achieved. The starting guidelines established by Stappenbelt and Cooper (2010) for this to occur are that the system should be sized such that the bottom surface area of the oscillating water column is roughly equal to approximately 90% of the total bottom surface area (oscillating water column plus the structure). This relationship is seen in equation 7.2.

$$0.9 = \frac{A_o}{A_s + A_o} \tag{8.2}$$

This recommendation will allow a large enough oscillating water column and enough structure bottom surface area to experience heave motion from the Froude-Krylov force.

The structure heave mass (added and real) in conjunction with the water plane stiffness must be such that the natural period of the structure is approximately 1.5 times the natural period of the water column.

The design flow chart for the structure is seen in Figure 8.3. This stage takes place only after the oscillating water column dimensions have been established.

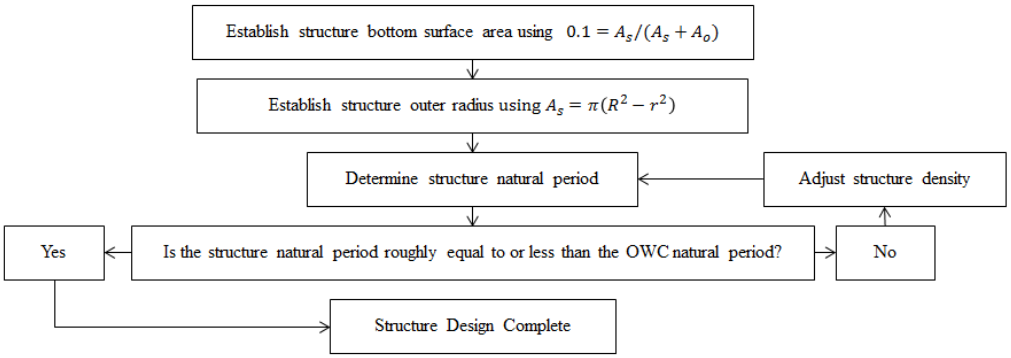

Figure 8.3: Structure design flow chart.

The design stage here calls for the untuned structure natural period to be approximately equal to, or less than, the oscillating water column natural period. This is because it is possible to increase the natural period of the structure through added mass tuning but it is not possible to decrease it because the lowest added mass value will occur when the cylinder has no heave plates. Hence, a lower initial natural period provides more scope to change the natural period of the structure through tuning. Starting with a lower value for the structure natural period allows the natural period to be reduced to this starting value during unfavourable storm conditions where the peak wave period is usually much greater than the mean wave period. This means that the structure natural period is sufficiently spaced from the wave peak period. It is suggested that the structure density be adjusted if this condition is not met. This can be achieved through use of a different material or by adjusting void spaces within the structure. The increase in density will cause a change in the bottom surface area to achieve the required draft calculated during the design of the oscillating water column. It is unlikely that this change will be significant. The natural period of the structure will be approximately equal to:

$$T_{ns} = 2\pi\sqrt{\frac{D}{g}} \tag{8.3}$$

This is slightly less than the natural period of the water column because the effect of the oscillating water column surface area is not included.

This research shows that these structure-oscillating water column relationships (structure natural period 150% of the oscillating water column natural period) are favourable with respect to both the power production phase and survivability. The large difference in structure and oscillating water column natural period is shown to increase the range over which the device can capture power when oscillated with a wave with peak period equal to the peak wave period of the oscillating water column. This difference creates an elevated efficiency between the natural periods of the oscillating water column and structure because a difference in natural periods will lead to different RAOs for the oscillating water column and structure at any given forcing period. Hence a velocity differential between each can exist. This is seen in Figure 5.16 on page 124 and again in Figure 5.32 on page 139.

What is the range of wave frequencies that this system can operate over?

Increasing the range of wave periods over which the structure can draw power from is essential in a practical application where the forcing periods are drawn from a spectrum rather than from a single wave. This range is increased by ensuring that there is adequate separation between the structure heave natural period and oscillating water column heave natural period. The device can capture power over wave frequencies that lie between the oscillating water column natural frequency and the structure natural frequency. The starting design guideline set by Stappenbelt and Cooper (2010) (having the structure natural period at least 1.5 times the oscillating water column natural period) was kept constant in this present research. It was shown in Chapter 5 that for single sinusoidal waves the axis length of the parametric function relating the structure heave velocity to the oscillating water column heave velocity (and hence system efficiency) is maximised at a forcing period ratio (forcing wave period to the oscillating water column natural period) of 0.9 and remains elevated at forcing period ratios between 0.9 and the ratio of the structure natural period to the oscillating water column natural period. This result is seen in Figure 5.16 on page 124.

The research concludes that when the device is subjected to wave spectra rather than single sinusoidal waves the operational wave frequencies lie between the structure natural frequency and water column natural frequency. Waves with peak wave frequencies matching the oscillating water column natural frequency produce the most efficient system. The results leading to this conclusion are seen in section 5.12 starting on page 132. Hence, an increase in separation of natural periods can increase the range of periods in which the system is capable of capturing power.

There is an upper limit of the separation of natural frequencies. Too large a separation will result in a loss of the structural movement with respect to the forcing wave. Hence, the velocity differential between the oscillating water column and structure will be equal to the velocity differential between the water column and forcing wave. This will be less than the previous velocity differential because the structure is able to experience a heave RAO greater than one in the mean sea conditions when subjected to wave frequencies equal to the natural frequency of the water column. This RAO is seen in Figure 5.3 on page 110. The RAO value at the oscillating water column natural frequency is equal to approximately 1.3. This work concludes that through tuning the structure natural period the wave periods over which increased capture can occur can be increased. This means that the spread of the wave spectrum can be larger but the peak wave period should still match the damper oscillating water column natural period.

Is a tunable system likely to increase the range of wave conditions in which the wave energy converter is able to experience increased motion?

and

What are the most viable methods to create a tunable system that is able to meet objective 2?

A structure with a tuneable heave added mass is likely to be needed to satisfy the two obligations the structure must meet; have a draft that allows the oscillating water column to have a natural period equal to the mean peak wave period, and to have a natural period approximately equal to 1.5 times the oscillating water column natural period. If the structure is designed to meet the size requirements of the oscillating water column then the mass of the structure, in conjunction with the water plane stiffness, will likely not result in a large enough natural period. An example of such a system is seen in Figure 4.8 on 73. The system with no increase in heave added mass has a natural period slightly less than the oscillating water column. It is suggest that heave plates be used to increase the natural period of the structure. Chapter 5 concluded that this tuning mechanism is more effective than changing the power take-off damping or mooring line stiffness. The use of heave plates will increase the added mass and hence overall heave mass and result in a larger structure natural period. The effect of increasing the heave mass on the structure natural period is seen in Figure 4.14 on page 76. This increase was shown to cause negligible changes in the value of the oscillating water column natural period. This change is seen in Figure 4.15 on page 76.

Care must be taken to use appropriately sized heave plates so that the structure viscous damping is not increased so much that the RAO peak is reduced. Koh and Cho (2011) have provided guidelines on heave plate sizing. Koh and Cho (2011) have also highlighted that numerous heave plates may be used with little increase in viscous damping. This approach may be needed if a single heave plate cannot increase the added mass to the required value without increasing the viscous damping. The present research concludes that this method of device tuning is superior to an increase in mooring line tensions to increase the structure stiffness.

To what extent is efficiency of a motion-dependent wave energy converter increased during periods of optimal wave induced motion?

Specifying exact numbers to answer this question is not easy because of the highly site specific nature of system efficiency. Spectra with a larger wave period standard deviation will lead to a less efficient system because fewer wave periods will be equal to the peak wave period. The system efficiency is mostly determined by the number of waves that have a period of approximately 90%-140% of the oscillating water column natural period encountered by the device. Because of the spread of the wave spectrum, this number will change at each site. This study shows that a system with an oscillating water column natural period equal to the peak wave period is more efficient than a system where the oscillating water column natural period is slightly larger than the peak wave period. The system is also more efficient than a system where the oscillating water column natural period is 150% larger than the forcing wave peak period. This result is seen in section 5.12.3 starting on page 136.

8.2.3 Survivability phase wave energy converter mooring

These questions focussed on the development of a system to operate efficiently in the mean sea state and be able to withstand unfavourable storm conditions and focus on whether tuning mechanisms are able to influence the chance of survival. These questions were investigated by testing the structure in two 1-in-100 year events defined by DNV-OS-301. These events defined the peak wave period, significant wave height, peak wind speed, and peak current speed. The survivability was determined by measuring the peak heave displacement, the peak mooring line tensions, and value of the wave and structure zeroth moments. The questions were as follows:

Can the system developed in objective 2 withstand unfavourable conditions through the tuning (i.e. reduce first order motion response), without compromising the operational phase motion of the wave energy converter?

It was determined that such a system could be created if the system natural period could be tuned. The peak displacements, peak mooring line tensions, and zeroth moments of the structure spectral density curve were all reduced when comparing the untuned system with the tuned system in both 1-in-100 year events tested. These results are seen in Table 6.4 on page 176 and Table 6.5 on page 179 for the Norwegian Sea spectrum and in Table 6.6 on page 197 and Table 6.7 on page 200 for the West Africa spectrum. This reduction likely to result in a structure that will withstand unfavourable storm conditions because the mooring line tension of the catenary mooring system was within permissible limits when compared to the chain mooring systems commercially available. These values are seen in Table 6.8 on page 209. A reduction in heave mass (changing the natural period though a change in added mass) is the best tuning mechanism for decreasing the natural period of the structure. Section 6.12 starting on page 206 concluded that this mechanism performed better than the increase in power take-off damping and provided fewer unfavourable side effects than stiffness increases through mooring line tensioning. An increase in stiffness (through mooring line tensioning) was also shown to perform well but the accompanying increase in oscillating water column heave and the exponential increase in mooring line tensions experienced when the line is no longer catenary in shape, suggest that this tuning mechanism is unlikely to be practical. This increase in tension is seen in Table 6.8 on page 207. The peak mooring line tension in the taught mooring line setup was at least two orders of magnitude greater than the tension in the catenary setup.

If the answer is negative: What is the most feasible system that will meet the survivability requirement of a wave energy converter?

This is answered in Chapter 5. The most feasible system will be one that employs a tuning mechanism that allows heave plates to be deployed and removed when needed.

The results of this investigation determined the mooring system characteristics. The mooring lines need to remain loose (catenary in nature). They should allow the structure to reach peak heave and surge displacement without the mooring lines becoming taught. This length defined by the maximum structure excursion should serve as the mooring line design length. The mooring line design flow chart is shown in Figure 8.4.

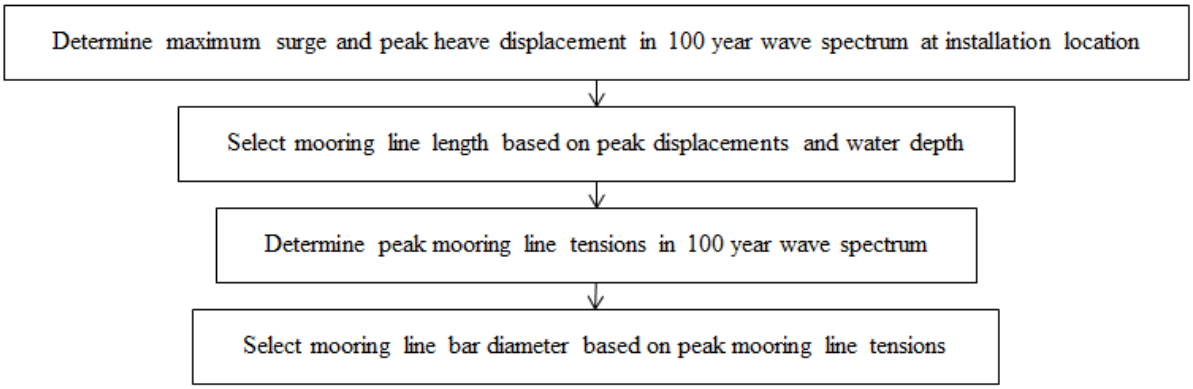

Figure 8.4: Mooring line design flow chart.

The structural dynamics will need to be verified after the mooring system has been chosen because the mooring lines will increase the weight of the structure. The mooring system will probably affect the heave mass of the structure and hence the draft of the oscillating water column. If this is the case then the structure mass will have to be reduced. This is likely to be the case unless the mooring system is more intricate in design where a floating buoy bears most of the weight of the chain or the mooring lines are the same density as the ocean. Either of these options is likely to lead to an unnecessary cost increase of the system. Hence this design stage will be an iterative stage. Once the mooring lines are selected, the structure will have to be resized to ensure the appropriate heave mass is achieved. The peak offsets and mooring line tensions during the storm conditions will have to be assessed. If the mooring system can withstand these values then the design is complete. If not, then new mooring lines will have to be chosen and the process repeated.

8.2.4 System Integration

These questions were asked so as to focus on whether or not the system designed to operate most efficiently in the mean sea state of the particular installation location can also be the system that is able to survive the 1-in-100 year storm event.

Can the operational system and survivability system be integrated into one system without compromising efficiency or increasing risk of failure?

and

If the answer is negative: Can both systems be implemented with one floating vessel?

and

If the answer is positive: What is the best method to transition between the systems?

Transition between the systems is unlikely to occur too frequently if calm areas are chosen. If this system is deployed off the east coast of Australia the system will probably only have to be in survival mode once a year on average. Comparing the conclusions to the research discussed in Chapter 4 and Chapter 5 shows that the operational system and the survivability system are able to coexist if the structure is developed in such a way that the heave plates are able to be retracted and deployed for a given sea state. This will allow the structure natural period to be adjusted as needed. The design of retractable heave plates will require further research.

What are the environmental conditions that determine which system is in use?

The system to use should be determined by the current or predicted sea state. This means that during the mean sea state the device should be setup such that it can operate most efficiently, and during the unfavourable storm conditions the device must be setup to ensure structural integrity. This means changing the heave mass to ensure the goal (power production for mean sea states, survivability for storm sea states) for the device matches the sea state it is in. Prediction of unfavourable conditions (each site will have a predetermined list of conditions classed as unfavourable) will be essential so that the device can be ready for unfavourable conditions. This will result in a small period of down time but will probably result in a device that withstands storm conditions. Unfavourable conditions are touched on in section 6.14 on page 211 concerning selection of installation location. As a guideline, peak wave periods

close to (±10% to 15%) of the structure natural period during the operation phase, and significant wave heights double the mean significant wave height, would be classed as unfavourable in a location with typically calm seas.

During the mean sea state, the heave system that allows the largest separation of natural periods between the oscillating water column and structure should be used. This will increase the range of wave periods over which power can be captured. When unfavourable storm conditions are predicted the system should be such that the structure natural period is sufficiently spaced from the predicted peak wave period of the unfavourable conditions. This will require the heave plates to be retracted as the storm conditions will most likely have a peak wave period greater than the mean peak wave period. This means that since the optimal power production state requires the structure to have a greater natural period than the oscillating water column, the structure natural period will be closer to the storm peak wave period. Hence, a reduction in heave added mass, and consequently the structure natural period, will move the structure natural period away from the storm peak period. This is best understood through the illustrations in Figure 8.5 and Figure 8.6.

Figure 8.5 shows the setup for the mean sea conditions. These are the conditions where the oscillating water column natural period and structure natural period should be spaced accordingly. The model used in this thesis has oscillating water column natural period of approximately 8.75 seconds. This value corresponds to a forcing period ratio of one. The structure natural period will be equal to approximately 13 seconds.

Figure 8.6 shows the desired setup in unfavourable storm conditions and highlights where the structure natural period should be moved to during unfavourable storm conditions. Here the storm peak wave period will be larger than the oscillating water column natural period; hence, it is closer to the structure natural period. This is disadvantageous because it will increase the structure heave. To counteract this, the structure natural period should be moved to either a higher or a lower value. Retracting heave plates will allow the value to be decreased (seen on the left of the horizontal bracket) to a value of approximately 8.75 seconds or less. Increasing the heave plates will allow the value to be increased (seen on the right of the horizontal bracket) to a value of approximately 17 seconds or more. This again highlights the importance of developing a structure where the natural period without the inclusion of heave plates is sufficiently low (close to the oscillating water column natural period).

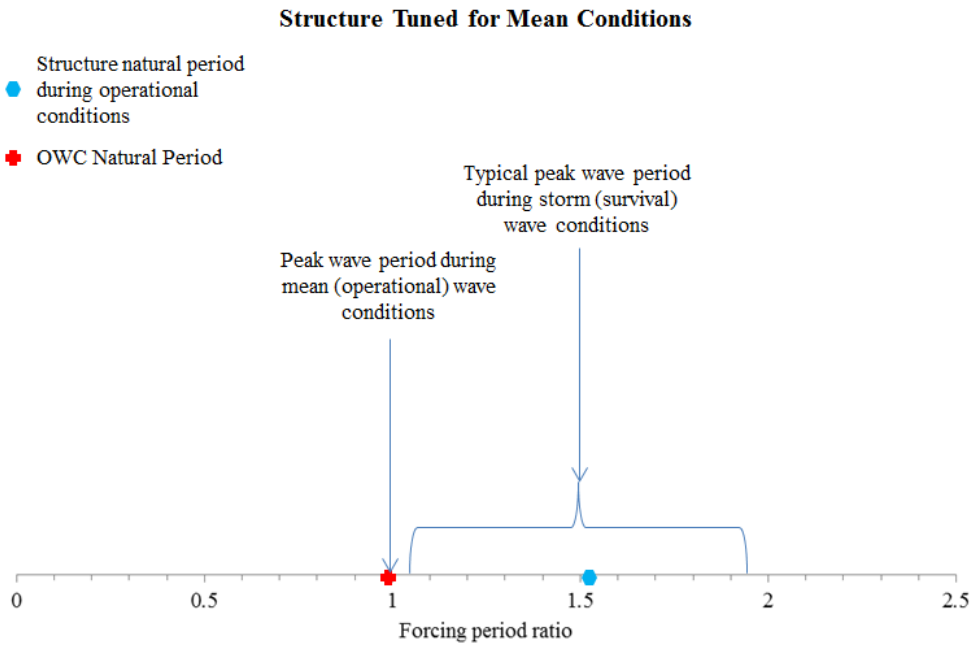

Figure 8.5: Relationship between the oscillating water column and structure natural period during favourable (mean) sea conditions

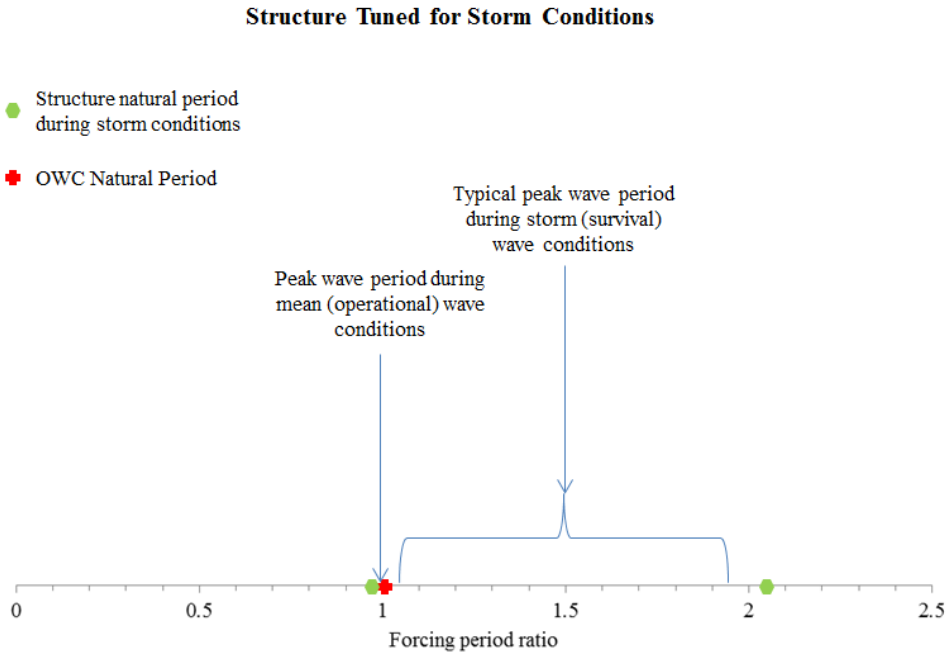

Figure 8.6: Location of the structure natural period after tuning for survivablity with respect to the oscillating water column natural period and the peak wave period of the sea state.

The exact extent of the tuning needed, and hence heave plate number and sizing, will be site-specific so exact recommendations cannot be provided.

8.2.5 Design parameters and concerns

The final questions this study focussed on are related to design factors for safety and the identification of installation locations for a wave energy device. The questions posed were:

What are appropriate factors of safety during analysis for wave energy converters?

It was outlined in Chapter 2 that the factors of safety required for traditional offshore vessels are perhaps too extreme for oscillating water column wave energy devices because they do not take into the account that movement is necessary for power production. Oscillating water column wave energy devices do not post the same risk to human life or to the environment that traditional offshore vessels such as oil and gas platforms do. The most significant risk posed is an economic risk for whoever is funding the project. DNV-OS-301 does provide a provision for certain devices to use lower factors of safety. These vessels are likely to be classed as Consequence Class 1 vessels. It is recommended that these safety requirements be used for the mooring system during the design of the mooring lines for the unfavourable conditions given the lack of specific wave energy device design codes. Argument could be made that a safety factor closer to 1 might appropriate if the overall cost of the device can be reduced. This is a possibility because the device investigated in this study is for use in calmer sea states. Consequence Class 2 vessel factors of safety are not recommended because they are aimed at more traditional offshore vessels where the cost of failure is more than just financial. Further research is needed to determine whether the functional objectives of the motion dependent device deserve a specific set of design parameters.

Where are the most feasible locations for the installation of the wave energy converter investigated in this thesis?

Chapter 5 considers results that highlight key installation site parameters. These parameters allow installation sites to be identified. The site should be such that the mean peak wave period is sufficiently different to the natural period of the structure in the operational phase. A selection matrix based on the mean and 1-in-100 year storm peak wave periods is shown in Figure 6.57 on page 213 The larger the difference between these two periods the less tuning will be needed to survive the unfavourable storm conditions.

The significant wave height of the 1-in-100 year storm should be as close to the significant wave height of the mean wave spectrum. This will ensure that the peak displacements, and hence mooring line tensions, during the storm conditions are not significantly different from the peak displacements and tensions experienced in the mean sea state. This will likely allow for a cheaper mooring system. A selection matrix detailing the optimal relationship between the significant wave heights in the two design states is presented in Figure 6.58 on page 215.

An example of an appropriate installation site is seen in Figure 6.2 on page 145. The Port Kembla site has a median peak wave period of 9.57 seconds and median significant wave height of 1.43 metres. The unfavourable conditions can be defined by the conditions at 1% exceedance. Here the peak wave period is 15.1 seconds and the significant wave height is 3.94 metres. The increase in significant wave height is small compared to the Norwegian Sea 100 year event tested in Chapter 5. This means that the increase in heave and surge will also be smaller. The 1% exceedance peak wave period is also sufficiently spaced from the median wave period. This location will require, however, tuning of the structure natural period during such a storm because the structure natural period will be approximately equal to the storm peak wave period of 15 seconds when the structure is setup for power capture.

8.3 Chapter Summary

This chapter ties together the work of this study and is most easily summarised by the answers to the research questions posed at the conclusion of the literature review. These research questions are seen in Chapter 1. Chapter 8 outlines the design methodology and suggests a design roadmap for an open bottom floating oscillating water column wave energy device. To provide an holistic overview of the topic it also contains commentary on other areas not explicitly examined in this study.

This chapter highlights the competing objectives of the power capture state and survivability state of the wave energy device. The device is required to increase heave to capture power from mild sea states but needs to nullify this heave motion during more powerful, unfavourable storm conditions. By answering the initial research questions this chapter has provided insight into how these objectives can be reached without comprise of either.

This chapter provides a brief overview of the literature review and the research undertaken to develop the guidelines for an oscillating water column wave energy device that is able to experience improved energy capture in low energy sea states and improve survivability in unfavourable storm conditions.

Chapter 9 Conclusions, Reflections, and Recommendations

9.1 Thesis Summary

This project has looked broadly at the need for renewable energy sources within mainly Australia. Wave energy is an abundant and viable source of energy but a capture system designed for use in sheltered areas is yet to be developed. This project began with a review of the existing offshore industry with an emphasis on the oil and gas industry. Comparisons between the oil and gas industry design methodology and the renewable energy methodology has highlighted the shortcomings with the current design standards and practices which include safety standards, vessel dynamics, and mooring line requirements. The existing offshore design methodologies and practices have been shown to be counterproductive to the goals of renewable energy devices, in particular, motion dependent energy devices.

Existing mathematical models and principles that are applicable to the offshore industry, renewable energy industry, and data analysis and processing were reviewed in Chapter 3. This includes investigation into sizing of an oscillating water column and the sizing of a wave energy device. Investigation of ocean wave modelling was undertaken and set the context for the wave models (ISSC and JONSWAP) used in the time domain analyses using OrcaFlex.

An oscillating water column wave energy converter was developed using various mathematical modelling principles. The characteristics of the device, which include weight, dimensions, damping, and stiffness, were explored in the frequency domain and conclusions have been drawn regarding these values. The mass of the structure should be so that the natural period of the structure is approximately one and a half times that of the oscillating water column. The larger the oscillating water column is with respect to the structure the greater the power output of the device is expected to be when subjected to a wave with peak period equal to the natural period of the water column. Investigation into the power take-off damping of the floating system reveals that the power take-off increases with damping up to a certain value and then declines.

Time domain analyses of the optimal power production system reveals that a single sinusoidal forcing wave with period matching a value corresponding to 90% of the natural period of the water column produces the most efficient system. This is not the case when the wave energy converter is subjected to wave spectra with peak periods matching that value

through a sensitivity analysis. Wave spectra with peak wave periods equal to the natural period of the water column produce a more efficient system than any other peak period value. These investigations were undertaken using a traditional power output comparison and by using a newly developed analytical assessment tool. This tool draws conclusions from the parametric equation relating the heave velocity of the oscillating water column to the heave velocity of the structure.

Investigation of tuning the device properties was also undertaken in the time domain. Potentially suitable tuning mechanisms were chosen from the results of the WAMIT frequency domain investigation. The tuning mechanisms investigated include decrease of the heave mass of the structure, increasing the stiffness, and increasing the power take-off damping. Investigation of the affect each tuning mechanism has on the natural period, and hence the motion of the device, was undertaken using OrcaFlex. Each tuning mechanism was investigated in isolation and in combination with each other tuning method. It is concluded that a reduction of the heave mass is the most viable method for reducing structure movement and hence mooring line tensions.

This project has developed a total design summary of a floating oscillating water column wave energy device. Methods have been developed to allow the most efficient system to be in action during optimal sea conditions. Investigation into unfavourable sea conditions show that if a suitable location is chosen then a reduction in heave mass is the most viable way to ensure structural integrity.

9.2 Original Contributions

This research presents a design methodology for a simple floating oscillating water column wave energy converter. This design methodology shows that it possible to develop an oscillating water column wave energy device that is able to fill the gap in the current technology outlined in Chapter 2. That is, a device that is able to experience improved energy capture in low energy sea states and improved survivability in unfavourable storm conditions through oscillating water column and structure heave period tuning using added mass. This design methodology begins with site selection and then moves on to the development the system. The methodology begins with sizing of the oscillating water column and the structure through to the optimal damping and stiffness levels for a given sea state. This has not previously been undertaken.

A new parametric design tool for oscillating water column wave energy devices has been developed through numerical analysis and confirmed experimentally. This tool suggests that a phase difference between the water column heave velocity and structure heave velocity is not as important as the magnitude of the difference between the heave velocities when concerned with power output. The length of the axis of the ellipse of the parametric equation has shown to be positively correlated with the efficiency of the device. This phenomenon is explained in Figure 9.1. In system A, the oscillating water column and structure are out of phase but moving slowly, leading to a net airflow velocity of 2 m/s. In system B the oscillating water column and structure are more in phase but the oscillating water column is moving at a greater velocity. This results in a system where the net airflow velocity is equal to 3 m/s. This is greater than in system A and more energy will be captured and hence power generated. It was shown that system B produces higher velocities than system A is moderate sea states.

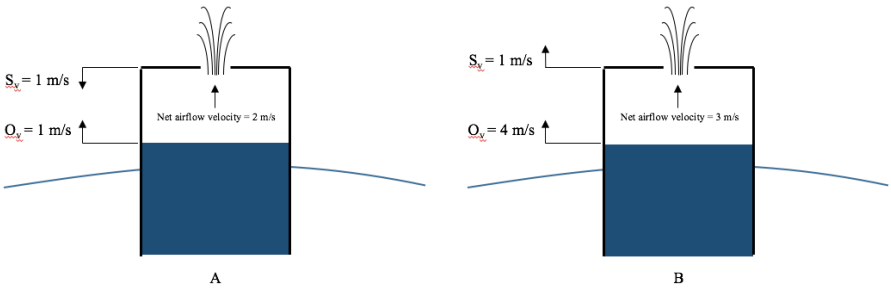

Figure 9.1: Illustration of design tool findings

This work was presented at ISOPE 2016 and can been seen in Stanham et al. (2016).

This project has led to a better understanding of the dynamics of the coupled system in a floating oscillating water column wave energy device. The research shows that with sufficient spacing between the damped oscillating water column natural period and the structure natural period, the range of forcing frequencies over which power can be captured in increased. It is now understood that a reduction in structure movement through heave mass changes during unfavourable conditions can lead to a reduction in peak mooring line tensions to values within the limits of current mooring lines. This structure movement is a function of the environmental conditions such as the significant wave height, the peak wave period and the coupled nature of the oscillating water column and structure. An increase in the oscillating water column motions is linked to an increase in the structure motions. The research also shows that a decrease in the structure heave through mooring line tensioning causes an increase in the oscillating water column response which, in turn, leads to an increase in structure movement. Tensioned mooring lines restrain the increase in structure movement and tension increases in the mooring lines to values above the maximum permissible.

This project concludes that controlling the device's structural dynamics in an effort to increase efficiency and structural robustness is best undertaken through adjustments of the heave mass of the device. This is most easily achieved by designing a device with heave plates. These heave plates can be used to achieve two outcomes. The first is to increase the device natural period during optimal conditions so that the spacing between the oscillating water column natural period and structure natural period is sufficient. The second is to reduce the natural period of the device so that it is not within the storm spectrum envelope during unfavourable conditions. This will ensure a more robust system by reducing structural excursion during unfavourable conditions. The work shows that tuning the device through adjustment of the heave mass will lead to lower peak mooring line tensions and a smaller, more cost efficient mooring system can be used.

Lastly, this project provides guidelines on installation locations for oscillating water column wave energy devices. The site must be such that the median wave period is small enough to ensure that an oscillating water column with required draft can be built. It is to ensure the draft is not so large that all wave attenuation at the required draft is lost. The site should also be a location where the unfavourable conditions (1-in-100 year storm) is such that the significant wave height is not too much larger than the median wave height and the peak wave period is sufficiently larger than the median wave period.

9.3 Review of Achievements

Objective	Evidence of Achievements
Investigate current offshore design methodologies and determine their applicability to OWC WEDs	Chapter 2 Section 2.4 - 'Existing offshore designs' Section 2.4.2 - 'Mooring system design' Section 2.4.3 - 'Design analysis methods' Section 2.5 - 'Literature critique'
Determine system dynamics that result in increased first order wave loading	Chapter 3 Section 3.3 - 'Water column sizing' Section 3.4 - 'Structure sizing' Chapter 4 Section 4.4 - 'System modification using WAMIT' Chapter 5 Section 5.7 - 'Operational state testing Section 5.8 - 'Structure-column velocity function' Section 5.12 - 'Wave spectra' Section 7.2 – ‘Results and Disucssion’
Determine whether the operational state of the WEC can withstand unfavourable sea conditions	Chapter 6 Section 6.7 - 'Results of the Norwegian Sea analysis' Section 6.8 - 'Discussion of the Norwegian Sea analysis results' Section 6.9 - 'Results of the West Africa storm analysis' Section 6.10 - 'Discussion of the West Africa storm analysis results' Section 6.11 - 'Discussion of result trends'
Determine possible tuning/optimisation methods to increase performance and robustness	Chapter 4 Section 4.4 - 'System modification using WAMIT' Chapter 5 Section 5.7 - 'Operational state testing Chapter 6 Section 6.12 - 'Tuning mechanism feasibility'
Determine wave spectra characteristics of appropriate installation sites	Chapter 6 Section 6.14 - 'Installation location guidelines'

9.4 Recommendations for Future Work

Because of the time sensitive nature and funding limits of a doctoral scheme, a complete analysis of a floating offshore wave energy system has not been possible. Secondary investigation into areas this study has not explored may be necessary. The results from this present study can be used as a stepping-stone for this further research.

Second order wave loading

Further investigation into the effects of second order wave loading is needed to ensure the device survivability is not compromised during the operation state by the low frequency wave clusters. The second order loading may cause higher than expected loading in the mooring lines caused by slow drift motions. Subsequent increased tensions will need to be accounted for in a real design. Analysis can be conducted through WAMIT version 6.4S. This is a second order module that needs to be purchased and is in addition to a WAMIT license.

Compressible air within the chamber

This present work does not account for the compressibility of the air within the chamber. It is assumed the airflow through the turbine is moving at the same flow rate as the water column. This can lead to an overestimation of the power output of the system. Since all calculations were undertaken with this assumption it is unlikely that the comparative results would differ. Despite this, further investigation into how the theoretical system behaves when investigated with the inclusion of compressible air may shed more light on the optimal system dynamics and, hence, design characteristics.

Best design of heave plate mechanism

It seems that adjustment using heave plates will be the most viable way to tune the system. The system proposed here utilises heave plates to increase the natural period of the structure during power production phases and to reduce the natural period of the structure during unfavourable storm conditions. A practical investigation into the sizing of the heave plates needed and how they can be deployed and retracted is needed to finalise the design of the oscillating water column wave energy device.

Risk Determination Study

It is suggested that the factors of safety employed in the oil and gas industry are an overestimation of the factors of safety that should be used in unmanned offshore wave energy devices. Investigation into appropriate factors of safety would determine the mooring line requirements and the extent to which the system would have to be detuned during unfavourable storm conditions. This area of research is likely to venture into insurance cost estimations and may fall outside the scope of 'engineering'.

References

Alcorn, R., (2000) Thesis, Wave station modeling based on the Islay prototype plant

API-RP-2SK, 2005. *Design and Analysis of Stationkeeping Systems for Floating Structures*.: American Petroleum Institute.

Astrid, S. and Iglesias, G. (2015) 'The economics of wave energy: A review', *Renewable and Sustainable Energy Reviews*, 45, pp. 397–408.

Bureau of Meterology, (2016). *Interactive Weather and Wave Forecast Maps*. [online] Bom.gov.au. Available at: http://www.bom.gov.au/australia/charts/viewer/index.shtml?type=pPeriod&tz=AEDT&area=Au&model=CG&chartSubmit=Refresh+View

Bayoumi, S., Incecik, A. and El-Gamal, H. (2014) 'Dynamic modelling of Spar-Buoy oscillating water column wave energy converter', *Ships and Offshore Structures*, 10(6), pp. 601–608.

Behrens, S., Griffin, D., Hayward, J., Hemer, M., Knight, C. and McGarry, S. (2012) *Ocean Renewable Energy: 2015 - 2050*. Available at: https://publications.csiro.au/rpr/download?pid=csiro:EP113441&dsid=DS2

Beirão, P.J.B.F.N. and dos Santos Pereira Malça, C.M. (2014) 'Design and analysis of buoy geometries for a wave energy converter', *International Journal of Energy and Environmental Engineering*, 5(2-3).

Benassai, G., Campanile, A., Piscopo, V. and Scamardella, A. (2014) 'Ultimate and accidental limit state design for mooring systems of floating offshore wind turbines', *Ocean Engineering*, 92, pp. 64–74.

Bernhoff, H., Sjöstedt, E. and Leijon, M. (2006) 'Wave energy resources in sheltered sea areas: A case study of the Baltic sea', *Renewable Energy*, 31(13), pp. 2164–2170.

Willcock, T., Che, N. and McCluskey, C. (2013) *Energy in Australia*. Available at: http://www.industry.gov.au/Office-of-the-Chief-Economist/Publications/Documents/energy-in-aust/bree-energyinaustralia-2013.pdf

Brommundt, M., Krause, L., Merz, K. and Muskulus, M. (2012) 'Mooring system optimization for floating wind turbines using frequency domain analysis', *Energy Procedia*, 24, pp. 289–296.

Brown, A.C., and Thomson, J. (2015) 'Heave Plate Dynamics for a Floating Point Absorbing Wave Energy Converter.' *Proceedings of the 3rd Marine Energy Technology Symposium*

Bull, D. (2015) 'An improved understanding of the natural resonances of moonpools contained within floating rigid-bodies: Theory and application to oscillating water column devices', *Ocean Engineering*, 108, pp. 799–812.

Carbon Trust (2011) *Accelerating Marine Energy*. Available at: https://www.carbontrust.com/media/5675/ctc797.pdf

Carnegie Wave Energy (2015) CETO6 Garden Island Project Western Australia: http://carnegiewave.com/wp-content/uploads/2015/06/CP115-0020-0_PRS-CETO-6-Community-Information-Sheet_Web.pdf

Clean Energy Australia Report (2012) https://www.cleanenergycouncil.org.au/

Chakrabarti, S.K. (2005) *Handbook of offshore engineering: V.1-2*. London: Elsevier Science.

Chakrabarti, S. (2009). State of Offshore Structure Development and Design Challenges. *Handbook of Coastal and Ocean Engineering,* 667-694.

Coles, S. (2001) *An introduction to statistical modeling of extreme values*. 2nd edn. London: Springer-Verlag New York.

Davis, A.F., Thomson, J., Mundon, T.R. and Fabien, B.C. (2014) 'Modeling and analysis of a multi degree of freedom point absorber wave energy converter', *Volume 8A: Ocean Engineering*, .

Day, A.H., Babarit, A., Fontaine, A., He, Y.., Kraskowski, M., Murai, M., Penesis, I., Salvatore, F. and Shin, H.. (2015) 'Hydrodynamic modelling of marine renewable energy devices: A state of the art review', *Ocean Engineering*, 108, pp. 46–69.

DNV OS-E301, Position Mooring. 2001, Det Norske Vertias

Evans, D.V. and Porter, R. (1995), "Hydrodynamic characteristics of an oscillating water column device", Appl. Ocean Res., 17, 155-164.

Falcão, A.F. de O. (2010) 'Wave energy utilization: A review of the technologies', *Renewable and Sustainable Energy Reviews*, 14(3), pp. 899–918.

Falcão, A.F.O. and Henriques, J.C.C. (2016) 'Oscillating-water-column wave energy

converters and air turbines: A review', *Renewable Energy*, 85, pp. 1391–1424.

Fiorentini, M. (2010), Evaluation of the frequency dependent parameters and optimization of a floating OWC device, Masters Thesis, University of Wollongong

Fitzgerald, J. and Bergdahl, L. (2008) 'Including moorings in the assessment of a generic offshore wave energy converter: A frequency domain approach', *Marine Structures*, 21(1), pp. 23–46.

Folley, M. and Whittaker, T. (2005) 'The effect of plenum chamber volume and air turbine Hysteresis on the optimal performance of oscillating water columns', *24th International Conference on Offshore Mechanics and Arctic Engineering: Volume 2*.

Fukuda, K. (1977) 'Behavior of water in vertical well with bottom opening of ship, and its effects on ship-motion', *Journal of the Society of Naval Architects of Japan*, 1977(141), pp. 107–122.

Godoy-Diana, R. and Czitrom, S.P.R. (2007) 'On the tuning of a wave-energy driven oscillating-water-column seawater pump to polychromatic waves', *Ocean Engineering*, 34(17-18), pp. 2374–2384.

Harnois, V., Weller, S.D., Johanning, L., Thies, P.R., Le Boulluec, M., Le Roux, D., Soulé, V. and Ohana, J. (2015) 'Numerical model validation for mooring systems: Method and application for wave energy converters', *Renewable Energy*, 75, pp. 869–887.

Harris, R. E., Johanning, L., Wolfram, J. (2004). 'Mooring Systems for Wave Energy Converters: A Review of Design Issues and Choices' *3rd Conference on Marine Renewable Energy, 2004 Blyth, UK.*

Herbich, John B. (2000). *Handbook of coastal engineering*. McGraw-Hill Professional. A.117, Eq. (12)

Hughes, M.G. and Heap, A.D. (2010) 'National-scale wave energy resource assessment for Australia', *Renewable Energy*, 35(8), pp. 1783–1791.

Iglesias, G. and Carballo, R. (2011) 'Wave resource in El Hierro—an island towards energy self-sufficiency', *Renewable Energy*, 36(2), pp. 689–698.

Imai, Y., Nagata, S., Toyota, K. and Murakami, T. (2014) 'An experimental study on primary efficiency of a wave energy converter "backward bent duct buoy" in regular wave conditions', *Journal of the Japan Society of Naval Architects and Ocean Engineers*,

19(0), pp. 79–88.

Johanning, L., Smith, G. H., & Wolfram, J. (2005) 'Towards design standards for wave energy converter mooring' *6th European Wave and Tidal Energy Conference, 2005 Glasgow, UK.*

Johanning, L., Smith, G.H. and Wolfram, J. (2006) 'Mooring design approach for wave energy converters', *Proceedings of the Institution of Mechanical Engineers, Part M: Journal of Engineering for the Maritime Environment*, 220(4), pp. 159–174.

Johanning, L., Smith, G.H. and Wolfram, J. (2007) 'Measurements of static and dynamic mooring line damping and their importance for floating WEC devices', *Ocean Engineering*, 34(14-15), pp. 1918–1934.

Kamath, A., Bihs, H. and Arntsen, Ø.A. (2015) 'Numerical modeling of power take-off damping in an oscillating water column device', *International Journal of Marine Energy*, 10, pp. 1–16.

Kasiulis, E., Punys, P. and Kofoed, J.P. (2015) 'Assessment of theoretical near-shore wave power potential along the Lithuanian coast of the Baltic sea', *Renewable and Sustainable Energy Reviews*, 41, pp. 134–142.

Kim, J. A. and Hong, S. Y. (2014). 'The Shape Design and Analysis of Floating Offshore Wind Turbine Structures with Damper Structure and Shallow Draft', *Journal of Ocean and Wind Energy,* ISOPE, 1(3), 170-176

Koh, H and Cho, I.H. (2011). 'Motion Response of a Circular Cylinder with a Heave Plate in Waves', *Proceedings of the Twenty-first (2011) International Offshore and Polar Engineering Conference* Maui, Hawaii, USA, June 19-24, 2011

Lake, M., He, H., Troesch, A.W., Perlin, M. and Thiagarajan, K.P. (2000) 'Hydrodynamic coefficient estimation for TLP and Spar structures', *Journal of Offshore Mechanics and Arctic Engineering*, 122(2), p. 118.

Lee, C.H., Maniar, H., Newman, J.N., and Zhu, X. (1996). "Computation of wave loads using a B-spline panel method" Proceedings, 21st Symposium on Naval Hydrodynamics, Trondheim, Norway.

Lee, C.H. (2014). WAMIT User Manual, Version 7.1. Massachusetts Institute of Technology.

Ponce de León, S., Bettencourt, J.H. and Kjerstad, N. (2011) 'Simulation of irregular waves

in an offshore wind farm with a spectral wave model', *Continental Shelf Research*, 31(15), pp. 1541–1557.

Lewis, A., S. Estefen, J. Huckerby, W. Musial, T. Pontes, J. Torres-Martinez. (2011) Ocean Energy. In IPCC Special Report on Renewable Energy Sources and Climate Change Mitigation [O. Edenhofer, R. Pichs-Madruga, Y. Sokona, K. Seyboth, P. Matschoss]

Lupton, R.C. and Langley, R.S. (2014) 'Assessing the importance of the slow drift motion of floating wind turbine platforms', *Volume 9A: Ocean Renewable Energy*.

Maniar, H. (1995) 'A three dimensional higher-order panel method based on B-splines' Ph.D. Thesis, Department of Ocean Engineering, MIT, Cambridge, Massachusetts.

Mei, C.C. (2011) 'Hydrodynamic principles of wave power extraction', *Philosophical Transactions of the Royal Society A: Mathematical, Physical and Engineering Sciences*, 370(1959), pp. 208–234.

Mombaerts, J. (2006). Mooring Course for ARIANE Users: Bureau Veritas.

Moreno, J., Cameron, M., Thiagarajan, K.P., and Mendoza,. C.A.G., (2015) 'Hydrodynamic Performance of Heave Plates on Floating Offshore Wind Turbine Platforms.' *Proceedings of the Twenty-fifth (2015) International Ocean and Polar Engineering Conference.*

Morris-Thomas, M., Irvin, R. and Thiagarajan, K. (2007). An Investigation Into the Hydrodynamic Efficiency of an Oscillating Water Column. *J. Offshore Mech. Arct. Eng.*, 129(4), p.273.

Morris-Thomas, M., Irvin, R. and Thiagarajan, K. (2007). An Investigation Into the Hydrodynamic Efficiency of an Oscillating Water Column. *J. Offshore Mech. Arct. Eng.*, 129(4), p.273.

Newman, J. (1985). Algorithms for the free-surface Green function. *Journal of Engineering Mathematics*, 19(1), pp.57-67.

Nielsen, J. and Sørensen, J. (2011). On risk-based operation and maintenance of offshore wind turbine components. *Reliability Engineering & System Safety*, 96(1), pp.218-229.

Ning, D., Shi, J., Zou, Q. and Teng, B. (2015). Investigation of hydrodynamic performance of an OWC (oscillating water column) wave energy device using a fully nonlinear

HOBEM (higher-order boundary element method). *Energy*, 83, pp.177-188.

Norton, M. (1990). Fundamentals of Noise and Vibration Analysis for Engineers. *The Journal of the Acoustical Society of America*, 88(4), p.2044.

Oceanlinx. (2016). *How Oceanlinx works*. [online] Available at: http://www.oceanlinx.com/oceanlinx-advantage/how-it-works/

Pelamis-Wave-Power-LTD. 2013. Pelamis Testing. *Pelamis Wave Power.*

Pérez, C. and Iglesias, G. (2012), 'Integration of Wave energy converters and Offshore Windmills', *ICOE (The International Conference on Ocean Energy) 2012 Proceedings, Dublin*

Rhinefrank, K., Schacher, A., Prudell, J., Cruz, J., Stillinger, C., Naviaux, D., Brekken, T., von Jouanne, A., Newborn, D., Yim, S. and Cox, D. (2013). Numerical Analysis and Scaled High Resolution Tank Testing of a Novel Wave Energy Converter. *J. Offshore Mech. Arct. Eng.*, 135(4), p.041901.

Rhinefrank, K., Schacher, A., Prudell, J., Hammagren, E., Zhang, Z., Stillinger, C., Brekken, T., von Jouanne, A. and Yim, S. (2011). Development of a Novel 1:7 Scale Wave Energy Converter. *Volume 5: Ocean Space Utilization; Ocean Renewable Energy*.

Silva, S. R., Gomes, R., & Falcão, A. (2016). Hydrodynamic optimization of the UGEN: Wave energy converter with U-shaped interior oscillating water column. International Journal of Marine Energy, 15, 112-126.

Roddier, D., Cermelli, C., Aubault, A. and Weinstein, A. (2010). WindFloat: A floating foundation for offshore wind turbines. *J. Renewable Sustainable Energy*, 2(3), p.033104. Ronalds, B. (2005). Applicability ranges for offshore oil and gas production facilities. *Marine Structures*, 18(3), pp.251-263.

Sarpkaya, T., & Isaacson, M. (1981). Mechanics of wave forces on offshore structures. New York: Van Nostrand Reinhold.

Sheng, W., Lewis, T., Alcorn, R., (2012), 'On wave energy extraction of oscillating water column device', 4th International Conference on Ocean Energy, Dublin, Ireland.SOFEC 2013. FSPO Kizomba A - Angola. *SOFEC.*

Sheng, W., Thiebaut, F., Babuchon, M., Brooks, J., Lewis, A. and Alcorn, R. (2013). Investigation to Air Compressibility of Oscillating Water Column Wave Energy

Converters. *Volume 8: Ocean Renewable Energy*.

Sims, R., et al. (2007), "Energy supply", In B. Metz, et al., (Eds.), Climate Change 2007: Mitigation, Contribution of Working Group III to the Fourth Assessment Report of the IPCC (Intergovernmental Panel on Climate Change), Cambridge University Press, Cambridge, and New York

"Space For News: How Hydrokinetic Energy Works." Space For News. N.p., n.d. Web. 29 Apr. 2012. http://space4news.blogspot.com.au/2010/07/howhydrokinetic- energy-works.html

Stanham, Y., McCarthy, T., Stappenbelt, B. (2016). 'Water column and structure heave velocity relationship for a floating oscillating water column wave energy device', ISOPE 2016.

Stappenbelt, B., & Cooper, P. (2010). Mechanical Model of a Floating Oscillating Water Column Wave Energy Conversion Device. *Annual Bulletin of the Australian* Institute of High Energetic Materials (1), 34-35.

Soomere, T. and Eelsalu, M. (2014). On the wave energy potential along the eastern Baltic Sea coast. *Renewable Energy*, 71, pp.221-233

Subbulakshmi, A., Jose, J., Sundaravadivelu, R. and Selvam, R. (2015). Effect of Viscous Damping on Hydrodynamic Response of Spar with Heave Plate. *Aquatic Procedia*, 4, pp.508-515.

Sykes, R., Lewis, A. and Thomas, G. (2008). A Numerical and Physical Comparison of a Geometrically Simple Fixed and Floating Oscillating Water Column. *Volume 6: Nick Newman Symposium on Marine Hydrodynamics; Yoshida and Maeda Special Symposium on Ocean Space Utilization; Special Symposium on Offshore Renewable Energy*.

Tao, L., and Cai, S., 2004. Heave Motion Suppression of a Spar with a Heave Plate. Ocean Engineering 31, 669-692.

Szumko, S. (1989). Mechanical Model for Oscillating Water Column with Compressibility. *J.* Eng. Mech., 115(9), pp.1851-1866.

Veer, R. V., & Tholen, H. J. (2008). Added Resistance of Moonpools in Calm Water. Volume 6: Nick Newman Symposium on Marine Hydrodynamics; Yoshida and Maeda Special Symposium on Ocean Space Utilization; Special Symposium on

Offshore Renewable Energy. doi:10.1115/omae2008-57246

Walkington, I. and Burrows, R. (2009). Modelling tidal stream power potential. *Applied Ocean Research*, 31(4), pp.239-245.

WAMIT, n.d.. WAMIT, Inc., Chestnut Hill, Massachusetts.

Wang, Zhuo, An evolutionary optimisation study on offshore mooring system design, Doctorate of Engineering thesis, School of Civil, Mining & Environmental Engineering, University of Wollongong, 2012. http://ro.uow.edu.au/theses/3808

Wave-Dragon 2005. Wave Dragon - Principles. *Simple and robust construction* - complex design.

Williamson, Robert, and Dopita. "Australia's Renewable Energy Future." Australian Academy of Science. N.p., 1 Jan. 2010. Web. 18 Mar. 2012. <http://www.science.org.au/reports/documents/AusRenewableEnergyFuture.pdf>

Wilson, J. (2003). *Dynamics of offshore structures*. Hoboken, N.J.: J. Wiley.

Zhou, G., Huang, J. and Zhang, G. (2015). Evaluation of the wave energy conditions along the coastal waters of Beibu Gulf, China. *Energy*, 85, pp.449-457.

Appendix A – WAMIT Theory

A.1 - WAMIT Theory and Background

Wave Analysis MIT (WAMIT) is software package developed at the Massachusetts Institute of Technology. WAMIT is a diffraction/radiation program used for the analysis of the interaction of surface waves with offshore structures. WAMIT is able to analyse a wide variety of offshore structures including free floating, restrained or fixed bodies. WAMIT is able to evaluate the following quantities:

- Hydrostatic coefficients
- Added-mass and damping coefficients for all modes
- Wave exciting forces and moments using the Haskind relations, or directly by pressure integration from the solutions of the diffraction or scattering problems.
- Motion amplitudes and phases for a free-floating body.
- Forces restraining a body that is free-floating in some but not all modes. This includes mooring forces.
- Hydrodynamic pressure and fluid velocity on the body surface.
- Hydrodynamic pressure and fluid velocity in the fluid domain.
- Free-surface elevation.
- All components of the drift force and moment by momentum integration over a control surface.
- Horizontal drift forces and mean yaw moment by momentum integration in the far-field.
- All components of the drift force and moment by local pressure integration over the body surface.
- Drift force and moment in bidirectional waves.

WAMIT is run through the command prompt and consists of two programs, POTEN and FORCE. POTEN is responsible for the radiation and diffraction velocity potentials on the body surface for the various modes, wave periods/frequencies and wave headings. FORCE then solves for the global quantities. These include the motion, hydrodynamic coefficients and first and second order forces. The user may specify additional quantities to be evaluated by FORCE. These include velocities and pressures at specified locations in the fluid domain

and wave elevations at the free surface. POTEN is usually significantly more computationally intensive than FORCE.

WAMIT is able to analyse offshore structures using both a lower order method and higher order method. The lower order method utilises flat panels to describe the structure. The vertex of each panel is specified in the geometric data file. The higher order method is able to specify the structure geometry through flat panels, B-spline approximations, geometry models developed in MultiSurf (a CAD program), and explicit analytical formulae. The higher order method is generally more accurate than the lower order method due to a smaller number of unknowns compared to the lower order method. The higher order method is used in this thesis. Both the higher order and lower order method are explained in more detail later in this chapter.

The higher order method requires the structure to be composed of a number of patches. These patches are then further reduced into panels (seen in Figure 9.3 and Figure 9.4). B-splines are then used to develop approximations on these surfaces. The panels are not restricted to flat surfaces but rather a continuous surface. This allows curves surfaces to be represented better more accurately than those using the lower order method. Reduction of the panel size will result in more accurate solutions; however this will also result in significantly longer computational times. Care must be taken to balance these two variables. The higher and lower order methods are discussed with more depth in the theory section of this chapter.

A.2 - WAMIT Input and Output Files

A.2.1 - Input Files

WAMIT requires four primary input files. These are the geometric data file (GDF.gdf), the potential control file (POT.pot), the force control file (FRC.frc), and the configuration file (CFG.cfg/config.wam). Each file is summarised here.

Geometric Data File

The geometric data file contains all data relating to the geometry of the body. The structure of this file is largely dependent upon the chosen method of analysis. The user must first select from the higher order and lower order method and then select the method by which they choose to define the body.

Potential Control File

The potential control file contains data that is used to determine the external parameters of the testing. These include the water depth, wave periods and the time between successive periods used in testing, the wave heading and number of waves, the number of bodies tested the location of the local axis with respect to the global axis, and also the allowable degrees of freedom for each body.

Force Control File

The potential control file stores information regarding the physical setup of the body. This includes any external damping or stiffness contributions, the mass matrix, the radius of gyration matric, and the centre of gravity of the body.

Configuration File

The configuration file is where the solving method and solving parameters are defined. This includes specifying the use of the lower or higher order method, and also whether to use a direct solver, iterative solver, or a block iterative solver. Other solving parameters defined include the panel size, the range of the solution and the type of input and output of the range (period, frequency, infinite depth wavenumbers or finite depth wavenumbers) and also the degrees of freedom of any additional patches added by the user.

A.2.2 - Output Files

WAMIT outputs one primary file, this file is known as the OUT file. The user specifies the contents of the OUT file in the force control input file. The following options are available. Each option will produce a separate output file with the relevant file name and extension.

Option	Description	Filename
1	Added mass and damping coefficients	frc.1
2	Exciting forces from Haskind relations	frc.2
3	Exciting forces from diffraction potential	frc.3
4	Body response amplitude operators	frc.4
5p	Hydrodynamic pressure on the body surface	frc.5p

5v	Fluid pressure vector on the body surface	frc.(5vx,5vy,5vz)
6p	Pressure and surface elevation at field points	frc.6p
6v	Flued velocity vector at field points	frc.(6vx,6vy,6vz)
7	Mean drift force and moment from control surface	frc.7
8	Mean drift force and moment from momentum	frc.8
9	Mean drift force and moment from pressure	frc.9

Each output file is produced as a simple text file. Analysis of the data is performed using a data analysis software package such as Microsoft Excel.

A.3 - Theory

A.3.1 - Introduction

WAMIT makes use of Cartesian coordinates for all calculations. These output is then non-dimensionalised through a combination of the wave height, A, gravity, g, frequency, ω, and the length scale defined through the input parameter, *ULEN*, in the GDF file.

WAMIT makes use of a local (x, y, z) and global (X, Y, Z) coordinate system to define the input and output of the system. The local coordinate system is also referred to as the body coordinate system. The body motions, geometry and forces are defined with respect to the body coordinate system. This allows multiple bodies to be analysed concurrently, each with their own point of reference. The body coordinates are defined with reference to the global coordinates in the input file XBODY. For simplicity the body and global coordinate systems will align when analysing a single body.

The global system is used to define the incident waves. The phase angles of the forces, motions, pressures, and fluid velocity are also defined with respect to the global system. The origin of the system ($X = Y = 0$) is used as the point of reference.

Fluid Theory

Boundary Value Problem

The boundary value problem is initial step used to solving fluid domain problems where a body interacts with incident waves. This is used to evaluate the oscillating hydrodynamic pressures, loads, velocity potentials and motions of the body in the fluid domain. The fluid flow is assumed to be linearized, free of uplift and to be potential; a harmonic time dependence is also adopted.

If the flow is assumed to be potential then the velocity potential, Φ, can be used to define the flow velocity. The flow velocity is the gradient of the velocity potential; hence this satisfies the Laplace equation in the fluid domain:

$$\nabla^2 \Phi = 0 \tag{A.1}$$

Using the harmonic time dependence assumption, an expression relating the complex velocity potential, φ, to the velocity potential, Φ, can be developed:

$$\Phi = \mathrm{Re}\left(\varphi e^{i\omega t}\right) \tag{A.2}$$

Where ω is the incident wave frequency and t is time.

Expressing the boundary value problem in terms of the complex velocity potential will allow for the complex solutions to be developed. The linearised form of the free surface is then:

$$\varphi_z - K\varphi = 0 \text{ on } z = 0 \tag{9.3}$$

Where K is the wave number of the incident wave in an infinite water depth. The velocity potential is then defined as:

$$\varphi_0 = \frac{igA}{\omega}\frac{\cosh[k(z+H)]}{\cosh kH} e^{-ikx\cos\beta - iky\sin\beta} \tag{9.4}$$

Where k is the real part of the root to the dispersion equation,

$$\frac{\omega^2}{g} = k\tanh kH \tag{9.5}$$

and β is the angle of propagation between the body and positive x axis. This will usually be 0 radians.

The dispersion equation assumes the water depth is not infinite. At infinite depth $k = K$.

The assumption of the linearization of the problem allows the velocity potential to be deconstructed into the addition of the radiation, φ_R, and diffraction potentials, φ_D:

$$\varphi = \varphi_R + \varphi_D \tag{9.6}$$

Where the radiation and diffraction potentials are equal to:

$$\varphi_R = i\omega \sum_{i=1}^{6} \xi_j \varphi_j \tag{9.7}$$

$$\varphi_D = \varphi_0 + \varphi_S \tag{9.8}$$

Here, ξ_j represents the complex motions of the body in each degree of freedom and φ_j represents the corresponding unit-amplitude radiation potential. Lastly, φ_S is the scattering disturbance of the incident wave by the body at its fixed, undisturbed location.

If the body is undisturbed then the following relationships on the body boundaries regarding the radiation and diffraction potential hold true:

$$\varphi_{jn} = n_j \tag{9.9}$$

$$\varphi_{Dn} = 0 \tag{9.10}$$

Where n = (n_1, n_2, n_3) and x × n = (n_4, n_5, n_6) where x = (x, y, z). n is a unit vector perpendicular to the body boundary and points out into the fluid.

Lastly, the radiation condition of outgoing waves is applied to the velocity potentials, φ_j, where j = 1,2,…,7.

Velocity Potentials

WAMIT makes use of Green's Theorem to develop integrals for the velocity potentials; this was first developed by Newman (1985). The radiation and diffraction potentials can each be expressed. The integral that satisfies the radiation component of the velocity potential on the body boundary is

$$2\pi\varphi_j(\mathrm{x}) + \iint_{S_b} \varphi_j(\xi)\frac{\partial G(\xi;\mathrm{x})}{\partial n_\xi}d\xi = \iint_{S_b} n_j G(\xi;\mathrm{x})d\xi \tag{9.11}$$

While the total diffraction velocity potential integral over the body surface is:

$$2\pi\varphi_D(\mathrm{x}) + \iint_{S_b} \varphi_D(\xi)\frac{\partial G(\xi;\mathrm{x})}{\partial n_\xi}d\xi = 4\pi\varphi_0(\mathrm{x}) \tag{9.12}$$

Where S_b is the wetted area of the body surface.

The Green function is represented here by $G(\mathbf{x};\boldsymbol{\xi})$ and is referred to as the wave source potential.

Hydrostatics

The Gauss divergence theorem allows WAMIT to define all hydrostatic data in the form of surface integrals over the wetted surface area of the body, S_b. This leads to the following definitions:

$$\text{Volume} = \begin{matrix} -\iint_{S_b} n_1 x\, dS \\ -\iint_{S_b} n_2 y\, dS \\ -\iint_{S_b} n_3 z\, dS \end{matrix} \tag{9.13}$$

All three volumes are calculated by WAMIT as a check on the panel coordinates. The average of the three calculations is used for the internal calculation.

WAMIT calculates the centre of buoyance through the following relationships:

$$x_b = \frac{-1}{2\forall} \iint_{S_b} n_1 x^2 \, dS \tag{9.14}$$

$$y_b = \frac{-1}{2\forall} \iint_{S_b} n_2 y^2 \, dS \tag{9.15}$$

$$z_b = \frac{-1}{2\forall} \iint_{S_b} n_3 y^2 \, dS \tag{9.16}$$

The dimensionalised terms of the 6x6 restoring coefficient matrix, C, is then defined as:

$$C(3,3) = \rho g \iint_{S_b} n_3 \, dS \qquad C(4,5) = -\rho g \iint_{S_b} xyn_3 \, dS$$

$$C(3,4) = \rho g \iint_{S_b} yn_3 \, dS \qquad C(4,6) = -\rho g \forall x_b + mgx_g$$

$$C(3,5) = -\rho g \iint_{S_b} xn_3 \, dS \qquad C(5,5) = \rho g \iint_{S_b} x^2 n_3 \, dS + \rho g \forall z_b - mgz_g$$

$$C(4,4) = \rho g \iint_{S_b} y^2 n_3 \, dS + \rho g \forall z_b - mgz_g \qquad C(5,6) = -\rho g \forall y_b + mgy_g$$

Further computation is able to be non-dimensionalise these terms:

$$\bar{C}(3,3) = C(3,3)/pgL^2 \qquad \bar{C}(4,5) = C(4,5)/pgL^4$$

$$\bar{C}(3,4) = C(3,4)/pgL^3 \qquad \bar{C}(4,6) = C(4,6)/pgL^4$$

$$\bar{C}(3,5) = C(3,5)/pgL^3 \qquad \bar{C}(5,5) = C(5,5)/pgL^4$$

$$\bar{C}(4,4) = C(3,3)/pgL^4 \qquad \bar{C}(5,6) = C(5,6)/pgL^4$$

Where $C(i,j) = C(j,i)$ for all i and j except $C(4,6)$ and $C(5,6)$ and all over values of $C(i,j) = 0$.

Added Mass and Damping

The added mass, A_{ij}, and damping, B_{ij}, are linked through the following expression:

$$A_{ij} - \frac{i}{\omega} B_{ij} = \rho \iint_{S_b} n_i \varphi_j \, dS \tag{9.17}$$

The added mass coefficient is defined as:

$$\bar{A}_{ij} = \frac{A_{ij}}{\rho L^k} \tag{9.18}$$

And damping coefficient as:

$$\bar{B}_{ij} = \frac{B_{ij}}{\rho L^k \omega} \tag{9.18}$$

Where:

k = 3 for (i,j = 1,2,3)

k = 4 for (i = 1,2,3, j = 4,5,6) or (i = 4,5,6, j = 1,2,3)

k = 5 for (i,j = 4,5,6)

Exciting Forces

WAMIT offers two options for the output of exciting forces. These options are computed through either Haskind relations or direct integration of hydrodynamic pressure.

The complex solution for the motion, X_i, for each case is defined as

Haskind relations

$$X_i = -i\omega\rho \iint_{S_b} \left(n_i \varphi_0 - \varphi_i \frac{\partial \varphi_0}{\partial n} \right) dS \tag{9.19}$$

Direct Integration

$$X_i = -i\omega\rho \iint_{S_b} n_i \varphi_D \, dS \tag{9.20}$$

The complex solution is non-dimensionalised:

$$\bar{X}_i = \frac{X_i}{pgAL^m} \tag{9.21}$$

Where m = 2 for i = 1,2,3, and m = 3 for i =4,5,6.

Both the Haskind relations and direct pressure integration approaches are a combination of the Froude-Krylov forces and scattering forces. In the Haskind relations the first expression

of the parenthesis, $n_i\varphi_0$, is the Froude-Krylov component and the second, $\varphi_i \frac{\partial \varphi_0}{\partial n}$, is the scattering component. The direct pressure integration methods accounts for both the Froude-Krylov component and scattering component of the forces through the total diffraction potential, φ_D.

Motions in Waves

WAMIT allows two input methods for evaluating the body motion in waves. The first input method, referred to as the Alternative 1 FRC input, is used when the body is without external constraints. This body has six degrees of freedom. With this, the following relationships hold true:

$$x_b = x_g$$

The *x* centre of the body is equal to the *x* centre of gravity.

$$y_b = y_g$$

The *y* centre of the body is equal to the *y* centre of gravity.

$$m = \rho \forall$$

The mass of the body is equal to the density of the fluid multiplied by the displaced volume of the fluid.

The user is required to input an inertia matrix of the body within the Alternative 1 FRC file. Newman (1977) defines the inertia matrix as:

$$M = \begin{bmatrix} m & 0 & 0 & 0 & mz_G & -my_G \\ 0 & m & 0 & -mz_G & 0 & mx_G \\ 0 & 0 & m & my_G & -mx_G & 0 \\ 0 & -mz_G & my_G & I_{11} & I_{12} & I_{13} \\ mz_G & 0 & -mx_G & I_{21} & I_{22} & I_{23} \\ -my_G & mx_G & 0 & I_{31} & I_{32} & I_{33} \end{bmatrix} \quad (9.22)$$

Where m is the mass of the body, (x_g, y_g, z_g) is the centre of gravity in the *x, y,* and *z* plane, and I_{ii} is the moment of inertia around the respective axis.

The moment of inertia can be further defined in terms of the radius of gyration, r_{ij}, density of the fluid and the displaced volume of the fluid:

$$I_{ij} = \rho \forall r_{ij} \left| r_{ij} \right| \tag{9.23}$$

The second input method, Alternative 2 FRC, allows for effects external factors to be included in the analysis. These factors may include the addition on heave plates, mooring lines, power take-off damping simulation, and also viscous damping effects. The added external stiffness and damping is introduced through two additional matrices, K_{ij}^{E}, and B_{ij}^{E} respectively. The additional mass components must be accounted for within the existing mass matrix, hence M_{ij} is now equal to $M_{ij} + M_{ij}^{E}$.

Once the matrices have been defined the complex amplitudes of motion, ξ_j are calculated using Newton's Law by solving the linear system:

$$\sum_{j=1}^{6} \left[-\omega^2 \left(M_{ij} + M_{ij}^{E} + A_{ij} \right) + i\omega \left(B_{ij} + B_{ij}^{E} \right) + \left(K_{ij} + K_{ij}^{E} \right) \right] \xi_i = X_i \tag{9.24}$$

WAMIT then non-dimensionalises the solution, $\bar{\xi}_i$, using the following relationship:

$$\bar{\xi}_i = \frac{\xi_j}{A/L^n} \tag{9.25}$$

Where n = 0 for i = 1,2,3 and n = 1 for i = 4,5,6.

Higher and Lower Order Methods

WAMIT has two options for developing solutions, the higher order method and lower order method. Both options will be detailed here along with the advantages and disadvantages of each method. Both are presented to develop context and reasoning for selecting the higher order method as the method of analysis in this thesis.

Lower Order Method

The lower order method required the user to specify the geometric coordinates of the body in the Geometric Data File (GDF). The body is discretised into a number of flat quadrilaterals; it is possible to specify a triangular panel by repeating the coordinates of a quadrilateral vertex. The user is required to specify twelve points to full describe each panel, an *x*, *y*, and *z* coordinate for each vertex. The panel numbering system is dependent upon how the user is viewing the body. If viewed from the wet side of the panel the vertices are numbered anticlockwise. The opposite applied when viewing the panel from the dry side. This is

illustrated in Figure 9.2 (WAMIT Manual). Panel *i* is viewed from the wet side and panel *j* is viewed from the dry side.

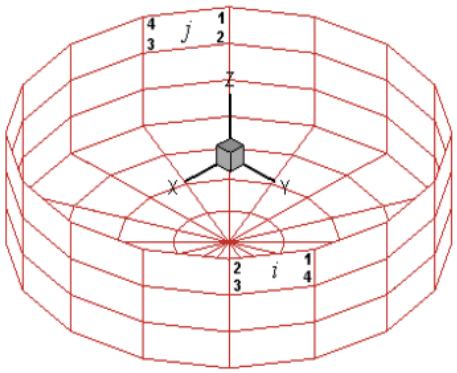

Figure 9.2: Lower order method discretization of an open cylinder

The solutions for the velocity potentials and the source strength are then calculated through an approximation of piecewise constants on each panel. The accuracy of the solutions is dependent on the number of panels (NPAN) the body is discretised into. Ideally the panels will be of similar width and thickness. This will call for a larger number of panels for larger bodies, potentially increasing the computational time. WAMIT does allow for two axis of symmetry to be established, one each for the X plane and Y plane.

The use of the lower order method allows two different solutions to be used; WAMIT refers to these as the potential source information. The potential source information is composed of two parts, the always-calculated potential formulation and the optional source formulation.

The potential formulation represents the velocity potential in terms of the surface distribution of sources and normal dipoles. The mathematics behind this can be found in Section 15.2 of the WAMIT manual. The potential formulation is used to determine the hydrodynamic quantities of the system. These include the first order pressure, drift forces based on the conservation of momentum, and the force coefficients.

The source information is optional and is chosen by the user. The source information is represented by the only source information. The source information must be used if the moment and mean drift force is solved through direct pressure integration.

Thin body sections may be represented through the lower order method by specifying a zero thickness and representing each panel as dipole panels, or by panelling both sides of the thin element with a finite thickness.

Higher Order Method

The higher order method does not reply on panelling but rather describes the body through a series of patches. Each patch can developed through a combination or singular use of B-spline approximations, flat panels, and analytical models developed in Multisurf. The velocity potential is solved through continuous B-splines rather than through piecewise approximations like the lower order method. The fluid velocity is solved through analytical differentiation. Both higher order solving differences generally results in a more accurate solution when compared to the lower order method.

The higher order method describes the body by reducing it into patches. These patches are further reduced into panels. Each panel is continuous surface and is therefore not limited to flat quadrilaterals or triangles like in the lower order method. This allows cylindrical shapes to be more accurately modelled when compared with the lower order method. B-splines approximations are then used to solve for the velocity potential and fluid velocity on each surface. The user is able to specify the number of patches and also the panel size. A decrease in panel size will result in a more accurate solution as the B-spline approximation will cover a smaller area, however, smaller panels will increase the computational time. Both the number of patches and panel size are specified in the GDF. WAMIT does allow for the maximum panel size to be set in the SPL file rather than specifying the number of panels each patch will be reduced to. WAMIT will then specify the largest panel size that will produce accurate solutions based on the parameters of the system. These parameters are the body size and wavelength. This can potentially allow for a quicker solution.

Likewise with the lower order method, WAMIT allows the user to specify an X and Y-axis of symmetry to reduce the number of input variables. The body is first described by patches; each patch is a continuous surface in 3D space. Various patches then meet at a common edge, this edge may be continuous or discontinuous. The intersection of a cylindrical patch and a plat patches is seen in the Figure 9.3 (WAMIT Manual). The blue sections of the patches are the only part specified by the user, reflecting the user defined patched on the X and Y-axis of symmetry produces the yellow part of the body.

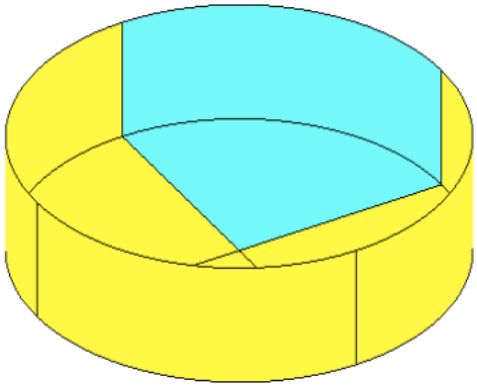

Figure 9.3: Discretisation of a cylinder using patches

To further increase accuracy WAMIT reduce the patches into smaller panels, each patch can be composed of a number of panels. Each panel can be described as rectangle in parametric space and as a curved surface in physical space. Each patch of Figure 2 has been reduced into four panels. This result of this is seen in Figure 9.4.

.

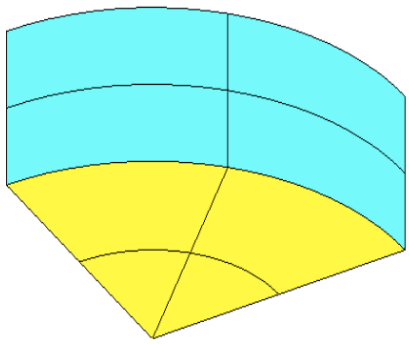

Figure 9.4: Reduction of patches into smaller panels

WAMIT makes use of a pair of normalised cylindrical coordinates (u,v) to define each point on each patch. Each coordinate varies for -1 to +1. To illustrate this the example from the

WAMIT manual will be discussed. This example is also relevant to this thesis as the model will be a cylindrical body composed of various patches.

Cylindrical coordinates typically make use of *r*, the distance of a point from the origin on the *x*-*y* place, *z* the height above the origin on the *z*-axis, and θ, the angle of rotation about the *z*-axis measured from the positive *x*-axis. Defining the draft of the structure as D, the cylinder radius as R, we can express *u* and *v* in terms of the known quantities of the body. The bottom patch is described as:

$$u = \frac{4\theta}{\pi} - 1 \quad \text{and} \quad v = 1 - 2\frac{r}{R} \tag{9.26}$$

While the cylinder is described as:

$$u = \frac{4\theta}{\pi} - 1 \quad \text{and} \quad v = -2\frac{z}{D} - 1 \tag{9.27}$$

Since the body is being specified in the first quadrant and reflected on the X and Y-axis the angle is defined for $0 \leq \theta \leq \frac{\pi}{2}$ while the draft of the structure must be less than zero, therefore $-D \leq z \leq 0$.

This allows any physical point on the body to be described by a combination of patches. Each Cartesian coordinate can also be described by the mapping functions:

$$x = X(u, v)$$

$$y = Y(u, v)$$

$$z = Z(u, v)$$

WAMIT makes uses of higher order geometry representation first presented by Maniar (1995) and also Lee *et al* (1996).

Defining the body

The body geometry in the higher order method is specified by first assigning a value to IGDEF in the GDF file. The following options for the body description are available:

Representation by Lower order panels (IDGEF = 0)

This is the simplest method to represent the body in the higher order method. The coordinates of the vertices of each patch are input sequentially. This method is useful when modelling

bodies composed of a small number of flat rectangular patches. Examples include barges and vessels with simple moonpools.

Representation by B-splines (IGDEF = 1)

Modelling the body through the use of B-splines is the most general approach to modelling the body in the higher order method. Here each patch is represented by a B-spline. This method is similar to finite element analysis. The user has the option to specify the panel subdivision of the geometry and velocity potentials independently.

The B-spline method models the mapping function on each panel in the tensor-product form. This makes use of the mapping functions in 1.3.7.2. Here X = (*X, Y, Z*).

$$\boldsymbol{X}(u,v) = \sum_{j=1}^{M_v^{(g)}} \sum_{i=1}^{M_u^{(g)}} \boldsymbol{X}_{ij} U_i(u) V_j(v) \tag{9.28}$$

$U_i(u)$ and $V_j(v)$ are the B-spline basis functions and $M_v^{(g)}$ and $M_u^{(g)}$ are the number of basis functions in *u* and *v* respectively. The number of basis function in *u* and *v* are calculated from the user input in the GDF file through the following relationship:

$$M_u^{(g)} = N_u^{(g)} + K_v^{(g)} - 1 \tag{9.29}$$

$$M_v^{(g)} = N_v^{(g)} + K_v^{(g)} - 1 \tag{9.30}$$

Here $N_v^{(g)}$ and $N_u^{(g)}$ are numbers of the panel subdivision of the *v* and *u* coordinates of on the i-th patch. $K_v^{(g)}$and $K_v^{(g)}$ are the orders of the B-splines. The user in the GDF file specifies these values, along with the Xij values.

Representation by Multisurf (IGDEF = 2)

Multisurf is a piece third party computer automated design software. Multisurf is able to export models directly to WAMIT. This method is desirable when dealing with irregular shapes that may be hard to easily represent with B-splines are or smaller patches. The user has the option to specify the number of patches the model will be discretised into however this can also be left to WAMIT to calculate. This method will not be used in this thesis because the desired system is able to be represented through the higher order method.

Representation by analytical geometry (IGDEF < -1)

This method is the easiest representation of the body if the body geometry can be defined explicitly. This method is advantageous over the other methods as the explicit definition of the body negates body approximation errors; only the velocity potential is approximated. The body geometry is coded in FORTRAN (a programming language) and saved in the WAMIT file, GEOMXACT.F. WAMIT includes thirty-three different pre-programmed geometric models within the GEOMXACT.F file. The user is able to specify the desired model by selecting the appropriate IGDEF value and also the dimension of each model in the GDF file.

A floating oscillating water column device will be modelled using IGDEF = -7. This subroutine is that of a floating spar type body. The body has a concentric moonpool in the centre of the structure. The user is required to specify the outer diameter of the structure, the moonpool diameter and the draft. This body consists of three patches, the outer cylinder, the inner cylinder and the base. This is illustrated in Figure 9.5. An additional fourth patch will be used in this chapter. The fourth patch will represent an added free surface pressure. This has been done so simulate power take-off damping found in oscillating water column wave energy converters. This fourth patch will also dampen any large non-physical responses. The fourth patch is located within the cylinder. It can be thought of as a permeable lid. The ‘permeability’ of the patch will be determined by the user. A higher level of permeability will represent lower power takeoff damping values and a higher lower level of permeability will represent a higher level of power takeoff damping. This method of body specification has been chosen because the model is able to be specified analytically by an existing WAMIT function. This will reduce errors involved with the creation of a new model.

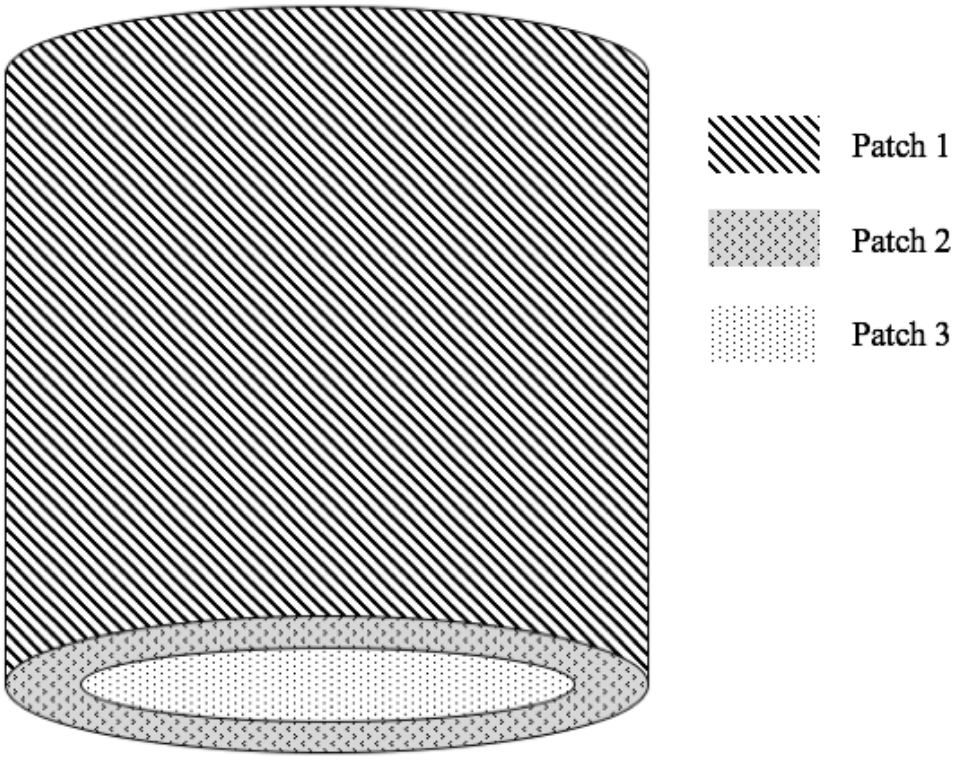

Figure 9.5: Physical representation of the model used in WAMIT

Advantages and Disadvantages of Each Method

Use of the lower order method or higher order method will be largely dependent on the structure geometry and desired output. Despite the simpler approach the lower order method does have some advantages over the higher order method.

The lower order method is able to better map the second order fluid pressure due to the square fluid velocity at unbounded edges than the higher order method. This is due to the higher order making the estimation more complicated. This can be overcome in the higher order method by ensuring that the flow singularity around these corners is accounted for.

The lower order method is also able to solve for the linearised velocity potentials more effectively than the higher order method. The higher order method can lead to a higher rate of non-convergence in the linear system.

Despite these advantages of the lower order system, the higher order method will be used in this chapter for a number of reasons:

Modelling cylindrical bodies using continuous surfaces available in the higher order method will produce a more accurate solution than that produced using the flat panels of the lower order method.

The higher order method contains less unknown variables than the lower order method. This will allow the solution to converge faster, saving computational time.

The higher order method will generally give a more accurate value for the free-surface elevation at the body waterline.

Appendix B - WAMIT Operational Files

Geometric Data File

TEST17 cylinder with moonpool

1. 9.80665 ULEN GRAV

1 1 ISX ISY

3 -7 NPATCH IGDEF

1 NLINES

5.67 12.3 5 radius, draft, moonpool radius

Potential Control File

TEST17 cylinder with moonpool, NPATCH=3

100

0 0 IRAD, IDIFF

-2501

0 0.01

1 NBETA (array BETA follows)

180.

1 NBODY

test17.gdf

0. 0. 0. 0. XBODY

0 0 1 0 0 0 IMODE(1-6)

Force Control File

TEST17b cylinder+moonpool, generalized modes, damping b33=.4, b77=.1

1 1 1 1 0 0 0 0 0 0

1.

0. 0. 0.

1 imass (mass matrix of body)

35625.66069 0.0 0.0 0.0 0.0 0.0

0.0 35625.66069 0.0 0.0 0.0 0.0

0.0 0.0 35625.66069 0.0 0.0 0.0

0.0 0.0 0.0 6522464.712 0.0 0.0

0.0 0.0 0.0 0.0 6522464.712 0.0

0.0 0.0 0.0 0.0 0.0 5771357.032

1 idamp

0.0 0.0 0.0 0.0 0.0 0.0

0.0 0.0 0.0 0.0 0.0 0.0

0.0 0.0 9000 0.0 0.0 0.0

0.0 0.0 0.0 0.0 0.0 0.0

0.0 0.0 0.0 0.0 0.0 0.0

0.0 0.0 0.0 0.0 0.0 0.0

1 istif

0.0 0.0 0.0 0.0 0.0 0.0

0.0 0.0 0.0 0.0 0.0 0.0

0.0 0.0 0.0 0.0 0.0 0.0

0.0 0.0 0.0 0.0 0.0 0.0

0.0 0.0 0.0 0.0 0.0 0.0

0.0 0.0 0.0 0.0 0.0 0.0

0

0

Configuration File

! TEST17.CFG file, cylinder with moonpool

ipltdat=5

ilowgdf=5

ILOWHI=1

IALTFRC=2

ISOLVE=1

PANEL_SIZE = 5 (use default .spl parameters)

IPERIN=1 (input period)

IPEROUT=3 (output period)

NUMHDR=1

noout= 1 1 1 1 0 1 0 0 0

Appendix C – Fast Fouier Transforms

Signal processing using Fast Fourier Transforms

Fast Fourier transformation (FFT) is used to covert a signal from one domain to another. This is often from the time domain to the frequency domain and vice versa. FFTs in this thesis are completed using Microsoft Excel and MATLAB. Both software packages utilise discrete calculations to produce the FFT. FFTs are useful when analyzing time domain data because they allow the amplitude and power spectra as a function of frequency to be developed. This allows further investigation into which forcing frequencies are likely to cause the most and by extension the least, power output of a particular system.

This process contains a number of steps. If the time series of the heave of vessel in the ocean is denoted as *z(t)*, and the motion is sampled at *N* times then t_k where k = 0,1,2,…*N*-1. Each measurement, z_k, has a complex value Z_n. These complex values are determined by satisfying the *N* number of equations:

$$Z_n = \sum_{k=0}^{N-1} z_k \, e^{ik\frac{2\pi n}{N}} \tag{C.31}$$

This sample function then has discrete Fourier expansion of:

$$z_k = \frac{1}{N} \sum_{k=0}^{N-1} Z_n \, e^{-in\frac{2\pi k}{N}} \tag{C.2}$$

Equation C.2 can be rewritten to incorporate the time step value t_k and the rotational frequency ω_o:

$$z_k = \frac{1}{N} \sum_{k=0}^{N-1} Z_n \, e^{-in\omega_o t_k} \tag{C.3}$$

Now z_k is equal to the discrete analogue of the complex form of the Fourier expansion:

$$z(t) = \frac{1}{N} \sum_{n=-\infty}^{\infty} c_n \, e^{in\omega_o t} \tag{C.32}$$

The complex coefficients at the sampled intervals are then equal to:

$$c_n = \frac{1}{T_o}\int_0^{T_0} z(t)\, e^{in\omega_o t}\, dt \tag{C.5}$$

This process required that the number of samples be a function of 2n. Microsoft Excel is limited to 212 but MATLAB contains no limitation. Both Microsoft Excel and MATLAB produce column vectors for the complex coefficients at the sampled intervals. The user is then required to process this data to produce the final FFT curve.

Microsoft Excel

The first example will be done using Microsoft Excel. This example will compute the FFT for the equation:

$$\mathrm{y} = \sin(2\pi t) + \cos(3\pi t) \tag{C.6}$$

The data will be sampled every 0.01 seconds. This gives a sampling rate, f_s, of 100 Hz. A total value of 4096 points will be used. To achieve this, the spreadsheet is setup in the following manner. The initial time domain data is contained in column A and column B. Column A contains the time value and column B contains the data points. Column C, D, and E will be used to compute the FFT. These columns are labled FFT Freq, FFT Mag, and FFT Complex respectively. FFT Freq will be the frequency values corresponding to the time at which the complex magnitude, FFT Complex, is calculated. FFT Mag will be the magnitude of the complex coefficient at sample. This setup is shown in Figure C.1:

	A	B	C	D	E
1	Time	Data	FFT Freq	FFT Mag	FFT Complex
2	0	1			
3	0.01	1.058352			
4	0.02	1.10762			
5	0.03	1.147675			
6	0.04	1.178466			
7	0.05	1.200024			
8	0.06	1.212452			
9	0.07	1.215934			

Figure C.1: Microsoft Excel setup for an FFT

The second stage of computing the FFT is to utlise the data analysis pack. Selecting the data in column B as the input and column E as the output produces the complex magnitudes of the data. The result of this process is seen in Figure C.2.

	A	B	C	D	E
1	Time	Data	FFT Freq	FFT Mag	FFT Complex
2	0	1			5.49211434174104
3	0.01	1.058352			5.49344754137229+0.430317080102723i
4	0.02	1.10762			5.49745257196008+0.861511180330416i
5	0.03	1.147675			5.50414579326388+1.29446629195645i
6	0.04	1.178466			5.51355468882275+1.73008048502744i
7	0.05	1.200024			5.525718197845+2.16927329411352i
8	0.06	1.212452			5.54068719210773+2.6129935345129i
9	0.07	1.215934			5.55852511084011+3.06222771811168i
10	0.08	1.210722			5.57930877132645+3.51800926223703i
11	0.09	1.197139			5.60312937866161+3.9814287178808i
12	0.1	1.175571			5.63009376506132+4.4536452879227i
13	0.11	1.146465			5.66032589778814+4.93589996468207i

Figure C.1: Complex amplitude output of FFT using Microsoft Excel

The FFT Freq column is the next to be filled. Since the data is sampled at 100 Hz, this needs to be even distributed over the number of sampled points, 4096. This means that each frequency step will be a multiple of f_s/N. Populating Column C produces the data seen in Figure C.3.

	A	B	C	D	E
1	Time	Data	FFT Freq	FFT Mag	FFT Complex
2	0	1	0		5.49211434174104
3	0.01	1.058352	0.024414		5.49344754137229+0.430317080102723i
4	0.02	1.10762	0.048828		5.49745257196008+0.861511180330416i
5	0.03	1.147675	0.073242		5.50414579326388+1.29446629195645i
6	0.04	1.178466	0.097656		5.51355468882275+1.73008048502744i
7	0.05	1.200024	0.12207		5.525718197845+2.16927329411352i
8	0.06	1.212452	0.146484		5.54068719210773+2.6129935345129i
9	0.07	1.215934	0.170898		5.55852511084011+3.06222771811168i
10	0.08	1.210722	0.195312		5.57930877132645+3.51800926223703i
11	0.09	1.197139	0.219727		5.60312937866161+3.9814287178808i
12	0.1	1.175571	0.244141		5.63009376506132+4.4536452879227i
13	0.11	1.146465	0.268555		5.66032589778814+4.93589996468207i

Figure C.3: Population of FFT Freq Column

The last stage before the FFT is complete is to compute the magnitude of the FFT Complex values. This is achieved by using the excel function *=2/N*IMABS(FFT Complex)* in the respective cells. After populating Column D the spreadsheet should resemble Figure C.4.

	A	B	C	D	E
1	Time	Data	FFT Freq	FFT Mag	FFT Complex
2	0	1	0	0.002682	5.49211434174104
3	0.01	1.058352	0.024414	0.002691	5.49344754137229+0.430317080102723i
4	0.02	1.10762	0.048828	0.002717	5.49745257196008+0.861511180330416i
5	0.03	1.147675	0.073242	0.002761	5.50414579326388+1.29446629195645i
6	0.04	1.178466	0.097656	0.002822	5.51355468882275+1.73008048502744i
7	0.05	1.200024	0.12207	0.002899	5.525718197845+2.16927329411352i
8	0.06	1.212452	0.146484	0.002991	5.54068719210773+2.6129935345129i
9	0.07	1.215934	0.170898	0.003099	5.55852511084011+3.06222771811168i
10	0.08	1.210722	0.195312	0.003221	5.57930877132645+3.51800926223703i
11	0.09	1.197139	0.219727	0.003356	5.60312937866161+3.9814287178808i
12	0.1	1.175571	0.244141	0.003505	5.63009376506132+4.4536452879227i
13	0.11	1.146465	0.268555	0.003667	5.66032589778814+4.93589996468207i

Figure C.4: Population of FFT Mag column

The data can now be plotted to visualise the FFT. Only half ($N/2$) data points need to be plotted due to the nature of FFTs being mirrored about the folding frequency. The folding frequency for this example is equal to 100Hz/2 = 50Hz. The time domain data (Column A and B) is plotted in Figure C.5 and the FFT is plotted in Figure C.6

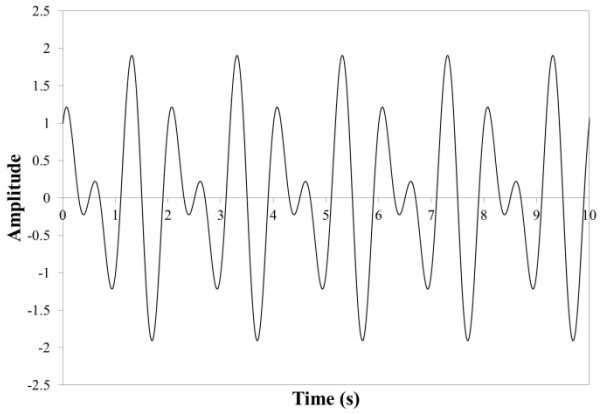

Figure C.5: Initial time domain data of equation (C.6) before FFT

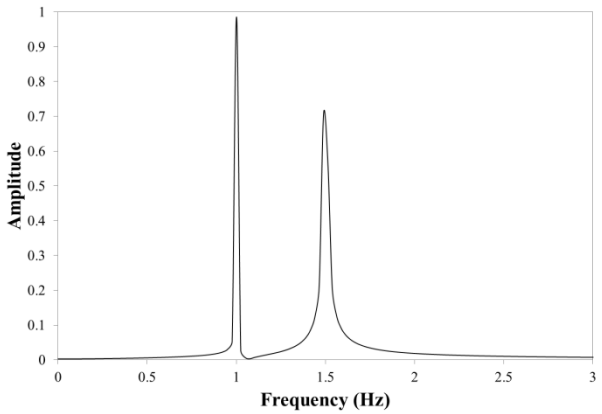

Figure C.6: Equation C.6 in the frequency domain after FFT

MATLAB

The MATLAB example will be completed with data imported from Microsoft Excel rather than data developed within the program itself. This is done because the time domain data produced in OrcaFlex will be of interest in this thesis. OrcaFlex produces spreadsheets of the data hence importing this into MATLAB will be necessary. The same number of data points (N=4096) and sampling rate (f_s = 100Hz) will be used in the MATLAB computation so comparison between the results produced by Microsoft Excel and MATLAB is possible.

The first step is to save the spreadsheet containing just the time domain measured data and not the time values in the MATLAB folder. The following code is then used to produce the time domain data graph and the FFT graph in MATLAB:

```
%---------- FFT of time domain data from Microsoft Excel ----------%


% Import time domain data
data=xlsread('TTD.xlsx');   % Imports the excel data


% Setting up the FFT parameters
Fs=100;                 % Sampling rate (Hz)
t=0:1/Fs:40.95;          % Time vector of 40 seconds
N=4096;                 % Number of sample points


% Computing the FFT
R=fft(data);            % FFT of the data - produces the complex values
R=R(1:N/2);              % Discards the repeated FFT
mr=abs(R)*2/N;           % Computes the magitude of the complex values
f=(0:N/2-1)*Fs/N;        % Computes the FFT frequency values


% Plotting the output
figure(1)               % Denotes first figure
```

```
plot(t,data);              % Plots the time domain data
xlabel('Time (s)');        % Labels the x axis
ylabel('Amplitude');       % Labels the y axis
axis([0,10,-2.5,2.5]);     % Stipulated minimum and maximum axis values

figure(2)                  % Denotes second figure
plot(f,mr);                % Plots the frequency domain data
xlabel('Frequency (Hz)');  % Labels the x axis
ylabel('Amplitude');       % Labels the y axis
axis([0,3,0,1]);           % Stipulated minimum and maximum axis values

%---------------------------------- end ----------------------------------%
```

Each step is labeled with what it does. This produces two figures. The first is the time domain output, seen in Figure C.7. The second is the frequency domain output seen in Figure C.8.

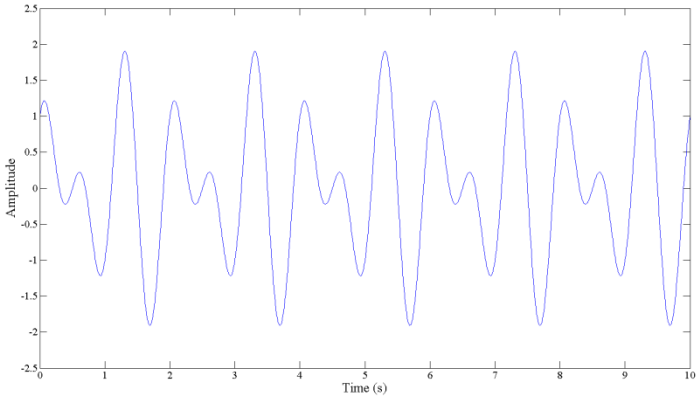

Figure C.7: MATLAB time domain output

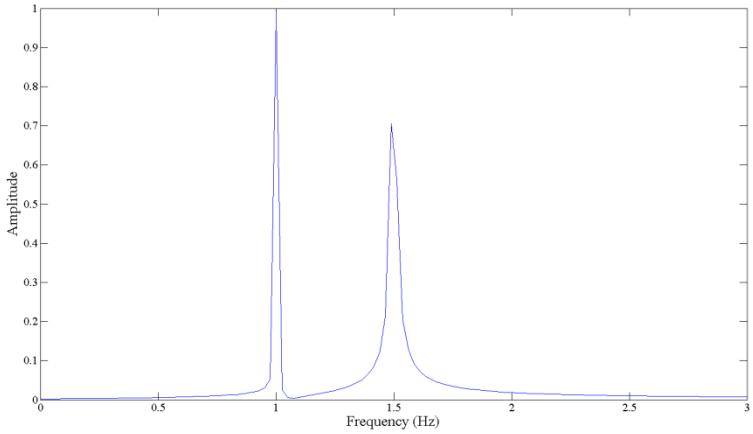

Figure C.8: MATLAB FFT output

The data produced in MATLAB and Microsoft Excel is an exact match. Both programs produced data in a timely manner. MATLAB might be preferred over Microsoft Excel when using non-uniform signals due to the ability to use more data points than Microsoft Excel.

Appendix D – MATLAB FFT Code

```
%---------- FFT of time domain data from Microsoft Excel ----------%
%housekeeping
clear                   % Clear stored data
clc                     % Clear input window

%import data
data1=xlsread('ISSC.xlsx','A:A');       % 7.875s data
data2=xlsread('ISSC.xlsx','B:B');       % 8.75s data
data3=xlsread('ISSC.xlsx','C:C');       % 11/67s data
f1=xlsread('ISSC.xlsx','E:E');          % Reading the frequency of the ISSC Spectra
p1=(1/8.75)*f1.^-1;                     % Converting the frequency to period
s1=100*xlsread('ISSC.xlsx','F:F');      % ISSC Spectrum with Tp = 7.875s
f2=xlsread('ISSC.xlsx','H:H');          % Reading the frequency of the ISSC Spectra
p2=(1/8.75)*f2.^-1;                     % Converting the frequency to period
s2=100*xlsread('ISSC.xlsx','I:I');      % ISSC Spectrum with Tp = 8.750s
f3=xlsread('ISSC.xlsx','K:K');          % Reading the frequency of the ISSC Spectra
p3=(1/8.75)*f3.^-1;                     % Converting the frequency to period
s3=100*xlsread('ISSC.xlsx','L:L');      % ISSC Spectrum with Tp = 11.67s

%Setup and perform the FFT
Fs=10;                  % Sampling frequency
t=0:1/Fs:1;             % Time vector of 1 second
nfft=16384;             % Number of sample points
X=fft(data1);           % Perform FFT on Data1
Y=fft(data2);           % Perform FFT on Data2
Z=fft(data3);           % Perform FFT on Data3
X=X(1:nfft/2);          % Disregard repeated FFT values
Y=Y(1:nfft/2);          % Disregard repeated FFT values
```

```
Z=Z(1:nfft/2);                % Disregard repeated FFT values
mx=(abs(X)*10/nfft);          % Compute magnitude of compled FFT values
smx=smooth(mx);               % Smooth the values
my=(abs(Y)*10/nfft);          % Compute magnitude of compled FFT values
smy=smooth(my);               % Smooth the values
mz=(abs(Z)*10/nfft);          % Compute magnitude of compled FFT values
smz=smooth(mz);               % Smooth the values
f=(0:nfft/2-1)*Fs/nfft;       % Determinig FFT frequency values
p=2/8.75*f.^-1;               % Converting frequencies values to period values
Q1=trapz(data1);              % Determine area under FFT of data1
Q2=trapz(data2);              % Determine area under FFT of data2
Q3=trapz(data3);              % Determine area under FFT of data3
SP1=trapz(s1);                % Determine area under ISSC curve with Tp = 7.875s
SP2=trapz(s2);                % Determine area under ISSC curve with Tp = 8.750s
SP3=trapz(s3);                % Determine area under ISSC curve with Tp = 11.67s

%plotting the output
figure(1);                    % First figure
%   Plotting three FFTs and three ISSC Spectra
plot(p,smx,'r',p,smy,'g',p,smz,'b',p1,s1,'-k',p2,s2,'--k',p3,s3,'-.k');
axis([0,2,0,110]);            % Stating minimum and maximum axis values
xlabel('Forcing period ratio');   % x axis label
ylabel('Power (J/s)');        % y axis label
%   Creating legend for figure 1
legend('Ratio = 0.90', 'Ratio = 1.00','Ratio = 1.33','Tp = 7.875s','Tp = 8.750s','Tp = 11.67s');

% Post FFT Calculations
PPW1=(Q1/nfft/7.875*10)/(1025*9.81/(64*pi)*7.875)    % Power efficiency ratio of ISSC curve with Tp = 7.875s
```

```
PPW2=(Q2/nfft/8.75*10)/(1025*9.81/(64*pi)*8.75)        % Power efficiency ratio of ISSC curve with Tp = 8.750s

PPW3=(Q3/nfft/11.675*10)/(1025*9.81/(64*pi)*11.67)   % Power efficiency ratio of ISSC curve with Tp = 11.67s


%---------------------------------- end ----------------------------------%
```

Appendix E – Numerical Analysis of a Water Column and Structure Heave Velocity Relationship for a Floating Oscillating Water Column Wave Energy Device

Appendix F – Experimental analysis of a water column and structure heave velocity relationship for a floating oscillating water column wave energy device